



UNIVERSITÀ
DEGLI STUDI
DI PADOVA

UNIVERSITA' DEGLI STUDI DI PADOVA
DIPARTIMENTO DI SCIENZE FARMACEUTICHE

SCUOLA DI DOTTORATO DI RICERCA IN : SCIENZE MOLECOLARI
INDIRIZZO: SCIENZE FARMACEUTICHE
CICLO XXIII

**NEW MOLECULAR DEVICES FOR SELECTIVE STRUCTURAL
MODIFICATIONS OF G-QUADRUPLEXES FOLDED
OLIGONUCLEOTIDES**

Direttore della Scuola : Ch.mo Prof. Maurizio Casarin

Coordinatore d'indirizzo: Ch.mo Prof. Adriana Chilin

Supervisore :Ch.mo Prof. Manlio Palumbo

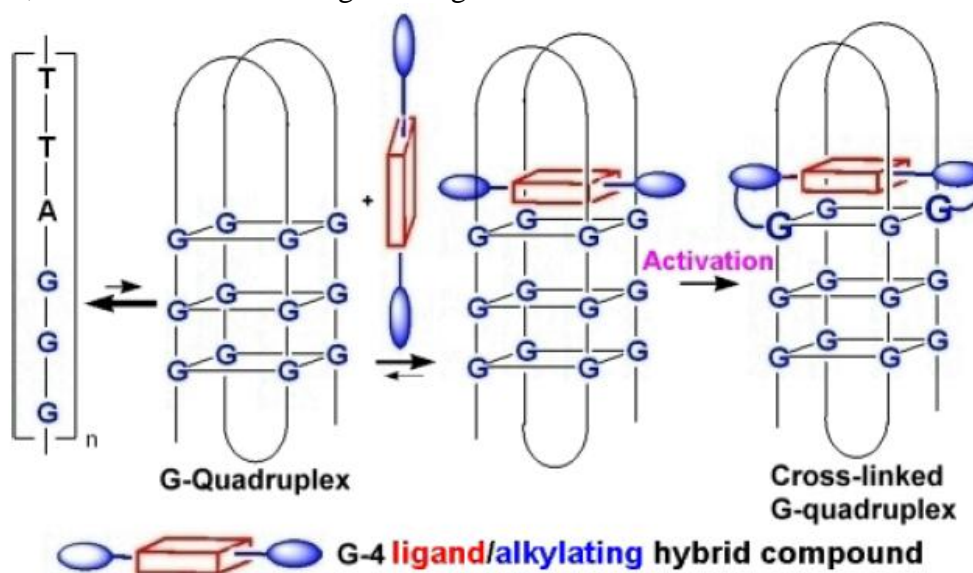
Dottorando : Marco Di Antonio

Scuola di Dottorato in Scienze Molecolari (XXIII Ciclo)
Indirizzo in Scienze Farmaceutiche
Candidato: Marco Di Antonio

Direttore Della Scuola: Chiar.mo. Prof. Maurizio Casarin
Supervisore: Prof. Manlio Palumbo

"Nuovi dispositivi molecolari per modifiche strutturali selettive di oligonucleotidi organizzati a quartetti di guanina."

Nell'ultimo decennio un sempre più crescente interesse è stato rivolto nei confronti del riconoscimento selettivo dei quartetti di guanina (G-quadruplex), strutture supramolecolari in grado di auto-assemblarsi in condizioni fisiologiche da oligonucleotidi ricchi di residui guaninici. La ragione di ciò risiede nel fatto che tali strutture sembrano agire come regolatori di processi a livello cellulare. Infatti, esistono svariati esempi in cui, soprattutto *in vitro*, molecole o anticorpi in grado di riconoscere e stabilizzare quartetti di guanina influenzano drasticamente il processo biologico in cui l'oligonucleotide stesso è implicato. L'inibizione indiretta della telomerasi e gli studi dell'effetto sulla trascrizione di oncogeni ne rappresentano le applicazioni più importanti, assieme ai più recenti effetti sulla traduzione di RNA. Ciò rende G-quadruplex un vero e proprio target terapeutico per lo sviluppo di nuove terapie antitumorali. Questo lavoro nasce con lo scopo di creare una nuova generazione di leganti di G-4 che manifestino proprietà alchilanti attivabili mediante protocolli biocompatibili. Proprietà alchilanti non intrinseche, ma attivabili attraverso modifiche chimiche e fisiche, permetterebbero un controllo temporale del processo di alchilazione, come illustrato nella seguente figura.



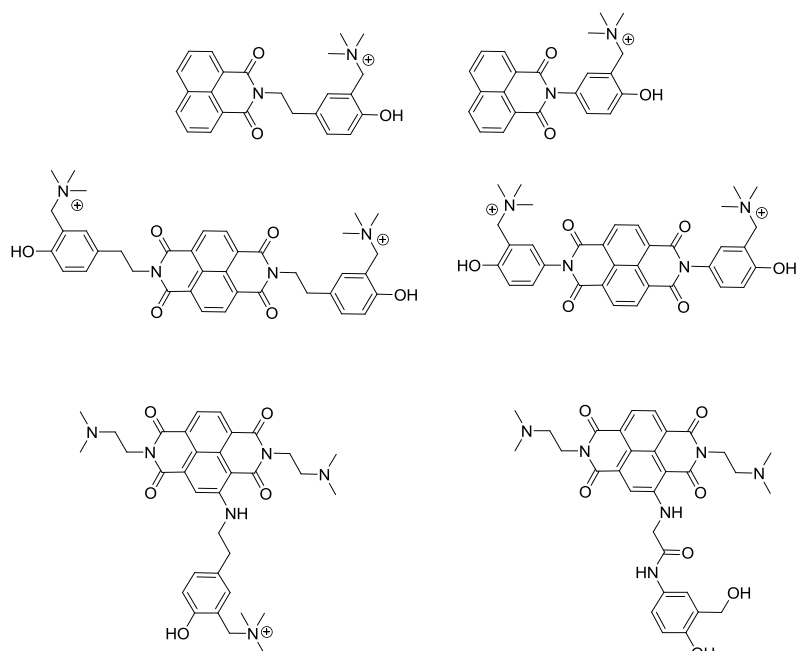
Tali molecole agirebbero pertanto da veri e propri dispositivi molecolari preconcentrandosi sul target e stabilizzando il complesso attraverso interazioni non covalenti per poi, mediante attivazione, generare la specie alchilante così da ancorare fortemente la molecola all'oligonucleotide. Queste caratteristiche renderebbero il danno indotto irreversibile o non riparabile dai comuni processi cellulari, aumentando notevolmente l'efficacia di azione in termini di effetti farmaco-biologici. L'idea pertanto è quella di sfruttare le proprietà di riconoscimento di

alcuni tra i leganti noti in letteratura equipaggiandoli, però, con una specie alchilante silente, il cui rilascio può essere controllato temporalmente mediante azione fisica o chimica. Questo nuovo tipo di molecole rappresenterebbe pertanto una classe di leganti irreversibili di **G-4**, mai progettata in precedenza.

Per far ciò la molecola da sintetizzare deve possedere:

- ✓ una superficie aromatica estesa ed elettrone-povera che conferisca le proprietà di riconoscimento molecolare attraverso interazioni di π stacking con il target biologico.
- ✓ un precursore di una specie alchilante che presenti una scarsa o assente reattività intrinseca modulabile mediante attivazione, possibilmente compatibile con condizioni fisiologiche.
- ✓ una porzione molecolare facilmente modificabile per interazioni con il substrato o per attivazione chimica, che funga da “grilletto” della reattività del precursore alchilante.

Nella fattispecie ci siamo concentrati sulla derivatizzazione di strutture, che dalla letteratura risultano dei buoni leganti di **G-4**, come Naftalendiimidi (**NDI**) o Naftalimmidi (**NI**), variamente sostituite con dei precursori di alchilanti tipo chinone metide (**QM**), come illustrato nello schema seguente. Questi ultimi risultano particolarmente adatti a questo scopo in quanto possono essere generati da precursori molto stabili, attraverso dei protocolli di attivazione biocompatibili. Soprattutto risultano elettrofili la cui reattività è modulabile variando la natura elettronica del precursore stesso.



In questo lavoro di tesi descriviamo la sintesi, la reattività e gli studi di interazione con oligonucleotidi riapribili a strutture tipo **G-4**, delle molecole progettate e preparate nel corso del dottorato di ricerca. Particolare enfasi verrà posta sull'effetto indotto dal danno da alchilazione osservato e sulle potenziali applicazioni sia terapeutiche che diagnostiche. Inoltre descriveremo brevemente un progetto parallelo svolto durante il periodo trascorso all'Università di Cambridge, presso il gruppo di ricerca del Prof. Balasubramanian.

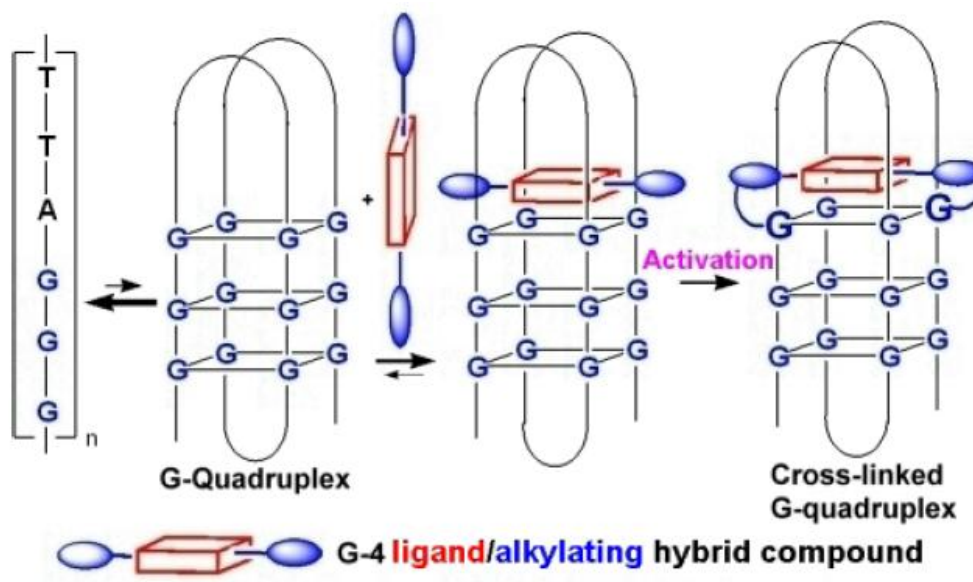
School Director: Chiar.mo. Prof. Maurizio Casarin

Supervisor: Prof. Manlio Palumbo

"New Molecular Devices for Selective Structural Modifications of G-4 Folded Oligonucleotides"

The attention around selective recognition of G-Quadruplex has steadily grown during the past 10 years. **G-4** are non-canonical DNA structures which can be generated from the self-assembling of guanine rich oligonucleotides. Such an interest is justified by the fact that it is widely recognized that the above structures could act as regulators of biological processes *in vivo*.

In fact, there are several examples of G-Quadruplexes stabilization, by small molecules or engineered antibodies, which is translated into a strong influence of the biological process in which the oligonucleotide is involved. The inhibition of telomerase enzyme as well as the gene transcriptional alteration induced by the stabilization of such structures, represent the most important applications, together with the more recently studied effect on translation mediated by **G-4** RNA structures. This makes G-Quadruplex a real therapeutic target useful for the developing of new antitumor drugs. The aim of this work is to develop a new generation of **G-4** ligands capable to undergo alkylation triggered by biocompatible protocols. The key aspect of this idea is to regulate the alkylation process, exploiting mild chemical or physical modifications, in order to temporally separate it from the reversible recognition. Such concept is depicted in the following figure.



These molecules would therefore act as molecular devices capable of pre-concentration onto the target and stabilizing the complex through non covalent interactions. These ligands after activation of the masked electrophile are capable to generate the alkylating specie and therefore to achieve a strong covalent interaction.

These features would induce an irreversible damage which would not be repaired by the common cellular process, enhancing the effectively drug potency in biological response terms.

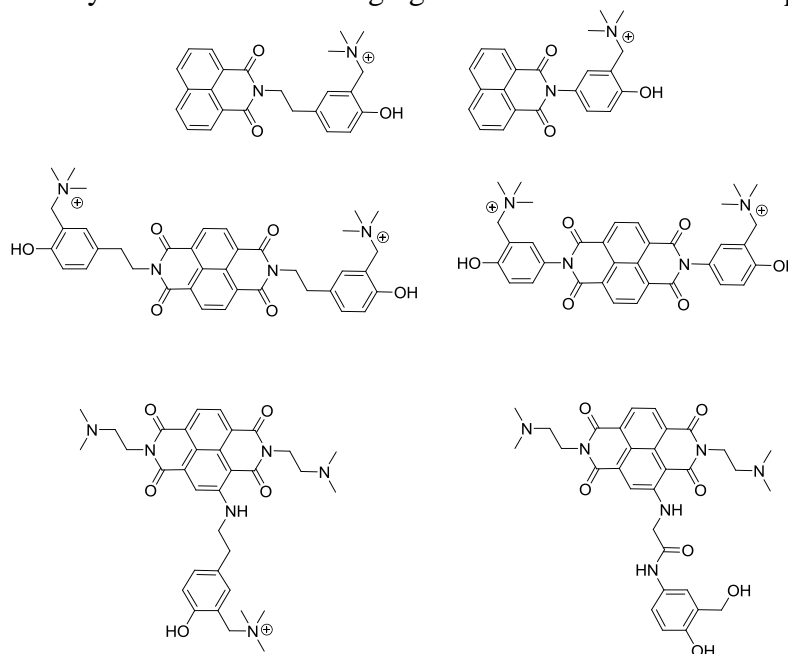
The basic idea is to exploit molecular recognition properties of already described ligands and tethering to them a masked electrophile. The releasing of the alkylating specie will be achieved exploiting physical or chemical triggers. Such molecules would represent a brand new class of irreversible G-4 ligands which has never been conceived before.

The common features that such a class of ligands must have are:

- ✓ A wide electron poor and flat surface, which confers molecular recognition properties, exploiting superficial π stacking interactions with the biological target.
- ✓ A precursor of an alkylating specie, triggerable by mild physical and chemical activation protocols, possibly exploitable under physiological conditions
- ✓ A moiety which can be easily modified through substrate interactions or chemical activation. Such moiety will represent the trigger of the alkylating reactivity.

In more details, we had focused our attention on the chemical functionalization of Naphthalimide (NI) and Naphthalendiimide (NDI) derivatives, which both are good **G-4** binders according to literature. Quinone Methide precursors (**QM**) electrophiles have been tethered to the above molecules as illustrated in the following scheme.

QM based alkylating species are particularly suitable for this project because they can be generated from very stable precursors through several biocompatible activation protocols. Moreover, their reactivity could be tuned changing the electronic nature of the phenolic precursor.



In this PhD thesis we describe the synthesis, the reactivity and the study concerning the interaction of the synthesized molecules with oligonucleotides capable of **G-4** folding.

Particular emphasis will be given to the consequences induced by the alkylation damage with potentially achievable application both therapeutic and diagnostic. Moreover, we will discuss a parallel project developed during a period spent in the Cambridge University in Prof. Balasubramanian's research group.

INDEX

INTRODUCTION	9
Molecular Recognition	9
G-Quadruplexes	10
Structural Features of G-Quadruplexes	11
G-Quadruplexes Topologies	18
G-Quadruplexes in the genome	22
The “end replication problem”	23
Telomerase an unusual way to make DNA.	24
Telomerase as validated cancer target.	25
Targeting telomerase towards G-4 ligands.....	29
G-Quadruplexes and oncogenes.....	31
G-Quadruplexes in RNA.	34
Targeting G-Quadruplex by using small molecules	36
“In situ” protonable G-Quadruplexes Ligands.	37
N-Methylated aromatic G-quadruplex ligands	43
Metallo-organic G-quadruplex ligands	46
Quinone Methides a useful tool for masked electrophiles delivering	48
Towards selective G-quadruplex alkylation: why using QMs?.....	50
Laser Flash Photolysis in QM transients characterization.	53
AIM	55
RESULTS AND DISCUSSIONS	59
Exploration and development of new QMs generation protocols	59
Quinone Methides Precursors Embedded to Naphthalimide Derivatives	59
Synthesis of Naphthalimide Derivatives.	62
Photoreactivity Study of Naphthalimide Derivatives.....	63
Base catalytic activation.	64
Hetero Diels-Alder Reactivity.....	65
Laser Flash Photolysis (LFP).	67
NDIs as Activable Precursors of bis-Alkylating Agents by Reduction	73
Synthesis of bis-alkilating NDIs triggerable by reduction.....	73
Base catalytic activation.	74

Reductive activation.	77
Diels-Alder reactivity of the transient electrophile.....	79
Detection of the transients by UV-vis-spectroscopy.	80
Computational evaluation of the basic and reductive activation processes.	82
New NDIs Tethered to Quinone Methides as Selective G-4 Alkylating Agents.	84
Synthesis of Naphthalene Diimides Tethered to Quinone-Methide Precursors and reactivity towards simple nucleophiles.....	84
Activation and Reactivity of Naphthalene Diimides 49-51.	86
Alkylation of DNA Folded into a G-quadruplex.	89
Drug Alkylation as a Function of DNA Folding.	90
G-quadruplex Folding Induction versus Alkylation.	92
CD Spectroscopic Study.	94
Alkylated G-quadruplex Properties.....	95
NDIs cytotoxicity.	96
Tri and Tetra substituted NDIs Tethered to Quinone Methides as More Efficient and Selective G-4 Alkylating Agents.....	97
Rational Design of new NDI derivatives.....	98
New NDI derivatives selectively bind human telomeric G-quadruplex folded DNA.....	104
NDI 71 drives towards the formation of a parallel-like G-4 topology.....	105
NDI compounds bind with a different stoichiometry to G-4 telomeric DNA.....	109
Both electrostatic and non-electrostatic interactions are involved in the binding of 5 to G-4 telomeric DNA.....	111
A Novel NDI Capable to Alkylate dG and the G-4 Telomeric DNA.	111
NDIs concentrate inside the nucleus and their cytotoxicity parallels binding to G-4 DNA.....	114
Compound 72 inhibits telomerase activity and induces cell senescence.	115
Changing QMP and Spacer in Tri NDI Derivatives. Effects on Binding Properties and Alkylation Efficacy.....	118
Fret Melting Assays.....	122
Does third generation NDIs induce parallel-like G-4 topology as consequence of the alkylation process? CD consideration.	123
New Raphaine Derivatives: Towards “in-situ” Synthesis of G-4 New Ligands.	125
CONCLUSIONS	128
EXPERIMENTAL SECTION	129
1,8 Naphthalimides Derivatives Synthesis and Characterization.	129
Microwave imidization of 1,8-Naphthalic anhydride (14-17): General Procedure.....	129
Mannich Reaction (10-13). General Procedure	130

Exhaustive Methylation of Mannich bases (15-18). General Procedure	130
Photoactivation of Naphthalimides 16 and 19. General Procedure	131
Activation by Base Catalysis of Naphthalimides 16 and 19. General Procedure	132
Naphthalendiimides as New Reductive Bis-Alkylating Agents. Synthesis and Characterization.	135
Activation by base catalysis. General procedure.	136
Electrochemical Measurements.	140
Methods and Computation Details.	141
Naphthalendiimides as selective G-4 Bis-Alkylating Agents. Synthesis and Characterization.	
Biophysical Assays.	141
Synthesis of the Intermediates	141
NDIs Activation of the bis-alkylating properties by mild thermal digestion. General procedures.	147
G-quadruplex DNA Alkylation and Folding Induction.	151
Exonuclease I Digestion Assay.	152
Circular Dichroism Measurements.	152
Cytotoxicity Assay.	153
Tri and Tetra Naphthalendiimides as selective G-4 Bis-Alkylating Agents. Synthesis and	
Characterization. Biophysical Assays.	154
Deprotection of tert-butylcarbamate: General Procedure	155
Preparation of Key Intermediate NDI 85	156
Synthetic procedures for the generation of alcoholic QMP in third generation NDIs development.	157
Microwave assisted synthesis of 70, 70a, 71, 71a, 75.	160
Exhaustive methylation of the amines 71, 71a	162
Nucleophilic aromatic substitution reaction at r.t.	163
FRET-melting assay.	166
CD analysis.	167
Alkylation Assays Experiments.....	168
Cytotoxicity.	169
Evaluation of telomerase activity. TRAP Assays.	170
Immunoblotting analyses.	170
New Raphaine Derivatives Synthesis	171
REFERENCES.	174

INTRODUCTION

Molecular Recognition.

Molecular recognition represents a crucial aspect in the drug discovery field. Such a term refers to the specific interactions involved between two or more molecules which can be considered, in terms of shape and chemical properties, complementary each other. The interactions involved in this kind of molecular process are essentially chemical non-covalent bonding such as hydrogen bonds, π -stacking interactions, hydrophobic Van Der Waals bonds, metal cation coordination and electrostatic interactions.¹ Therefore small molecules with defined chemical and physical properties are able to selectively interact with specific biological targets such as proteins. This is the basic principle based on the interaction enzyme-substrate or neurotransmitter-receptors. One of the most striking example of molecular recognition involved in drug action is represented by the antibiotic Vancomycin. Such a molecule is capable to bind tightly the dipeptide D-Alanine-D-Alanine, which represent the final component of the peptidoglycan.² Owing to the crucial role of peptidoglycan in the plasma membrane of Gram positive bacteria, the molecular recognition process between Vancomycin and peptidoglycan is translated in the very effective antibiotic action of this natural molecule.

Nowadays, thanks to the efforts and the development of molecular biology, biotechnologies and chemistry, researchers are able to clone and study in details proteins and oligonucleotides. Information concerning the oligonucleotide structures, enzyme active sites as well as receptor binding sites, together with the computational simulations, are actually giving to the chemists the tools to synthesize more and more specific and effective drugs. On the other hand, the lack of a total specificity shared between most of the common drugs confers the possibility to interact with different targets, which is one of the main causes of drugs side effects. Indeed, improvement of molecular recognition properties of the common used molecules is a widely recognized demand for the development of new and more potent drugs. A lot of efforts have been dedicated in the

attempt to confer higher molecular recognition properties to the chemotherapeutic drugs.³⁻⁶ In fact, the improvement of such a class of drugs is probably one of the most expanding research area both for its medical relevance and for the well known side effects associated to the treatment. Molecular recognition, together with the expanding knowledge of cancer biology, represents a highly useful tool in the purpose to achieve the ambitious goal of chemotherapeutics selective for cancer cells. Several example of cancer cells peculiar targets could be discussed, herein we will focus the attention to the G-Quadruplexes. The attention around these supramolecular structures has steadily grown during the last years because of their probable involvement in cancer crucial bio-processes.

G-Quadruplexes.

For several years DNA has been considered “The” target of anticancer drugs. Because of that the research and development of new antitumor drugs has so far grown around the DNA structure. Most of them are DNA alkylating or intercalating agents such as *Cisplatin*⁷ or *Doxorubicin*.⁸ Unfortunately such a target is shared between somatic and cancer cells and, despite the effectiveness of the chemotherapeutics, a lot of efforts have been spent in the attempt to find molecules with comparable potency but lower cytotoxicity towards somatic cells. Beside the classic Watson e Crick double helix conformation (B-DNA), oligonucleotides strands can adopt other biologically relevant supramolecular structures. One of these is represented by the **G-Quadruplex**. Indeed, Guanine rich oligonucleotide strands have high tendency to self-assemble into a tetrameric G-Quartet. The latter is capable to undergo self association to generate unusual structures called G-Quadruplex (**G-4**), which have been studied and characterized for the first time by Davies’s group in 1962.⁹ Polymorphism and unique features of **G-4** justify easily the relevant role that they can play in several biological processes. Indeed, guanine rich oligonucleotides strands are situated in crucial position of the eukaryotic genome. In particular only in the human genome there are 376000 sequences capable to fold into G-4 structures.¹⁰ The most relevant genomic zones capable to fold into such structure and discussed in the present work

are: the telomeric G-4 DNA, oncogenes and proto oncogenes G-4 and, RNA G-4. The systematic presence of G-rich sequences in these relevant genome portions suggests that such supramolecular structures can actually have a crucial role in the regulation of biological processes. In more details, it has been thought that the main role associated with the formation or stabilization of the G-4 structures could be the up or down regulation of some physiological events such as genes transcription or telomerase enzyme action. The latter represent a widely investigated translation of G-4 formation into a biological response. Indeed, it is well known how G-4 structures stabilization by small molecules could be exploited for the development of new telomerase enzyme inhibitor. For all these reasons, these DNA secondary structures actually represent one of the most promising and debated field in antitumor drug discovery.¹¹

Structural Features of G-Quadruplexes.

The high tendency of G-rich oligonucleotides to self-organize into supramolecular structures has already been described. Indeed, guanine and its derivatives always resulted very hard to handle in the common laboratory practice because of their low solubility and their tendency to jellify towards oligomers generation.^{12,13} Such a peculiar feature could be easily justified if we consider the guanine structure. In fact, the presence of complementary donor and acceptor hydrogen bonding portions together with its wide aromatic and polarized surface,¹⁴ confer to the guanine the ideal properties to generate tetramers capable to interact each other towards superficial π -stacking interactions. The self-association of guanine occurs in many settings. Some spiders have cells known as guanocytes that are filled with crystalline plates of guanine. When disturbed, these spiders change color instantly by retracting the guanocytes from their surface.¹⁵ The eyes of certain deep-sea fish contain layered guanine crystals that focus light to the photoreceptors.¹⁶

The essential components of G-4 are the tetrameric structures called G-quartet or G-tetrad. Such structures have been first described more than 40 years ago and are characterized by the association of four guanines in a cyclic structure mediated by *Hoogsteen* hydrogen bonding motif.⁹ In a G-Quartet each guanine interacts with two hydrogen bonds and monovalent metal cations can be coordinated and stabilize the structure as depicted in **Figure 1**.

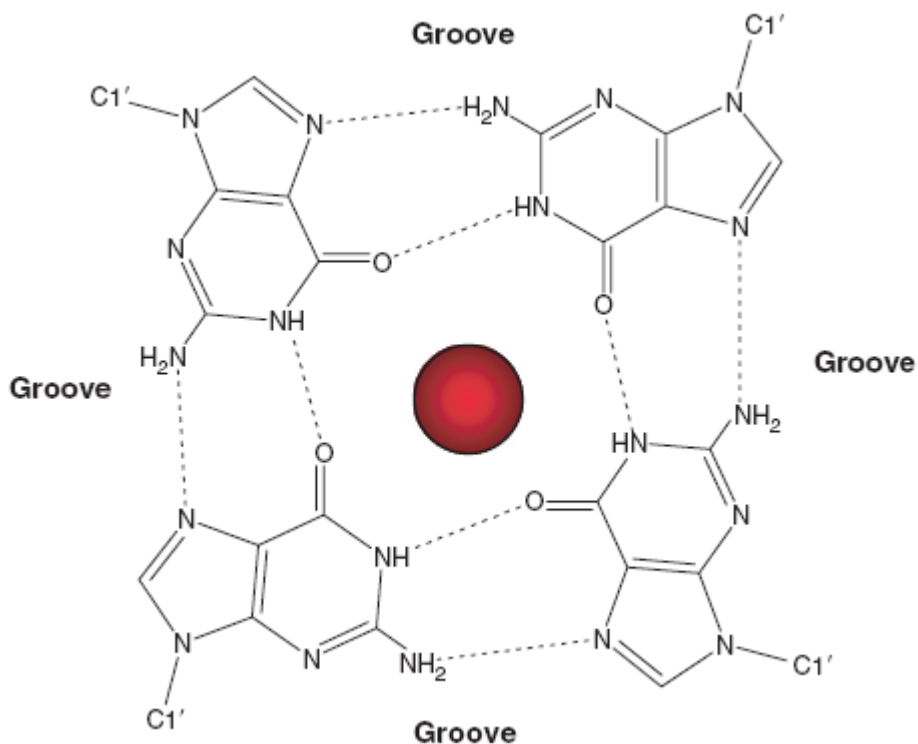


Figure 1. The chemical structure of a tetrameric G-Quartet stabilized by metal coordination

During his investigations, Gellert, observed that even the simple 3' GMP as well as the 5' GMP were capable to form tetrameric structures in solution. Diffractometric studies suggested that N-H bonds of guanine nitrogen N₁ and N₂ coupling with the N₇ and O₇ of another adjacent guanine. Thus, allowed the formation of a planar tetrameric structure in which each guanine is tethered each other by the formation of 8 hydrogen bonds (**Figure 1**).¹⁷⁻¹⁹ Moreover, each quartet is still capable to tether one other by superficial π -stacking interaction in order to generate a polymer

with an helicoidally structure comparable to the double helix Watson and Crick DNA, even though with considerable bigger dimensions as underlined in **Figure 2**.^{20,21}

This pioneeristic studies have been followed by always raising discovers concerning guanine supramolecular structures and about the dynamic of the self-assembling processes involved. It became clear that such a process was extremely pH dependent and more important that the supramolecular aggregates generated could have been detected and characterized by NMR.

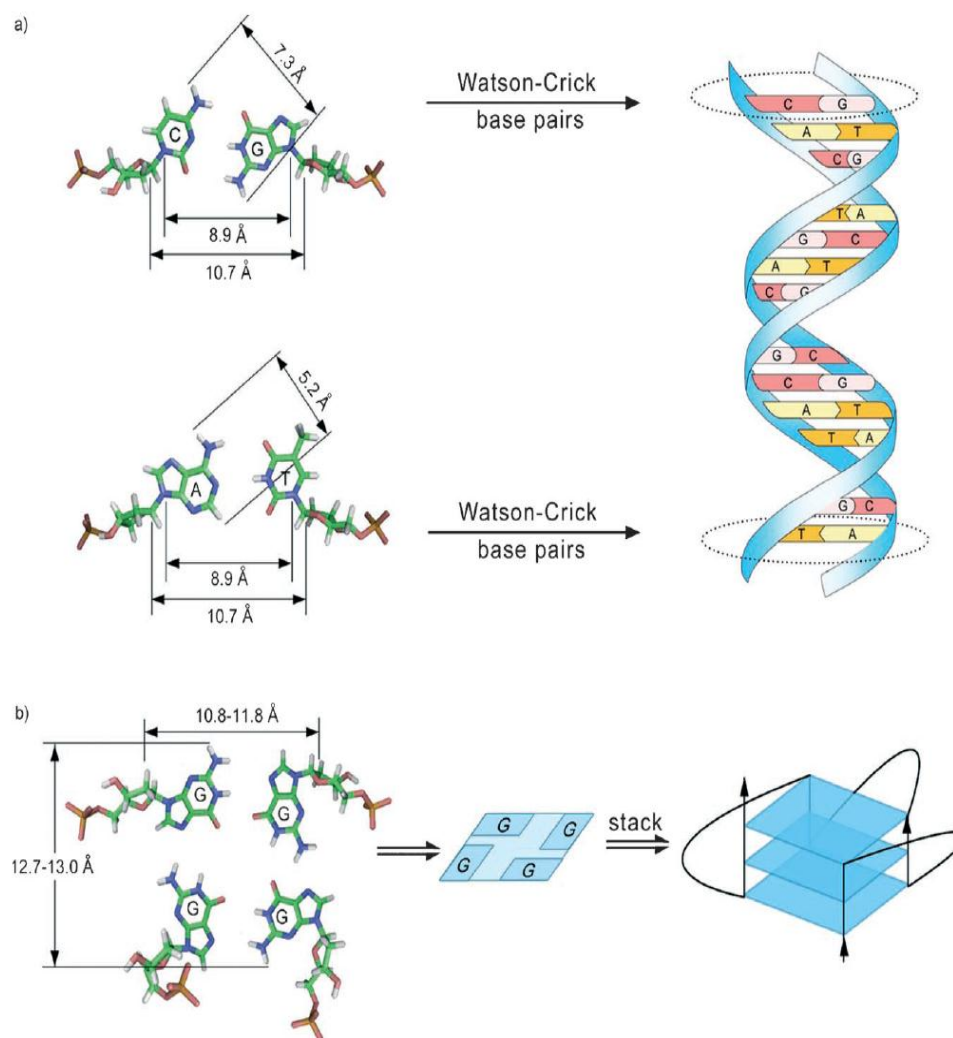


Figure 2. Comparing of DNA double helix and G-4 structures. **a)** Structure and surface dimensions of complementary bases in DNA double helix. **b)** Structure and surface dimensions of a G-Quadruplex

A cornerstone in the G-Quadruplex structure study has been represented by the discovery of the stabilizing effect of such structures by alkaline cations such as Na^+ and K^+ , while a negligible effect was observed under treatment with Li^+ and Cs^+ .²² This experimental evidence suggested that alkaline metals were able to drive the self-assembling of nucleotide based structures by using a selective coordination mechanism extremely dimension dependent. The G-4 tendency to coordinate alkaline cations is fairly understandable. In fact, the four oxygens surrounding the hole in the middle of the G-4 represent a classic alkaline coordination center, somehow comparable to a crown ether. Moreover, the presence of a metal cation centered in the quartet obviates to the electrostatic repulsion between the adjacent oxygens. Therefore, the presence of a cation is crucial as template of the G-4 and to stabilize the structure minimizing the electrostatic repulsions involved in the formation of the tetrameric quartet. As already mentioned, the dimension of the cations plays a significant role in such a process. In more details the K^+ ions are too big to fit inside the quartet, therefore they induce the formation of octameric G_8K^+ structures in which the cation is displaced in a sandwich motif (**Figure 3**).^{17,23,24} The theoretical K-O bond distance calculated for the above structure is super impossible to the already described octameric potassium coordination complexes. The octameric G_8K^+ structures represent the building blocks for the formation of extended G-4 based polymers.

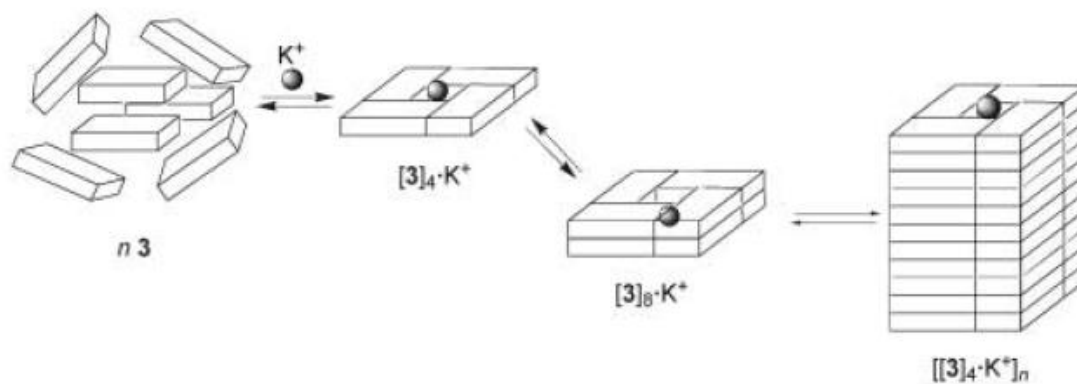


Figure 3. The potassium template effect on the 5' GMP self-assembly.

It has been possible to clarify several key features concerning G-4 folding and underline non covalent interaction capable to induce guanine self-assembly thanks to Davis efforts.²⁵ Indeed, Davis showed how in the presence of template cations also the 5'-silyl-2',3'-O-isopropylidene guanosine (**G,1**) forms a lipophilic G-quadruplex that is stable in nonpolar solvents and that also gives single crystals with long-range order. Such a crystal formed in the presence of picrate anions is depicted in **Figure 4**.

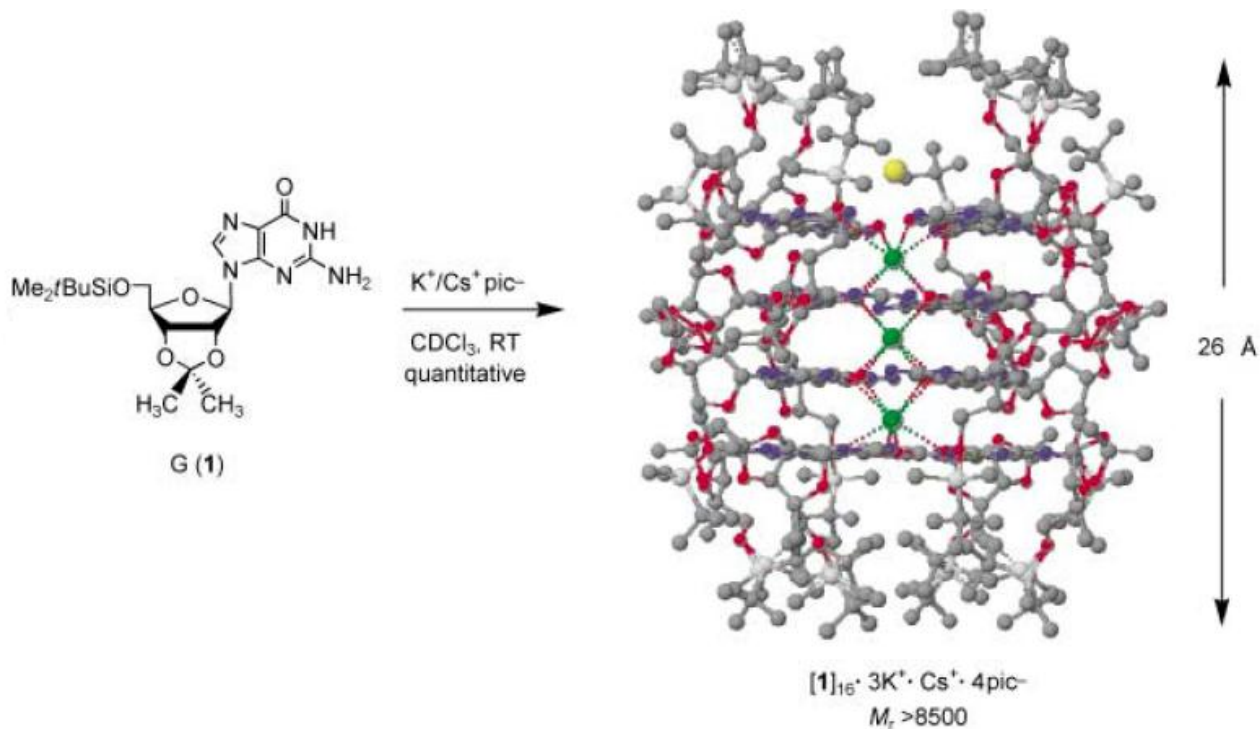


Figure 4. 16 equivalents of **G1** mediated by metal cations lead to the formation of the lipophilic $\text{G}_{16}\text{K}_3^+/\text{Cs}^+ \text{pic}^-_4$ G-quadruplex described by Davis. (K green, Cs yellow, N blue, O red).

Therefore it is possible to summarize G-4 folding dynamics in 3 separate and sequential steps:

- ✓ In the first step four guanosine molecules arrange into a tetrameric planar structure by using complementary hydrogen bonds, as depicted in **Figure 5a**
- ✓ The second step is represented by the π stacking superficial interactions between two tetrameric G-quartets to generate an octameric structure in which the distance between the two quartet is 3.3 Å. In this step the presence of cationic metals is crucial. Indeed, by coordination of the 8 oxygens present in each quartet, the metal is capable to enhance

the stacking interaction and to emphasize the hydrogen bonding web. The formation of a C4 symmetric octameric G_8K^+ therefore occurs (**Figure 5b**).

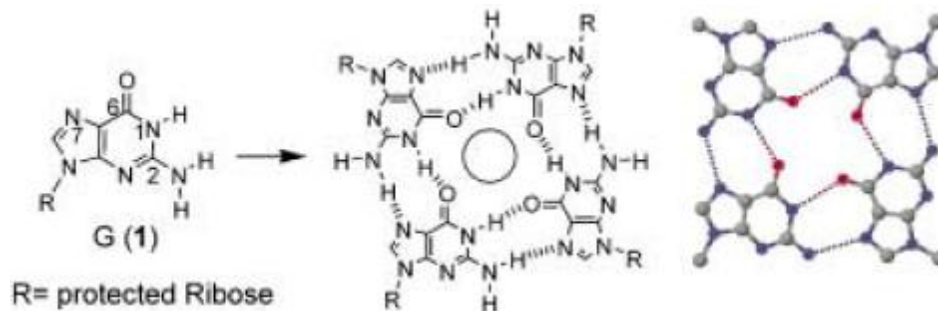


Figure 5a. The G-quartet formation from four molecules of 5'-silyl-2',3'-O-isopropylidene guanosine

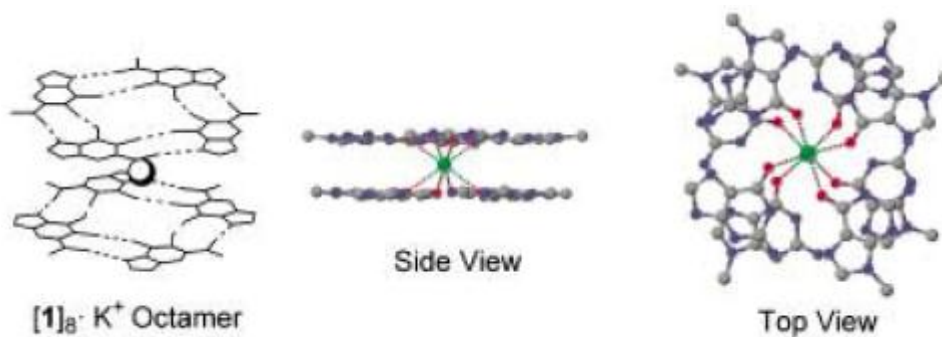


Figure 5b. Octameric G_8K^+ generated by template effect and π -stacking.

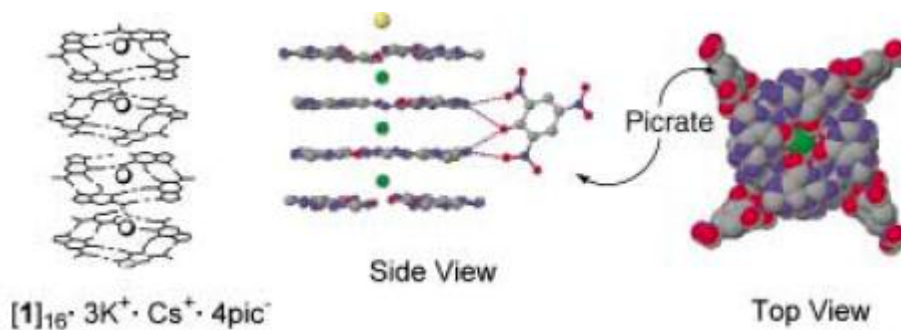


Figure 5c. Anion mediated exadecameric G-Quadruplex formation.

- ✓ The third step involves anions, such as picrate in the Davis cited work. The interaction between anions and G-Quartet is mainly electrostatic and involves the amine groups of the nucleobase. The hydrogen bonds formed with the internal quartets and the anion lead to the formation of an exadcameric specie $G_{16}M^+_4 \text{pic}^-_4$ provided with a D4 symmetry. Such a structure is illustrated in **Figure 5c**.

The NMR spectrum of the assembly also raised issues about supramolecular stereochemistry, which is still representing an intensely studied area today.^{26,27} Stacking two chiral G-quartets can give at least six possible diastereomers for a $G_8 \cdot M^+$ octamer, depending on the stacking orientation and relative rotation about the central axis.²⁸ The NMR spectra for $5'$ -GMP \cdot Na⁺ indicated, however, the presence of only two stable diastereomers, thus indicating a high stereo selectivity in this self-assembly process. Another important finding concerning the stability of the assembly towards dissociation was represented by the ¹H NMR spectra of $5'$ -GMP \cdot Na⁺ which showed separate signals for the monomer and the assembly.²⁹ This slow exchange was remarkable since such kinetically stable systems are rare, especially in water. Hydrogen-bonded assemblies and their components are usually in fast exchange and give averaged NMR signals. The self-assembly of $5'$ -GMP 3 is also relevant today, since obtaining discrete non-covalent assemblies that are thermodynamically and kinetically stable in water is still challenging.³⁰⁻³³ In retrospect, these early studies on the self-association of $5'$ -GMP involved much of what motivates studies in supramolecular chemistry today, namely structure and stereochemistry, mechanism, and function. However, recognition of the name G-quartet really developed in the late 1980s, when it was proposed that G-quartets might be biologically functional.³⁴⁻³⁷ In particular, Sen and Gilbert suggested that G-quartets were involved in chromosome association during meiosis.³⁵ Sundquist and Klug proposed that the G-quadruplex was an important secondary structure regulating biochemical processes in the telomeric region of the chromosome.³⁷ A massive research explosion on G-quadruplexes followed.

G-Quadruplexes Topologies.

Beside the pure supramolecular aspects it has quickly become clear that, from the biological point of view, different G-4 could have different roles and, most important, could have been targeted by different molecules. Indeed, it has been demonstrated that G-4 structures are mainly formed in DNA and RNA oligonucleotides with sequences that occur in chromosomal telomers, gene promoter regions, recombination sites, RNA packaging sites and dimerization domains.^{38,39} If we compare the G-4 to the classic double helix DNA a wider polymorphism and structural diversity could be observed for the guanine supramolecular structures. Such a higher molecular complexity is due to several factors namely the loop (portion of the oligonucleotide not involved in the quartet) nature, the oligonucleotide base stoichiometry and polarity, the spatial distribution of the loops dedicated to the G-rich strands connection and the strain angle of the glycosidic bonds.⁴⁰ Beside these principal factors, G-4 topologies could be also influenced by the nature of the environment. As mentioned the presence of different alkaline metal cations could strongly influence the nature of the folding as well as the presence of molecules capable to bind tightly to only one topology. Also the concentration of the oligonucleotide is a key factor for the topology preferred in the folding process. Since the variety of topologies is so wide it has become mandatory to make a simple classification of the different conformations. Herein we first report a stoichiometry classification of different G-4:

- ✓ ***Tetramolecular*** in which the association of four different oligonucleotides with at least one G-rich strand each generates the G-4 structure.
- ✓ ***Bimolecular*** in which the association of two different oligonucleotides with at least two G-rich strands each generates the G-4 structure. A very well known example of such a structure is represented by the telomeric *Oxytricha nova* sequence d(G₄T₄G₄).
- ✓ ***Monomolecular*** (intramolecular) in which a single oligonucleotide with four guanine rich strands self-assemble into the G-4 structure.

Several natural sequences containing four or more G-rich strands has been identified so far. This peculiar feature gives to the oligonucleotide the possibility to fold into different G-4 and equilibrium between all the possible conformation often results.⁴¹ Such sequences have been rationalized and herein summarized in **Table 1**.⁴⁰

Table 1. G-rich sequences with the potential to form G-quadruplexes.		
Name	Sequence	Description
Intramolecular G4	$G_m X_n G_m X_o G_m X_p G_m$	m represents the number of G residues in each short G-tract; X_n , X_o and X_p can be any combination of residues, including G, forming the loops.
Bimolecular G4	Two $X_n G_m X_o G_m X_p$	X_n and X_p are any non-guanine nucleotide of length n and p , G_m is any number of guanines involved in tetrad formation of length m , and X_o is any nucleotide of length o involved in loop formation.
Tetramolecular G4	Four $X_n G_m X_o$	X_n and X_o are any nucleotide of length n and o , and G_m is any number of guanines involved in tetrad formation of length m .

Table 1. G-rich sequences with the potential to form G-Quadruplexes

Since the guanines of a G-Quadruplex are conformationally blocked by the stacking and coordination interactions, the chemical nature of the loops connecting the G-rich sequences may play a crucial role for the G-4 stability. In other words, the connective function of the loops drives through the formation of a preferential topology. In particular, different loops and consequently different G-4 topologies are strictly related to the strand polarity. Indeed, the four oligonucleotide strands can assume different spatial orientations: i) all parallels ii) 3 parallel strands and one antiparallel (mixed type) iii) parallel adjacent strands iv) alternate parallel strands.

We can distinguish two different topologies according to the strands polarity as depicted in **Figure 6**.

- ✓ **Chain reversal loop (propeller type)** characteristic of G-4 with parallel strands in which the loop has to connect the higher tetrad with the lower one. **Figure 6a**.
- ✓ **Diagonal or Lateral loop (edgewise)** characteristic of G-4 with antiparallel strands in which the loop can be diagonal or lateral if the antiparallel strands result adjacent or opposite respectively. **Figure 6b**.

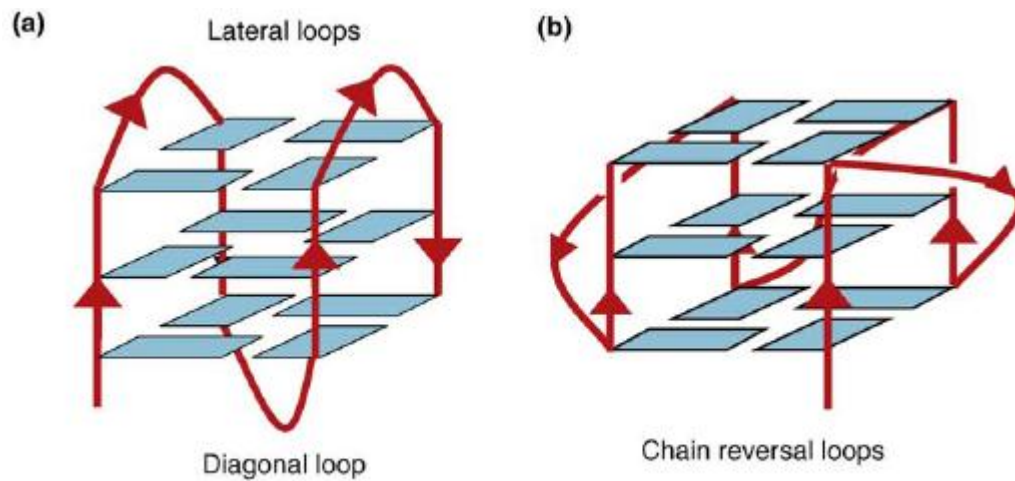


Figure 6. Schematic representation of two intramolecular G-4 topologies.

Several of the above described loop combinations result sterically impossible,⁴² and moreover, just 26 of the possible combinations have been so far considered as stable.⁴³

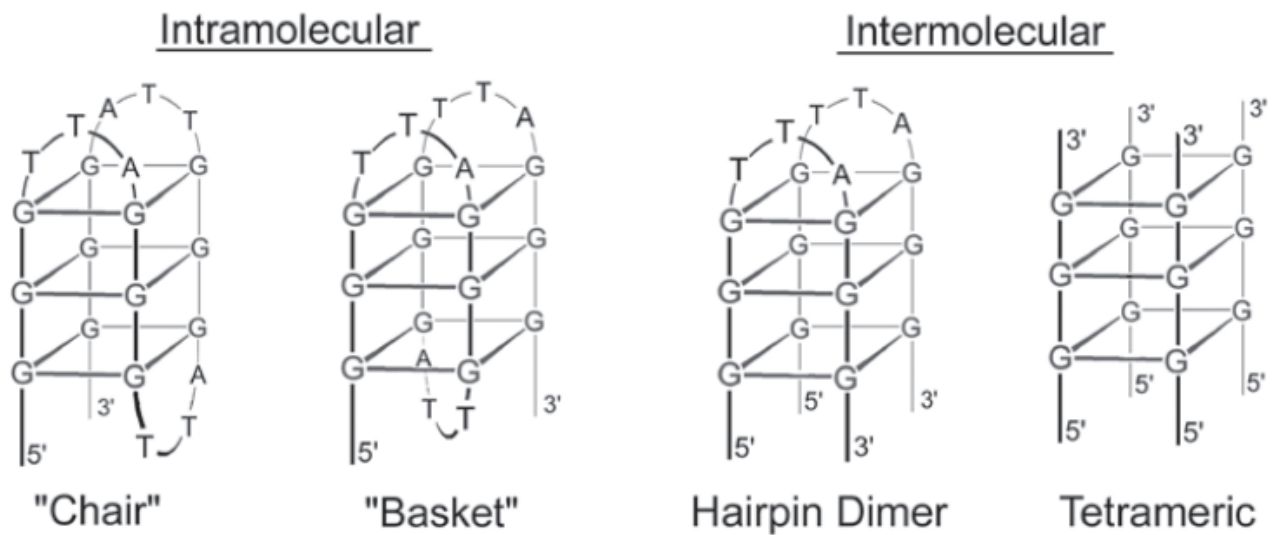


Figure 7. Two of the 26 intramolecular G-4 possible topologies: Chair and Basket type.

Tetramolecular and bimolecular G-4 examples are also shown.

Also the conformation of the glycosidic bond between the guanine and the ribose can play an essential role in the strand spatial orientation. In fact it is well known how such a bond can assume a *syn* orientation as well as an *anti* orientation as underlined in **Figure 8**.

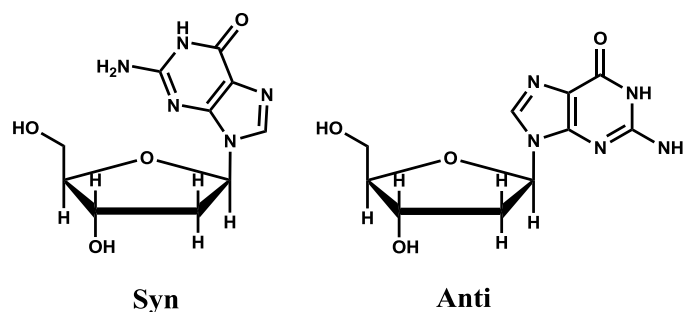


Figure 8. Torsional angle between the nucleobase and the ribose can lead to *syn* or to *anti* conformations.

Beside the pure stereochemical aspects, strand orientation and guanine conformation are strictly related each other. Indeed, a G-4 with four parallel strands drives all bases through the *anti* conformation and the backbone grooves result equally dimensioned, whereas in a fully antiparallel strands G-4 bases can assume both the *syn* and the *anti* orientation typical of the involved strand. The combination of the strands position with the torsional angle orientation directly influence the dimension and the spatial orientation of the related backbone grooves.⁴⁴ Therefore it is clear that different G-4 topologies can be populated depending on the distance between the quartet, loops nature and dimension as well as the cation involved in the template coordination. Moreover, the G-4 overall dimension depending on the loop's regions orientation, grooves dimension, negative electrostatic charge of the phosphate backbones and the central G-4's groove are all crucial elements which must be taken in consideration in order to clarify the differences between different G-4 and, therefore, maximize the ligands selectivity towards these targets. Indeed, the development of ligands selective towards different G-Quadruplexes topologies will be crucial for the development of new drugs capable to interact selectively with single bio-targets G-4 dependent.

G-Quadruplexes in the genome.

Several guanine rich sequences capable to fold into G-4 structures have been so far characterized in the human genome. In fact, more than 370000 sequences containing the typical motif $(G_3+N_{1-7})_4$ have been founded in the human genome.⁴⁵ Such sequences are mainly concentrated in biologically crucial regions such as the regulation portion of genes, immunoglobulin heavy chains, telomeres and 5' or 3' UTRs RNA.^{45,46} Although a direct evidence of the G-4 biological relevance is still missing, such a high number of putative G-4 in crucial genomic regions suggests that these structures can play an important role in biological processes regulation. Therefore in past few years G-4 had become an interesting target for the development of new antitumor drugs. Indeed, several small molecules acting as G-4 ligands have been synthesized with the aim to explore new pathways in chemotherapeutics development. This is mainly due to the fact that G-Quadruplex ligands have shown *in vitro* cancer grown inhibition properties, according two different strategies (**Figure 10**):

- ✓ Acting as transcriptional inhibitors of oncogenes such as *c-myc* and *c-kit* by deactivation of its promoter.⁴⁷
- ✓ Acting as indirect telomerase inhibitors by the stabilization of the G-4 present in the single stranded telomeres end.⁴⁸⁻⁵²

For both the above strategies G-4 stabilization acts as a switch of a biological process. In fact, in the first case the stabilization of a G-4 in a gene promoter region acts as a transcriptional regulation factor. For the telomerase inhibition, which also represent the most studied and detailed strategy so far, the G-4 targeting acts as enzyme inhibitor. Although none of the above strategies is actually used in therapeutic treatment, the G-4 represents nowadays one of the most attractive targets for the development of new classes of antitumor drugs.⁵³

The “end replication problem”.

In order to clarify the role of telomerase and its implication in tumor cell growing it is better to introduce the “end regulation problem”, which represent the main cause of the telomerase action. Linear DNA molecules such as eukaryotic nuclear chromosomes require mechanisms in addition to the conventional DNA polymerases to complete the replication of their very extreme termini. The normal replication apparatus of cells carries out semiconservative DNA replication, copying a parental DNA strand as originally suggested by Watson and Crick in their famous Nature paper.⁵⁴ Furthermore, all DNA polymerases can synthesize DNA only in the 5' to 3' direction, and DNA polymerases require a primer, usually an RNA or a DNA. As a result of these inherent properties, a consequence of the normal mechanism of semi-conservative DNA replication would be attrition of sequences from the ends of chromosomes, as shown in **Figure 9**.

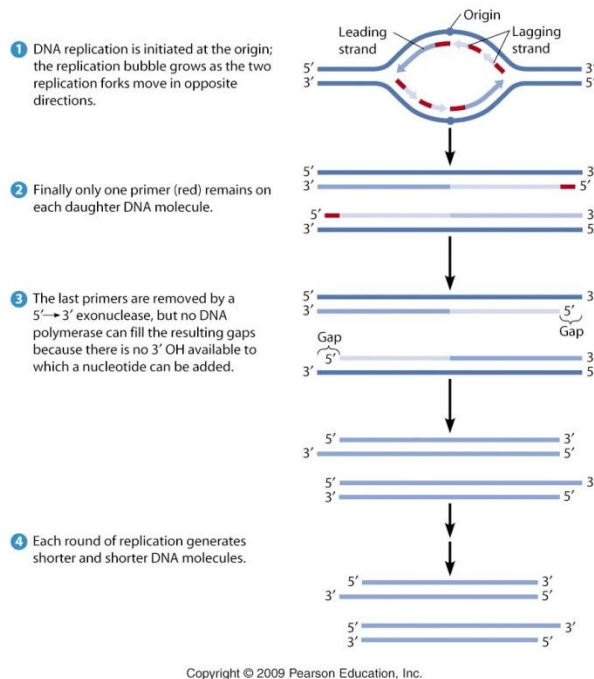


Figure 9. Schematic representation of the *end replication problem*.

Without some other mechanism, as it was predicted by Watson in 1972, such attrition would eventually lead to loss of genetic information, preventing cells from continuing to multiply.⁵⁵ Bacteria generally get around this problem by having circular chromosomal DNAs. Many

bacteriophage and viruses with linear genomes bypass this problem in a variety of other ways: some use a circular or concatamerized DNA replication intermediate. Others use a covalently attached terminal protein for DNA priming. Some viruses, such as poxviruses, actually have the end of their linear DNA genome closed in a covalently closed loop, with replication proceeding all the way around the end of the loop, and then the two daughters separating by being cut apart.⁵⁶ In contrast to these solutions, eukaryotic nuclear chromosomes use a very different mechanism to solve the problem of completing the replication of their ends: telomerase.

Telomerase an unusual way to make DNA.

The discovery of telomerase provided the general solution to the end-replication problem in eukaryotes.⁵⁷ Telomeric DNA consists of tandem repeats of a simple, often G-rich, sequence. This sequence is determined by the action of telomerase, which lengthens terminal regions of eukaryotic telomeric DNA by RNA-templated addition of the repeated DNA sequence. Complete replication of telomeric DNA requires telomerase. Telomerase was originally discovered by directed biochemical assays in vitro, using cell extracts and substrates designed to mimic telomeric DNA termini.⁵⁷ Telomerase is a specialized cellular Reverse Transcriptase (RT). It is a ribonucleoprotein (RNP) complex and it synthesizes one strand of the telomeric DNA namely, the strand running 5' to 3' towards the distal end of the chromosome, by copying a short template sequence within its intrinsic RNA moiety.⁵⁸⁻⁶⁰ This action extends the 3' terminal, single-stranded overhang found at the ends of telomeric DNA (**Figure 10a**). Discovery of this polymerization action of telomerase established the role of telomerase as a polymerase that extends one telomeric DNA strand. Synthesis of the complementary strand of the telomeric repeats is presumed to occur through lagging strand synthesis by the normal cellular DNA replication machinery. The resulting array of telomeric DNA repeats attracts and binds a set of DNA sequence-specific binding proteins. These in turn bind a further set of proteins to build an inferred higher order complex nucleated on the telomeric DNA. Addition of telomeric DNA onto chromosome ends by

telomerase serves to counterbalance the losses predicted from the end-replication problem and from nuclease action,⁶¹ or potentially other DNA damage at telomeric DNA ends.⁶² Interestingly, although the telomerase mechanism for telomere maintenance is very widespread among eukaryotes, and seems to have appeared early in eukaryotic evolution,⁶³⁻⁶⁶ it is not completely universal. The best studied natural exception to the telomerase mediated mode of telomere maintenance is, ironically, *D. melanogaster*, the species for which the term telomere was originally coined by Muller. *Drosophila melanogaster* has no telomerase. Instead, it maintains its telomeres by periodic addition of large retroelements to the chromosomal ends, building a complex array of repeats that form heterochromatin at the chromosomal end regions.⁶⁷ This chromosome-terminal heterochromatin provides the telomeric end protection. This was seen when a known heterochromatin protein, normally present at *D. melanogaster* telomeres, was mutated: such flies show frequent telomere–telomere fusions indicative of loss of end protection.⁶⁸ The essential core components of the telomerase enzyme are the RT protein subunit TERT, and TER. TERT has several other essential telomerase-specific domains besides the RT domain.⁶⁹ Telomerase in yeast and humans has been shown to be a dimeric complex containing two active sites, and with two telomerase RNAs and two TERTs that can functionally interact,⁷⁰ but it is not certain if dimerization is a universally conserved or even absolutely required feature of the enzyme. Genetics and biochemistry have revealed a number of other proteins which are associated with the core telomerase RNP.⁶⁶

Telomerase as validated cancer target.

Validation of a cancer target encompasses information on the prevalence and role of the target or pathway in human cancer. Conversely, modulation of the target or pathway in preclinical model systems results in a robust anticancer phenotype such as growth inhibition, induction of apoptosis or prevention of angiogenesis, migration and invasion. Therefore small-molecule or biological modulators provide a benefit to cancer patients.⁷¹ Pioneering studies done over the past

2 decades have shown that one of the above-described and to date therapeutically untapped phenotypic hallmarks of cancer, unlimited replicative potential, is intimately related to the maintenance of telomeres, repetitive TTAGGG sequences of DNA located on the ends of human chromosomes. Whereas mortal cells shorten their telomeres during each round of replication due to the “*end-replication problem*,” in tumor cells telomere length is stabilized mainly *via* reactivation of the reverse transcriptase termed telomerase. Such an enzyme is composed of a RNA component hTR or hTERC and a catalytic protein hTERT.⁷² Moreover, the introduction of hTERT into normal human cells extends their life span⁷³ and hTERT (along with two oncogenes, large T and H-ras) expression results in the direct tumorigenic conversion of normal human epithelial and fibroblast cells.⁷⁴ Other studies, however, suggest that telomerase may also play a role in maintaining telomeres in some normal human cells⁷⁵ and may possess additional roles to telomere maintenance, such as regulation of chromatin state and DNA damage responses, as cells lacking hTERT possessed a diminished capacity for DNA double-strand break repair and fragmented chromosomes.⁷⁶ In addition, in some tumors such as those of neuroepithelial and mesenchymal origin, telomeres are maintained by an alternative lengthening of telomere mechanism.⁷⁷ In patients with glioblastoma multiforme tumors, alternative lengthening of telomere is associated with mutant TP53 and a favorable prognosis.⁷⁸ Characteristics of alternative lengthening of telomere cells are alternative lengthening of telomere–associated promyelocytic leukemia bodies and circular extrachromosomal telomeric DNA.⁷⁹ Moreover, a group of six telomere-associated proteins, collectively termed shelterin, comprising TRF1 and TRF2 that bind to double-stranded telomeric DNA, POT1 that binds the single-stranded 3′ G-rich overhang, and three interconnecting proteins (TIN2, TPP1, and RAP1), acts to shape and safeguard telomeres as depicted in **Figure 10**.^{80,81}

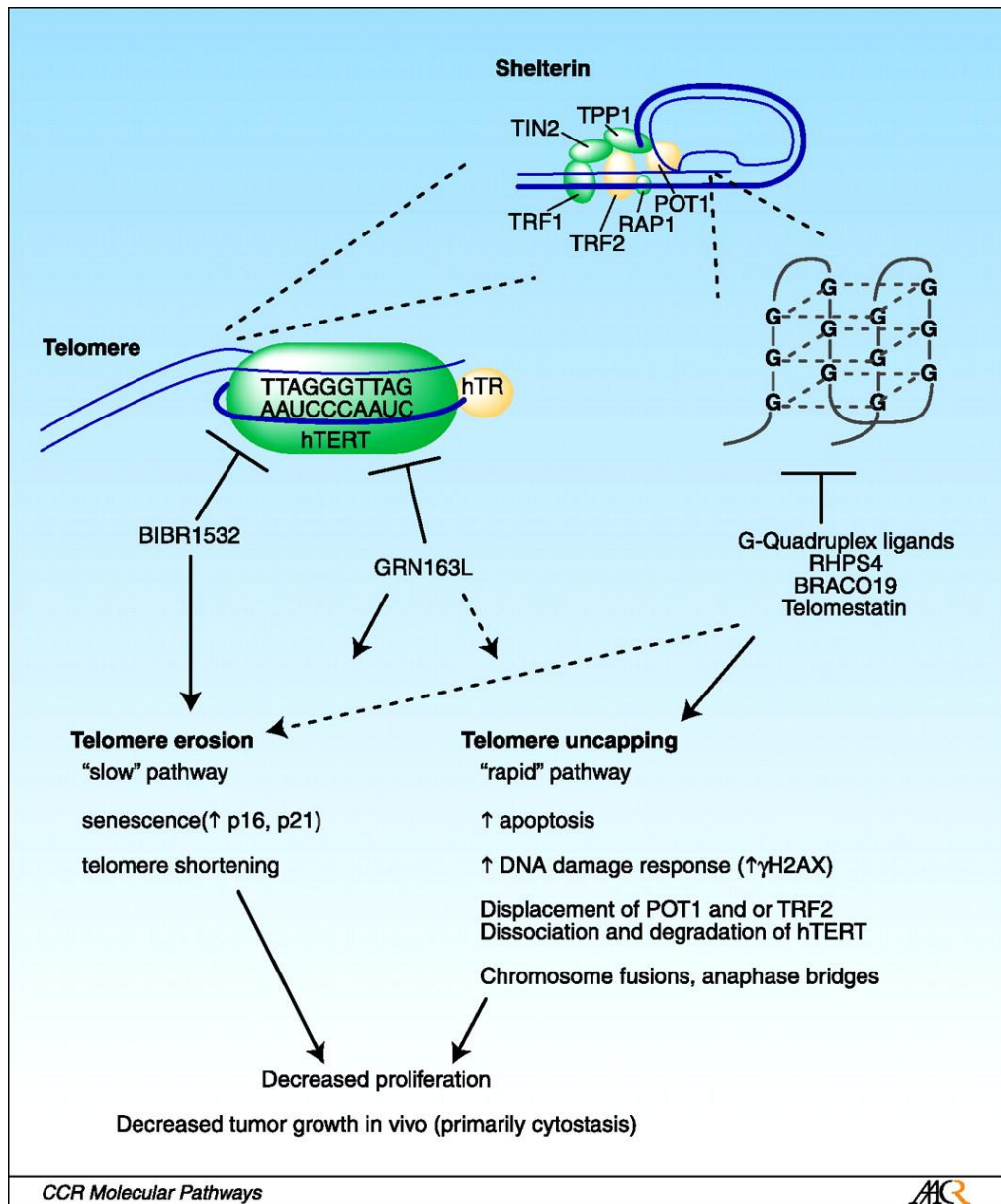


Figure 10. The telomerase/telomere pathway and main points of possible therapeutic intervention. Pathway modulators may result in either mainly telomere erosion (e.g., BIBR1532) resulting in relatively slow phenotypic anticancer effects or predominantly telomere uncapping (e.g., RHPS4) producing more rapid anticancer effects. Agents such as GRN163L probably mainly affect telomere erosion but also seem to induce telomere uncapping.

The interest in telomerase and telomeres in a cancer therapeutics context has emerged from two main observations: first, telomerase activity, typically using a PCR-based assay, telomeric repeat amplification protocol, is elevated in the great majority (~85%) of tumor types in comparison

with normal tissues, and second, telomeres are generally shorter in tumors than in corresponding normal tissues.^{82,83} Furthermore, several studies provide genetic validation of telomerase as an anticancer target in that inactivation of hTR and/or hTERT by dominant-negative mutants or antisense strategies resulted in an inhibition of tumor cell proliferation. For example, transfection of a dominant-negative mutant of hTERT into cancer cell lines of differing initial telomere length resulted in growth inhibition but this occurred with a different lag time dependent on this initial telomere length.⁸⁴ Such studies supported the view that, following inhibition of telomerase, telomeres needed to be gradually eroded down to a critical length before any phenotypic effect occurred. Hence, small-molecule mimics of this effect would be best suited to the treatment of tumors possessing very short telomeres.

Subsequent studies, however, targeting components of telomerase or telomeres/shelterin have shown that much more rapid apoptosis or induction of senescence effects can unfortunately occur. For example, antisense oligonucleotide-mediated inhibition of hTERT, but not hTERC, caused a rapid reduction in cell growth and induction of apoptosis without telomere shortening in human prostate cancer cells.⁸⁵ Second, the introduction of mutant template telomerase RNA into human tumor cells rapidly decreased cell viability and increased apoptosis, possibly via a telomere uncapping mechanism and triggering a DNA damage response.^{86,87} Third, ribozymes targeting murine telomerase RNA induced antitumor effects, including reducing melanoma tumor invasion and metastases *in vivo*. These studies also showed that telomerase activity may control the glycolytic pathway.⁸⁸ Finally, other genetic and biochemical studies suggest that targeting components of shelterin, such as TRF2⁸⁹ or POT,^{81,90,91} or exposing the telomere 3' overhang⁹² can induce apoptosis or telomere-initiated senescence and thereby activate a DNA damage checkpoint response.⁹³

Because telomerase activity is relatively high in many tumors and telomeres are generally shorter in tumors than normal tissues, taken together with the above-described genetic-based validation studies, provide a compelling argument to suggest that the telomerase/telomere

pathway is a well-validated target at the preclinical level. Therefore, appropriate modulators should be tested in patients.

Targeting telomerase towards G-4 ligands.

Telomerase enzyme recognizes as its substrate only the linear telomeric DNA. Indeed, the telomere ending is a single stranded sequence acting as a template substrate for the RNA telomerase active. Because of its intrinsic RT nature, telomerase can recognize as substrate only the linear telomeric ending form. On the other hand the G-rich nature of such a substrate gives it the possibility to fold into supramolecular structures such as G-Quaruplexes. Therefore, stabilizing the G-4 folded form by using small molecules or specific antibodies is translated into an indirect telomerase inhibition.⁹⁴ The first *in vitro* evidence concerning the formation of telomeric DNA G-4 structures has been reported in the late 80s, whereas the experimental proof about their formation *in vivo* is more recent and has been published in the 2000 by Schaffitzel's group.⁹⁵ Such a proof of concept has been achieved by using single chain antibodies engineered for intermolecular G-4 structure recognition typical of the *Stylonichia lemnae* protozoa. Although great efforts have been spent in order to demonstrate G-4 formation in eukaryotics cells a direct demonstration about their formation *in vivo* and their actual relationship with telomerase activity and chromosome stability is still missing. This makes the G-Quadruplex one of the most debated fields in the biochemistry research. 2 intermolecular G-4 structures derived from human telomeric DNA have been described to date: the *basket-type* and the *propeller-type*. These structures have been already mentioned in this work during the discussion of the G-4 topologies. NMR studies revealed that in the presence of Na⁺ an antiparallel *basket type* conformation with diagonal loops is adopted.⁹⁶ Conversely in the presence of K⁺ as well as in the solid state the *propeller-type* conformation is preferred.⁹⁷ The G-4 folding could not only interfere with the telomerase activity towards an indirect inhibition mechanism. In fact, also the proteins interacting with the telomeric DNA can be displaced or influenced by the folding equilibrium. As already mentioned the

chromosome ending is associated with several nucleoproteins, capable to interact both with the *ds* and the *ss* telomeric DNA. The hexa-proteic complex *shelterin* is crucial for chromosome stability and results tightly bound in between the *ds* and the *ss* telomeric DNA as depicted in **Figure 11**. Shelterin protects the telomere from shortening and DNA repairing processes. In particular the subunit **POT1** (*protection telomerase 1*) is capable to modulate telomerase activity.⁹⁸

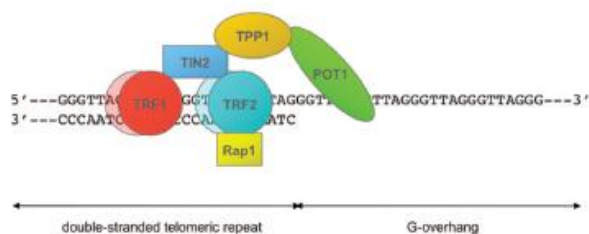


Figure 11. Representation of the *shelterin* bounded to the human telomeric DNA.

The stabilization of the telomeric G-4 by small molecules has been proven to be capable of POT1 displacement. Therefore, G-4 targeting by small molecules causes telomere uncapping inducing a DNA damage response by p53 activation. The latter allows selective telomerase dependent apoptotic pathways. This makes the G-Quadruplex formation and stabilization within the human telomeric DNA a potential cell cycle regulator as summarized in **Figure 12**.⁹⁹

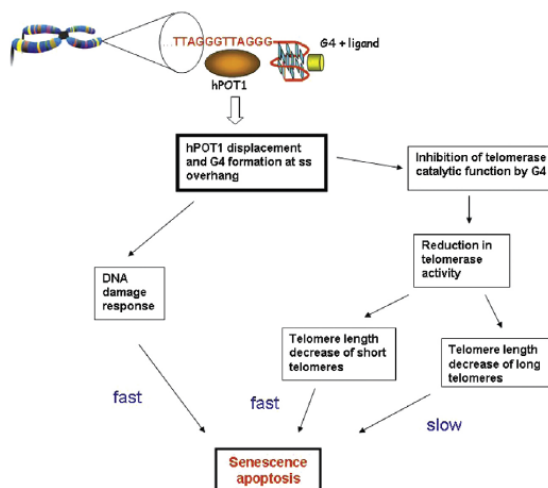


Figure 12. hPOT1 displacement consequences on telomerase active cell stability.

Indeed, several quadruplex-binding ligands, such as the acridines BRACO-19 and RHPS4 induce replicative senescence in cancer cells with a few days of exposure (the effects on some cell lines are more immediate and may be telomere-length dependent). This activates the same DNA damage response that follows DNA double-strand breaks, and involves in particular ATM, p16INK4a kinase and p53 pathways^{100,101} which can be visualized by, for example, the appearance of characteristic DNA damage foci using an antibody to the damage-response protein γ H2AX,⁹⁸ or by a significant population of cells undergoing end-to-end fusions in metaphase.¹⁰² Such changes are analogous to those produced when the telomeric protein TRF2 is knocked out. This response is a consequence of the displacement of bound proteins from the single-stranded overhang, chiefly hPOT1 (**Figure 12**), as well as possible uncapping of telomerase from the ends. There are likely to be multiple mechanisms involved, some of which at least have crosstalk between them. For example, hPOT1 interacts with the telomeric protein Tpp1 and so facilitates telomere-length regulation by telomerase, and hPOT1 displacement deregulates telomerase function.^{99,103} In addition, although the classic telomerase inhibition model does not appear to be followed by G-quadruplex-binding agents, most if not all cancer cells have marked telomere-length heterogeneity, with some having extremely short (<1 kb) telomeres. It has been suggested that these cells are not only sensitive to senescence, as one would expect, but also their viability is critical to the cell population overall.^{104,105} A Q-FISH technique has been used to determine that telomestatin is localized at telomeres during replication and has found that telomere replication is unaffected in mouse embryonic fibroblast (i.e. untransformed) cell lines.¹⁰² The analogous experiments in cancer cells have not as yet been reported.

G-Quadruplexes and oncogenes.

There is now a growing body of work that has explored a hypothesis linking the existence of G-quadruplex forming sequences in gene promoters to the transcriptional activity of the proximal gene. The “promoter-quadruplex” hypothesis is elucidated in **Figure 13** in its most general form

and depicts the formation of G-quadruplex structures in gene promoters in a process that is temporally and mechanistically coupled to transcriptional activity. This hypothesis has inspired the suggestion that small molecules that interact with such DNA G-quadruplexes may exert functional changes by specifically modulating the expression of the gene(s) regulated by these promoter sequences. The prospect of small-molecule gene regulators that act via a G-quadruplex mechanism presents attractive opportunities for the design of novel therapeutic agents that target disease-related genes both in humans and in a wide range of anti-infective targets.

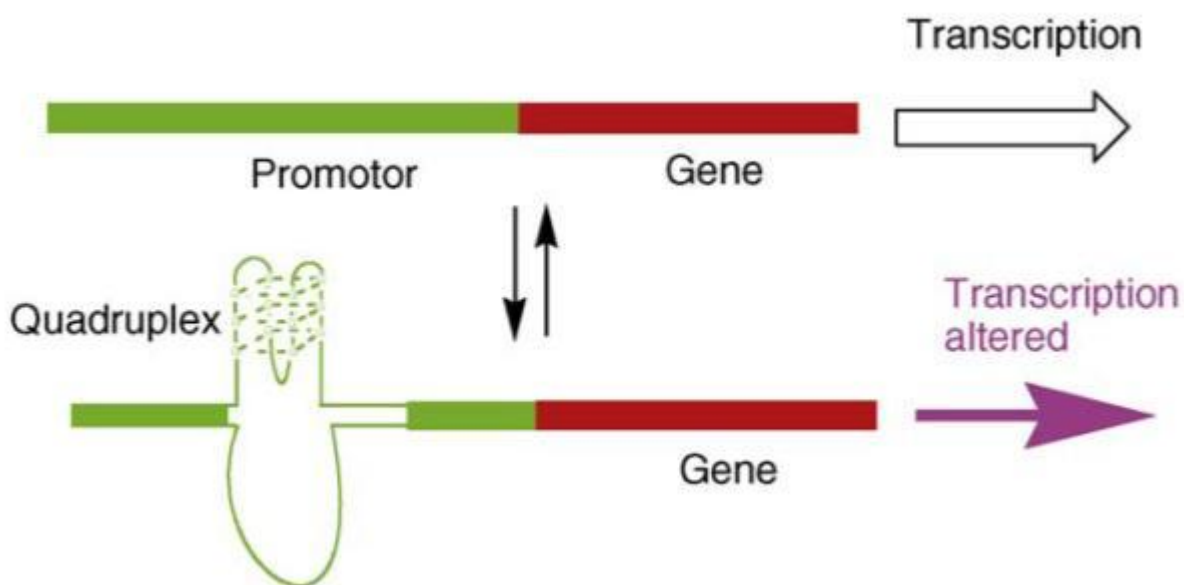


Figure 13. Schematic of the promoter-G-quadruplex hypothesis. G-quadruplex-forming sequence motifs in the upstream (promoter) region (in green) of genes (in red) may fold into G-quadruplex structures. The formation of G-quadruplex, rather than duplex, DNA structure in the promoter is associated with an altered state of transcription. This hypothesis would suggest that any molecule capable of interacting with the specific G-quadruplex could modulate the transcriptional activity of the associated gene.

The proposed association between G-quadruplexes and transcription has its origins in studies that set out to explore the relationship between nuclease hypersensitivity sites, indicative of non-duplex DNA structure and the transcriptional activation of genes. A number of such non-duplex structures were found upstream of transcription start sites and close analysis of the sequence

content of such regions revealed a prevalence of G-rich sequence. Indeed, many such sequence stretches would today be recognized as intramolecular G-quadruplex-forming motifs,^{45,46} and it was probably the chicken- β -globin gene the first to have a G-quadruplex sequence formally identified within its promoter.¹⁰⁶

A number of genome-wide computational studies have since been carried out to explore whether G-quadruplex sequence motifs are particularly prevalent near transcription start sites. A study that focused on human protein coding genes revealed that more than 40% of the genes had at least one G-quadruplex motif within 1 kb upstream of the transcription start site.¹⁰⁷ Furthermore, the quadruplex motifs within these upstream regions showed a strong positional bias towards the site at which transcription starts.¹⁰⁸ These features are analogous to those exhibited for 'classical' transcription factor binding regulatory sites¹⁰⁹ and would be consistent with G-quadruplex sequence motifs being *cis*-acting regulatory elements of transcription. Indeed, other computational studies have concluded that promoter-associated G-quadruplex motifs are proximal to¹¹⁰ or overlapping with¹¹¹ transcription factor binding sites. Thus, suggesting a possible mechanism whereby G-quadruplex motifs may interact with transcription factor binding events. Although, such data do not distinguish whether it is G-quadruplex structure formation rather than the sequence *per se*, to be relevant to transcription.

Detailed investigations have been carried out on G-quadruplex motifs found within the promoters of a number of medically related genes, particularly proto-oncogenes. The first-studied and best-studied case, of relevance to this hypothesis, was that of the human *c-myc* for which a G-quadruplex-forming sequence was identified in a nuclease hypersensitive element upstream of the P1 promoter.¹¹² NMR spectroscopic studies have elucidated the complexity of G-quadruplex structures formed by the motif, with a well-defined G-quadruplex structure being obtained for a truncated sequence comprising just four sets of G-tracts.^{113,114} Genetic point mutations that destabilized the *c-myc* G-quadruplex structure, led to an increase in transcriptional activity,

whereas the G-quadruplex interactive small-molecule **TMPyP4** was found to reduce the transcriptional activity, supportive of the promoter-G-quadruplex hypothesis.¹¹⁵

Two distinct G-quadruplex-forming sequence motifs were identified in the core promoter of the human *c-kit* oncogenes.^{116,117} Interestingly, both motifs flanked the binding site of the activating transcription factor *sp1* by ~10 nucleotides. The structure formed by one of the *c-kit* G-quadruplex-forming motifs (*c-kit1*) was solved by NMR.¹¹⁸ Single molecule Förster resonance energy transfer spectroscopy has suggested that the sequence of the second (*c-kit2*) G-quadruplex motif is sufficient to programme the formation of non-duplex structures within the context of an extended duplex.¹¹⁹ An isoalloxazine small-molecule G-quadruplex ligand that binds both *c-kit* G-quadruplexes was shown to reduce the levels of *c-kit* mRNA in *c-kit* expressing cell line.¹²⁰ Studies have also confirmed the presence of a G-quadruplex-forming sequence within the promoter of *k-ras*,¹²¹ which is also sensitive to a reduction in transcriptional activity induced by the G-quadruplex interactive ligand **TMPyP4**. Experiments using nuclear extracts identified Ku, PARP-1 and hnRNP-A1 as proteins that bind the G-quadruplex-forming sequence.¹²² Interestingly, PARP-1 has also been found to be enzymatically activated upon binding to G-quadruplex DNA,¹²³ and hnRNP-A1 has been found to unwind G-quadruplex DNA,¹²⁴ which may both be related to promoter-G-quadruplex function.

Promoter-G-quadruplexes have now been reported for a number of other cancer-related genes for which there is *in vitro* biophysical data, such as *VEGF*, *PDGF*, *HIF1a*, *bcl-2* and *RET* and in some cases also preliminary chemical biology evidence in support of the “promoter-G-quadruplex” hypothesis.⁴⁷

G-Quadruplexes in RNA.

While our knowledge of the DNA G-quadruplexes present in the human genome is increasing, our understanding of biologically relevant RNA G-quadruplexes remains limited. It is known that for a given sequence *in vitro*, an RNA G-quadruplex is usually more stable than its DNA

counterpart.¹²⁵ Moreover, unlike DNA, which is constrained mainly to a duplex form in the cell, RNA has no complementary strand limiting its structure. These two features make G-rich RNA sequences more susceptible to folding into a G-quadruplex structure *in vivo*. Several bioinformatic analyses searching for PG4 in the different regions of an mRNA have been reported such as in the 5'-UTR, the 3'-UTR and the RNA processing sites.^{126,127} Moreover, in some cases, RNA G-quadruplexes have been demonstrated to have functional roles.¹²⁸ For instance, one G-quadruplex structure was shown to direct the discrimination of a proper target by the fragile X mental retardation protein, while another was reported to regulate an alternative splicing event, to name two examples.^{128,129} The original study showing a G-quadruplex structure acting as a translational repressor was performed in a cell-free system using the full-length NRAS 5'-UTR that includes such a structure.¹²⁴ Subsequently to this Balasubramanian's and Bugaut's pioneering work, two other studies showed similar effects *in cellulo* using either a 27-nt Zic-1 RNA G-quadruplex, or a complete MT3-MPP 5'-UTR bearing a special purine-only RNA G-quadruplex.^{130,131} In each of these studies, only one RNA G-quadruplex was analyzed. More recently, the characterization of artificial cis-acting G-quadruplex repressors revealed an interesting correlation between the loop length and the number of G-tracks in terms of the translational inhibition level.¹³² Indeed, Bugaut et al showed that a naturally occurring RNA G-quadruplex element within the 5' UTR of the human NRAS proto-oncogene is a target for a small molecule that inhibits translation *in vitro*. That study provided the first demonstration that natural 5' UTR mRNA G-quadruplexes have potential as molecular targets for small molecules that modulate translation (**Figure 14**).¹³³

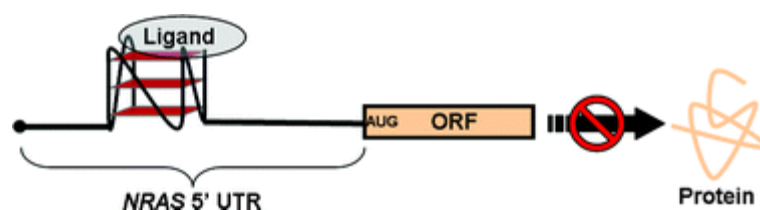


Figure 14. Schematic of the translation inhibition mediated by a RNA G-4 stabilization.

Despite all of these studies, both the impact and the importance of the 5'-UTR G-quadruplex structures on the biology of the cell remain, most likely, underestimated.

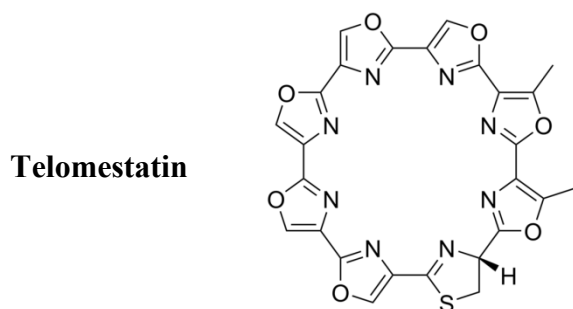
Targeting G-Quadruplex by using small molecules.

Because of the biological relevance of the G-4 based structures, the development of small molecules capable to selective interact and stabilize such structures has been one of the major goals of the medicinal chemists so far. Although the supramolecular differences between the classic double strand DNA and the quadruplexes are relevant, a total selectivity between these two structures is not an easy task at all. Such an issue is mainly due to the fact that the electrostatic contribution in this molecular recognition process is very high. Therefore researchers in the past years found some peculiar features that a good G-4 binder should have in order to increase the so called duplex *vs* quadruplex selectivity. Herein we summarize the main features shared among the G-4 best ligands:

- ✓ The presence or the potential for a wide flat aromatic or hetheroaromatic molecular surface, in order to enhance the superficial stacking interactions.
- ✓ The presence of physiological protonable or cationic side chains such as amines and ammonium salts, in order to maximize the electrostatic interaction with DNA.
- ✓ The potential for metal cation coordination or a strongly electron poor aromatic surface to mimic the metal coordination at the top of the Quadruplexes.

Even though most of the ligands reported in literature to date so far share such features, several exceptions can be reported. This underline how we are still far away of a complete understanding concerning the drug-target interaction mode in this field. One of the biggest exception is represented from the natural product Telomestatin (**1**), a potent G-4 selective binder as well as telomerase inhibitor, which still represent of the best ligand to date.¹³⁴ Indeed this ligand does not have any protonable moiety and, moreover is not a planar structure. Telomestatin structure herein

reported in **Scheme 1** is commonly employed in the laboratory practice as standard reference in the measurement of G-4 ligands goodness.



Scheme 1. The Telomestatin Macrocyclic Structure.

Beside the Telomestatin exception the above common features of G-4 binders have been, and still are, commonly used in the drug design practice. Indeed, from the Telomestatin discover¹³⁵ several synthetic molecules have been developed and studied as G-4 binders/antitumor agents. Some of them must be cited because of the relevance they had in the past decade, even though most of them did not pass the phase II of clinical trials. Since we have already described the common features shared among these ligands, we are now going to classify them herein into 3 different classes with the aim to better describe them and to rationalize the decisions taken during this work period.

“In situ” protonable G-Quadruplexes Ligands.

The key issue in the development of compounds that target G-Quadruplex-DNA is to conceive large flat aromatic systems prone to π -stacking with a G-tetrad platform, while retaining reasonable water solubility. In other words, the molecule has to exhibit both hydrophobic and hydrophilic characteristics. A usual way to ensure this duality is to introduce protonable side arms such as amine groups, around an aromatic core. That makes the molecule water soluble, thanks to the charge(s) possibly far from the hydrophobic center. This line has been followed 10 years ago by Neidle, Hurley and co-workers with the promotion of a bis-amidoanthraquinone as G-quadruplex ligand and telomerase inhibitor.⁵² The bisamido-anthraquinone family has been

further developed and subsequently evaluated by cytotoxicity and direct telomerase inhibition assays, revealing **IC50** values in the low micro-molar range.^{136,137} However, these studies concluded that the quadruplex- vs. duplex-DNA selectivity of this series was insufficient for further biological applications. Modifying the core and the side arms of the initial ligands: from anthraquinone to fluorenone,¹³⁸ then acridone¹³⁹ and acridine,¹⁴⁰ better selectivity has been achieved. A member of the 3,6-disubstituted acridine series was particularly useful for the G-quadruplex ligand design, **BSU6039** (**Scheme 2**), since a crystal structure of its complex with G-quadruplex was obtained as depicted in **Figure 15**.¹⁴¹

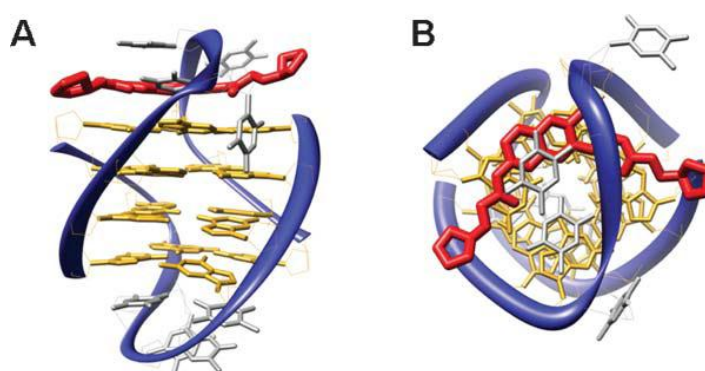
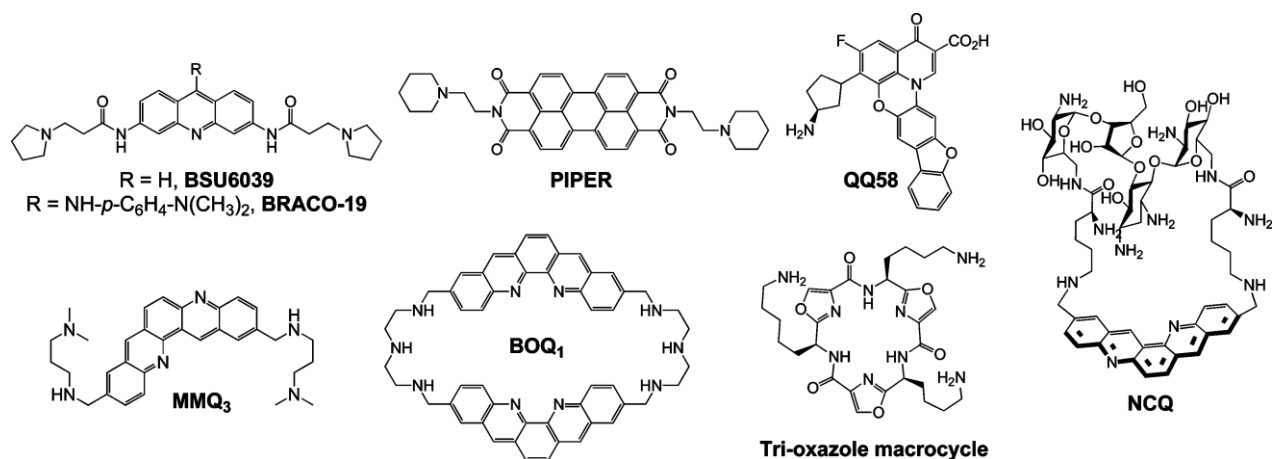


Figure 15. Side- (**A**) and top-views (**B**) of the X-ray structure of **BSU6039** complex with bimolecular quadruplex-DNA (d[G.T.G₄]) (PDB entry: 1L1H).

As expected, this structure showed an interaction driven by hydrophobic π -stacking interactions between the flat aromatic core of the ligand and two guanine residues of the accessible G-tetrad doubled by electrostatic interactions between the two protonable side chains of the ligand and the quadruplex-grooves. On this basis, an optimized prototype was designed, **BRACO-19** (**Scheme 2**), able to interact concomitantly with three G-quadruplex grooves thanks to three side-arms. **29** This optimized target adaptation appears through the high level of quadruplex-stabilization, evaluated by FRET (fluorescence resonance energy transfer)-melting assay,¹⁴² ($\Delta T_{1/2} = 27$ °C $1\mu\text{M}$) and selectivity evaluated by the SPR (surface plasmon resonance) method,¹⁴³ which both revealed a 31 fold binding preference for the quadruplex-structure. In addition, a strong potency for telomerase inhibition was evaluated by TRAP (telomeric repeat amplification protocol assay)

(IC₅₀ -TRAP = 115 nM).¹⁴⁴ Further biological investigations have recently demonstrated the efficiency of **BRACO-19** as an inhibitor of cancer cell proliferation, 34 which has been somewhat limited by pharmacological parameters such as cellular uptake or membrane permeability.¹⁴⁵ These limitations seem to be on the way of being avoided, by modification of the 9-amino substituent of the **BRACO-19** (from an aniline to a difluorobenzylamine group).¹⁴⁶ Hurley's orientations pointed toward more extended aromatic molecule such as the perylene diimide **PIPER** (Scheme 2).¹⁴⁷ This molecule is characterized by a broader hydrophobic core, with two external amine appendages. This family of compounds was shown to be moderately active as telomerase inhibitors (IC₅₀ -TRAP ~20 μM) but has been extensively studied by Hurley's then Kerwin's group, for the peculiar relationship between aggregation state and quadruplex- vs. duplex-DNA selectivity. Indeed, the latter increases from almost none to 42-fold quadruplex selectivity under a free (pH 7) or aggregated state (pH 8.5).^{148,149} Recent extensions confirmed that hydrosolubility does not necessarily imply better in vitro characteristics, as demonstrated by multi-substituted perylene and coronene ligands, either symmetrically substituted or not.^{150,151} Hurley's group also diverted the quinobenzoxazines from their usual anti-bacterial activity, to propose the fluoroquinolone **QQ58** (Scheme 2) as a G-quadruplex ligand.¹⁵² A NMR study confirmed the stacking onto an external G-tetrad as the main binding mode, and extended biological investigations demonstrated the cellular activity of such ligands.



Scheme 2. Some of the in situ protonable ligands cited and described in this work.

Other compounds from various natural sources and well-known for their affinity for duplex-DNA have been tested as G-quadruplex ligands: these are intercalators such as daunomycin, which wonderfully crystallized as a trimer with G-quadruplex (**Figure 16**),¹⁵³ or groove binders such as distamycin, whose NMR structure demonstrated quite a surprising binding mode with quadruplex, based on two molecules lying side by side in an anti-parallel fashion either in the groove or on the terminal G-quartet.¹⁵⁴ This study re-proposed old antitumor drugs for new purposes.

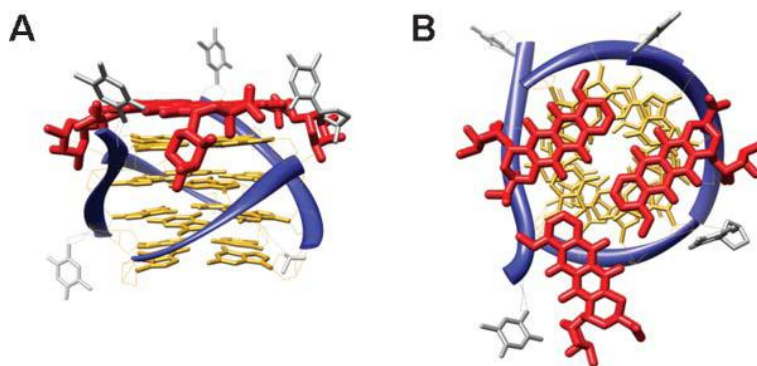
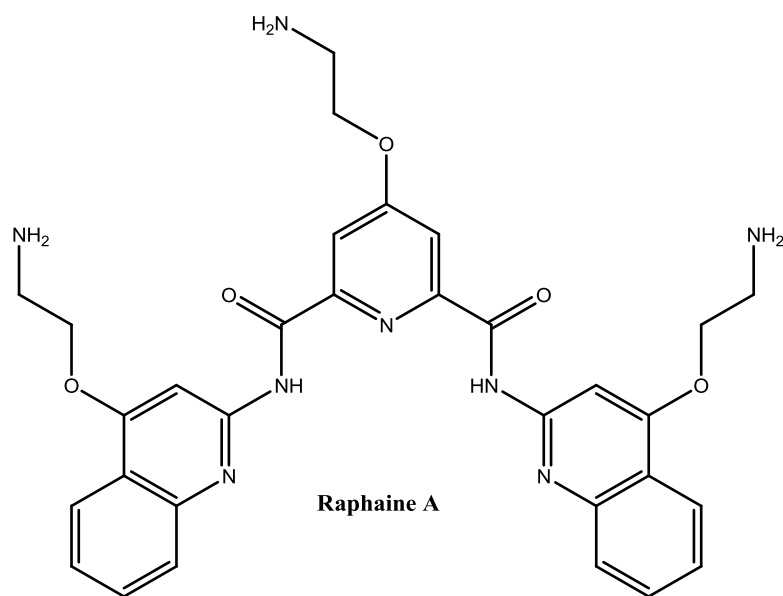


Figure 16. Side- (**A**) and top-views (**B**) of the X-ray structure of the **daunomycin** trimer with tetramolecular quadruplex-DNA (d[**TG₄T**])₄(PDB entry: 1O0 K).

Another dimension in the G-quadruplex ligand design has been introduced in 2001 by Teulade-Fichou, Mergny and coworkers with the use of pentacyclic quinacridines that display a crescent shape likely to maximize the overlap with the guanines of the accessible G-quartet. **MMQ3** (**Scheme 2**) was the leading compound of the quinacridine family, which shows remarkable G-quadruplex stabilization ($\Delta T_{1/2} = 20^{\circ}\text{C}$) and high telomerase inhibitory activity ($\text{IC}_{50}\text{-TRAP}=28$ nM).¹⁵⁵ Recently, an NMR structure was determined with **MMQ1**, the dipropylamino analogue of **MMQ3**, and a tetramolecular quadruplex.¹⁵⁶ This study not only shows the simultaneous overlap of three guanines by the quinacridine unit, but also pinpointed the role of the protonated side arms, which actively participate in quadruplex recognition via interactions in the grooves. A dimeric macrocyclic quinacridine was subsequently proposed, **BOQ1** (**Scheme 2**), that proved to be an improved quadruplex-stabilizer ($\Delta T_{1/2} = 28^{\circ}\text{C}$), with a better overall selectivity than

themonomeric series (~10-fold, evaluated by SPR) and an efficient telomerase inhibitor (IC₅₀ - TRAP = 130 nM). This selectivity, attributed to the enhancement of the ligand aromatic surface, is also likely a consequence of the steric hindrance of the macrocyclic scaffold that impedes duplex binding. Recently, it was suggested that BOQ1 can adopt a semi-closed conformation that might result in a particular binding mode, probably based on specific interactions with loops.¹⁵⁷ Interestingly, the efficiency of such a dimeric macrocyclic scaffold appears clearly dependent on the nature of the aromatic unit, since macrocycles derived from quinacridine (**BOQ1**) or acridine (**BisA**)¹⁵⁸ are efficient quadruplex binders, whereas those comprised of phenanthroline or naphthalene units, which have poor ability to stack on DNA bases,^{156,158} lead to more modest results. Some of the previous examples perfectly illustrate the difficulty in obtaining ligands with high quadruplex-selectivity. A novel trend in the G-quadruplex ligand design is currently emerging based on the enhancement of G-quadruplex recognition by the introduction of additional structural elements. This relies on the fact that quadruplex- vs. duplex-DNA selectivity has to be addressed in terms of the difference between the surface area of a G-quartet and of a base-pair, but also in terms of loop- and groove recognition. This basic principle was applied to the conception of the neomycin capped quinacridine series (**NCQ**, **Scheme 2**) that has been designed to concomitantly target the G-quartet and the loop of a quadruplex structure with the quinacridine moiety and the neomycin motif respectively.¹⁵⁹ The preferential binding of **NCQ** to loop-containing quadruplexes as compared to non-loop containing ones was evidenced. This result along with the good quadruplex stabilization ability of the series ($\Delta T_{1/2} = 14^\circ\text{C}$) and its strong telomerase inhibitory activity (IC₅₀ -TRAP = 200 nM) fully validates this ditopic design. The efficiency of trioxazole macrocycles (**Scheme 2**) originates probably in a similar phenomenon, thanks to the three amino appendages located on the same face of the macrocycle and putatively implicated in loop and groove interactions.¹⁶⁰ Interestingly, these secondary interactions raise the possibility of selectively stabilizing a particular type of quadruplex-DNA. This is illustrated by the binding preference of the tri-oxazole macrocycles for the quadruplex

formed by the *c-kit* sequence as compared to the human telomeric one. This particular macrocyclic oligoamide scaffold has been very recently confirmed as valuable for the design of efficient G-quadruplex ligands by two independent studies.¹⁶¹ Finally, Balasubramanian and coworkers also succeeded very recently in targeting another structural element of the quadruplex architecture, namely the central cation channel, thus opening interesting perspectives as for a ligand-mediated control of the quadruplex polymorphism.¹⁶² A real cornerstone in protonable G-4 ligands has been recently reached with the development, by Rodriguez and Balasubramanian, of **Raphaine A** molecule depicted in **Scheme 3**. Such a molecule is the best telomeric G-4 ligand to date ($\Delta T_{1/2} = 33^\circ\text{C}$ $1\mu\text{M}$) capable, moreover, to displace hPOT1 protein *in cellulo*.⁹⁸



Scheme 3. The **Raphaine A** Structure.

However, and as mentioned above, interactions of ligands with peculiar quadruplex elements such as loops, grooves, cation channel are still poorly investigated, suffering from the availability of firm structural data. We can schematically summarize such interaction modes as depicted in **Figure 16** as: a) superficial stacking b) lateral interaction c) loop interaction d) dual loop and superficial stacking interaction

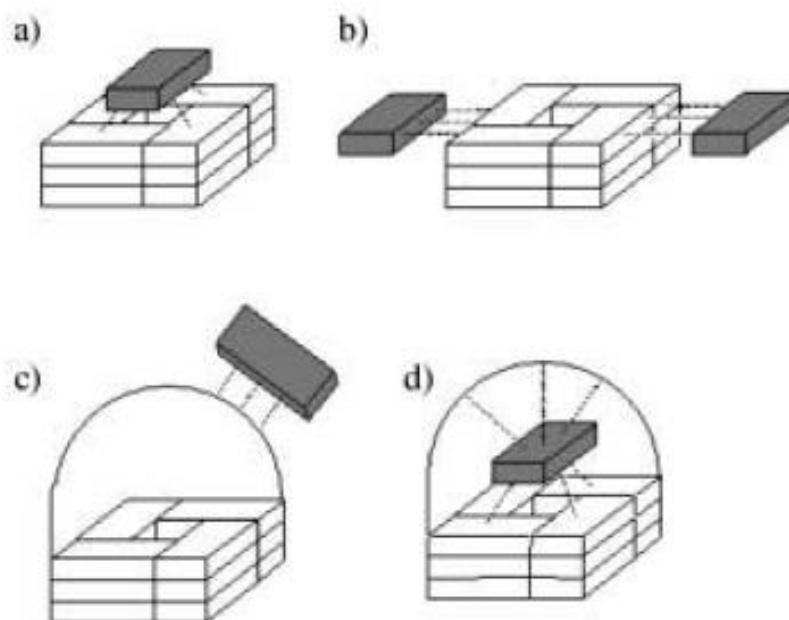
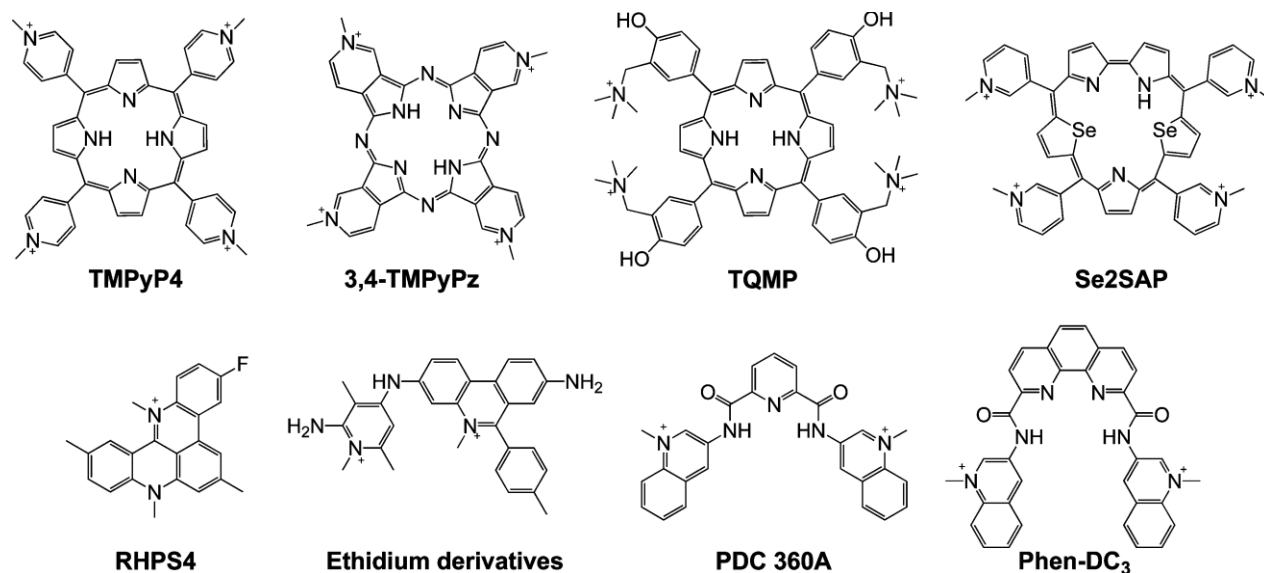


Figure 16: G-4 ligand possible binding modes above described.

N-Methylated aromatic G-quadruplex ligands

Beyond quaternization of amine side-chains via in situ protonation, an alternative pathway was thoroughly exploited with the use of N-methylated ligands especially on the aromatic ring nitrogen. The success of this design relies on the double advantage of N-methylated aza-aromatic moieties, affording water solubility without the need for cationic side-chains and increasing the π -stacking ability of the ligand because of the reduction of the electron density of the aromatic part. **TMPyP4** (Scheme 4) is the pivotal example of this family of ligands. **TMPyP4** has been shown to have a high affinity for G-quadruplex ($\Delta T_{1/2} = 17^\circ\text{C}$ $1\mu\text{M}$), to efficiently inhibit telomerase ($\text{IC}_{50}\text{-TRAP} = 6\mu\text{M}$), but also to down-regulate the expression of oncogenes such as *c-myc* or *k-ras* and to convert antiparallel topologies to parallel forms of quadruplexes.^{115,163-166} Interestingly, despite the fact that **TMPyP4** soon became known to be poorly to non-selective for quadruplex-structure,¹⁶⁷ the interest for this particular molecule has never declined. Indeed, the diverse

binding modes of **TMPyP4** include intercalation between adjacent G-tetrads and stacking of the porphyrin onto the external G-quartet which has represented a cornerstone in G-4 binding mode study.¹⁶⁸ Furthermore, X-ray studies have described an unexpected alternative binding mode based on external stacking onto the **TTA** nucleotides but without any direct contact with G-quartets.¹⁶⁹ Several structurally-related ligands have been described over the past years: the porphyrin **TQMP68** and the porphyrazine **3,4-TMPyPz (Scheme 4)**¹⁷⁰ are two examples of tetracationic macrocycles, which have been shown to bind efficiently to quadruplex DNA. In particular in the case of the porphyrazine derivative, a 100-fold increase in affinity as compared to **TMPyP4** has been measured by SPR, but also a significant improvement of the specific recognition of quadruplex-over duplex-DNA was observed (>30-fold preference for quadruplex-DNA). Finally, an important breakthrough in the porphyrin series came with the design of a diseleno-sapphyrin **Se2SAP (Scheme 4)**, with an expanded porphyrin core.¹⁷¹ This ligand was shown to bind strongly and selectively to quadruplex and to convert parallel (*c-myc* sequence) or anti-parallel (human telomeric sequence) topologies to a mixed anti-parallel/parallel hybrid structure. More importantly, this ligand was the first of a promising series able to discriminate among the various forms of the G-quadruplex-DNA, a crucial task for drug development. Nevertheless, the very low-yielding preparation of the **Se2SAP** may be a serious drawback for future exploration of its biological potential. Beyond the canonical macrocyclic pattern of porphyrins and derivatives, several small molecules have been reported with quite exceptional properties. Among the first was **RHPS4 (Scheme 4)**,¹⁷² a N-methylated pentacyclic acridinium molecule. In vitro studies (IC₅₀-TRAP = 330 nM) and *in cellulo* investigations demonstrated the ability of this highly condensed aromatic ligand to decrease telomere length and to act in synergy with the classical anti-cancer agent Taxol. Recently, **RHPS4** has also been reported as an efficient telomere uncapping agent, as well as a telomere binding proteins modulator.¹⁰¹



Scheme 4. Some of the cationic ligands cited and described in this work.

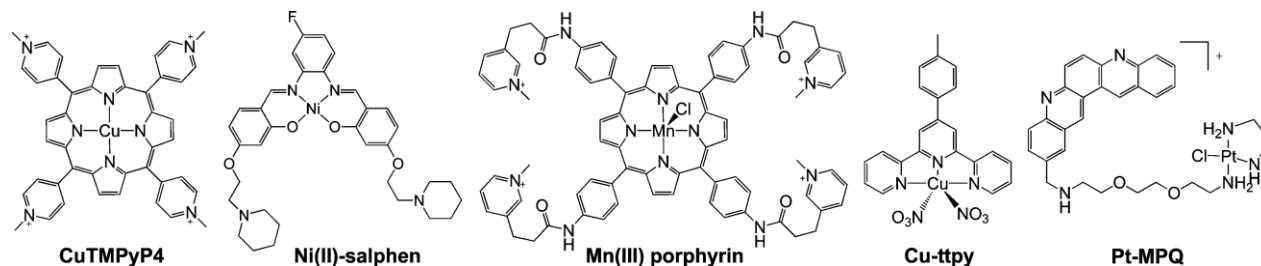
As expected, the cationic molecule sandwiches the quadruplex structure thanks to strong stacking interactions between the ligand and the two external G-quartets of the G-quadruplex. In 2001, Mergny and co-workers reported on the use of ethidium derivatives (**Scheme 4**) as G-quadruplex ligands.¹⁷³ However, the well-known toxic and mutagenic properties of ethidium bromide led these co-workers to develop a novel and safer series of G-quadruplex ligands, derived from triazine.¹⁷⁴ The member of the series known as **12459** and identified by FRET melting screening was particularly interesting thanks to its ability to stabilize selectively G-quadruplex ($\Delta T_{1/2} = 8^\circ\text{C}$) and to strongly inhibit telomerase activity ($\text{IC}_{50}\text{-TRAP} = 130 \text{ nM}$). Nevertheless, triazines were also rapidly superseded by the emergence of a structurally-related bisquinolinium series containing a pyridodicarboxamide (**PDC**) core.¹⁷⁵ The **PDC** series mimic the Raphaine A structure and, therefore has shown quite exceptional properties. The two leading compounds, **307A** and **360A** (**Scheme 4**), exhibit a good degree of quadruplex-stabilization ($\Delta T_{1/2} = 21^\circ\text{C}$), an exquisite quadruplex-over duplex-selectivity (>150-fold) and induce efficient inhibition of telomerase ($\text{IC}_{50}\text{-TRAP} = 300 \text{ nM}$). These results are particularly impressive with regard to the structural simplicity of the series and its two-step synthesis. Tritiated **360A** has been shown to localize preferentially at telomeric regions of chromosomes as **Raphaine A** structures,

thus providing new evidence of quadruplex existence in a cellular context.¹⁷⁶ Finally, a recent extension of this family of ligands was achieved by the synthesis of phenanthroline analogues **Phen-DC (Scheme 4)** that show a perfect geometrical match with a G-quartet. Remarkably, the selectivity of the Phen-DC series revealed to be higher than that of telomestatin, thus confirming the great potential of the bisquinolinium compounds, which represent an ideal compromise between rapid synthetic access and efficient target recognition.²¹

Metallo-organic G-quadruplex ligands

An alternative to the use of classical organic molecules is currently emerging from the literature, with the use of metallo-organic complexes. This class of ligands is highly interesting because of their easy synthetic access and their very promising G-quadruplex binding properties. This approach is based on the assumption that the central metal centre could be positioned over the cation channel of the quadruplex, thereby optimizing the stacking interactions of the surrounding chelating agent with the accessible G-quartet.¹⁷⁷ Their cationic or highly polarized nature is also a clear advantage to promote the association with the negatively charged G-quadruplex-DNA. The very first reported examples described the insertion of a metal in the central cavity of **TMPyP4**,^{51,166} and their use as Cu(II)¹⁷⁸ (**Scheme 5**), Ni(II) or Mn(III)-complexes.¹⁷⁹ **Mn-TMPyP4** deserves particular attention since it showed a 10 fold preference for quadruplex over duplex DNA, as evaluated by SPR, despite modest telomerase inhibition.¹⁸⁰ Among the subsequent examples of transition metal complexes like Ru(II),¹⁸¹ Zn(II)¹⁸² or Pt(II) complexes,¹⁸³ **Ni(II) salphen**¹⁸⁴ and **Mn(III)-porphyrin**¹⁸⁵ appeared to stand amongst the most potent reported G-quadruplex ligands (**Scheme 5**). Their performances are indeed impressive both in terms of quadruplex-stabilization ($\Delta T_{1/2} = 33^\circ\text{C}$ for Ni(II)) and quadruplex selectivity that were evaluated by FRET melting assay and SPR. These compounds also display good level of telomerase inhibition (IC₅₀-TRAP = 120 and 580 nM for Ni(II) and Mn(III) complexes respectively). Finally very simple structures such as Cu(II) and Pt(II)-terpyridine complexes that

can be obtained in one-step or two-step processes have proved to be high-affinity and highly selective G-quadruplex ligands (**Scheme 5**).¹⁸⁶ Importantly, this study highlighted that the geometry of the metal centre is a key parameter governing selectivity.



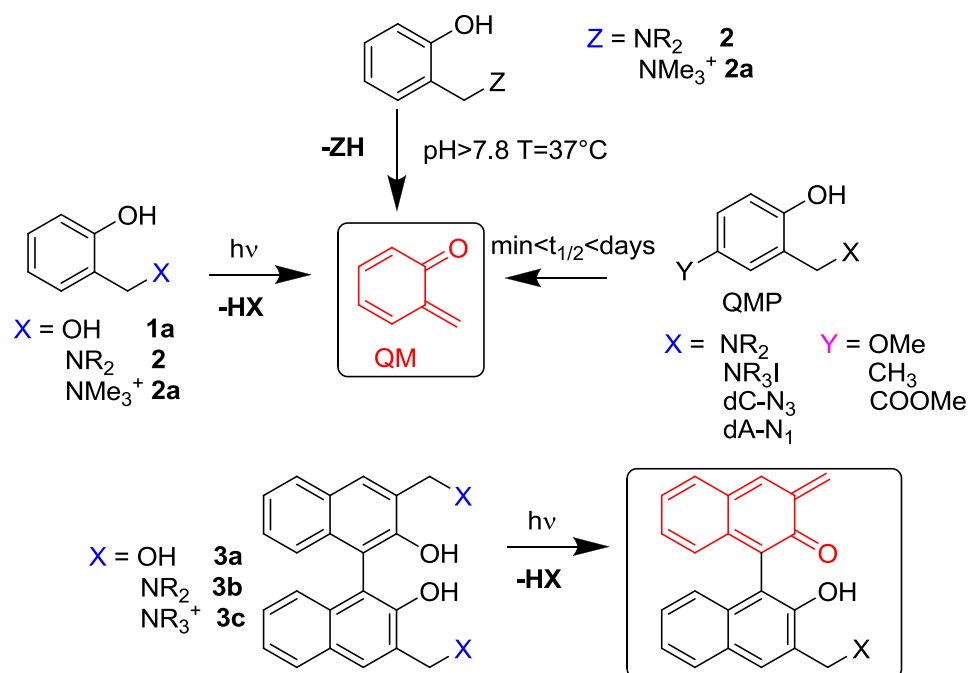
Scheme 5. Some of the metallo-organic ligands cited and described in this work.

Lastly, the use of a metal moiety grafted in the periphery of the central aromatic core of a G-quadruplex ligand has also been reported for various purposes. Fe(II) terminated appendages have been for example linked to a perylene or a naphthalene diimide core, in the design of probes devoted to quadruplex selective chemical cleavage or to electrochemical detection of immobilized quadruplex-DNA.^{187,188} Pt(II) complexes have also been exploited to provide additional anchorage of a G-quadruplex binding motif inside the DNA target. This work was stimulated by previous investigations of Bombard and co-workers who demonstrated the ability of terminal G-quartets to be platinated.¹⁸⁹ This approach has led to the design of the hybrid compound **Pt-MPQ** (**Scheme 5**) that interacts with quadruplex DNA via a dual covalent non-covalent binding mode due to the concomitant presence of the quinacridine unit and the platinum moiety.¹⁹⁰ This unprecedented synergism between π -stacking-directed association and a covalent trapping mediated by a mono-functional Pt complex opens up new perspectives for the development of novel quadruplex-binding modes. Indeed, the goal of this PhD work is partially inspired to the development of new third generation ligands, and has as main purpose the alkylation of the G-4 structure *via* cross-linking. Such an alkylation process, which is in term of chemical nature is impossible to those achieved with classic alkylating agents, it has been achieved by using masked electrophile specie which are herein illustrated.

Quinone Methides a useful tool for masked electrophiles delivering.

Over the past 10 years, several groups have achieved covalent modification of DNA by photo-activation of o-hydroxy benzylic alcohols (**1**), Mannich base derivatives of phenols (**2**) and binols (**3**), in water solution, and such reactivity can also be triggered by thermal digestion, base catalysis and presence of fluoride anions.¹⁹¹⁻¹⁹⁸ More recently binols derivatives, functionalized with benzylic amino acids side chains, showed DNA photo-alkylation properties and photo-cytotoxicity comparable to, and in some cases higher than, psoralen.¹⁹⁹

The key intermediates shared between all these processes are the transient Quinone Methides (**QMs**) depicted in **Scheme 6**. What make QMs so interesting from the medicinal chemistry point of view is that their formation showed a strong dependence on the leaving group attached at the benzylic position of their precursor (**QMP**). Furthermore, the generation of QMs has been proven to be highly responsive to the presence of electron-withdrawing and electron-donating groups. In more details, electron-donating groups greatly facilitate QM generation, whereas electron withdrawing substituents strongly suppress such a process.²⁰⁰ Thus makes such a class of triggerable electrophiles perfect for medicinal chemistry purpose. Indeed, a QMP could be engineered to release the electrophile under physiological conditions such as by pH modification or light exposure. Therefore, at least theoretically, by using these molecules a magic bullet antitumor drug synthesis can be achieved. Very recently and as part of this PhD thesis work, a purine selective alkylation towards DNA has been afforded by photo generated naphthoquinone methides.²⁰¹ The proof of concept of the flexibility in QM using has been given in the very first part of this PhD work, by developing a brand new reductive protocol for the release of the QM transient. In particular, the mono-electronic reduction of a naphthalendiimide (**NDI**) acts as a reactivity switch for the directly tethered QMP, owing to the electron donating group properties of the stable NDI radical anion generated, as depicted in **Figure 16** and better discussed in the experimental part of this thesis.²⁰²



Scheme 6. Thermal and Photoinduced Generation of QM. Substituent Effect on the Reactivity of QM Precursor (QMP).

Moreover, the reductive protocol applied for alkylating agents release is a widely recognize tool in the new antitumor drug discovery, owing to the well known oxygen absence in tumor environments. Indeed, pH, reductive and photo based protocols for the release of alkylating agents such as Quinone Methides is one of the key aspects of this PhD work.

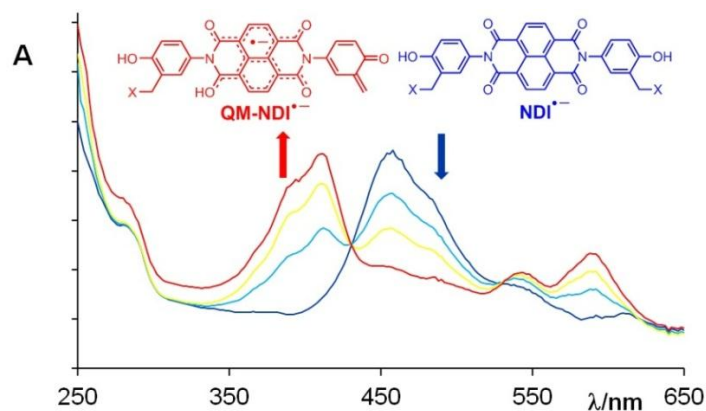


Figure 16. Generation of the NDI radical anion ($\text{NDI}^{\cdot-}$) as electron donating substituent, triggering the QM formation, detected by UV-vis spectroscopy, developed in this work.

Towards selective G-quadruplex alkylation: why using QMs?

As already described, Quinone Methides thanks to their tunable properties can represent a real useful tool for medicinal chemistry drug discovery. Moreover, such a class of reactive transients presents a very wide range of bio-compatible activation protocols which make QMs key transients for the development of a new generation of alkylating antitumor drugs. Because of the relevance of these transient in this PhD thesis work, it is mandatory to cite the most important development in the past 10 years concerning QMs as well as the techniques exploited to characterize them. The wide ranging activation protocols for such masked electrophiles are one of the most important characteristics. There are several activation protocols developed to date, the most relevant are herein summarized:

- ✓ Chemical or Enzymatic oxidation
- ✓ Chemical reduction (developed in this work)
- ✓ Photochemical activation
- ✓ Thermal activation
- ✓ Fluorine ions activation

Among the others, the photochemical activation is one of the most studied. The direct irradiation of the precursor represents the classic trigger protocol for QMs photo reactivity. In this work we have developed a brand new photo activation protocol mediated by a photo-induced electron transfer. Such a novel pathway for QM release will be better discussed in the experimental part of this work but here anticipated with the schematic **Figure 17**.

Although Quinone Methides have been largely employed in the past 15 years as DNA cross-linking agents, the reversibility of the alkylation damage is the peculiar feature that makes such transients special, especially for G-4 targeting purpose.

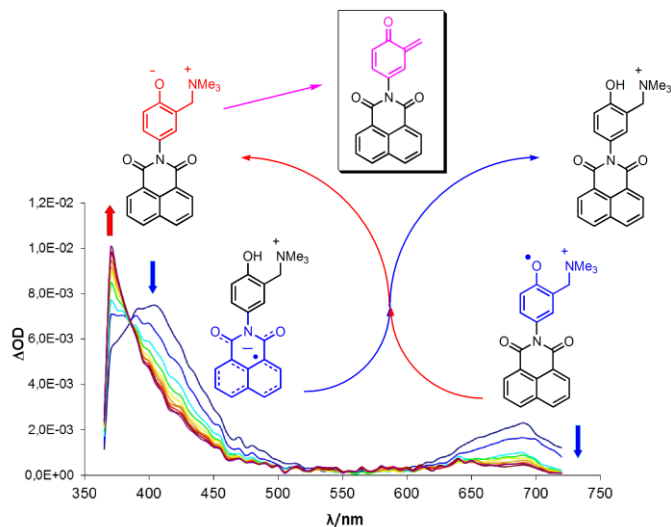
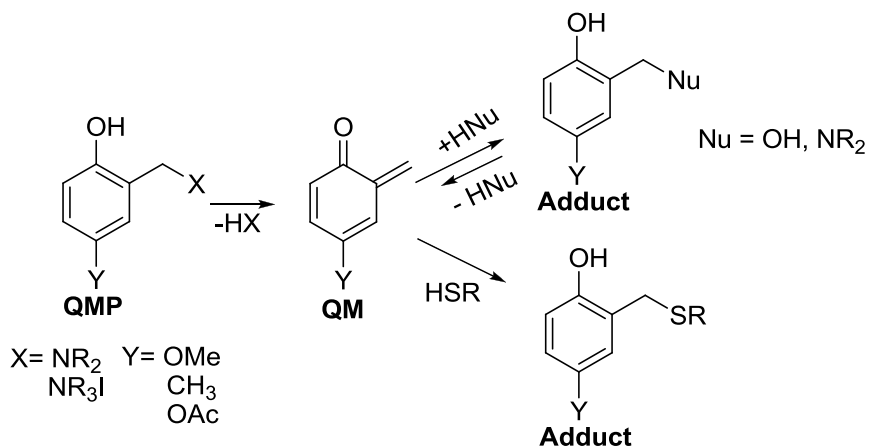


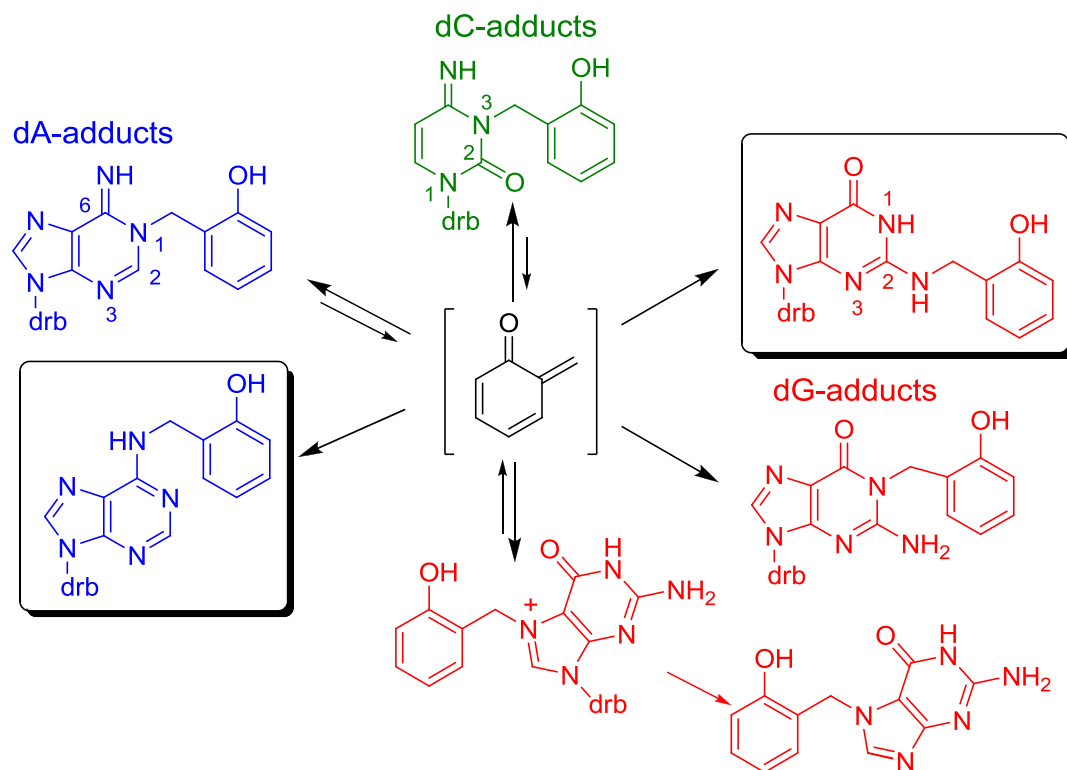
Figure 17. Novel QM photo generation mediated by a photo-induced electron transfer, developed in this work.

In fact, it has been shown that depending from the nature of the alkylation adduct, such a chemical damage could be either reversible or not. This should not sound surprisingly if we consider that the QM alkylation adduct is still a Quinone Methide Precursor; its reactivity will be dictated from the leaving group goodness, thus linked. This is a key aspect of QMs reactivity and represents the main reason based on the choice to use such transient in this PhD work. The underlying concept is depicted and summarized in **Scheme 7**.



Scheme 7. Reversibility of QM Alkylation dictated by the chemical nature of the trapped nucleophile. In more details, good leaving groups generate reactive adducts while bad leaving groups such as thiols generate an irreversible damage.

Reactivity of Quinone Methides towards nucleobases has been also studied. In order to clarify such reactivity it is better to distinguish between thermodynamic and kinetic reactivity. In fact, if we consider nucleobases as nucleophiles we will obtain this reactivity scale **N-7 guanine** >> **N-3 adenine** > **N-1 adenine** > **N-1 cytosine**. We can call this scale kinetic, because is proportional to the reactivity rate between the electrophile QM and the nucleophilic base. However, the kinetically formed adducts are still reactive to generate QMs and even though their formation is quicker, they will slightly decompose to generate less reactive and, therefore, more stable adducts. Following the reaction between a prototype QM and all the 4 DNA nucleobases we will report a high concentration of kinetic adducts in the very beginning which will slightly decrease to generate the thermodynamic adducts. Such a concept is herein depicted in **Scheme 8**.



Scheme 8. The chemical equilibrium between the kinetics and thermodynamics adducts. With double arrows the quickly formed but unstable kinetic adducts, whilst with the single arrow the irreversible thermodynamic adducts.

Thanks to the potential reversible and activable alkylation, QMs have been chosen in the present work as transient electrophiles to tether to a G-4 ligand in order to achieve a dual reversible/irreversible stabilization.

Because of their very reactive nature, QMs cannot be isolated or characterized with common spectroscopic and spectrometric techniques. Indeed, the average life time of such transients is in the millisecond timescale, herein we are going to briefly describe the laser flash photolysis technique which has been crucial for part of this work development.

Laser Flash Photolysis in QM transients characterization.

Laser flash photolysis (**LFP**) is a technique for the spectroscopic detection of photogenerated transients with half lifetime in the nanosecond or femtosecond timescale. Flash photolysis is a pump-probe laboratory technique, in which a sample is firstly excited by a strong pulse (called pump pulse) of light from a laser of nanosecond, picosecond, or femtosecond pulse width or by a short-pulse light source such as a flash lamp. This first strong pulse starts a chemical reaction or leads to an increased population for energy levels other than the ground state within a sample of atoms or molecules, the time dependence of which can be therefore detected by UV-Vis. Typically the absorption of light by the sample is recorded within short time intervals (by a so-called test pulses) to monitor relaxation or reaction processes initiated by the pump pulse as well as kinetic dependence between the so generated transients. As already introduced, QMs are very reactive transients which could be generated by photo activation. In fact, such photochemical process is easily followed by LFP as depicted in **Figure 18**. In particular in **Figure 18** it is represented the typical ortho-QM or para-QM UV profile (λ_{\max} 350-410 nm) and their time dependence over the millisecond time scale. The composition of the classical LFP instrument is depicted instead in **Scheme 9**.

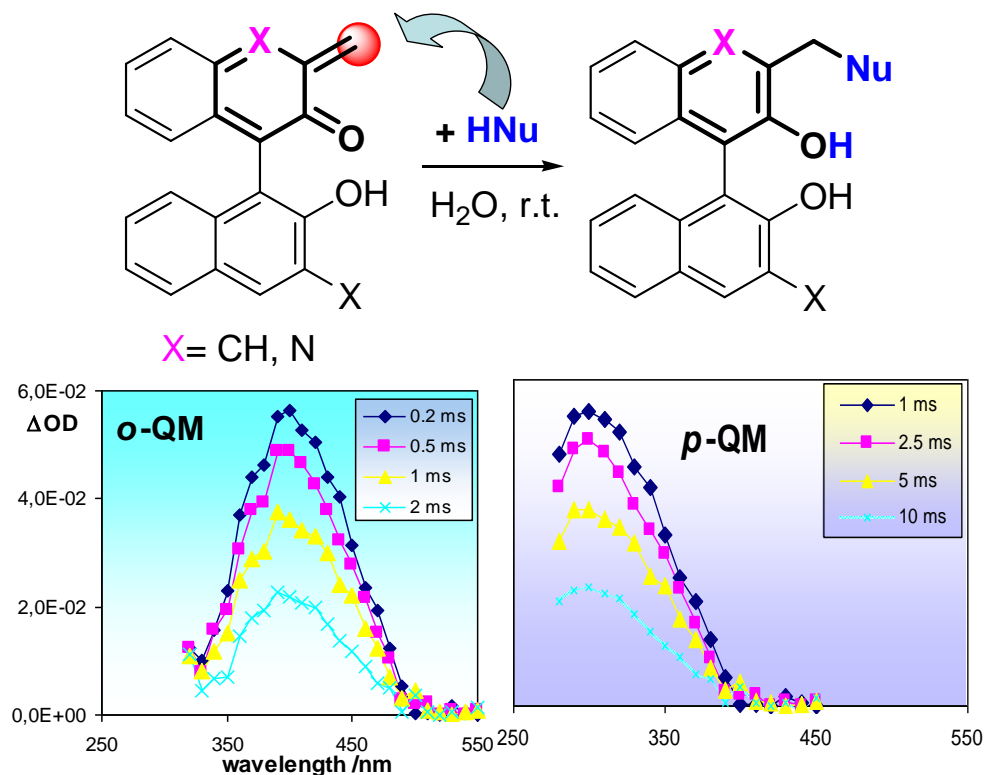
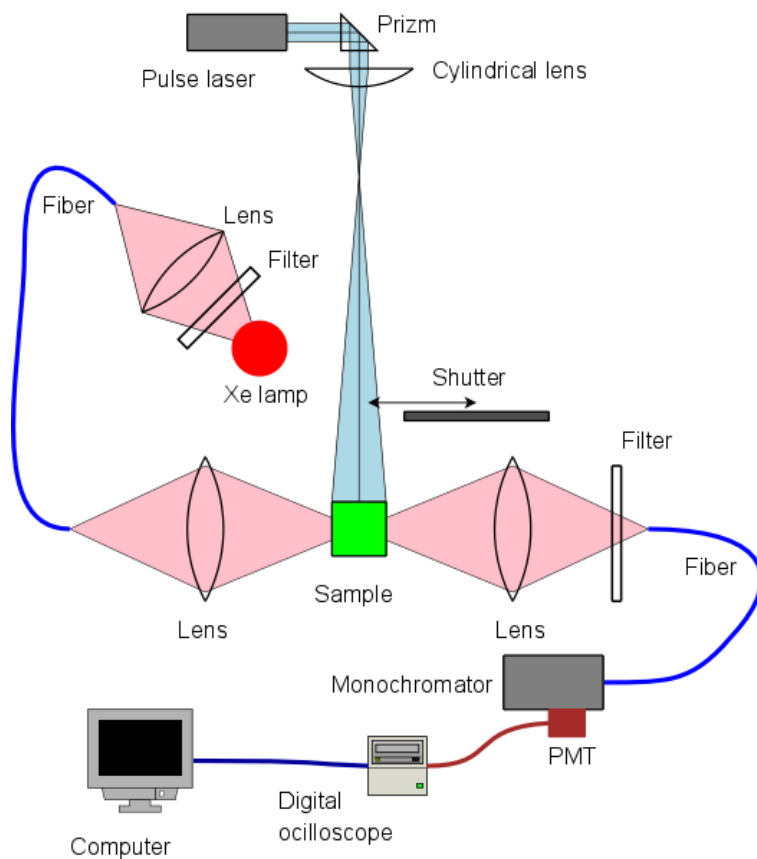
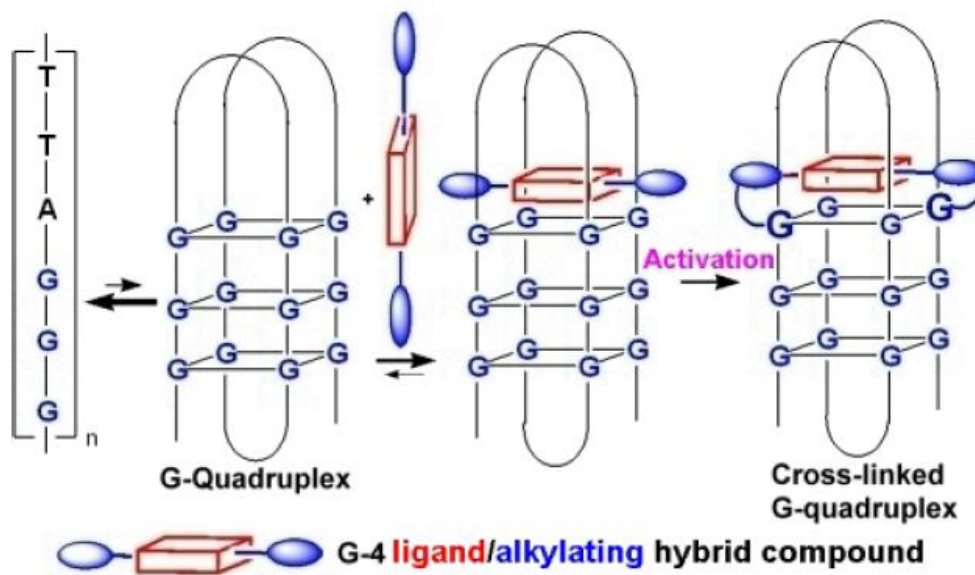


Figure 18. QMs photo generation profiles followed by LFP.



Scheme 9. Schematic representation of a generic LFP instrument composition.

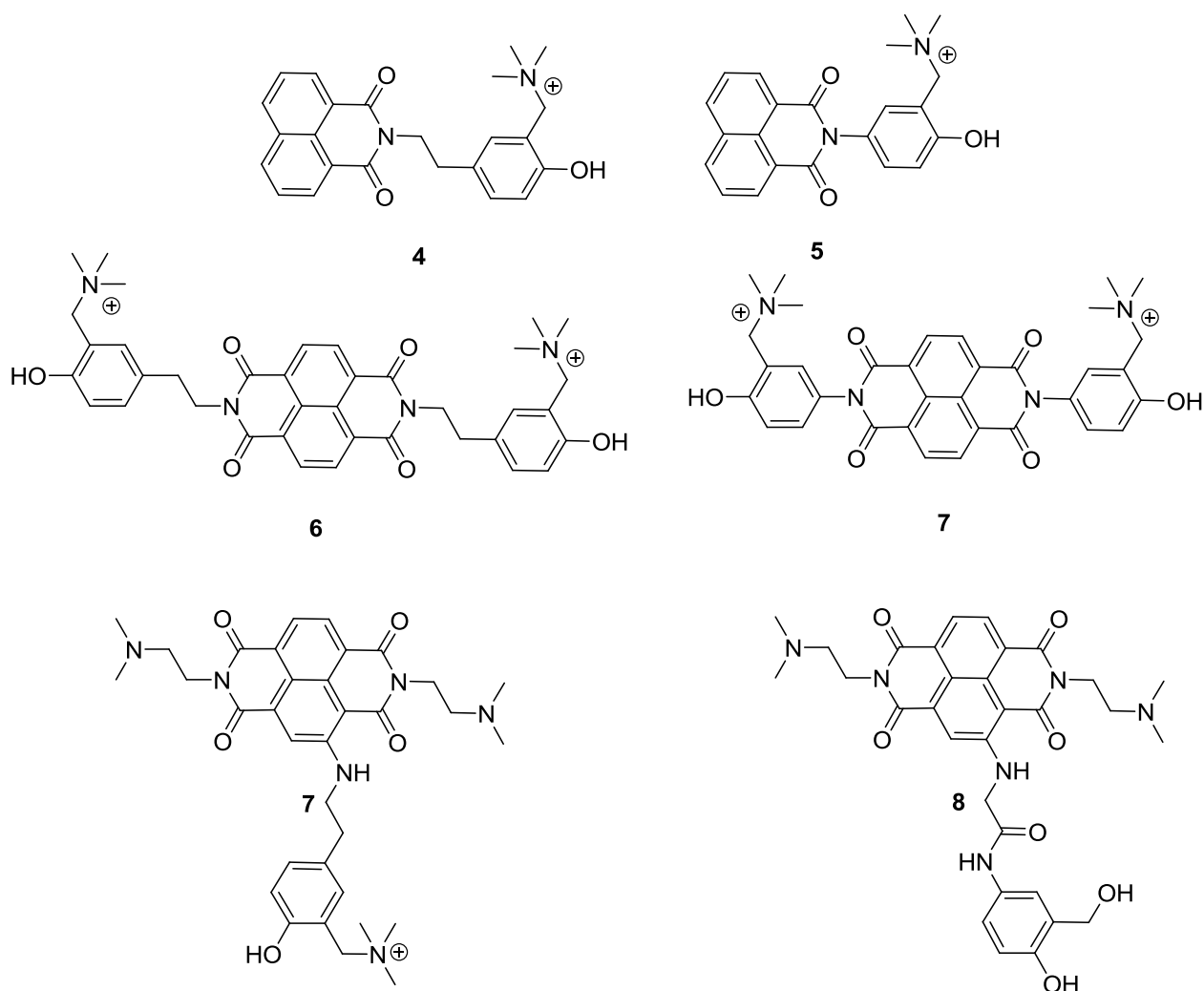
The aim of this PhD work is to develop a new class of G-4 ligands with triggerable alkylating properties. The strategy followed in order to reach this goal deals with tethering activable Quinone Methides Precursors (QMPs) to already described G-4 reversible ligands, thus creating a second generation of quadruplex binders with masked electrophiles embedded. The use of triggerable electrophiles such as QMs, allows the control of the alkylation by a defined chemical activation protocol of the precursors. Moreover, it allows a timing separation of the irreversible alkylating interaction with the reversible one given by the ligand. Therefore, we had defined such a class of molecules as molecular devices capable of pre-concentration onto a biological target and chemical releasing of a QM based electrophilic species.



Scheme 10. Mode of action of the new hybrid ligand/alkylating agents developed and studied in this work. The reversible interaction given by the ligand is depicted with the double arrows, whilst after the activation of the precursor the irreversible alkylation process occurs.

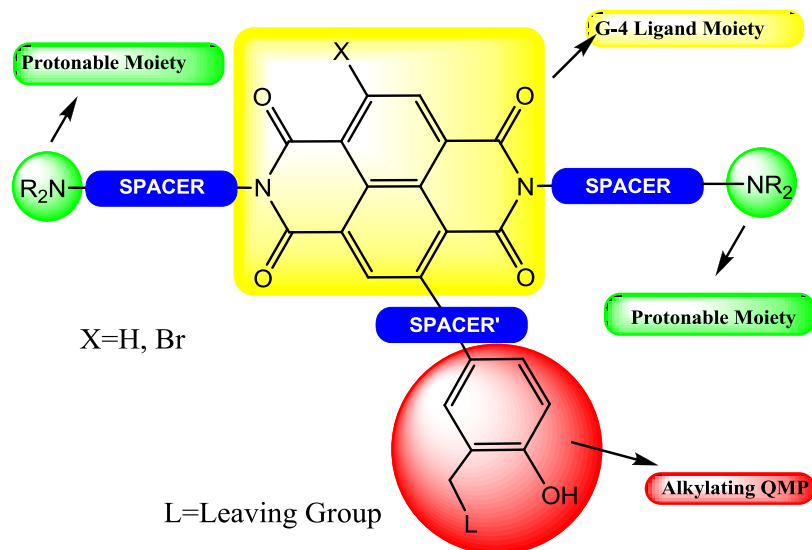
The decision to explore and study the stabilization by alkylation of G-4 structures is based on i) the possibility to achieve, at least theoretically, a complete shift of the equilibrium to the folded form, enhancing the goodness of the ligand and ii) the possibility to study selective DNA damage

responses eventually triggered by the alkylation process (i.e protein G-4 complexes displacement). Moreover, the conformationally rigid structure generated *via* cross-linking of the ligand onto the G-4 target, could be topology-selective or otherwise induce a conformational switch in response of the covalent binding. In order to chemically achieve the synthesis of the above molecular devices, we decided to focus our attention to Naphthalimide (NI) and Naphthalendiimide (NDI) derivatives. In particular we succeeded in the synthesis of the molecules depicted in **Scheme 11**.



Scheme 11. Some of the best hybrid ligand/alkylating molecules synthesized and studied during this PhD work.

All the above molecules has been rationally chosen and synthesized with the aim to combine the alkylating properties of Quinone Methides with the biophysical and chemical properties of NIs and NDIs. The general idea summarizing the chemical engineering of tri substituted NDIs as G-4 selective molecular devices is depicted in **Scheme 12**.



Scheme 12. General design of the molecular devices developed in this thesis. To a G-4 recognition moiety (Yellow) have been tethered by using chemical spacers water solubilizing amine units (Green) as well as alkylating appendages (QMP, Red).

Because of that, I have structured this PhD thesis in four distinct phases which will be described in dedicated chapters in the Result and Discussion part of this work, and herein summarized:

- ✓ Exploration and development of new QMs generation protocols “*ad hoc*” for G-4 alkylation purposes, exploiting new QMPs tethered to NDIs and NIs. Spectroscopic characterization of the new transients.
- ✓ Synthesis and spectroscopic study of new NDIs and NIs based molecules. Functionalization and chemical reactivity towards simple nucleophiles of different QMPs tethered to them.
- ✓ Evaluation of the above molecules as G-4 ligands before and after alkylation triggering.

- ✓ Evaluation of biological responses and selectivity towards different G-4 topologies, *in vitro* and *in cellulo*.

This PhD project has been developed in collaboration with Prof. Mauro Freccero's research group in Pavia, in which the chemical part of the project has been performed. Moreover, some of the *in cellulo* experiments have been performed in the Istituto Tumori Milano facilities by the Prof. Nadia Zaffaroni's group.

A parallel project has been conducted in collaboration with the G-4 expert Prof. Balasubramanian in his research group in Cambridge University. The project and the results concerning the Cambridge experience will be discussed in a dedicated chapter.

RESULTS AND DISCUSSIONS

In this section we are going to discuss the main results obtained during the PhD working period, with particular emphasis to both the synthetic and the biophysical aspects. Moreover, an analysis of the obtained data compared to the already cited state of the art will be discussed. More detailed experimental procedures and protocols will be discussed in the experimental part of this thesis.

As before mentioned, this section will be divided into dedicated chapters which will follow the rational evolution of the project from the synthesis of the new ligands and the choice of the suitable alkylating agent, to their behavior towards G-4 DNA.

Exploration and development of new QMs generation protocols.

As the very first task of this PhD project we aimed to explore new protocols for the generation of transient Quinone Methides. Particular emphasis has been given to the reductive and photochemical activation pathways, which are both amongst the better suitable for antitumor drugs development. Moreover, we attempt to achieve such new activation protocols for Quinone Methide Precursors directly tethered to NDIs or NIs scaffolds, with the aim to eventually exploit the latter cores as G-4 reversible moieties. Two original activation protocols have been developed during the PhD working period, namely a photochemical and a reductive one. The first has been explored for Naphthalimide (NIs) derivatives, while the second has been developed for Naphthalendiimides (NDIs) derivatives. Herein we are going to describe the new protocols developed, and the obtained results concerning the development of the above projects.

Quinone Methides Precursors Embedded to Naphthalimide Derivatives.

8-naphthalimide derivatives (NIs) have been studied extensively over the past few years because of their very interesting photo physical properties²⁰³⁻²⁰⁷ as well as their wide biological applicability. In fact, these compounds present two characteristic features namely, their high and

tunable fluorescence properties and the excellent accepting character of the NI core, which has greatly increased the use of NI based molecules for the synthesis of new devices with peculiar emission behavior, such as dyes,²⁰⁸ organic LEDs,²⁰⁹ pH and metal cation sensors,²¹⁰⁻²¹³ as well as anions sensors.²¹⁴⁻²¹⁶ These features make such a class of molecules very promising both for DNA targeting and sensing purposes.

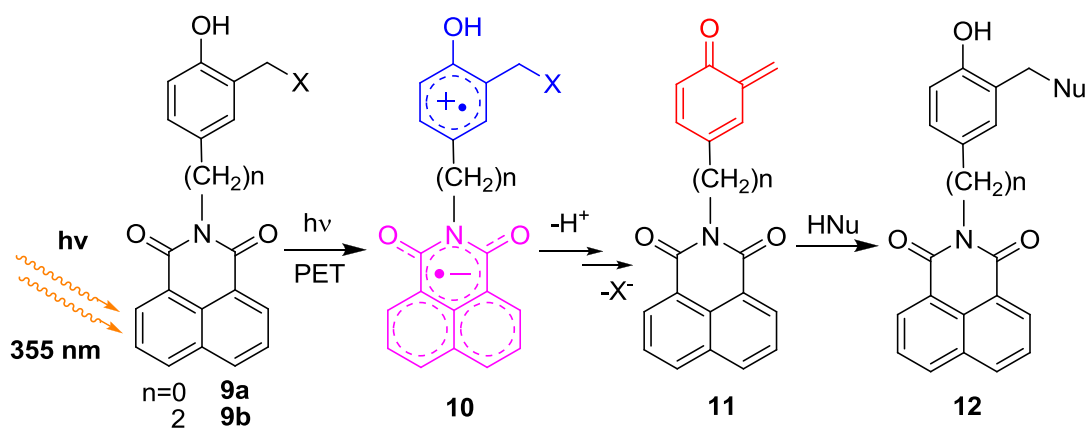
Moreover, it has been shown that such a class of molecules acts both as effective DNA intercalating agents,^{217,218} and potent topoisomerase II inhibitors.^{219,220} This has resulted in the wide ranging applications of NI based molecules for the development and design of new antitumor drugs.²²¹⁻²²⁵

The high tendency of the NI core to undergo photo-induced electron transfer (**PET**) as well as the affinity towards biological substrates such as DNA, has also been exploited to induce selective DNA damage. In particular, selective photo-oxidation²²⁶ and photo-cleavage²²⁷ processes, have been extensively investigated in the last few years. Furthermore, it has been demonstrated that NIs directly tethered to double stranded oligonucleotides, provided with a variable length A-T base pair spacer, are capable of undergoing intra-molecular **PET**, generating a couple of radical ions, namely NI^- and A^+ . Although the charge recombination process should be favored, the quick re-oxidation of NI^- by O_2 and the possibility of a hole hopping between A^+ and G to form G^+ , can strongly compete with the latter. By confirmation of that, it has been observed that DNA damage is greatly affected by the rate of the re-oxidation process, both by the length of the A-T base pair linker and G oxidation potential.^{228,229}

Such features have been exploited in this PhD work for the synthesis of a new class of NI derivatives bearing two different QMPs at the imide moiety (**Scheme 12**). These molecules showed an unprecedented photochemical reactivity by photochemical irradiation of the NI core. After several experiments we have finally rationalized the photo-generation of the transient QM (**11**) through a **PET** mechanism between the phenolic QM precursors and the NI core. Such a process, as summarized in **Scheme 13**, generates a radical ions pair (**10**) and the generation of a

phenolate anion eventually results. Because the electronic richness of the QMP strongly affects the reactivity, the phenolate generation results into the activation of the precursor itself. Thus allows the formation of the **new QM** transient which has been trapped by several nucleophiles in solution. All the transient specie involved have been detected and characterized by **LFP**.

At the best of our knowledge, this reactivity represents the very first case of alkylating QM photo-generation triggered by a photoinduced electron transfer with a peripheral moiety. The reactivity of the photo-generated QM towards several nucleophiles, together with a thorough **LFP** investigation, revealed that the phenolate anion is unequivocally the key intermediate generating the electrophilic QM. Owing to the wide applicability of NI based molecules in selective biological targeting, such a reactivity developed in this work represents the first step towards the development of engineered molecular devices capable to undergo photo-delivering of masked electrophiles



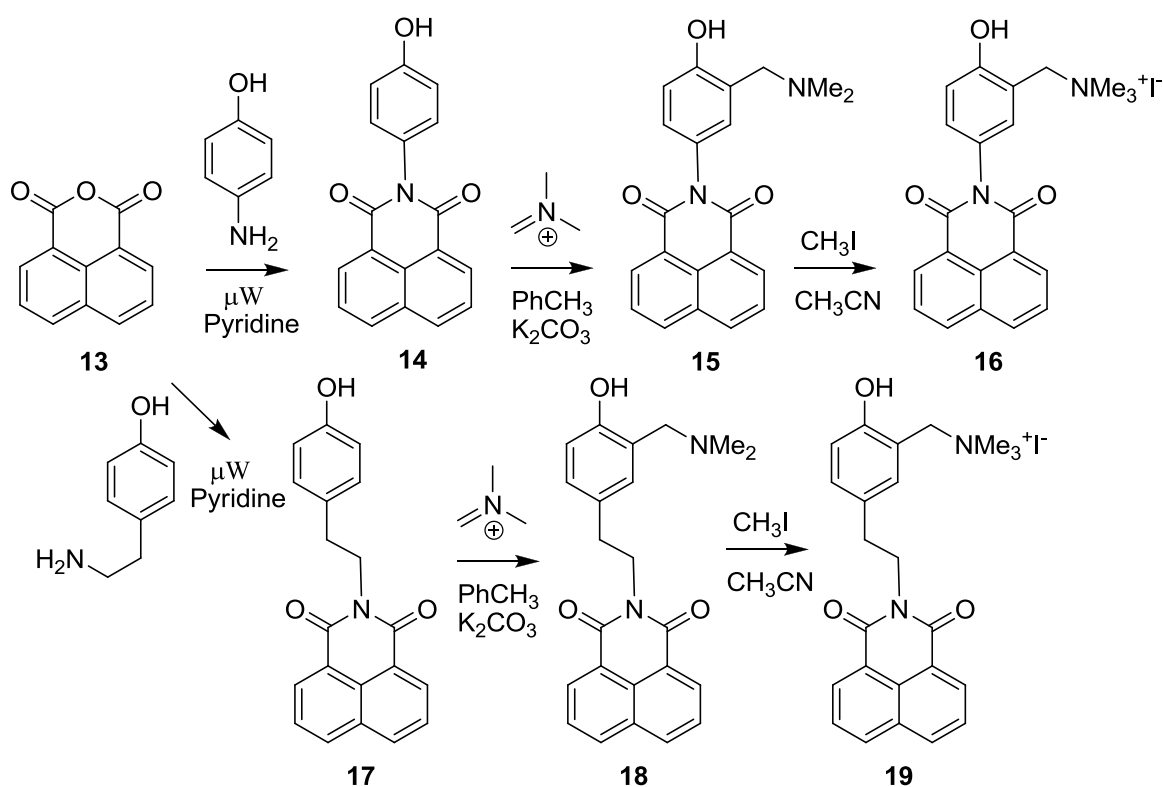
Scheme 13. Generation of QMs by PET Activation of Substituted NIs at 355 nm..

Also thermal reactivity towards nucleophiles under basic catalysis (45°C pH 10) has been studied and observed only for longer reaction time. This evidence suggests that phenolate anion is the involved intermediate for the generation of the QM transient for both processes.

Therefore this reactivity represents a novel activation pathway in which QM species generation occurs with the same efficiency of the thermal base catalyzed activation protocol but in the absence of any base and for shorter reaction times.

Synthesis of Naphthalimide Derivatives.

Already published studies showed how the PET mechanism in naphthalimide-donor dyads is strongly affected by the linker length between the NI accepting core and the donor.^{204,206} In order to evaluate how this effect could be translated in terms of photo reactivity, we decided to synthesize two different NI derivatives. By tethering the (5-amino-2-hydroxybenzyl)trimethylammonium iodide, as QMP precursor, to the 1,8 naphthalene anhydride (**13**) we obtained molecule **16**. The latter represents a directly linked donor-acceptor system. Alternatively, using the (5-(2-aminoethyl)-2-hydroxybenzyl)trimethylammonium iodide, we obtained molecule **19**, which allowed us to separate the donor QMP from the NI core with a conformationally flexible spacer as depicted in **Scheme 14**.



Scheme 14. Synthesis of the NIs Derivatives (**11** and **14**).

Attempts to achieve a direct coupling between the anhydride **8** and (5-amino-2-hydroxybenzyl)trimethylammonium iodide, according published procedures,²⁰⁸ were hampered by the thermal instability of the quaternary ammonium salts. In fact, we had already described

how such substrates can easily decompose into free QM and amine in the presence of electron donating groups on the aromatic ring.²⁰⁰ Consequently, both the adduct **16** and **19** were synthesized by a three step procedure starting from the coupling of the anhydride **13** to *p*-aminophenol or tyramine respectively, exploiting a brand new microwave synthetic protocol developed in this PhD work. The above coupling was followed by a Mannich reaction and CH₃I methylation (**Scheme 14**). This synthetic route allowed us to obtain NI **16** and **19** by using only one chromatographic purification step in excellent yield. (As described in the Experimental Section)

After the synthesis of **16** and **19** was accomplished, we started to investigate photo-activation protocols under mild conditions, in order to study the reactivity of such molecules as new photo alkylating agents. Moreover, to evaluate their thermal intrinsic reactivity and to discriminate it from the photoreactivity, two more activation pathways have been studied: (i) buffered neutral thermal digestion and (ii) base catalysed thermal digestion. In both last two cases, the reaction of **16** and **19** was performed at 45°C in the presence of several nucleophiles (thiols and amines), in aqueous acetonitrile solutions (CH₃CN/H₂O 1:1).

Photoreactivity Study of Naphthalimide Derivatives

The photo activation of *o*-hydroxybenzyl alcohols, Mannich bases and their quaternary ammonium salts as alkylating agents *via* QM generation has been studied. In fact, it is well known how QMs could be efficiently generated by direct irradiation of phenol-like chromophores. Indeed, the acidic QMPs singlet excited state leads to a facile deprotonation which eventually result in QM generation.^{197,230} Surprisingly, we found that the photo reactivity observed for the NI derivatives herein synthesized was not due to such a mechanism. This conclusion was suggested by two key experimental observations: (i) the high absorptivity of the NI core in the 310 and 360 nm spectroscopic window, compared to the negligible absorbance of the QMP moiety and (ii) the absence of photo reactivity of the amine analogues (**15**, **18**). In fact,

it is widely known that QM generation by direct irradiation of Mannich bases and their quaternary ammonium salts occurs with very similar photo efficiency. Despite this, irradiation of molecules **16** and **19** showed high photo reactivity towards basic nucleophiles such as piperidine, ethylbutylamine and *t*-butylamine. In fact, both molecules upon irradiation at 310 nm in a 1:1 CH₃CN/H₂O Ar purged solution, gave conversion into the corresponding alkylated adducts ranging between 15 and 50%, after only 5 min of irradiation (using 4 lamps, 15 W, **Table 2** and **3**). A similar behavior towards neutral nucleophiles such as water and thiols has been observed for longer irradiation times (30 min, **Table 2** and **3**), resulting in the hydration adducts **20** and **26**. This difference could easily be explained by the higher electron donor character of the phenolate anion generated in the presence of basic nucleophiles. Indeed, conducting the photo-reaction in carbonate buffer (pH 10, condition F **Table 2** and **3**) a comparable reactivity observed for basic nucleophiles has also been recovered for water. Almost complete conversion to the hydration adducts **20** and **26** was observed after 30 min irradiation under this condition (**Table 2** and **3**), whereas conversions similar to those observed for amines were obtained for 5 min irradiation. Notably, poor photoreactivity towards thiol based nucleophiles has been observed, which is in marked contrast to the reactivity studied generating the transient QM by direct irradiation. Therefore, in order to clarify the conditions of the thermal and photo activation, a blank has been prepared for each photoreaction batch, which were made and treated under the very same conditions but not exposed to light. Alkylating adducts have never been detected for the non-irradiated blank solutions, in the presence of the same nucleophiles for equal or longer reaction times (at least for an additional hour). This result confirmed that the observed conversions were due to photochemical process only.

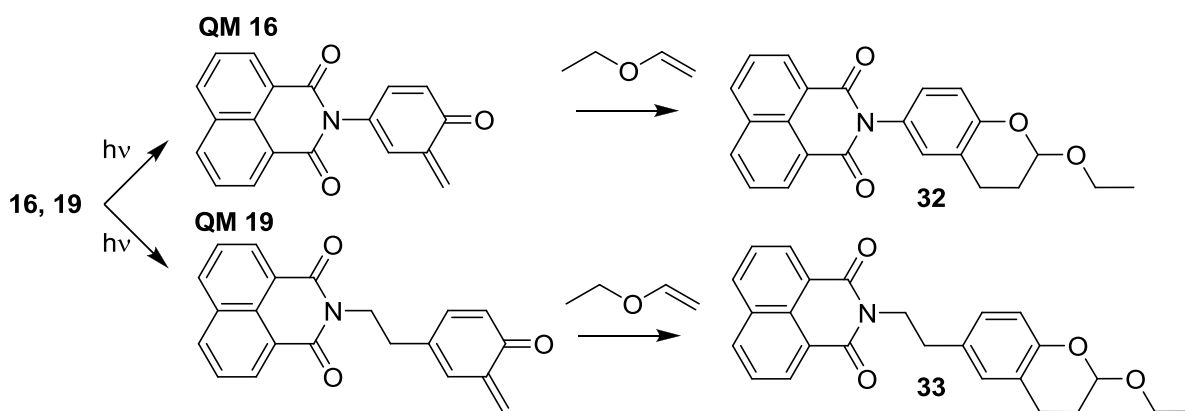
Base catalytic activation.

Activation by base catalysis takes advantage of the low pK_a (~8) of the quaternary ammonium salts of the Mannich bases, which allows the generation of a reactive zwitterionic form at pH ≥8

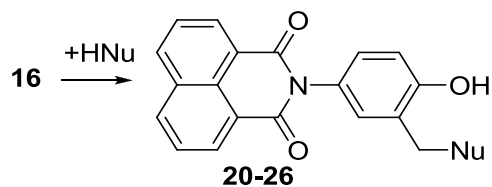
and, generates alkylating QM after mild thermal activation. Basic amines such as piperidine, *t*-butylamine and ethyl-butylamine ($pK_a > 10.7$) gave almost quantitative conversion after 1h digestion (45°C , in $\text{CH}_3\text{CN}:\text{H}_2\text{O}=1:1$; reaction condition A, **Table 2** and **3**). Amines displaying lower basicity ($pK_a \leq 8$), namely morpholine, as well as neutral nucleophiles, such as water and thiols, require carbonate buffered conditions ($\text{pH} \geq 8.5$, reaction condition C) and longer reaction times (**Table 2** and **3**). Remarkably, under these conditions reactivity towards thiols has been recovered. The results described above suggest that the activation of **16** and **19** as alkylating agent is not efficient at r.t. but only under strong basic conditions ($\text{pH} > 8.5$, 45°C), when the phenol is mainly deprotonated, and under higher temperatures. Similarly to the prototype quaternary ammonium salt **2a**, also for **16** and **19**, the zwitterionic form has to be populated to lower the barrier for the QM generation.

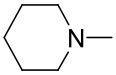
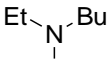
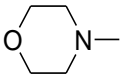
Hetero Diels-Alder Reactivity.

In order to confirm that a QM transient species was responsible of the alkylating reactivity observed, irradiation in the presence of ethyl vinyl ether (EVE) has been carried out. Although the QM-hydration pathway is competitive in aqueous acetonitrile ($[\text{EVE}] = 0.1 \text{ M}$), the irradiation of the NIs **16** and **19** leads to the formation of the 2-ethoxychromanes **32** and **33**. Such reactivity could be allowed only by the formation of a QM transient capable to react with EVE via [4+2] hetero Diels-Alder cycloaddition, as depicted in **Scheme 15**.

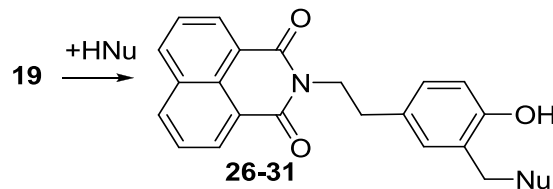


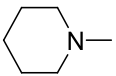
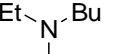
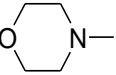
Scheme 15. Generation of Ethoxychromanes **32** and **33** by Trapping QMs (QM **16** and QM **19**).

Table 2. Reactivity of **16** by Base Catalysis and Irradiation at 310 nm.

Adduct	Nu	Base Catalysed Activation	Photoactivation
		Conditions, (Yield) ^[a]	Conditions, (Yield) ^[b]
20	HO-	30 min; 45°C; (10) ^[c]	30 min; 25°C; (33) ^[e]
		90 min; 45°C; (-) ^[d]	30 min; 25°C; (76) ^[f]
21		5 min; 45°C; (3) ^[d]	5 min; 25°C; (49) ^[e]
		30 min; 25°C; (1) ^[d]	10 min; 25°C; (99) ^[e]
22		5 min; 45°C; (8) ^[d]	5 min; 25°C; (55) ^[e]
		30 min; 25°C; (4) ^[d]	10 min; 25°C; (100) ^[e]
23		5 min; 45°C; (-) ^[d]	5 min; 25°C; (13) ^[e]
		30 min; 25°C; (-) ^[d]	30min; 25°C; (65) ^[e]
24	<i>t</i> -BuNH-	5 min; 45°C; (5) ^[e]	5 min; 25°C; (15) ^[e]
		60 min; 25°C; (-) ^[d]	30 min; 25°C; (45) ^[e]
25	HO-(CH ₂) ₂ S-	60 min; 45°C; (23) ^[c]	30 min; 25°C; (7) ^[e]
		90 min; 25°C; (-) ^[d]	60 min; 25°C; (22) ^[e]

[a] Reaction time T/°C, CH₃CN:H₂O=1:1, [**15**] or [**19**]= 5x10⁻⁴M, [HNu]=5x10⁻³ M, kept in the dark. [b] Reaction time T/°C, CH₃CN:H₂O=1:1, [**15**] or [**19**]= 5x10⁻⁴M, [Hnu]=5x10⁻³ M, 310 nm irradiation. Reaction yields (%) are reported in parenthesis. [c] Condition A, carbonate buffered (pH ≥ 8.5). [d] Condition A, not buffered. [e] Condition B, not buffered. [f] Condition B, carbonate buffered (pH ≥ 8.5)

Table 3 Reactivity of **19** by Base Catalysis and Irradiation at 310 nm.

Adduct	Nu	Base Catalysed Activation	Photoactivation
		Conditions, (Yield) ^[a]	Conditions, (Yield) ^[b]
26	HO-	30 min; 45°C; (17) ^[c]	30 min; 25°C; (22) ^[e]
		90 min; 25°C; (-) ^[c]	30 min; 25°C; (58) ^[f]
27		5 min; 45°C; (19) ^[c]	5 min; 25°C; (24) ^[e]
		60 min; 25°C; (6) ^[d]	30 min; 25°C; (56) ^[e]
28		5 min; 45°C; (19) ^[c]	5 min; 25°C; (25) ^[e]
		60 min; 25°C; (4) ^[d]	30 min; 25°C; (52) ^[e]
29		5 min; 45°C; (-) ^[c]	5 min; 25°C; (3) ^[e]
		30 min; 25°C; (-) ^[c]	30 min; 25 °C; (22) ^[e]
30	<i>t</i> -BuNH-	5 min; 45°C; (11) ^[d]	5 min; 25°C; (5) ^[e]
		60 min; 25°C; (-) ^[d]	30 min; 25°C; (31) ^[e]
31	HO-(CH ₂) ₂ S-	60 min; 45°C; (39) ^[c]	30 min; 25°C; (2) ^[e]
		90 min; 25°C; (-) ^[d]	60 min; 25°C; (12) ^[e]

[a] Reaction time T/°C, CH₃CN:H₂O=1:1, [**15**] or [**19**]= 5x10⁻⁴M, [Hnu]=5x10⁻³ M, kept in the dark. [b] Reaction time T/°C, CH₃CN:H₂O=1:1, [**15**] or [**19**]= 5x10⁻⁴M, [Hnu]=5x10⁻³ M, 310 nm irradiation. Reaction yields (%) are reported in parenthesis. [c] Condition A, carbonate buffered (pH ≥ 8.5). [d] Condition A, not buffered. [e] Condition B, not buffered. [f] Condition B, carbonate buffered (pH ≥ 8.5)

Laser Flash Photolysis (LFP).

We have been able to infer the nature of the key transient species (QMs) studying the photoactivation of the NIs **16** and **19** by product distribution analysis and investigating the

parallelism between the photo activation and the base catalyzed process. Nevertheless, from the above, we could not get any direct evidence regarding the generation of short-living species acting as precursor of the alkylating QM, in the early events after excitation of the NIs. Therefore, we performed a study of **16** and **19** by LFP. Photolysis of an argon-purged acetonitrile solution of **16** ($5 \times 10^{-4} \text{M}$) resulted in a transient spectrum exhibiting, at pulse end, an absorption centered at 470 nm (**Figure 19**). This transient decaying with the rate constant $k = 3.6 \times 10^6 \text{ s}^{-1}$ (τ 280 ns) in Ar-purged CH_3CN , that was quenched by O_2 was assigned to the triplet state of **16**, on the basis of published triplet-triplet absorption spectra of similar NIs.^{231,232} The quantitative effect of O_2 on the triplet lifetime is reported in **Figure 20a** (Air purged CH_3CN , $k = 6.33 \times 10^6 \text{ s}^{-1}$, $\tau = 158 \text{ ns}$; O_2 purged CH_3CN , $k = 1.22 \times 10^7 \text{ s}^{-1}$, $\tau = 82 \text{ ns}$). A longer timescale ($> 1 \mu\text{s}$) revealed the evolution of the triplet into a blue shifted transient absorption, centered at 410 nm with a broad and weak absorption around 700 nm. **Figure 20b** shows the parallel time course of the absorbance at both wavelengths 470, 410 and 700 nm. At the shorter wavelength, the formation kinetic of this transient was seen, and this buildup was mirrored by the decay at 470 nm.

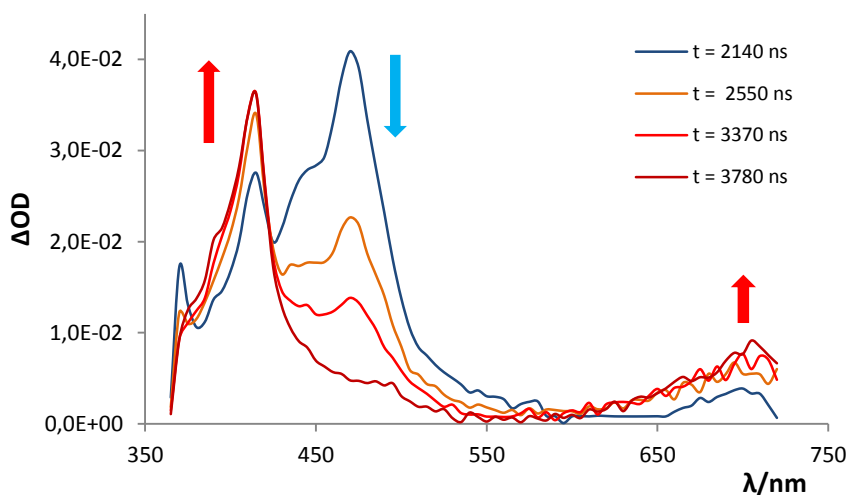


Figure 19. Transient absorption spectrum of **11** in oxygen free CH_3CN , recorded 2.14, 2.55, 3.37 and 3.78 μs after the 355 nm laser pulse.

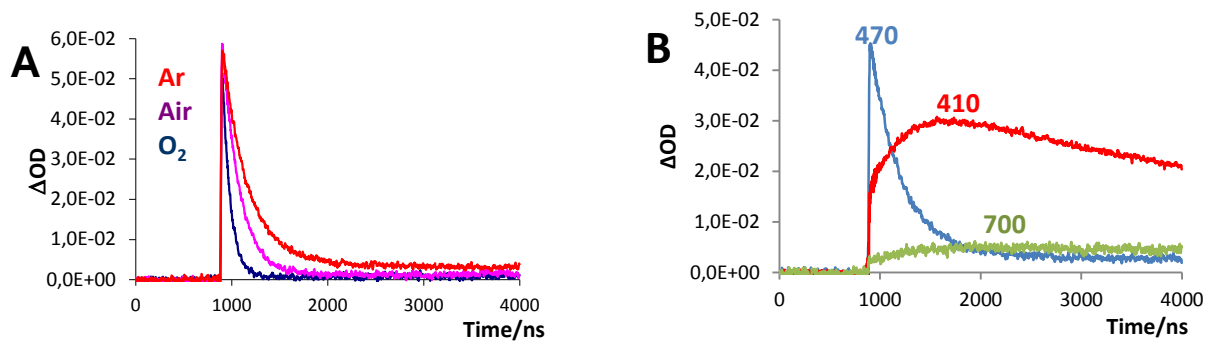


Figure 20. (a) Decay traces at 470 nm recorded flashing at 355 nm a CH₃CN diluted solution of **11** (5×10^{-4} M) under Argon (red), air (fuchsia) and oxygen (blue line). (b) Overlapping decay traces at 410, 470 and 700 nm, under Argon.

The transient that was generated from the decay of the triplet excited state, with a maximum absorbance at 410 nm, exhibited a longer lifetime $\tau = 22.3 \mu\text{s}$ ($k = 4.48 \times 10^4 \text{ s}^{-1}$) and it was partially quenched by O₂ (Air purged CH₃CN, $k = 6.29 \times 10^6 \text{ s}^{-1}$, $\tau = 158 \text{ ns}$; O₂ purged CH₃CN, $k = 2.02 \times 10^7 \text{ s}^{-1}$, $\tau = 49.6 \text{ ns}$). The oxygen did not bleach completely the transient centered at 410 nm leaving a decay trace that did not returned back to zero absorbance. Recording a full transient spectra in the presence of O₂ (**Figure 21**) it became clear that a second weaker transient centered at 390-400 nm (retaining the broad band at 700 nm) was present, but it was partially hidden by the intense absorbance at 410 nm in the absence of O₂. The absorption spectra of the transient centered at 410 nm was almost super imposable to the published NI radical anion spectra (NI⁻, $\lambda_{\text{max}} 410 \text{ nm}$).²³³ This spectroscopic evidence, together with its quenching by O₂, suggests that the intense absorbance at 410 nm has to be ascribed to the radical anion of the NI **16** (**16**⁻). The weaker transient absorbance centered at 390-400 nm (clearly visible only in the presence of O₂) together with the broad absorption around 700 nm have been assigned to the phenoxyl radical of the Mannich base moiety (**16**), due to its similarity to phenoxyl radical spectra already published.^{234,235} Such a radical is stable in a ms timescale in the presence of O₂, which efficiently

quenched the radical anion $16^{\cdot-}$, but in the presence of the radical anion $16^{\cdot-}$ (Ar-purged CH_3CN) it became a short living transient with a lifetime $\tau = 67\mu s$ ($k = 1.49 \times 10^4 s^{-1}$).

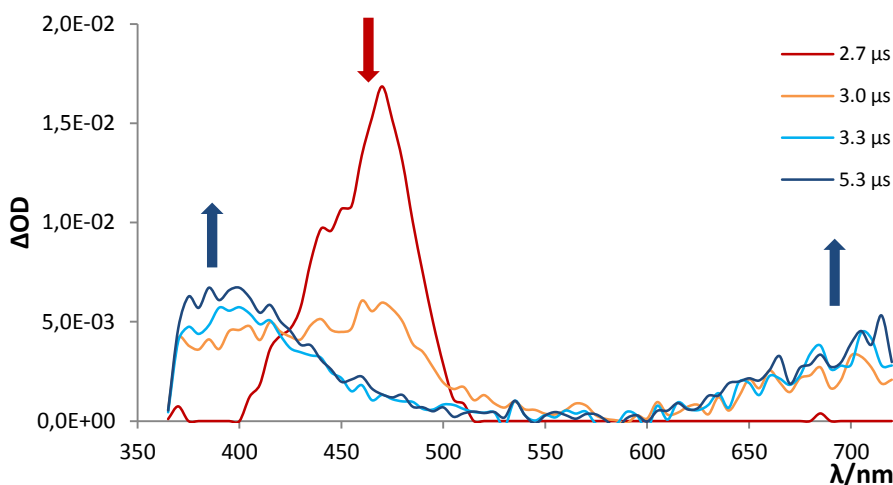


Figure 21. Transient absorption spectrum of **11** in an oxygen saturated CH_3CN solution recorded 2.7, 3.0, 3.3 and 5.3 μs after the laser pulse.

LFP of **11** was then carried out in diluted aqueous CH_3CN containing a variable amount of water from 5 mM to 100 mM. After the laser pulse all the transient due to (i) the triplet, (ii) the NI radical anion $16^{\cdot-}$ and (iii) the phenoxyl radical were observed at 470, 410 and 700 nm respectively. In aqueous CH_3CN the triplet lifetime was unaffected; conversely both the transients absorbing at 410 nm ($16^{\cdot-}$) and 700 nm (16^{\cdot}) showed a strong water dependence on their lifetimes. In more details, both ($16^{\cdot-}$) and (16^{\cdot}) decay at the same rate following a second order kinetic in CH_3CN solutions, in which the increasing of the water concentration from 5mM to 50mM is responsible of a dramatic reduction of both their lifetimes (on a 4 μs timescale). Nevertheless, for water concentrations $\geq 75mM$, the formation of a third species with an absorption tail at 410 nm, partially overlaps, at microsecond timescale, with the $16^{\cdot-}$ absorption. Such a physical limit, hampered a systematical study of the water effect on the kinetic decays for the above transients but, on the other hand, suggested that parallel decay of both $16^{\cdot-}$ and 16^{\cdot} generating a third species.

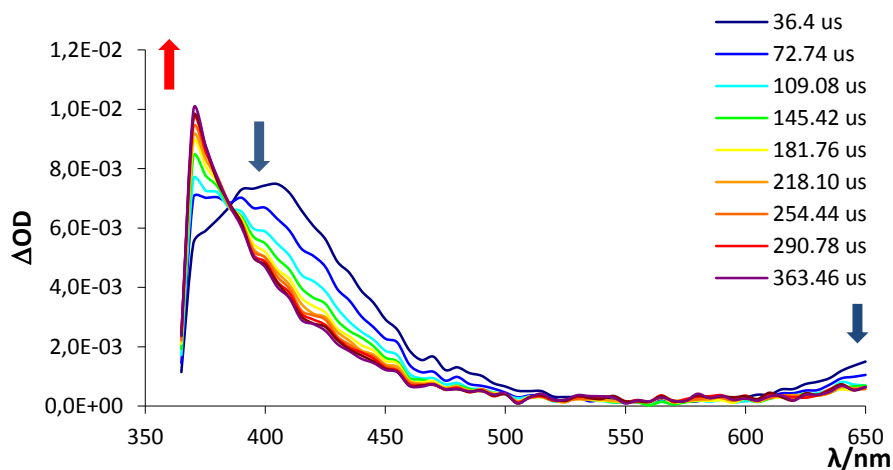
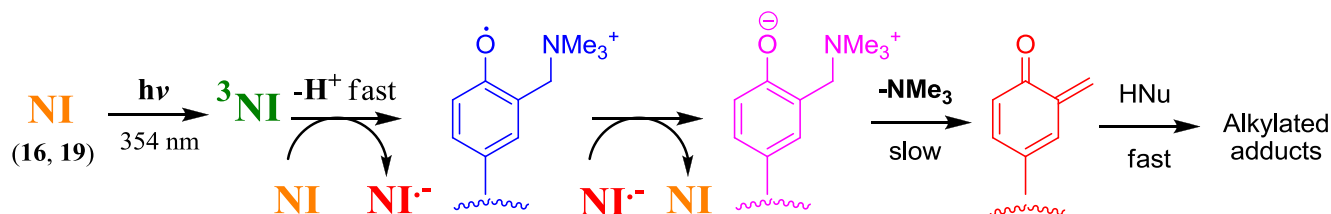


Figure 22 Transient absorption spectrum of **11** in an oxygen free CH_3CN solution recorded from 36.4 to 363.5 μs after the laser pulse.

In fact, longer timescale ($> 30 \mu\text{s}$) revealed the parallel evolution of $\mathbf{16}^-$ and $\mathbf{16}^\cdot$ into a blue shifted (370 nm) stable absorption (on our detection time scale) and a broad tail up to 450 nm (**Figure 22**). The straightforward comparison with the UV-Vis spectra differential of **16** under basic (pH 12) and in neutral (pH 7) conditions, suggested that the last absorbance has to be ascribed to the conjugate based of **16**. Such experimental evidence could easily justify the water effect observed in the photochemical generation of the phenolate anion. Nevertheless, the phenolate anion generation has also been observed in organic solvents. Indeed, $\mathbf{16}^-$ generation by laser pulse at 355 nm, has been monitored by UV-Vis spectroscopy in pure organic solvents such as CH_3CN , in which it showed stability over hour time scale. We finally investigated the reaction order of the PET reaction, with the aim to clarify if an *intra* or *inter* molecular process was involved. Surprisingly, we found concentration dependence for the triplet, radical anion and phenoxyl radical decays, suggesting that the photo reactivity was mainly due to an intermolecular PET (**Figure 22a**). The NI **14** exhibited a very similar LFP behavior, with the generation of (i) the triplet excited state of **19**, (ii) its NI radical anion $\mathbf{19}^-$ and (iii) the homologue phenoxyl radical $\mathbf{19}^\cdot$ observed at 470, 410 and 700 nm respectively. Therefore, the photoreactivity of both **15** and **19** has to be rationalized according to the mechanism depicted in **Scheme 16**, where the final

phenolate anions (**16⁻** and **19⁻**) decompose to give the alkylating QMs as confirmed by the product distribution analysis which are superimposable to those arising from the base catalyzed process. In this photochemical process, water revealed to be crucial for the QMPs decomposition into the QMs. In fact, the phenolate generation has also been observed in neat organic solvents, but no alkylating reactivity is associated with its formation under these conditions.



Scheme 16 The Intermolecular PET Mechanism Triggering the QM Reactivity.

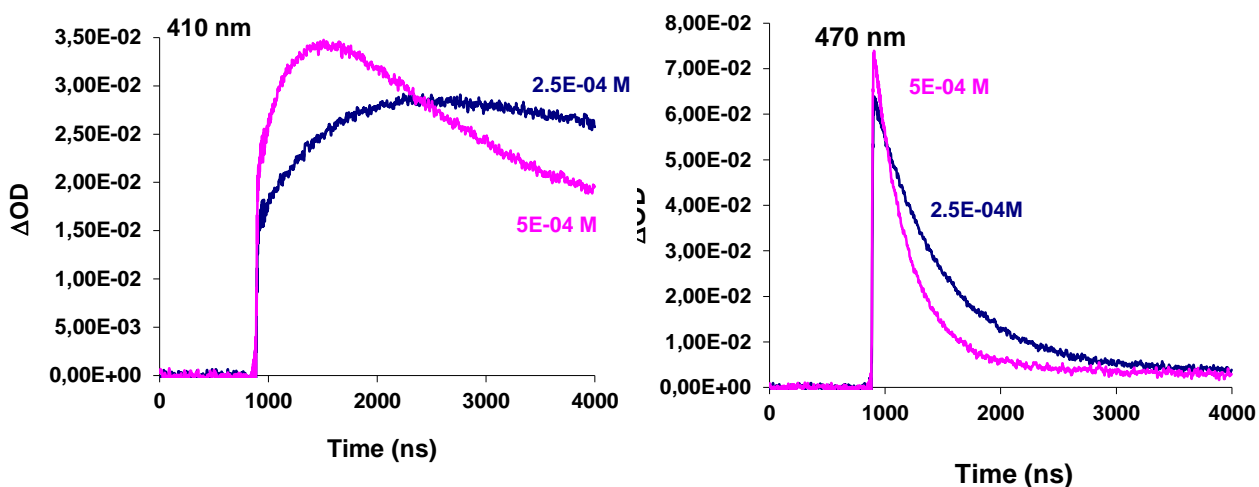


Figure 22a: Concentration dependence on the kinetics of both transient centred at 410 nm and 470 nm.

Therefore, according to the experimental evidences, we could rationalize the reactivity observed with an intermolecular PET process, which generates a couple of radical ions NI^- QMP^+ . The presence of a proximal quaternary ammonium salt moiety, strongly increases the acidity of the phenolic radical cation,²³⁵ which undergoes fast deprotonation. Thus, efficiently hampers the charge recombination process, forcing the system through an intermolecular electron transfer

pathway, generating **NI-QMP[•]**. Indeed, according to the already reported reduction potentials of phenoxyl radicals,²³⁶ as well as the good reductive character of the **NI⁻**,²³⁷ the reduction of the phenoxyl radical to phenolate results a very favored process. Such a mechanism is consistent with the poor reactivity observed in the presence of radical scavengers and oxidants such as thiols and oxygen.

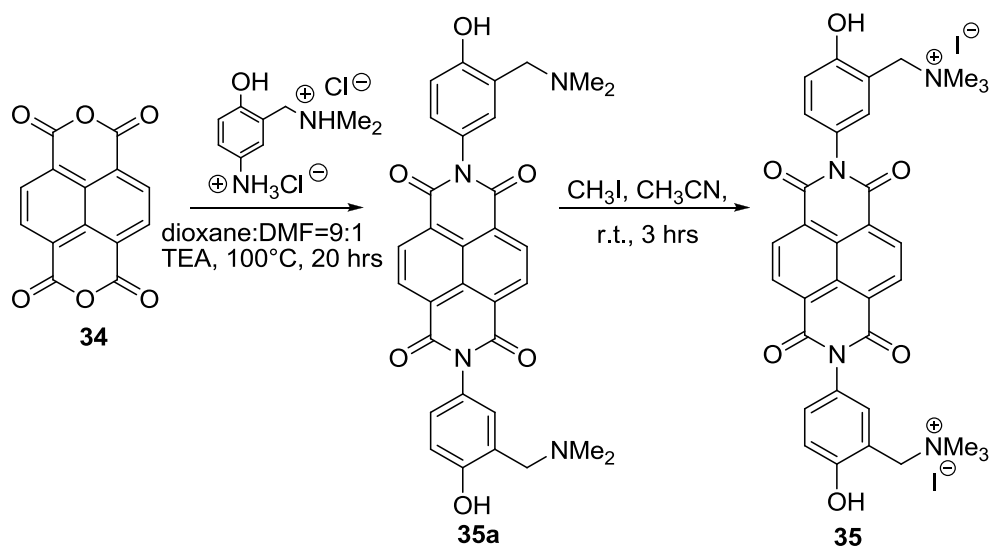
NDIs as Activable Precursors of bis-Alkylating Agents by Reduction.

Derivatives of 1,4,5,8-naphthalene tetracarboxylic diimides (**NDIs**) and perylene analogues have been extensively studied in recent decades owing to their interesting photophysical properties^{238,239} and their applications as molecular probes with recognition properties toward guanine rich oligonucleotides by intercalation, or end-stacking.^{240,241} In many cases such binding interactions function to stabilize duplex, triplex, or tetraplex structures, and it may contribute to stabilize complexes designed for gene-specific regulation of protein expression, as well as therapeutic agents.²⁵ Selective covalent modification of nucleotides has been achieved tethering these naphthalimides with molecular moieties exhibiting alkylating reactivity.²⁴²

Synthesis of bis-alkylating NDIs triggerable by reduction.

Because of the thermal instability of the quaternary ammonium salts already described in this work, at the beginning, the bisimide **35** was synthesized by a three steps procedure starting from the coupling of the anhydride **34** to *p*-aminophenol, followed by Mannich reaction and CH₃I methylation, exploiting a synthetic route similar to that used for the NIs derivatives. Due to solubility problems of the intermediate imide and also to poor yield in the Mannich reaction step (mainly due to the formation of both mono- and bis-CH₂NMe₂ adducts), the adduct **35** was synthesized in higher yield by a two steps procedure, starting from the coupling of the anhydride

34 to the preformed Mannich base 4-amino-2-dimethylaminomethyl-phenol generated in situ from its dichloride salt, followed by methylation (**Scheme 17**).



Scheme 17. Synthesis of **35** developed during this PhD work.

After the synthesis of **35** has been achieved, we began to investigate the activation of such NDI as bis-alkylating agents, under mild conditions. Two different activation protocols have been used: (i) base catalysis and (ii) a new $\text{S}_2\text{O}_4^{2-}$ reduction. In both cases we performed the reaction of **35** at both 25 and 40°C in the presence of several nucleophiles (thiols and amines), in aqueous solutions.

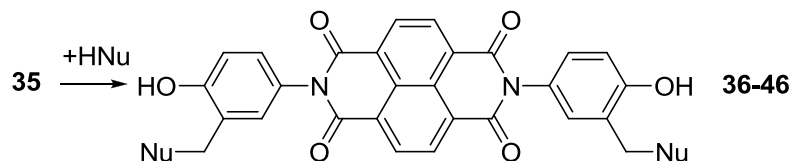
Base catalytic activation.

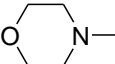
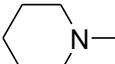
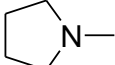
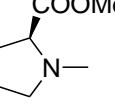
Activation by base catalysis takes advantage of the low pKa (~8) of the quaternary ammonium salts of the Mannich bases, which allows the generation of a reactive zwitterionic form at $\text{pH} \geq 8$, thus efficiently generates alkylating QM (**Scheme 18**).

Basic amines such as piperidine, pyrrolidine and diethylamine ($\text{pK}_a > 10.7$) gave almost quantitative conversion under mild conditions (25°C, in $\text{CH}_3\text{CN}:\text{H}_2\text{O}=1:1$; reaction condition A, **Table 4**). Amines displaying lower basicity ($\text{pK}_a \leq 8$), such as morpholine and L-proline methyl ester, require higher temperature (40°C), carbonate buffered conditions ($\text{pH} \geq 8.5$, reaction

condition B **Table 4**) and longer reaction times. **35** is much less reactive in the absence of basic nucleophiles, affording the diol **36** in low yield only in the presence of carbonate buffer at pH 8.5. In the presence of aniline (pKa 4.6), adduct **46** formation was detected at 40°C after 24 hrs, only under buffered conditions. In the absence of good nitrogen nucleophiles the reaction was sluggish and beside unreacted starting material an uncharacterized oligomeric product was formed. Monoalkylated adducts were not detected by HPLC under the reaction condition described, and therefore, if they formed at all, their yields were very low (i.e., <5%).

The results described above suggest that the activation of **35** as bis-alkylating agent at r.t. is efficient only under strong basic conditions (pH>8.5), when the phenol is mainly deprotonated. This suggests that, similarly to the prototype quaternary ammonium salt **2a**, also for the QMP **35** the zwitterionic form has to be populated to lower the barrier for the QM generation. Beside the pure kinetically aspects the above results suggest that molecule **35** could act as reversible G-4 ligand at r.t, whereas at 40 °C a dual alkylating/reversible effects should be observed. Although the last statement is an assumption based on the chemical experiments, which do not take in count the entropic effects, at least theoretically a big difference in binding properties should be observed in the range between 25 and 40 degrees. Moreover, exploiting the reductive activation protocol such an effect will be empathized in terms of discrimination between alkylation contribution and reversible one. A detailed study of the chemical reactivity of molecule **35** in both thermal and reductive conditions, is crucial to understand an unravel its potential as selective G-4 cross linking agent.

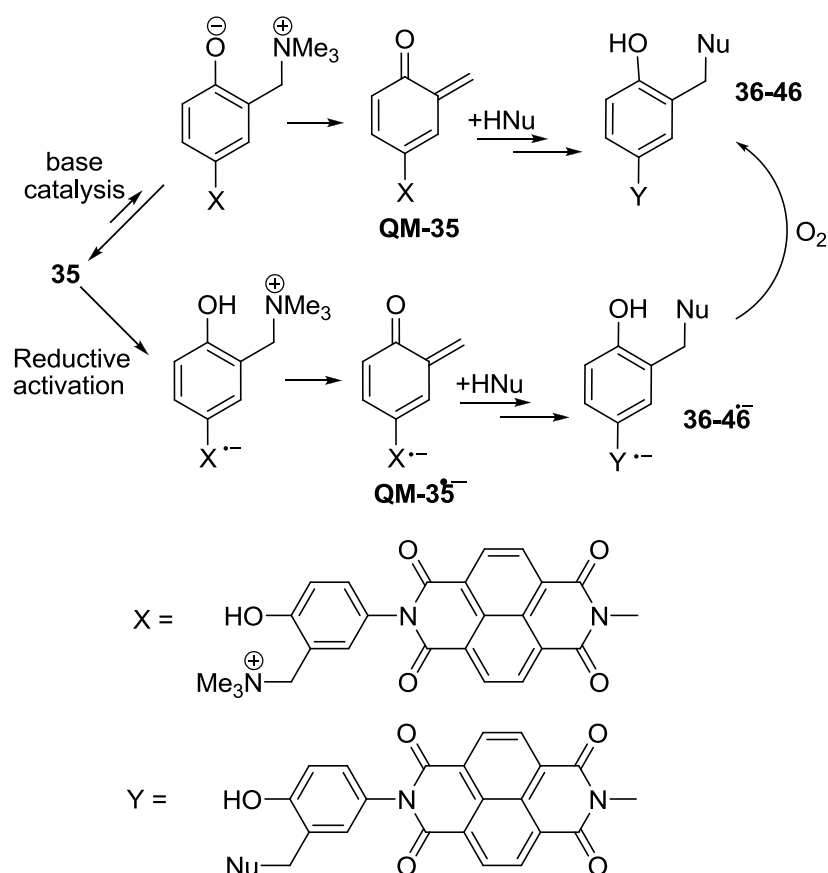
Table 4. Reactivity of **35** by base catalysis and S₂O₄²⁻ reduction.

Adduct	Nu	Base Catalyzed Activation	Reductive Activation
		Conditions, (Yield) ^[a]	Conditions, (Yield) ^[b]
36	HO-	4h; 40°C; (15) ^[c] 2h; 25°C; (-) ^[c, d]	2h; 25°C; (55)
37	Et ₂ N-	1h; 40°C; (85) ^[e] 0.5h; 25°C; (10) ^[e]	0.5h; 25°C; (86)
38	Et-N ₁ -Bu	0.5h; 40°C; (90) ^[e] 0.5h; 25°C; (24) ^[e]	0.5h; 25°C; (90)
39	iPr ₂ N-	0.5h; 40°C; (90) ^[e]	0.5h; 25°C; (93)
40		1h; 40°C; (75) ^[c] 0.5h; 25°C; (16) ^[c]	0.5h; 25°C; (95)
41	<i>t</i> -BuNH-	4; 40°C; (65) ^[e]	0.5h; 25°C; (70)
42		1; 40°C; (95) ^[e]	0.5h; 25°C; (90)
43		1; 40°C; (85) ^[e]	0.5h; 25°C; (90)
44		4; 40°C; (65) ^[c] 1; 25°C; (10) ^[c]	1h; 25°C; (75)
45	<i>t</i> -BuS-	0.5; 40°C; (85) ^[c]	0.5h; 25°C; (80)
46	PhNH-	24; 40°C: (20) ^[c] 24; 40°C: (-) ^[e, d]	2; 40°C: (56)

[a] Reaction time/hrs, T/°C, CH₃CN:H₂O=1:1, [4]= 5x10⁻³M, [HNu]=5x10⁻² M. [b] Reaction time/hrs, T/°C, CH₃CN:H₂O=1:1, in the presence of Na₂S₂O₄ 10⁻²M, [4]= 5x10⁻⁴ M, [HNu]=5x10⁻³M. Reaction yields (%) are reported in parenthesis. [c] Condition B, carbonate buffered (pH ≥ 8.5), as reported in the experimental. [d] Undetected by HPLC. [e] Condition A, not buffered.

Reductive activation.

The second activation procedure should switch the electron properties of the NDI moiety from strongly withdrawing to donating by mono-electronic reduction, with formation of the NDI radical anion. Very interestingly, the activation of **35** as bis-alkylating agent became even more facile under chemical reduction by dithionite anion ($S_2O_4^{2-}$), both in absence and in the presence of nucleophiles, yielding the adducts **36-46**, after incubation at 25°C, followed by workup with O_2 . Oxygen oxidizes the adducts generated as radical anions ($36^{\cdot-}$ - $46^{\cdot-}$) to the stable adducts (**36-46**), also quenching the excess of dithionite anion (**Scheme 18**).



Scheme 18. Base catalytic and reductive activation of **35** as bis-alkylating agent through the generation of **QM-35** and **QM-35 $^{\cdot-}$** , respectively.

The conversions into adducts **36-46** were obtained at lower temperature and shorter reaction time in comparison to the thermal incubations in the absence of dithionite. Data in **Table 4** show

that the reductive condition activates the bis-alkylation process by diimide **35**. Such an activation is effective also with less basic nucleophiles namely L-proline methyl ester and aniline. Thus the diimide **35** does not react with aniline in aqueous acetonitrile at 40°C for one day, but it undergoes bis-alkylation under $S_2O_4^{2-}$ reducing conditions. **35a**, unlike **35**, is stable under both base catalysis and $S_2O_4^{2-}$ reduction.

The reactivity as bis-alkylating agent of the NDI **35** is related to its favorable redox properties, which were characterized by cyclic voltammetry (**Table 5**). Both the amine **35a** and its quaternary ammonium salt **35** exhibit two one electron reduction peaks. In DMF, using Bu_4NBF_4 , compound **35a**, used as dichloride salt, showed two redox couples at -0.46 V and -0.96 V (vs Ag/AgCl/KCl). Although the first wave is perfectly reversible (in the sense that the peak separation for the reductions is exactly 60 mV), the second reduction is slightly less reversible (peak separation 120 mV). Apparent E^0 values in **Table 5** were taken as the center of the anodic and cathodic peak potentials and are consistent with those reported for other aromatic imides.²⁴³ Compound **35**, with quaternary ammonium groups had reduction potentials at slightly more positive potentials, -0.40 V and -0.85 V, but both reduction processes were strongly irreversible, with dependence on the sweeping rate (peak separation >180 mV and 300 mV at 200 mV/s). Although in aqueous solution both substrates are more easily reduced (**Table 5**), the compounds **35a** and **35** behave similarly to that described for the DMF solution. The process is chemically reversible for the amine **35a** and chemically irreversible for the quaternary ammonium **35**. In fact, after a few redox cycles the amine **35a** was recovered unreacted, unlike the quaternary ammonium **35** which was completely consumed, with diol **36** as the only detectable adduct (yield 20%). After a few redox cycles in an acetonitrile:water=1:1 solution containing morpholine (10^{-2} M), the quaternary ammonium **35** was converted into the adduct **40** (yield >80%).

Table 5. Redox properties of the NDI derivatives **35** and **35a**.

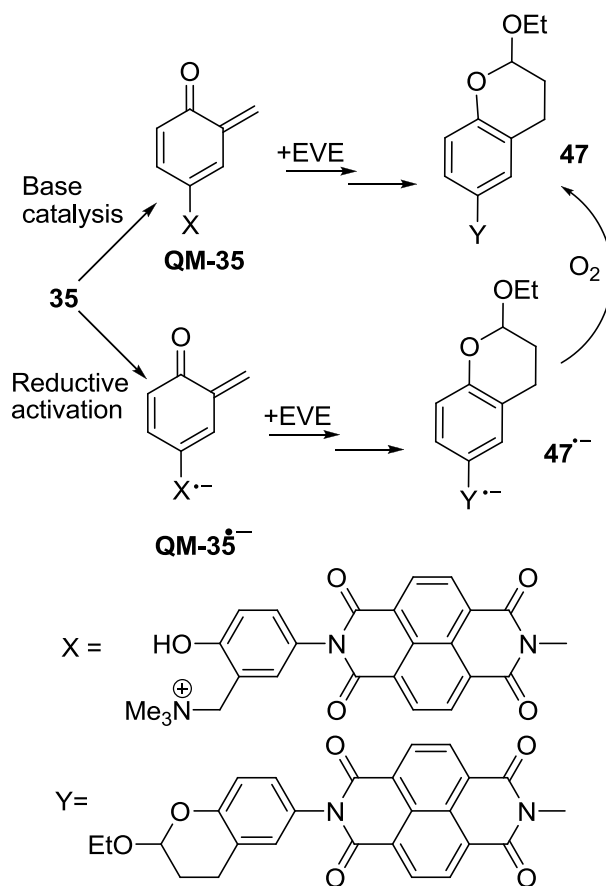
NDI	DMF		CH ₃ CN:H ₂ O=1:1	
	Bu ₄ NBF ₄ 0.1M		Bu ₄ NBF ₄ 0.1M	
	E _{1/2} ^{o[a]}	E _{1/2} ^{o[b]}	E _{1/2} ^{o[a]}	E _{1/2} ^{o[b]}
35	-0.40	-0.85	-0.32	≤-0.65
35a	-0.46	-0.96	-0.44	≤-0.85

[a] First wave potential (NDI/NDI^{•-}). [b] Second wave potential (NDI^{•-}/NDI²⁻). E_{1/2} values in V, were taken as the center of the anodic and cathodic peak potentials, vs Ag/AgCl/KCl (4 M KCl saturated with AgCl).

Diels-Alder reactivity of the transient electrophile.

In order to clarify the nature of the electrophilic intermediate involved in the alkylation process, we run two set of experiments in the presence of EVE (ethyl vinyl ether), under basic catalysis and reductive activation. Similarly to what we found for the NIs study, **35** gave the adduct **47** as the main adducts under (i) basic conditions (pH 9, CH₃CN/H₂O) at 40°C and (ii) in the presence of S₂O₄²⁻ at r.t. pH 7, followed by oxygen quenching (**Scheme 18**).

The formation of the adducts **36-47** by base catalysis is rationalized by the generation of a transient electrophilic QM (**QM-35**) from the reactive zwitterionic form, followed by nucleophile (**Scheme 18**) or EVE trapping in an hetero Diels-Alder [4+2] cycloaddition (**Scheme 19**). The formation of the same adducts **36-37** by reduction, following oxygen quenching, reveals that it is possible to switch the electron properties of the NDI as a substituent to a **QMP**, from electron withdrawing to donating group simply by monoelectronic reduction. In this way it has been possible to generate a QM directly tethered to a NDI radical anion (**QM-35^{•-}**), which retains electrophilicity at the exocyclic methylene group and heterodiene reactivity as the prototype *o*-QM.



Scheme 19. Reactivity of **QM-35** and **QM-35^{•-}** as heterodiene in an [4+2] cycloaddition.

Detection of the transients by UV-vis-spectroscopy.

The QM generation by base catalysis had been previously rationalized, thus we decided to corroborate the generation of a similar electrophilic intermediate by chemical reduction, producing further independent evidences. To this end we managed to achieve the activation of **35** as bis-alkylating agent by coulombometric reduction at $E = -0.5\text{V}$ [vs Ag/AgCl/KCl (4 M KCl saturated with AgCl)]. In fact, under these conditions, the salt **35** was efficiently consumed affording the diol **36** as the only detectable adduct in aqueous acetonitrile, after O_2 workup. A similar experiment performed with morpholine (10^{-2} M) afforded only the adduct **40** in quantitative yield. The electrochemical reduction was also monitored as function of the time, by UV-visible spectroscopy, which revealed two sequential transient species on the time scale of few

hours. The reduction of **35**, in CH₃CN:H₂O=1:1, bleached the reactant absorbance (360 and 378 nm) generating a new specie with maximum absorbance centered at 458 nm (**Figure 23a**). Such a transient was assigned to the radical anion of the diimide **35** (**35^{-•}**) on the basis of (i) its rapid quenching in the presence of O₂, (ii) the spectroscopic similarity to NDI radical anions, bearing cationic substituents to the imide nitrogen atom [such as -(CH₂)_nNMe₃⁺ (λ_{max} 449nm)],²⁴³ generated by electrochemical reduction and by intramolecular photoinduced single electron transfer.²⁴⁴ The radical anion **35^{-•}** decays with a first order kinetic (k₁=8.1x10⁻⁴s⁻¹, r²=0.99), in the absence of O₂, to generate another specie with absorbance centered at 412, 542 and 590 nm (**Figure 23b**).

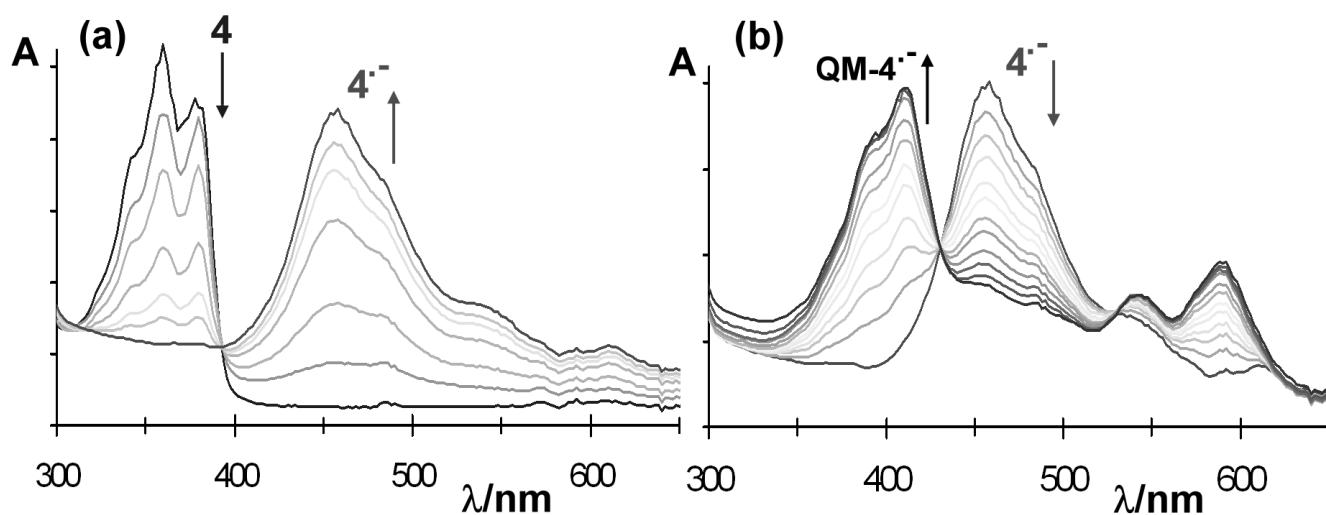


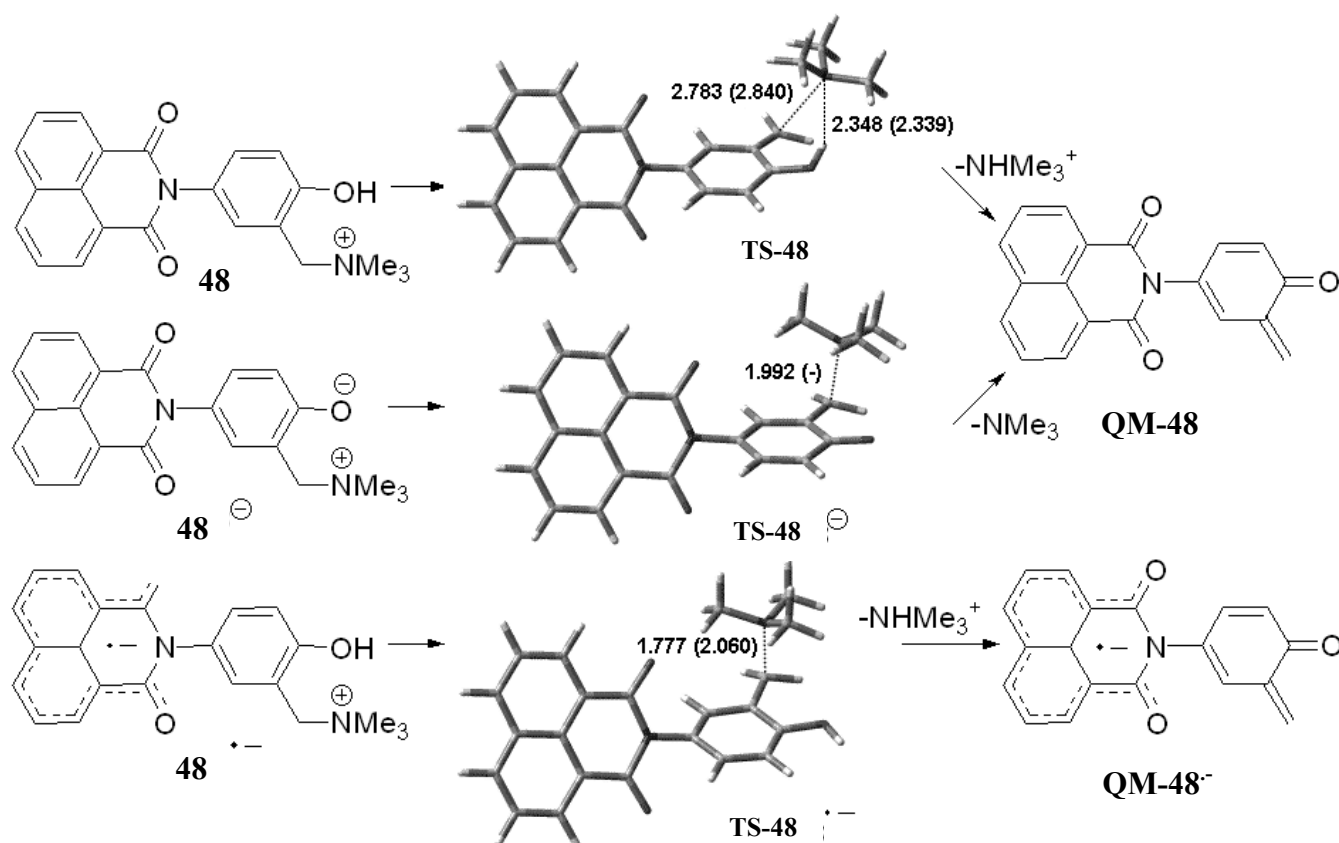
Figure 23 Generation, from 0 to 20 min. (a) and reactivity, from the following 2 hrs (b), of **4^{-•}** monitored by UV-visible spectroscopy.

This UV-vis spectrum display the features of both the radical anion NDI^{-•} (542 and 590 nm) and the *ortho*-QM (410 nm).²⁴⁵ This species decays within few hrs under aqueous acetonitrile, in the absence of O₂, and it is rapidly quenched by O₂, morpholine and EVE. The electrolyzed solution of **35** in the presence of morpholine (10⁻³ M) and EVE (10⁻² M), after 30 min at r.t. and work-up with O₂, gave the adducts **40** and **47**, respectively, in good yields (≥85%), with no hydration adduct **46** detected. Therefore, we assigned the absorbance of this specie to a QM tethered to a NDI^{-•} (**QM-35^{-•}**), displaying benzylating reactivity. Similarly, the NDI **35a** can be easily reduced

to its radical anion ($35a^-$) with $\lambda_{\max}=473$ nm, which unlike 35^- is stable in the presence of nucleophiles in aqueous acetonitrile. Such an evidence is in accord with the lack of reactivity of $35a$ in preparative experiments.

Computational evaluation of the basic and reductive activation processes.

The final proof that NDIs tethered to quaternary ammonium salts of a Mannich bases are activable QMP by both base catalysis and monoelectronic reduction, was given by a computational investigation at R(U)B3LYP/6-31+G(d,p) level of theory both in gas phase and in aqueous solution (by PCM solvation model) on the model imide **18** (Scheme 20).



Scheme 20. Generation of QM-48 and QM48^{•-} through the TSs TS-48, TS-48⁻ and TS-48^{•-}. Bond lengths are in Å. Data in parentheses are for full R(U)B3LYP/6-31+G(d,p) optimization in aqueous solution.

The activation free energies computed both in gas phase and in aqueous solution (**Table 6**), suggest that the generation of an alkylating QM (**QM-48**) becomes a much easier process passing from the protonated quaternary ammonium salt **48** to its zwitterionic form **48⁻**. The catalytic effect of the base is massive both in gas phase and in solution (>30 kcal/mol). The reduction of the naphthalimide moiety to its radical anion **48^{-•}**, which generates the QM tethered to the imide moiety **QM-18^{-•}**, also induces a similar activation, lowering the barrier in the gas phase by 35 kcal/mol. Geometry optimization in the solvent bulk of the **TS-18** and **TS-18^{-•}** suggest a slightly lower catalytic effect, since the activation free energy in aqueous solution is reduced by 29.5 kcal/mol. We were unable to optimize **TS-18^{-•}** in aqueous bulk, therefore for this **TS** we only compute the solvation by single point calculation on B3LYP/6-31+G(d,p) gas phase geometry.

Table 6. Activation free energy in gas phase and in aqueous solution at R(U)B3LYP/6-31+G(d,p) level of theory, for the generation of the QMs starting from **48**, its anion **48⁻** and its radical anion **48^{-•}**.

QMP	$\Delta E^{[a]}$	$\Delta G_{\text{gas}}^{[b]}$	ΔG_{aq}
48	37.0	32.1	46.5 ^[c]
			41.1 ^[d]
			41.4 ^[e]
48⁻	3.7	1.0	- ^[f]
			8.5 ^[d]
			8.5 ^[e]
48^{-•}	3.8	1.4	17.0 ^[c]
			6.3 ^[d]
			6.7 ^[e]

[a] Activation electronic energies in kcal/mol. [b]. Activation free energies in gas phase. [c]. Optimized in aqueous solution at R(U)B3LYP/6-31+G(d,p) using PCM (UA0 radii) solvation model. [d] Single point calculation at B3LYP/6-31+G(d,p) on gas phase geometries (UA0 radii). [e] Single point calculation at B3LYP/6-31+G(d,p) on gas phase geometries (UAHF radii). [f] We failed to locate the TS-18.- in aqueous solution.

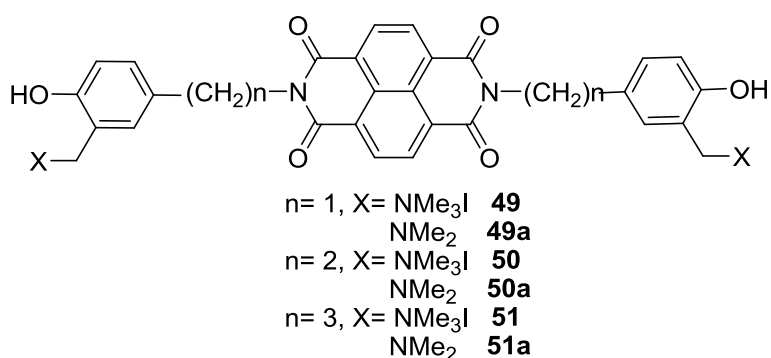
New NDIs Tethered to Quinone Methides as Selective G-4 Alkylating Agents.

The described activable bis-alkylating properties of the NDI moiety tethered to a quaternary ammonium salt of Mannich base exploring mild reduction protocols has been thought as bio-applicable. In addition, owing to the NDI recognition properties, these results suggested applications of **35** and its derivatives as triggerable and selective cross-linking agents toward guanines rich oligonucleotides. Although the reductive mono-electronic activation is unique and bio-friendly, compound **35** revealed unemployable for G-4 targeting. Such a limit has been rationalized analyzing the molecular shape of NDI **35**. Indeed, the orthogonal conformation between the QMP and the NDI core strongly depress the possibility of superficial π -stacking. Therefore, the G-4 binding properties of molecule **35** were negligible. Because of that we decided to investigate a new class of NDIs derivatives in which flexible methylene spacers separate the QMP from the NDI core, conferring higher conformational freedom to the molecules. Such a chemical modification enhances the possibility to generate π -stacking interactions but, on the other hand, suppresses the reductive activation. As consequence only thermal reactivity has been achieved and observed for this class of molecules. The DNA recognition and alkylation properties of these new derivatives were investigated by gel electrophoresis, circular dichroism and enzymatic assays. The alkylation process occurred preferentially on the telomeric G-4 structure in comparison to other DNA conformations. By dissecting reversible recognition and alkylation events, we found that the reversible process is a prerequisite to DNA alkylation which, in turn, reinforces the G-quadruplex structural rearrangement.

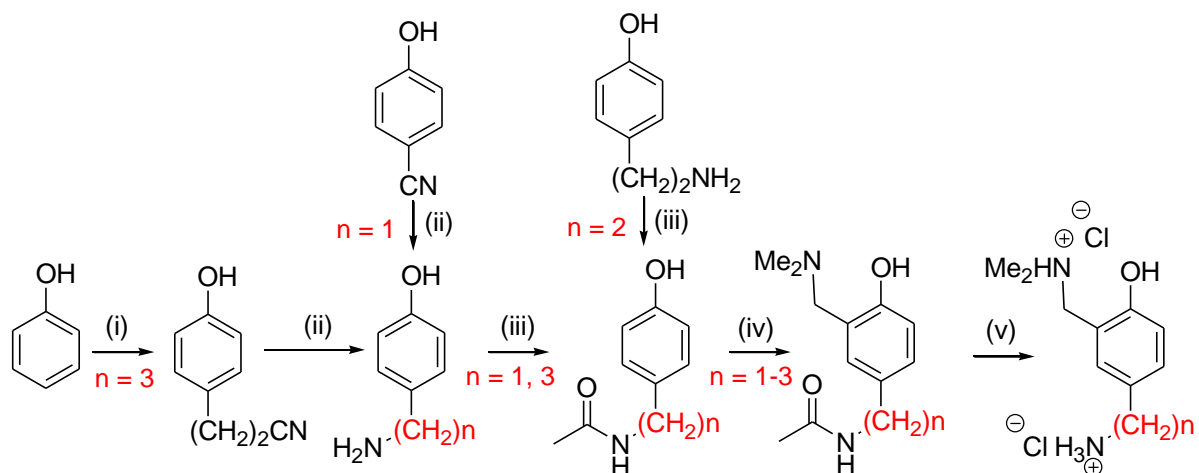
Synthesis of Naphthalene Diimides Tethered to Quinone-Methide Precursors and reactivity towards simple nucleophiles.

The quaternary ammonium salts **49-51** used as ligand-alkylating hybrid compounds were prepared by exhaustive methylation of the diamines **49a-51a** which are depicted in **Scheme 20**. The NDIs **49a-51a** were synthesized in a one-pot synthesis from the commercially available

dianhydride and 4-aminomethyl-, 4-(2-aminoethyl)- and 4-(3-aminopropyl)-2-dimethylaminomethylphenols, respectively. The above intermediates have been prepared according the general synthetic procedure depicted in **Scheme 22** and described in detail in the Experimental Section of this thesis. Although the synthetic protocols herein described are based on very simple chemistry, they have been completely explored and developed during this PhD working period. The 3 different synthetic routes have been planned in order to separate with different chemical spacers the QMP precursor from the NDI central core. In more details molecule **49**, **50** and **51** presents respectively mono, bis and tris methylene spacers between the phenolic precursor and the NDI core, as elucidated in **Scheme 21**.



Scheme 21. Bis-substituted NDIs **49-51** Exploited as G-4 Ligand-Alkylating Hybrid Compounds.



Scheme 22. Synthesis of 4-aminomethyl-, 4-(2-aminoethyl)- and 4-(3-aminopropyl)-2-dimethylaminomethylphenols, ($n = 1, 2$ and 3 , respectively). (i) Acrylonitrile as solvent, AlCl_3 .

(ii) LiAlH₄, THF, Δ , 4 hrs. (iii) Ac₂O, NaHCO₃, H₂O, r.t. (iv) paraformaldehyde, dimethylamine in anhydrous EtOH Δ , 2 hrs. (v) HCl aq. 10%, 2 hrs, Δ .

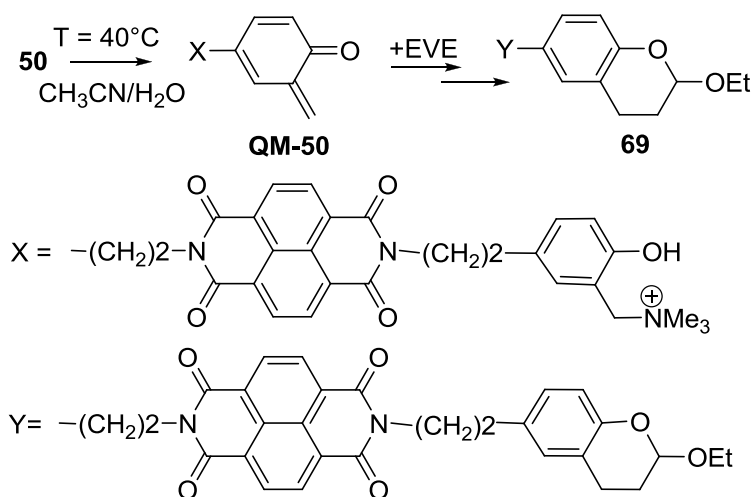
Activation and Reactivity of Naphthalene Diimides 49-51.

Our study began with the investigation of the reactivity of the NDIs **49-51** in order to define the more convenient protocol for their activation as bis-alkylating agents. We performed digestion of **49-51** at both 25 and 40°C in the presence of several simple nucleophiles (thiols and amines), in aqueous buffered and un-buffered solutions. The results of such chemical reactivity are collected in **Table 7**. As already mentioned only thermal activation protocols have been investigated for such a class of molecules. Activation by base catalysis in the presence of amines under un-buffered conditions takes advantage of the low pK_a (~7.8) of the quaternary ammonium salts of the three NDIs **49-51**, which, in the presence of basic nucleophiles, allows the generation of reactive zwitterionic forms of **49-51** at pH \geq 8. The latter promptly releases the alkylating QM (**Scheme 23**) at 25°C. In the presence of non-basic nucleophiles such as thiols a longer reaction time (6-12 hrs) is required at 40°C under neutral conditions. Specific base catalysis in buffered solutions at pH 8.5 triggered the alkylation of the less basic nucleophiles at lower temperature (25°C) affording the alkylated adducts in good yields (\geq 90%). These results are in agreement with those concerning the base activation for the above described NDI **35**.

In the absence of a nucleophile, hydration reaction occurred, affording diols **52**, **59** and **62** in low yield at 25°C. Higher yields in a shorter reaction time were achieved at 40°C. Moreover, data shown in **Table 7** suggest that the NDIs **49-51** exhibit a very similar reactivity, since they can be activated as bis-alkylating agents under the very same mild conditions (pH 7, at 40°C, for less than 12 hrs). No reactivity differences between NDIs **49-51** have been observed during these experiments, thus suggesting that the alkylation is triggered by the phenolate anion of NDIs **49-51** which is very similar for all the 3 molecules. Amines **49a-51a**, unlike their quaternary ammonium

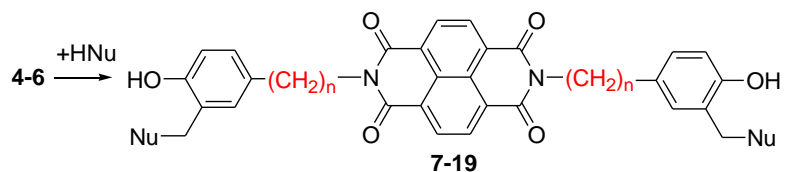
salts analogues, are stable for at least 24 hrs at 40°C at both pH 7.0 and 8.5. Therefore, they cannot generate alkylating **QMs** under these mild conditions.

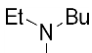
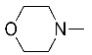
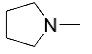
In order to unequivocally clarify the nature of the electrophilic intermediate involved in the alkylation process, we ran additional trapping experiments in the presence of EVE (ethyl vinyl ether), in acetonitrile aqueous (1:1) buffered solution. **50** gave **65** (58%, yield), as the main product, in the presence of the hydration adduct **52** (38%). Formation of the substituted 2-ethoxychroman **65** is rationalized by the generation of transient **QM** (**QM49**), trapped by EVE in a hetero Diels-Alder [4+2] cycloaddition reaction (**Scheme 23**), as already described for the previously described NIs derivatives and the NDI **35**.



Scheme 23. Bis Generation and Reactivity of the **QM-50** (tethered to the NDI moiety) as Heterodiene.

Table 7. Reactivity of **49-51** in the Presence of Nucleophiles.



Adduct	n	Nu	Conditions, (Yield %)^[a]
52	2	HO-	12h; 40°C; (25) ^[c]
			2h; 25°C; (20) ^[d]
53	2	Et ₂ N-	0.5h; 40°C; (95) ^[b]
54	2		0.5h; 40°C; (97) ^[b]
55	2		0.5h; 40°C; (85) ^[b]
56	2		0.5h; 40°C; (90) ^[b]
			2h; 25°C; (86) ^[d]
57	2	<i>t</i> -BuNH-	6h; 40°C; (88) ^[b]
58	2	<i>t</i> -BuS-	12h; 40°C; (96) ^[b,c]
			2h; 25°C; (90) ^[d]
59	1	HO-	12h; 40°C; (27) ^[c]
			2h; 25°C; (25) ^[d]
60	1	Et ₂ N-	0.5h; 40°C; (97) ^[b]
61	1	<i>t</i> -BuS-	12h; 40°C; (98) ^[b,c]
			2h; 25°C; (92) ^[d]
62	3	HO-	12h; 40°C; (30) ^[c]
			2h; 25°C; (32) ^[d]
63	3	Et ₂ N-	0.5h; 40°C; (98) ^[b]
64	3	<i>t</i> -BuS-	12h; 40°C; (95) ^[b,c]
			2h; 25°C; (94) ^[d]

[a] Reaction time/hrs, T/°C, CH₃CN:H₂O=1:1, [4]= 10⁻³M, [HNu]=10⁻² M. [b] Unbuffered [c] Buffered at pH 7.0. [d] Buffered at pH 8.5.

Alkylation of DNA Folded into a G-quadruplex.

The initial assessment of the ability of compounds **49-51** to alkylate DNA in a G-4 conformation was achieved by reacting increasing concentrations (0.25-16 μM) of compounds at 40°C for 24h in buffer Li_3PO_4 10 mM, KCl 50 mM, pH 7.4, with a ^{32}P 5'-end labeled synthetic oligonucleotide formed by four human telomeric repeats, 5'-AGGGTTAGGGTTAGGGTTAGGG-3' (4GGG). In these conditions, 4GGG can fold into an intramolecular G-4 preferentially assuming a hybrid-type (mixed parallel/antiparallel) conformation.^{246,247} The alkylated oligo was separated from the non-reacted DNA by denaturing polyacrylamide gel. Compound **50** exhibited the most promising alkylating properties, as shown in **Figures 24A** and **24C**. These data suggested that the two methylene spacers confer the ideal distance between the alkylating moiety and the NDI recognition core. When the reactivity of NDIs with different linkers was monitored, compound **49** was able to alkylate only 5% of total DNA at the highest tested concentration (16 μM), whereas compound **51** gave no appreciable adduct with 4GGG (**Figure 24C**). Additionally, compound **50a**, the amine analogue of **50**, did not generate any alkylation product, confirming that only the quaternary ammonium salt derivative is active in the test conditions (**Figure 24C**), as already observed in preparative experiments during the chemical reactivity study.

The covalent adduct was detectable at a concentration as low as 0.25 μM as depicted in lane 2, **Figure 24A** and reached 15% over total DNA at compound **50** concentration of 2 μM in lane 5. At higher ligand concentrations no further increment in the alkylated adduct was observed. This is likely related to the NDI-DNA complex precipitation (lanes 6-8) inevitably occurring under high molar ratios. Reactivity of **50** lead to maximal 4GGG alkylation adduct formation in 24 h at 40°C whereas alkylation was substantially absent at 20°C. In addition, the identified alkylation product resulted stable upon incubation at 20÷70°C. Degradation of such adducts was appreciable only at higher temperature.

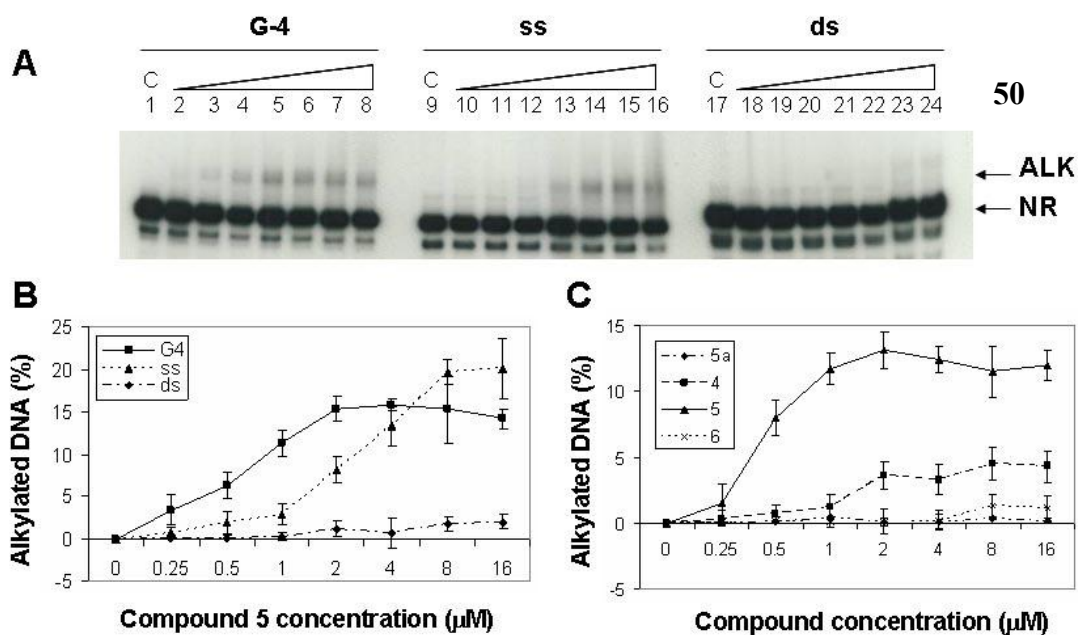


Figure 24. Specificity of NDI-mediated alkylation. **A)** Increasing concentrations of compound **50** (0.25, 0.5, 1.0, 2.0, 4.0, 8.0, 16.0 μM) were incubated with labeled 4GGG (G-4), ss-scrambled-4GGG (ss) or ds-scrambled-4GGG (ds) DNA for 24h at 40°C in Li_3PO_4 10mM, KCl 50 mM, pH 7.4. Alkylated DNA (ALK) was separated from non-reacted oligo (NR) in 20% denaturing polyacrylamide gel (8M urea). **C** refers to labeled 4GGG DNA without compound **50**. **B)** Quantification of the specificity of the alkylation experiment reported in A). **C)** Quantification of alkylation of G-4 DNA by compounds **50a**, **49**, **50**, **51**. Increasing compound concentrations (0.25, 0.5, 1.0, 2.0, 4.0, 8.0, 16.0 μM) were reacted with 4GGG DNA for 24h at 40°C in Li_3PO_4 10mM, KCl 50 mM, pH 7.4. Adducts (ALK) were separated from non-reacted DNA (NR) by 20% denaturing polyacrylamide gel.

Drug Alkylation as a Function of DNA Folding.

Selective recognition of G-quadruplex DNA by **50** was assessed by comparing its reactivity toward 4GGG with i) single stranded DNA exhibiting the same base composition of 4GGG DNA, but unable to fold into a G4 conformation (ss-scrambled-4GGG) and with ii) ss-scrambled-4GGG annealed to its complementary oligo (ds-scrambled-4GGG) (**Figure 24A**). Double stranded DNA

turned out to be the poorest substrate for **50** adduct formation. Interestingly, comparison of reactivity towards G-4 folded and ss-scrambled oligos showed a concentration window where alkylation occurs more efficiently on the G-4 folded DNA (**Figure 24B**). Indeed, at concentration below 1 μM , **50** was able to form a covalent adduct with 4GGG DNA only (lanes 2-4, **Figure 24 A and B**). Conversely, ss-stranded 4GGG was alkylated at only higher concentrations (2-16 μM) (lanes 13-16, **Figure 24 A and B**). This clearly underlines a modulation of drug reactivity upon DNA folding which is translated in terms of reactivity driven by entropic effects.

To unequivocally demonstrate that this behavior derived from a selective drug-DNA interaction, competition experiments were performed. Thus, a constant concentration of compound **50** was incubated with a fixed amount of ^{32}P 5'-end labeled 4GGG DNA in the presence of increasing concentrations of cold 4GGG, ss-scrambled-4GGG or ds-scrambled-4GGG DNA. As shown in **Figure 25**, cold 4GGG DNA was able to effectively compete for adduct formation (adduct amounts decreased to less than 2% of total labeled DNA in the presence of a tenfold excess of 4GGG DNA competitor) (lane 5, **Figure 25A and B**). On the contrary, the alkylated adduct was only modestly affected with ss and ds-scrambled 4GGG competitor DNAs as depicted in **Figure 25**. These data clearly demonstrate that compound **50** can specifically alkylate G-4 conformed DNA. Indeed, although the alkylation process could occur for ss oligonucleotides also, a marked difference has been observed for G-4 folding oligonucleotides. Such a substrate dependent reactivity has not been observed in preparative experiments with simple nucleophiles as well as with free nucleobases. This reactivity could be only justified by a molecular recognition which concentrates the alkylating molecule on the target. This data represent the very first case of molecular device capable of pre-concentration on the biological target and chemical release of an electrophilic species, as proposed in the aim of this work.

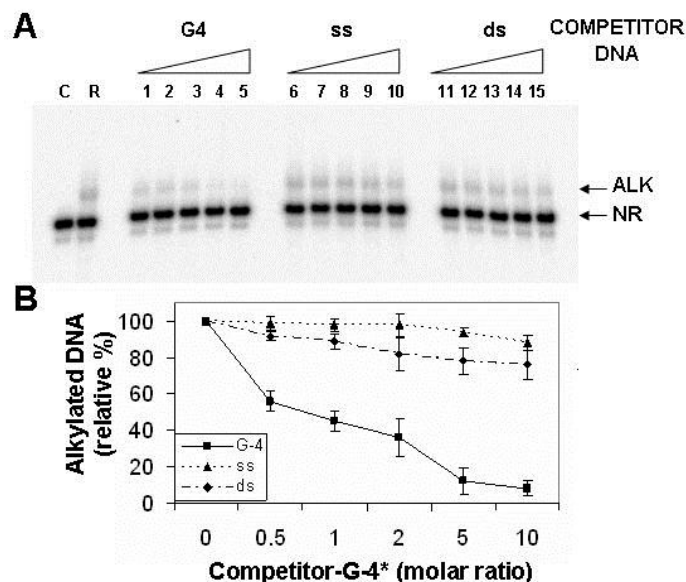


Figure 25. Competition of NDI-mediated alkylation. **A)** Compound **50** (2 μ M) was incubated with labelled 4GGG (3.9 pmol) in the presence of increasing molar ratios (0.5, 1, 2, 5, 10) of cold 4GGG (G-4), ss-scrambled-4GGG (ss) or ds-scrambled-4GGG (ds) DNA for 24h at 40°C. Alkylated DNA (ALK) was separated from non-reacted oligo (NR) in 20% denaturing gel. C refers to labelled 4GGG (3.9 pmol) treated at 40°C for 24 h, R to the 4GGG-compound **50** reaction product in the absence of any competitor DNA. **B)** Quantification of the competition experiment in A). Adduct amount obtained in sample R was indicated as 100% and quantification of adduct amount in lanes 1-15 was calculated as relative %.

G-quadruplex Folding Induction versus Alkylation.

In order to clarify how this selectivity is related to DNA recognition step, we used a 32 P 5'-end labeled synthetic oligonucleotide containing only two repeats of the human telomeric sequence, 5'-TACAGATAGTTAGGGTTAGGGTTA-3' (2GGG). This oligo can fold into G-4 arrangements only by intermolecular pairing leading to dimeric or tetrameric species resolvable by native gel electrophoresis. This process is poorly efficient in the absence of a G-4 stabilizer thus allowing us to compare the ability of compound **50** to induce G-4 folding and alkylation on the same DNA

sequence. DNA-ligand incubation was performed using alkylating (40°C) and non-alkylating (20°C) conditions in the presence/absence of 100 mM K⁺, to promote G-4 conformation. At variable time, samples were loaded onto 16% native and 20% denaturing polyacrylamide gels, to check for folding stabilization and alkylation, respectively.

According to previous results with NDI derivatives,¹⁵¹ using reversible conditions, **50** is poorly effective in inducing G-4 structures. Indeed, incubation of 2GGG with 25 μM **50** at 20°C induced only 28% of G-4 dimer over DNA adduct obtained at 40°C for 24 h (lanes 1-6 and lane 12, **Figure 26A**). In these incubation conditions, the presence of KCl was demanding. Indeed, no quadruplex stabilization was observed in the absence of KCl. Correspondingly, negligible alkylation occurred according to this protocol.

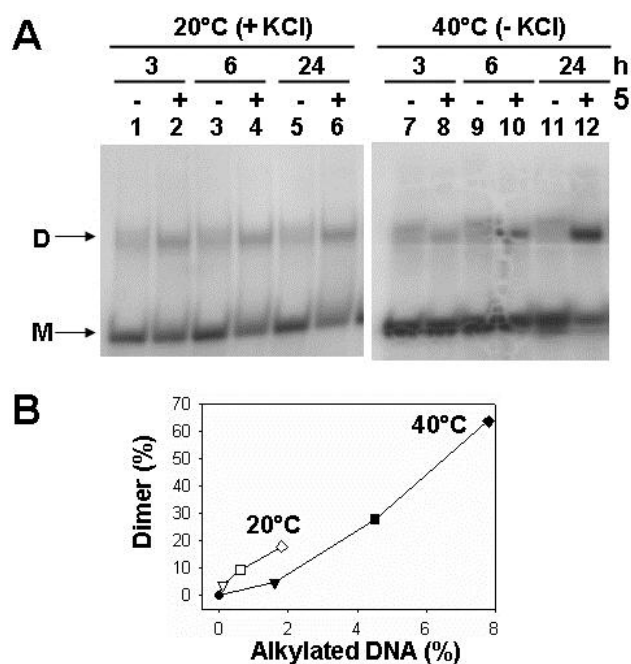


Figure 26. Comparison of induction of G-4 conformation and alkylation by NDI **5**. 2GGG DNA was incubated in the presence (+) or absence (-) of compound **50** (G-4/5 molar ratio 0.04) for variable times at 20°C or 40°C. **A**) The monomeric DNA (M) was separated from the dimeric G-4 DNA (D) by 16% native polyacrylamide gel. **B**) Quantification data. Dimer formation is reported as a function of DNA alkylation. Values were taken at 0 (circles), 3 (rectangles), 6 (squares) and

24 (diamonds) h time intervals. Dimer formation and DNA alkylation were calculated as % over total DNA.

Remarkably, the G-4 folded dimeric conformation was potently and time-dependently induced by **50** upon incubation at 40°C (lanes 7-12, **Figure 25 A**). Denaturing gel showed that in these conditions 2GGG alkylation products were detectable after 6 and 24 h of incubation. Direct comparison of G-4 folding induction and alkylation indicates that the amount of DNA adduct is linearly related to the extent of G-4 folding. However, since compound **50** induces a larger amount of G-4 structure than it undergoes alkylation, we infer that G-4 folded DNA stabilization occurs prior to and is a pre-requisite for DNA alkylation, which in turn irreversibly stabilizes the NDI-G-4 complex. On the other hand, because of the partial reversible character of QM alkylation damage, a striking comparison between the two techniques could not be done. In particular, denaturing conditions could also revert the some alkylation adducts giving only a partial percentage of overall alkylation.

CD Spectroscopic Study.

The above conclusion is also supported by an analysis of the chiroptical properties of 4GGG alone, and in the presence of **50** reported in **Figure 27**. As already described, in our experimental conditions, 4GGG preferentially folds into a mixed type G-4 structure.²⁴⁸ Upon 24 h incubation with **50** at 20°C, hence almost in complete absence of alkylation events, modest changes occurred in the DNA dichroic spectra that represent the sum of DNA folding rearrangements and ligand induced CD. It is interesting to note that after 24h incubation at 40°C, a larger modulation of the dichroic response occurred. In particular, a significant increment of the 265 nm band associated to a reduction of the 295 nm one emerged. This suggests that DNA can undergo a conformational rearrangement in the presence of **50**. In line with the gel shift data, the modest level of alkylation obtained in these conditions should not justify the extensive conformational change presented in **Figure 27**. Hence, reversible interaction between derivative **50** and G-4 appears to represent the

prodrome to alkylation. However, NDI structures reported in literature to date do not result able to induce such a conformational change, therefore further investigation should follow this study in order to clarify unequivocally if the change is dictated by the alkylation or a reversible interaction of the molecule.

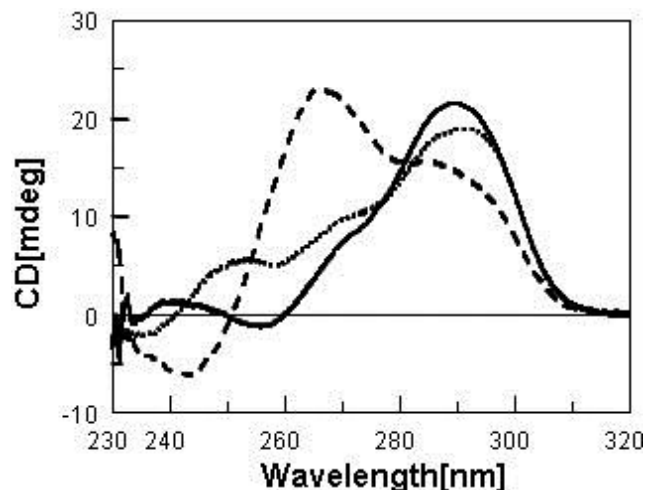


Figure 27. CD spectra of 4 μM 4GGG incubated 24 h alone (solid line) and in the presence of 26 μM **5** at 25°C (dotted line) or 40°C (dashed line) in Li_3PO_4 10 mM, KCl 50 mM, pH 7.4.

Alkylated G-quadruplex Properties.

With the aim to identify a potential selective alkylation site along the G-quadruplex folded 4GGG we used an enzymatic assay.²⁴⁹ In particular, the ^{32}P 5'-end labeled alkylated G-4 DNA was gel purified and treated with increasing amounts of exonuclease I at 50°C for 30 min, alongside the non-alkylated G-4 DNA treated in the same conditions. As shown in **Figure 28**, the enzyme could not process the alkylated G-4 DNA even at the highest tested enzyme amounts, whereas it was able to digest the non-alkylated oligo, with an efficiency linearly related to enzyme concentrations.

These data indicate that the alkylated DNA is a poor substrate for enzyme processing. The fact that no enzyme stop positions were observed likely reflects a lack of DNA-enzyme recognition. Based on the data obtained by circular dichroism studies, this behavior is likely related to the structural rearrangement occurring on the 4GGG bound by compound **50**, which prevents

anchoring/processing by Exonuclease I. However, we cannot exclude a 3'-end DNA alkylation event which would result in a similar experimental outcome.

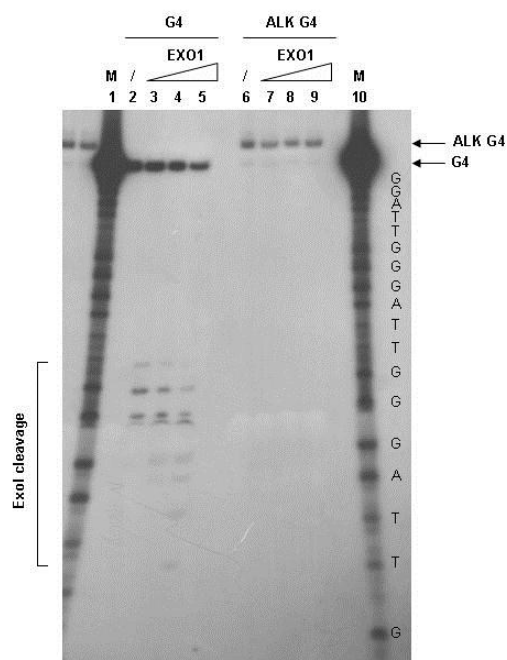


Figure 28. Digestion of alkylated and non-alkylated G-4 DNA by Exonuclease I. Labeled 4GGG DNA (G4) and the purified labeled-, 50-alkylated 4GGG DNA (ALK G4) were incubated with increasing amounts of Exonuclease I (ExoI) (10, 20 and 40 units) for 30 min at 50°C. Cleavage products were analyzed in 20% denaturing polyacrylamide gel. M indicates purine markers run aside samples.

NDIs cytotoxicity.

Cytotoxic effects of NDI derivatives **49**, **50** and **51** were investigated on the human embryonic kidney 293T cell line. Cells were exposed to increasing concentrations of the tested compounds (12 nM-40 μ M) at 37°C for 48 h, after which cell damage was assessed by MTT assay. The effective drug concentration able to kill 50% of cell population after drug exposure (EC_{50}) was $4.5 \pm 0.3 \mu$ M, $10.5 \pm 3.5 \mu$ M and $> 40 \mu$ M for compounds **50**, **49** and **51**, respectively. Hence, the cytotoxic potency of these compounds parallels their DNA alkylating ability.

Tri and Tetra substituted NDIs Tethered to Quinone Methides as More Efficient and Selective G-4 Alkylating Agents.

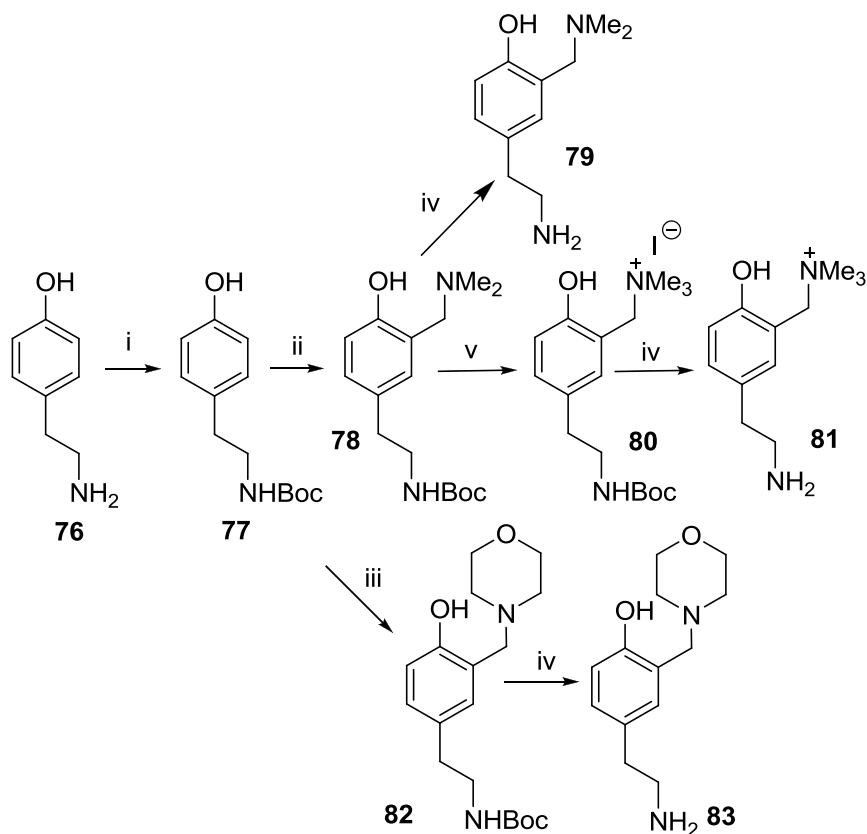
After the encouraging results achieved with simple NDIs such as molecule **50** we decided to explore synthetic route in order to improve selectivity and alkylation yields. With such an aim we developed a new small library of tri-substituted NDI which resulted capable of acting as potent ligand and hybrid ligand/alkylating agents selective for G-quadruplex structures. Some of these new molecules such as **71** and **71a** exhibit excellent reversible binding properties towards parallel G-quadruplex. In addition, for the first time tri-substituted NDI have been shown to bind in a 4:1 mode and stimulate the parallel G-4 conformation in solution, which represent a cornerstone for our aim to develop always more selective molecular devices. This feature is probably promoted by the presence of a protonable amino group directly linked to the aromatic ring (compounds **71** and **71a**). In fact, we are going to illustrate in this section that ligands lacking this functional moiety, namely **60** and **60a**, bind with a 2:1 stoichiometry to the antiparallel G-4 DNA. The new ligands have been structurally engineered in order to merge the reversible binding to the alkylating properties, resulting from the mild generation of a quinone methide. Such a strategy, has been developed for the hybrid structure **73**, and resulted in a superior cytotoxicity toward two human carcinoma cell lines (lung and colon). The data collected during the development of this PhD work, showed that is possible to tether only one fairly bulky triggerable reactive moiety, such as a Mannich base, to the tri-substituted NDI core without compromising its binding property. In fact, the tetra-substituted NDI **75**, bearing two Mannich base moieties is a very poor ligand, in contrast to other tetra-substituted NDIs exhibiting alkylamino side chains. These are crucial observation which will guide our future development of the project and which represented one of the main task in the chemical understanding of the G-4 chemical interactions. Remarkably, non-cationic NDIs capable to penetrate cell membrane showed cytostatic properties towards telomerase active cancer cells. This feature associated with the notable telomerase inhibition properties, pointed up by the TRAP assays, suggests a clear telomerase dependent antitumor

activity carried out by this new class of molecules. Further investigation on the selective targeting of different G-quadruplex with intrinsic parallel topology by tri-substituted NDIs as hybrid ligand/alkylating agents is in progress. These compounds represent the rational chemical evolution of the molecular devices developed in this PhD thesis and which fortunately turned into a higher selectivity and potency of the pro-drugs. Moreover *in cellulo* experiments allowed the obtaining of crucial information concerning the possible *in vivo* applicability of such molecules.

Rational Design of new NDI derivatives.

As described in literature the addition of proper side chains to di-substituted NDIs, giving tri- and tetra-substituted NDIs, causes a dramatic improvement of the G-4 binding properties.²⁵⁰ Moreover such a chemical implementation also lead to much more topology selective molecules which are capable to induce a conformational switch from mixed type to parallel type.²⁵⁰ This evidence suggested us to translate this structural feature also to the alkylating NDIs already developed and above described (**NDI-QMPs 50**) with the aim to point up interactions with telomeric DNA. Therefore, in the attempt to design new tri- and tetra-substituted NDIs as G-4 ligand/alkylating hybrids **Scheme 24**, during the last PhD year we have defined an original and efficient two steps synthetic route for tethering cationic arms and the reactive moieties both to the imide group and the NDI core, respectively. In particular, this synthesis requires two orthogonal steps: (i) imidization and (ii) nucleophilic aromatic substitution (S_NAr), using the already described *ortho* functionalized tyramine derivatives [4-(2-aminoethyl)phenols] as QMPs . The new NDIs so synthesized and highlighted in **Scheme 24** can be classified as (i) new G-4 reversible ligands such as **70**, **70a**, **71**, **71a**, **72**, **72a** and **75**) and (ii) hybrid ligand/alkylating agents (**73**, **74** and **74a**) according to the nature of the leaving group at the benzylic position (substituent Y in **Scheme 24**) which dictate the reactivity of the corresponding Quinone Methide Precursor. The tri- and tetra-substituted NDI analogues exhibit two protonable side chains on the imides moieties [$(CH_2)_2NMe_2$, or $(CH_2)_2NMe_3^+$] and a Mannich base or its quaternary ammonium

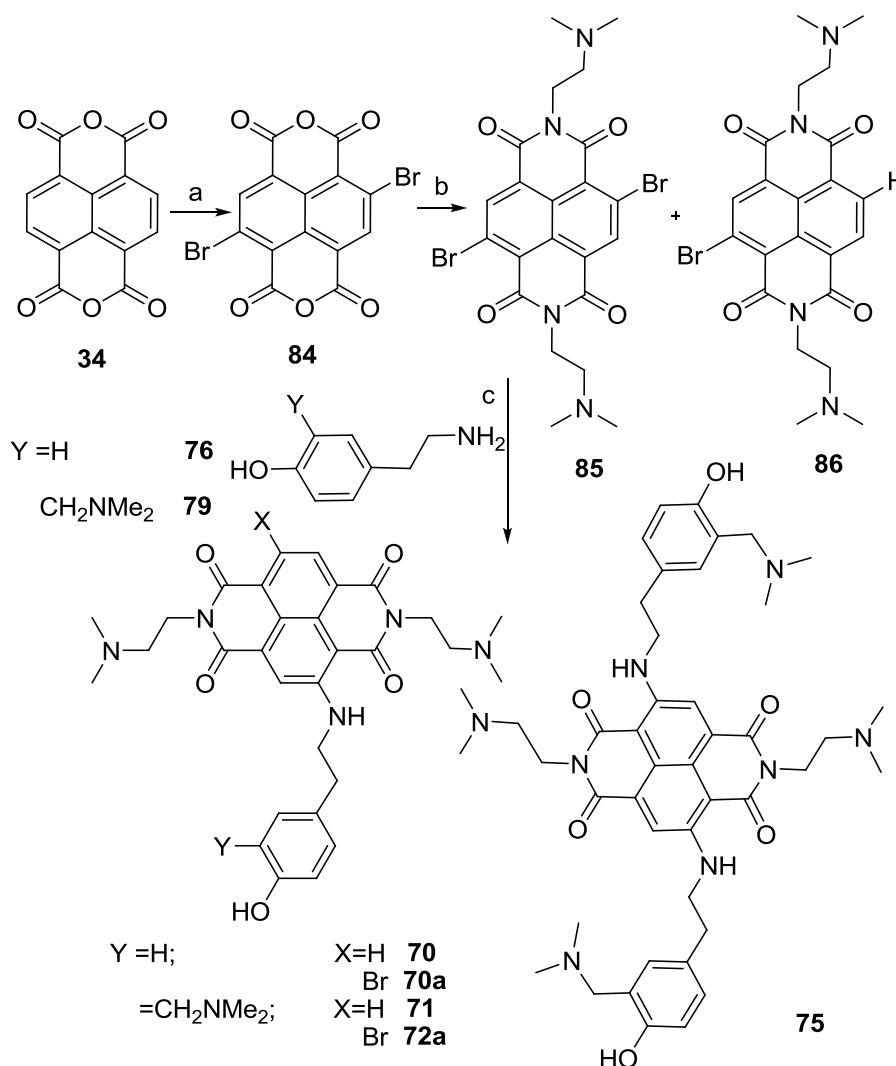
(Scheme 26) with the purpose of acting as additional side chain or as potentially reactive conjugate (QMP). The synthesis requires a stepwise protocol including a Mannich reaction and a protection/deprotection strategy. By using this synthetic route it has been possible to recover the intermediate **79** and the QMPs **81** and **83** in good yields.



Scheme 25. Synthesis of **79**, **81** and **83**. (i) Boc_2O , THF, r.t., (ii) paraformaldehyde, dimethylamine in anhydrous EtOH, Δ , 2hrs. (iii) paraformaldehyde, morpholine in anhydrous EtOH, Δ , 2hrs. (iv) TFA, Et_3SiH , CH_2Cl_2 , r.t., 25 min. (v) MeI, CH_3CN , Δ , 30 min.

After the synthesis of the precursors has been achieved and maximized we started to investigate chemical routes for the synthesis of the final ligands (**70**, **70a**, **71**, **71a**, **72**, **72a**, and **75**) as well as the hybrid ligand/alkylating compounds **73**, **74** and **74a**. In particular such goal has been achieved by exploring two different synthetic strategies both starting from the dibromodiimide **85** as depicted in **Scheme 26**. In more details, all compounds have been prepared starting from the 2,6-

dibromo-1,4,5,8-naphthalene tetracarboxylic acid dianhydride **84**, which was obtained by bromination of the naphthalene dianhydride **34** adding 2.5 equivalents of dibromoisocyanuric acid (DBI), in conc. H₂SO₄, according to the already published Wurthner's procedure.²³⁸



Scheme 26. Imidization of the anhydride by dimethylethylamine, according to the first synthetic protocol. Reagent and conditions: (a) dibromoisocyanuric acid (DBI), H₂SO₄, reflux, 12h, yield 93% of **84**; (b) dimethylethylamine, glacial acetic acid, 130 °C, 30 min. (c) Amine **76** and **79**, DMF, 180 °C, closed vessel, microwave assisted, 3-10 min (see conditions in **Table 8**).

Imidization of the dianhydride **84** has been performed in acetic acid as reported in published procedures, giving **85** in fairly good yield (45%), together with the mono-dehalogenated product **86** (26% yield). Both the subsequent mono- and bis-SNAr reactions on **85** were performed in a dedicated microwave reactor. Product distribution was dramatically affected by irradiation time as summarized in the data reported in **Table 8**.

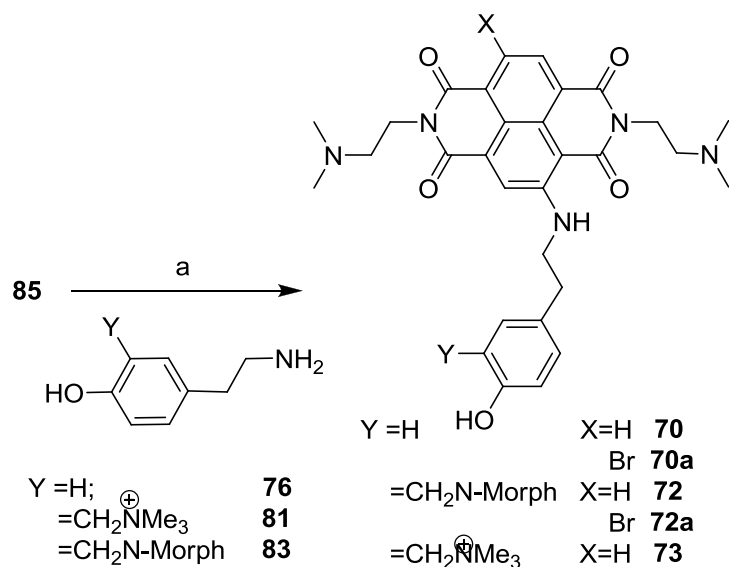
Table 8. Reactants and Conditions for the Nucleophilic Aromatic Substitution on the dibrominated NDI **85**.

Reactant	Conditions ^a	Products (% yield)
79	DMF, MW, 180°C, 200 W, 3 min.	71 (35), 71a (62)
79	DMF, MW, 180°C, 200 W, 5 min.	71 (25), 71a (40), 75 (30)
79	DMF, MW, 180°C, 200 W, 10 min.	71 (5), 75 (70)
76	DMF, MW, 180°C, 200 W, 3 min.	70 (66), 70a (37)
76	DMF, r.t., 8h.	70 (15), 70a (74)
81	DMF, r.t., 48h.	73 (6)
83	DMF, r.t., 24h.	72 (12), 72a (45)

^a Reaction performed under Argon.

The reaction has been optimized using amine **79** as reacting nucleophile at 180 °C, 250 psi, 200 W, in three different time conditions as shown in **Table 8**. After ten minutes, the microwave assisted synthesis, generated the tetra-substituted adduct **75** as main product. A shorter microwave irradiation (5 min) gave, instead, a mixture of three compounds tetra- and tri-substituted NDIs **75** (30%) and **71a** (40%), respectively, together with the tri-substituted byproduct **71** (25%) resulting from a reductive dehalogenation process. In order to improve the synthesis of tri-substituted NDIs such as **71a**, minimizing the tetrasubstituted NDIs side product, we managed to carry out the reaction in 3 minutes. Ligand-alkylating hybrid compounds **74** and **74a** have been prepared instead by exhaustive methylation of the amines **71** and **71a**. Unfortunately, this

microwave assisted protocol was unsuitable for the synthesis of the hybrid ligand/alkylating agents bearing a thermally triggerable QMP moiety. In fact, under the harsh conditions required by the S_NAr , the QMP moieties of the NDIs **72**, **72a** and **73** undergo fast degradation through QM generation. To avoid such a limit, we have studied and developed a new efficient protocol for the mono-functionalization via S_NAr reaction at room temperature herein summarized in **Scheme 27**. Under definitely milder conditions, the generation of the dehalogenated NDI was minimized below 15% and, moreover, the S_NAr reaction was achieved without QMP decomposition. In more details, the NDI **85** stirred at room temperature in the presence of the amines **76**, **81** and **83** for 8-48 h in DMF gave the tri-substituted NDIs **70**, **70a**, **71**, **71a** and **33**, respectively, which have been successively purified by preparative HPLC. This mild synthetic route has been developed *ad hoc* during this PhD and, moreover, allows a selective mono- S_NAr outcome. Therefore the latter has been exploited for building hybrid ligand/alkylating agents triggerable by mild thermal digestion ($T = 40^\circ\text{C}$).



Scheme 27. Synthesis of **70**, **70a**, **71**, **71a** and **73** according to the second synthetic protocol above described. Reagent and conditions: (a) generic amine, DMF, 25°C , 8-48 h.

New NDI derivatives selectively bind human telomeric G-quadruplex folded DNA.

To evaluate the stabilization and selectivity of NDI derivatives for telomeric G-quadruplex (G-4) DNA, FRET melting experiments has been carried out. **Table 9** reports the enhance of the melting temperature (ΔT_m) of the labeled oligonucleotide F21T in K^+ solution caused by the treatment with 0.8 μM NDI derivatives. F21T represents the human telomeric DNA sequence. The FRET-melting data clearly demonstrate that, derivatives **71** and **71a** effectively stabilize the telomeric G-quadruplex, with ΔT_m values above 20°C (**Table 9**). Moreover, these data strongly underline that proper side chains are crucial for achievement of good binding properties.

Table 9. ΔT_m of reversible binding NDI compounds at 0.8 μM conc, measured by FRET of the labeled oligonucleotide F21T in K^+ solution.

Compound	ΔT_m °C (0.8 μM)
71	22.2±0.3
71a	20.3±0.8
70	18.2±0.3
70a	15.6±0.5
72	4.5±0.4
75	3.2±0.6

70 and **70a** were slightly less efficient with a ΔT_m in the range of 15.6-18.2°C, whereas the tetra-substituted compound **75** and the morpholine derivative **72** were very poor stabilizers ($\Delta T_m = 3.2^\circ C$ and $4.5^\circ C$, respectively). Compounds **73**, **74** and **74a** were not included because high temperature required in FRET cycle experiments would activate them and trigger alkylation. Next, G-4 selectivity for all compounds was assessed by a FRET-based competition assay, where the ability of ligand to retain G-4 stabilizing affinity was challenged by non-fluorescent duplex

(ds26), single-stranded (scrambled G-4) DNA, or G-4 forming DNA (27NHEG). The latter, demonstrated to be the only oligonucleotide sequence capable of competing effectively with the labeled sequence. Indeed, under 27NHEG:F21T molar ratio of 1.5, ΔT_m decreased of about 50%, whereas 100% decrease was reached for all compounds for a molar ratio of 5. In the presence of various amounts of competitor ds26, the thermal stabilization of F21T enhanced by the NDI compounds was affected only starting from ds26:F21T molar ratio of 15, when the decrease in the ΔT_m value was around 20% for all compounds (**Figure 29**). Conversely, single-stranded scrambled G-4 DNA did not affect ΔT_m at any molar ratio and for any compound. These results demonstrate that the present NDI derivatives can be considered as a new class of highly selective G-quadruplex binding ligands.

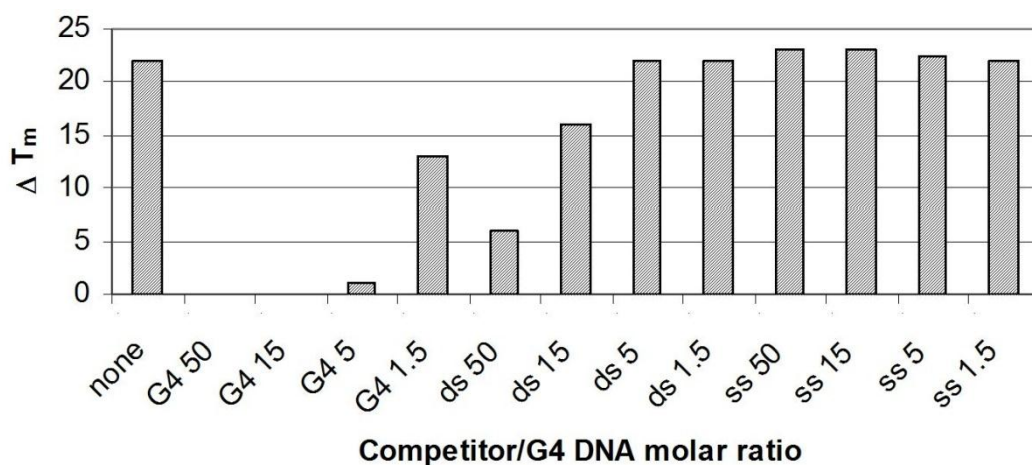


Figure 29. FRET-based competition assay. Binding of NDIs to the fluorescence-labelled F21T oligo was challenged by non-fluorescent duplex (ds), single-stranded scrambled G-4 DNA (ss), or a telomere non-related G-4 forming DNA (G4). Data for the representative NDI 71 are shown.

NDI 71 drives towards the formation of a parallel-like G-4 topology.

It is well known that the human telomeric DNA in K^+ solution folds in a 3:1 topology, in which three strands are oriented in one direction and the fourth is in the opposite direction, one loop is

double-chain reversal and two are edgewise, one G-tetrad has *anti/syn/syn/syn* glycosidic conformation and two have a *syn/anti/anti/anti* conformation.²⁵¹ In circular dichroism, this hybrid-type G-4 conformation has shown a strong positive peak around 290 nm with a shoulder peak around 260 nm, and a smaller negative peak at 240 nm, as already illustrated in the CD experiments for NDI **50**.²⁵² In general, a positive band at 265 nm and a negative peak at 240 nm are characteristic of a parallel G-4 topology, while two positive bands at 290 nm and 245 nm, and a negative peak at 260 nm are diagnostic of the antiparallel G-4 conformation,²⁵³ which features are mainly attributed to the specific guanine stacking in various G-quadruplex structures.²⁵⁴ Therefore, we will hence attribute peaks at 265 and 290 nm to parallel-like and anti-parallel-like G-4 structures, respectively. The hybrid G-4 form will be designed as mixed antiparallel/parallel.

To check the preferred G-4 conformation stabilized by the NDIs, CD analysis of the 4GGG oligonucleotide upon binding with the different NDI compounds was performed. Compounds were added either before (around 80°C) or after folding (20°C) of the G-4 DNA. Subsequently, samples were left to equilibrate prior to CD spectra measurement. In these conditions 4GGG oligonucleotide is present in its mixed antiparallel/parallel form as attested by a major positive peak at 290 nm and a shoulder at 265 nm (**Figure 30A-C**). Compounds **71**, **71a**, **70** and **70a**, incubated after DNA folding, induced a comparable stabilization of the mixed antiparallel/parallel G-4 structure as proved by a similar increase in the positive peak at 290 nm (**Figure 30A-C**). However, when compounds were incubated before DNA folding, a markedly different behavior has been observed. In particular, **71** and **71a** showed a remarkable stabilization of the parallel G-4 topology, as evinced by the increased peak at 260 nm which matched a decrease in the 290 nm peak, and a minor negative peak at 240 nm (**Figure 30A and B**). This behavior was the ligand **5a**, whereas **4** and **4a** did not show any significant difference between “after” and “before” incubation samples (**Figure 30C**) displaying in both cases a stabilization of the mixed antiparallel/parallel form. Finally, the tetra-substituted NDI **75** showed a similar behavior to these latter compounds, but with a significant minor intensity.

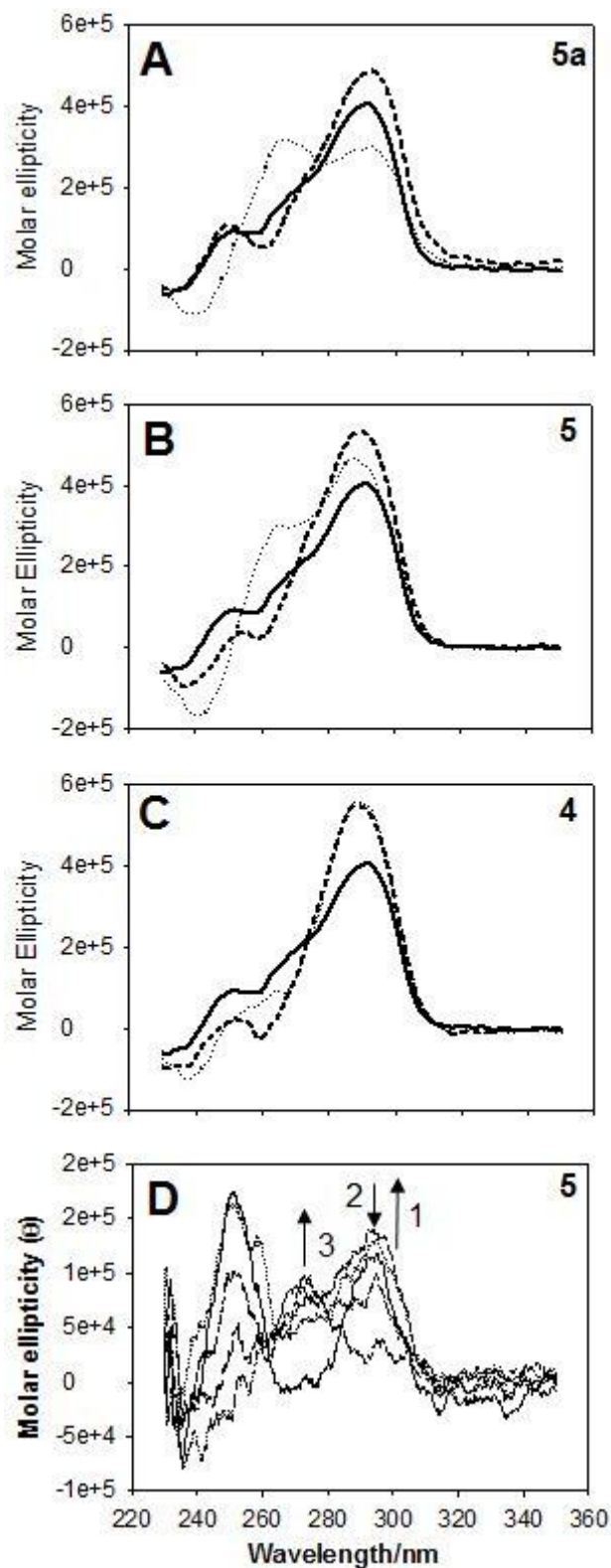


Figure 30. CD analysis of NDIs. Compounds **71a** (A), **71** (B) and **70** (C) (16 μ M) were incubated with 4GGG oligo (4 μ M) after (dashed lines) or before (dotted lines) DNA annealing in the presence of K^+ 50 mM. The spectrum of 4GGG DNA annealed in the absence of NDIs is shown

as a solid line. (D) Spectra obtained by incubation of increasing amounts of compound **71** with 4GGG DNA in the absence of K^+ .

Other G-quadruplex ligands, such as 1,3-phenylene-bis(piperazinylbenzimidazole) are also capable of inducing and stabilizing the parallel stranded quadruplex from randomly structured DNA in the absence of any stabilizing cation.²⁵⁵ Very recently other tetra-substituted NDIs, bearing alkylamine moieties, have been shown to induce formation of a parallel G-quadruplex topology at room temperature.²⁵⁰ It has been reported in the literature, and we have also proved in our experimental conditions, that K^+ and Na^+ ions drive towards different conformations of the human telomeric sequence in solution.^{96,251} In particular, K^+ favors a mixed antiparallel/parallel topology, while Na^+ maintains a full antiparallel conformation. We hence performed FRET-melting experiments in the presence of Na^+ , instead of K^+ , for the best performing NDI derivative, i.e. compound **71**: at NDI concentration of 0.8 μ M, we found a ΔT_m value of 5.5°C which, compared to ΔT_m of 22.2°C in K^+ in the same conditions (see above), points to a much disfavored binding of compound **71** to a full antiparallel G-4 conformation.

Since alkali-metal cations stimulate G-4 folding and influence topology, we checked the potential of compound **71** to bind the telomeric DNA sequence and induce its G-4 conformation in the absence of K^+ ions. Increasing NDI concentrations were incubated with 4GGG oligonucleotide in Li cacodylate buffer and samples were assayed by CD spectroscopy. In these conditions, 4GGG DNA in the absence of the compound showed a minor positive peak at 290 nm and a major positive peak at 250 nm, indicating a poor G-4 folding (Figure 2D). Upon addition of **71**, the peak at 290 nm initially slightly increased and then decreased at higher compound concentration, when a peak at around 265 nm appeared. These data indicate that **71** is able to induce a G-4 folding of the telomeric sequence in the absence of K^+ ions in a mixed antiparallel/parallel topology, with a preference for the parallel form (**Figure 30 D**).

To test the stabilization of the antiparallel versus parallel G-4 topology of the telomeric sequence induced by **71**, we performed CD thermal unfolding experiments. The CD spectra of **71** incubated with the folded 4GGG DNA were recorded at increasing temperature (range 20-95°C). At 20°C the spectrum showed a positive peak at 290 nm (see above), which remained stable up to 55°C. At 60°C the peak at 290 nm started to decrease and a positive peak at 260 nm appeared. This latter reached its maximum at 75°C, after which temperature it began to decrease. At 95°C no evident peak was present indicating the completeness of DNA unfolding. The van't Hoff equation was separately applied to the denaturation of the antiparallel form (measured at 290 nm) and to the unfolding of the parallel conformation (signal at 260 nm). The first transition gave a ΔT_m of 9.2°C and the second of 18.8°C. The sum of the two gave a ΔT_m of 23.9°C which perfectly matches the ΔT_m found in the FRET melting experiments (22.2°C) for the same 4:1 DNA:drug molar ratio. This data indicate a higher stabilization of the G-4 parallel topology than the antiparallel one by **71**. Hence the G-4 conformation preferentially stabilized by NDI compounds is different from that naturally adopted by the human telomeric sequence in K⁺-containing solution. The apparent ΔH value between the unfolding of the G-4 DNA alone or in the presence of **71** was 20 Kcal/mol, indicating a strong stabilization of the G-4 conformation upon drug binding.

NDI compounds bind with a different stoichiometry to G-4 telomeric DNA

The vast majority of reversible ligands that bind to the human telomeric intramolecular G-4 structure have been reported to display a 2:1 ligand:DNA molar ratio,²⁵⁶⁻²⁵⁸ and seldom a 1:1.²⁵⁹ Tetra-substituted NDI derivatives have been co-crystallized in a 6:2 stoichiometry with the parallel G-4 conformation of the human telomeric DNA.²⁶⁰ Recently, isaindigotone derivatives have been reported to bind in a 4:1 mode in solution and to stabilize the antiparallel topology of the human telomeric DNA.²⁶¹

Reaction stoichiometry of compounds **71**, **71a**, **70** and **70a** against 4GGG DNA in 10 mM Li cacodylate and 50 mM KCl buffer, at 20°C, was evaluated by CD titrations. In these conditions, we observed that NDIs reached binding saturation at different drug:DNA molar ratios (Figure 3A). In particular, for **71** and **71a**, 4 molecules of drug were necessary for binding to one DNA molecule, while for **70** and **70a**, 2 molecules were sufficient. In addition, at each intermediate molar ratio (i.e. 1, 2 and 3) a partial stabilization of the signal was detected. These data indicate that drugs with an amino group in the side chain (i.e. **71** and **71a**) bind in a final 4:1 drug:DNA mode, while drugs lacking the amino group linked to the aromatic ring (i.e. **70** and **70a**), bind in a 2:1 drug:DNA mode.

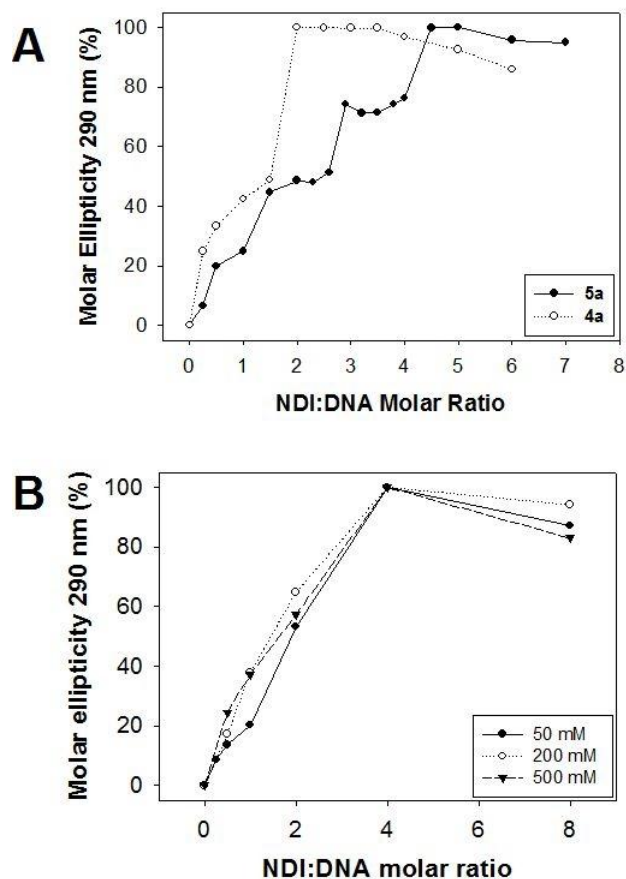


Figure 31. Stoichiometry of NDI binding to 4GGG DNA analyzed by CD. (A) Increasing molar ratios of NDIs were incubated with 4GGG DNA. Relative molar ellipticity values at 290 nm were plotted against NDI molar ratio. Shown are results for representative compounds **70a** and **71a**. (B) Increasing molar ratios of compound **71** were incubated with 4GGG in the presence of increasing

concentrations of K^+ . Relative molar ellipticity values at 290 nm were plotted against NDI molar ratio.

Both electrostatic and non-electrostatic interactions are involved in the binding of 5 to G-4 telomeric DNA.

Since the NDIs **71** and **71a** contain three protonable amino groups, we checked for the contribution of electrostatic forces to G-4 DNA binding. FRET melting experiments of **71** and F21T DNA were performed at increasing ionic strength concentrations (i.e 60, 110, 160, 260, 460, 1000 mM). ΔT_m , at 0.8 μ M NDI **71**, decreased from 22.2°C at 60 mM ionic strength to 6°C at 1 M, indicating that even though important electrostatic forces are present, non-electrostatic contribution is also evident, as indicated by the stabilization of the G-4 folded telomeric DNA even at very high ionic strength (1 M). We next evaluated if ionic strength could affect binding stoichiometry: **71** was incubated with 4GGG DNA in the presence of increasing buffer ionic strength (60 mM, 200 mM, and 500 mM) and CD spectra were recorded. We found that 4 molecules of NDI were in any case necessary to reach binding saturation (**Figure 31B**), independent of buffer ionic strength, indicating that each of the 4 compound molecules bind G-4 DNA through important non-electrostatic interactions. These data altogether point to a dual binding mode where both non-electrostatic (π -stacking and H-bonds) and electrostatic forces play important roles in NDI binding to G-4 telomeric DNA.

A Novel NDI Capable to Alkylate dG and the G-4 Telomeric DNA.

Since we have proved that NDIs compound can effectively and selectively recognize the G-4 folded telomeric sequence, we next tested the ability of the alkylating NDIs to covalently bind to G-4 DNA. We first looked for the alkylation properties of **74** against single nucleosides in

solution. The NDI **74** was incubated with 2'-deoxyguanosine (dG), 2'-deoxyadenosine (dA), 2'-deoxycytidine (dC) and thymidine (dT) at 60°C for 24 h. The reaction products were monitored by HPLC and MS. The initial HPLC analysis showed that adducts with dG, dC and dA were formed with 9%, 12% and 1% yields, respectively. MS analysis was subsequently performed for the most abundant adducts, i.e. NDI:dG and NDI:dC. For NDI:dG two major peaks at m/z values of 368.2 Da and 426.2 Da were found (**Figure 32A**): the first one corresponded to a positively double-charged molecule formed by **74** and dG with loss of ribose. Since ribose loss typically derives from alkylation at N7 of dG, we suggested that this adduct was formed by the attack of the QM to dG-N7, which in turn loses the sugar moiety. The second peak corresponded to a positively double-charged adduct formed by **74** and dG, corresponding to the attack of QM to one pyrimidine N of dG. Since the activations of the alkylating NDIs have been performed under thermodynamic control (60°C for 24 h) and knowing from literature data that N2-dG conjugate adduct with the prototype *o*-QM is the most stable alkylated product,^{262,263} we have assumed this is the alkylation site. MS analysis of NDI-dC conjugate adduct showed only one major peak at 406.2 Da (**Figure 32 B**), which corresponds to a positively double-charged molecule formed by the attack of the QM to a nucleophilic moiety of dC. Once again, previous experimental²⁶⁴ and computational reports²⁶⁵ indicated that QM should react preferentially at the exocyclic NH₂ of dC (N4), under thermodynamic control. Similar results were obtained for compounds **74a** and **73**. We next investigated the ability of compounds **73**, **74**, and **74a** to alkylate the G-4 folded telomeric sequence. Hence, alkylating NDIs were incubated with P³²-labeled 4GGG folded DNA at 40°C for 24 h to activate the QM precursor. Alkylation products were visualized by polyacrylamide sequencing gels. As shown in **Figure 32 D**, compounds induced the formation of an alkylation band migrating slower than the full length oligonucleotide. The NDI **74** was more efficient than the Br-substituted derivative **74a**: at the highest compound concentration (50 μM) the alkylated adduct was 12% and 7%, respectively (lanes 10 and 18, **Figure 32 D**). Similar results with yields of 5% were obtained for NDI **73**.

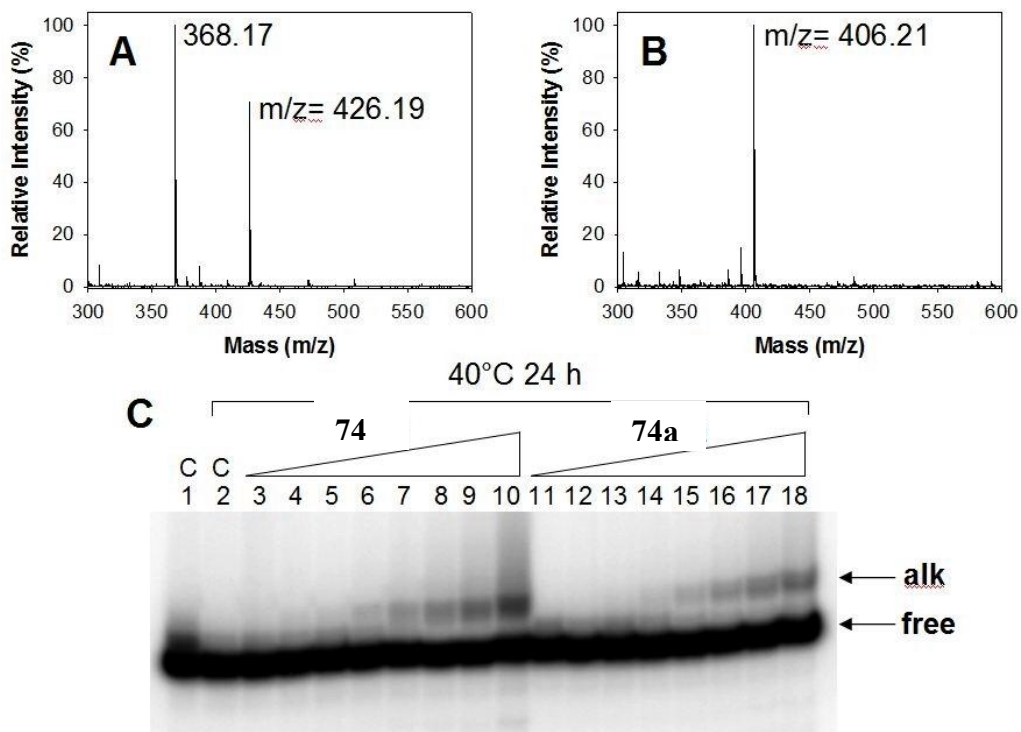


Figure 32. Alkylation effects of NDIs **73** and **73a**. (A) and (B) Mass spectra of the HPLC-separated adducts of compound **74** with dG and dC, respectively. (C) Alkylation of NDIs **74** and **74a** at the 4GGG DNA level. The P^{32} 5'-end labeled 4GGG oligo was incubated with increasing amounts of NDIs (0.34 - 50 μ M) at 40°C to activate alkylation. The alkylated DNA (alk) was separated from the unreacted DNA (free) by 20% polyacrylamide 7 M urea denaturing gel.

Although adduct amount was modest at the highest concentration, its formation was appreciable at compound concentration as low as 12 nM and 50 nM for **74** and **74a**, respectively (lanes 4 and 13, **Figure 32 D**). In addition, alkylation was selective for G-4 folded DNA. In fact, no discrete adduct band was observed when **74** was incubated in alkylating conditions with a double-stranded scrambled 4GGG DNA whose forward sequence base composition, but not order, corresponded to that of 4GGG oligo, similarly to what happened with the already described experiment with **NDI 50**. Since we have found that compound **74** reacts at N7 of dG inducing depurination, we investigated if this process could happen on a G-4 folded oligonucleotide. The **74**-4GGG

conjugate DNA adduct was hence incubated with hot piperidine which is known to stimulate glycoside bond cleavage at alkylated purines.²⁶⁶ However, we did not find any bond breakage, indicating that alkylation of the G4 folded DNA conformation does not involve the N7 site of guanines and probably no guanines at all.

NDIs concentrate inside the nucleus and their cytotoxicity parallels binding to G-4 DNA.

Cytotoxicity of the NDI derivatives was first tested against two human carcinoma cell lines (lung and colon) (**Table 10**) exploiting a collaboration with Professor Nadia Zaffaroni in the Istituto Tumori Milano.

As shown in **Table 10**, the reversible ligands **72**, **72a** and **70** were active at the low micromolar range in both cell lines, followed by **70a**, **72**, **72a** and tetra-substituted NDI **75**. Incidentally, the EC₅₀ scale perfectly matched the ΔT_m scale observed for the reversible compounds, indicating an excellent correlation between G-4 recognition and cytotoxicity. However, the best performing compound, with EC₅₀ in the nanomolar range, was the alkylating **73**, whereas the other two NDIs owning alkylating ability **74** and **74a** were not cytotoxic at concentration below 100 μ M, probably because of their cationic properties. Although a direct comparison of cytotoxicity values and FRET T_m could not be done, such a parallelism between the two data could be symptomatic of an alkylation involvement translated in drug efficiency.

Furthermore, taking advantage of the fluorescence properties of the NDIs, Nadia Zaffaroni's laboratory was able to visualize drug entry and localize it by confocal microscopy. Indeed, we found that **71** immediately entered the cells after 30 min exposure and preferentially concentrated inside the nucleus (**Figure 33**). Conversely, **74** and **74a**, the tricationic hybrid alkylating/ligands, were not able to enter the cells, which also explains their low cytotoxicity.

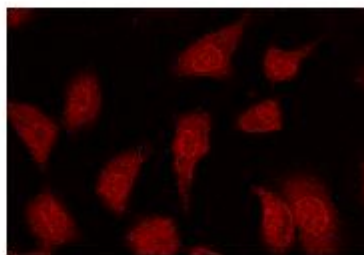


Figure 33. Cellular entry of NDIs. Compound **72** was incubated for 30 min with 293T cells.

Table 10. Cytotoxicity of NDIs towards colon (HT29) and lung (A549) carcinoma cell lines.

NDIs	EC ₅₀ (μM) HT29	EC ₅₀ (μM) A549
71	1±0.1	1.2±0.2
71a	1±0.1	1.3±0.1
60	1.25±0.4	1.1±0.1
60a	4±1.4	3.2±0.2
72	1.2±0.8	3±1.1
72a	4±1.3	9±0.9
75	2.5±0.7	7.6±1.0
73	0.4±0.1	0.9±0.1
74	> 100	> 100
74a	> 100	> 100

Compound 72 inhibits telomerase activity and induces cell senescence.

To evaluate the biological effects induced by **72**, human melanoma SK-Mel5 cells, constitutively expressing telomerase activity as determined by TRAP assay^{140,267} were used. Cells were exposed to different concentrations of tested derivatives, ranging from 5 nM to 50 μM, for

24 and 48 h. Results showed a dose-dependent inhibition of cell growth, with IC₅₀ values of 2.4 and 1.7 μ M at 24 and 48 h, respectively (**Figure 34A**).

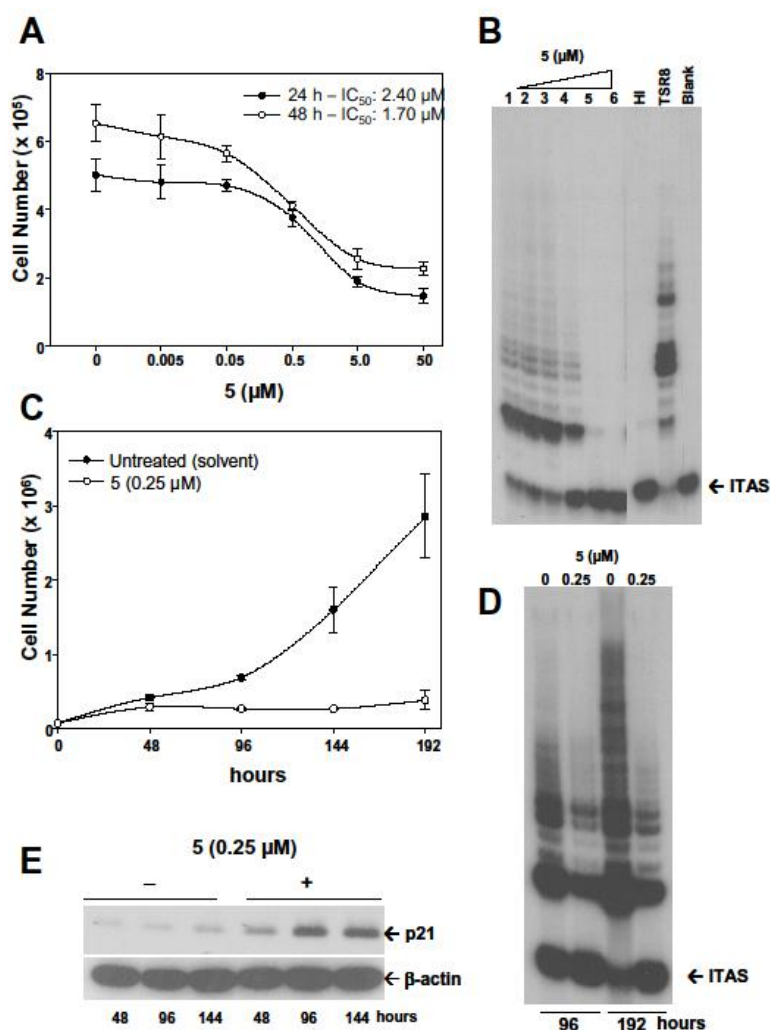


Figure 34. Cellular and antitelomerase effects of NDI 72. **(A)** Cell growth inhibition curves of SK-Mel5 after 24 (●) and 48 (○) h of exposure to increasing concentrations (0.005-50 μ M) of compound 72. Data are reported as cell number and represent mean values \pm SD of three independent experiments. **(B)** Representative TRAP assay showing the inhibition of telomerase activity in SK-Mel5 cells after a 48h exposure to increasing concentration (lanes 2-6) of compound 72. Lane 1: untreated cells; HI: heat-inactivated sample; TSR8: quantitation standard; Blank: no protein extract; ITAS: 36-bp internal TRAP standard. **(C)** Cell growth curves of

untreated (●) or SK-Mel5 treated cells after reiteration of treatment (○) using a fixed concentration (0.25 μ M) of compound **72**. Data are reported as cell number and represent mean values \pm SD of three independent experiments. **(D)** Representative TRAP assay showing the inhibition of telomerase activity in SK-Mel5 cells assessed at 96 and 192 h after the reiteration of treatment with 0.25 μ M of compound **72**. **(E)** Representative western blotting showing the time-dependent expression of p21^{waf1} in SK-Mel5 cells, in the absence or in the presence of 0.25 μ M compound **72**, reiterated every 48 h. An anti- β -actin monoclonal antibody was used to ensure equal loading of proteins.

With the aim to better understand the relevance of telomerase inhibition for the cell growth impairment induced by the tested compound, we analysed telomerase activity in protein extracts after a 48 hour exposure to different drug concentrations and compared it with the cell growth data. Results showed a dose-dependent decline of the enzyme's catalytic activity (**Figure 34 B**). Interestingly, such an inhibition of telomerase activity was already appreciable at 0.5 μ M concentration of **72**, a drug concentration that did not significantly impair the growth of SK-Mel5 cells, thus suggesting the possibility of a narrow selectivity window between antitelomerase activity and cell growth impairment.

On the basis of this evidence, we assessed whether **72** could induce a delayed effect on cell growth, by prolonging cell treatment with the compound up to 8 days. Cells were exposed to a fixed concentration of **72** (0.25 μ M), the treatment was reiterated every 48 h and the cell number was assessed every 2 days.

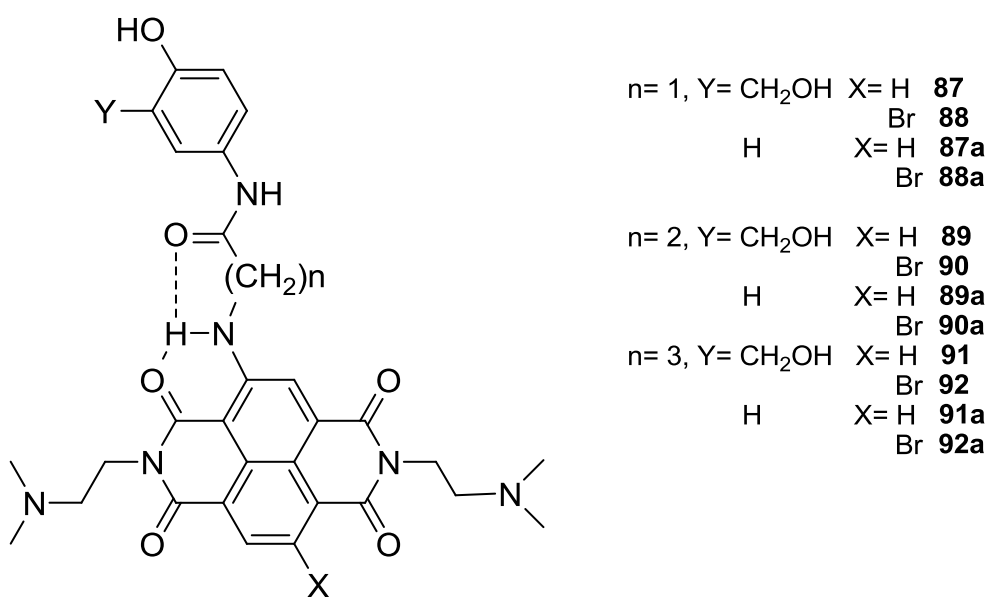
As reported in **Figure 34 C**, control cells showed an exponential growth during the time-course of the experiment, whereas the total number of treated cells remained essentially constant at the different time points. Such a cell growth arrest was paralleled by a marked inhibition of telomerase activity, as assessed by TRAP assay at days 4 and 8 (**Figure 34 D**). To test the

hypothesis that **72** caused growth arrest could be due to the induction of senescence, we preliminary analysed the expression of the cyclin-dependent kinase inhibitor p21^{waf1}, which is known to be involved in a senescence pathway triggered by telomere dysfunction. We found that p21^{waf1} protein expression was markedly enhanced in a time-dependent fashion in SK-Mel5 cells following drug exposure, as gauged by western immunoblotting (**Figure 34 E**). Further experiments aimed at better characterize cell senescence induced by **72** are now on-going in Nadia Zaffaroni's lab. More experiments must be focused on molecule **73**, in order to achieve a striking comparison between the biological effect induced by the reversible ligand **72** and the alkylating one **73**. Moreover, conformational strain induced by the alkylation could be strongly translated in biological effects such as telomerase inhibition or protein G-4 complexes displacement. It does worth to further investigate the above points, in order to clarify the benefits as well as the drawbacks brought by the alkylation.

Changing QMP and Spacer in Tri NDI Derivatives. Effects on Binding Properties and Alkylation Efficacy.

Although the aim of this work could be considered partially reached, in the very last part of this PhD working period we decided to exploit the synthetic routes so far developed for the generation of new NDI derivatives. In particular, we decided to focus on the issues raised during the development and the investigation of the above molecules, especially molecule **50** and **73**, in order to chemically engineer more specific molecular devices. In fact, we already showed in this thesis that the chemical nature of the molecule studied (i.e. the length of the spacers and the QMP characteristics) could strongly affect the binding properties of ligand. For instance, even though molecule **35** resulted an excellent and original bis-alkylating agent triggered by reduction, it also revealed unsuitable for G-4 alkylation purposes because of its molecular shape. On the other hand a less original bis-alkylating agent but conformationally more flexible ligand such as molecule **50**, showed G-4 selective alkylation properties. The right balance among all these characteristics and

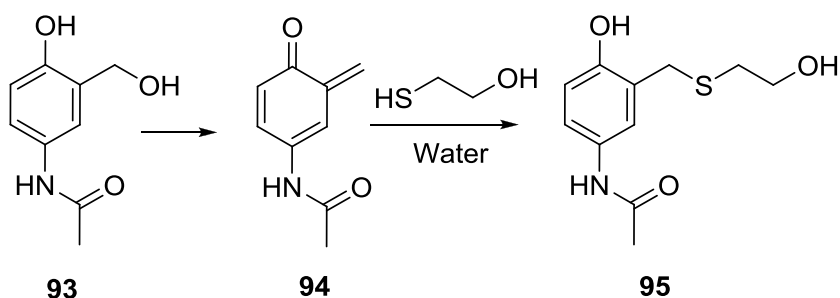
molecular requirements has to be found in order to improve the selectivity of our molecular devices. In this chapter we discuss the last generation of NDIs derivatives synthesized during the present PhD work. The rational evolution of these molecules brought us to improve the potential for an overall molecular flat conformation without compromising the flexibility needed for the binding process. In order to achieve that, we decided to explore tri NDIs with amido side chains, conversely to the amino ones used so far. Such a chemical modification should lead to planarity induced by an intramolecular hydrogen bond, as depicted in **Scheme 28**.



Scheme 28. New amido NDIs derivatives synthesized and object of this PhD work

Beside the planarity conferred by the hydrogen bond highlighted in **Scheme 27**, which should increase duplex/quadruplex selectivity, another substantial change concerning the QMP has been introduced in these new NDIs derivatives. Indeed, the phenolic QM precursor has now got an alcoholic substituent as benzylic leaving group. This last modification was crucial because it allowed to avoid the use of the quaternary ammonium salt group, which caused cell permeability issues. On the other hand such a modification suppressed the reactivity of the QMP which has been therefore compensated by the addition of an amido electron donating substituent directly

tethered to the aromatic ring (**Scheme 27**). In fact, as already mentioned substituent and leaving groups on Quinone Methide Precursors strongly influence the reactivity. A systematic temperature and pH reactivity dependence of the new alcoholic QMP prototype (**93**) has been investigated. The results summarized in **Scheme 29** show how the precursor is much more reactive in acidic conditions conversely to what observed for the quaternary ammonium salts derivatives. This experimental observation is crucial both because it represents a case of QM triggerable under acidic condition and because of its potential applicability in selective antitumor drug discovery, thanks to the lower pH characteristic of cancer cells environment.

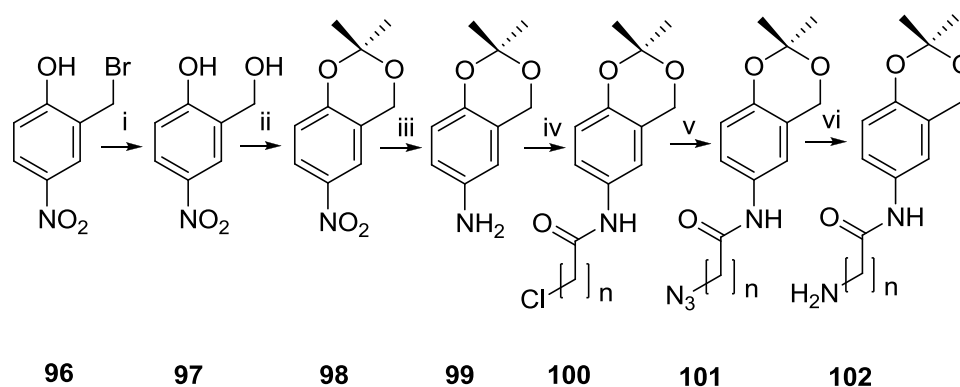


pH	°C	t _{1/2}
4.5	60	4 h
4.5	50	10 h
4.5	40	26 h
7	60	8,58 h
8	60	6,26
8	40	20

Scheme 29. Reactivity study of the prototype QMP developed in this PhD thesis.

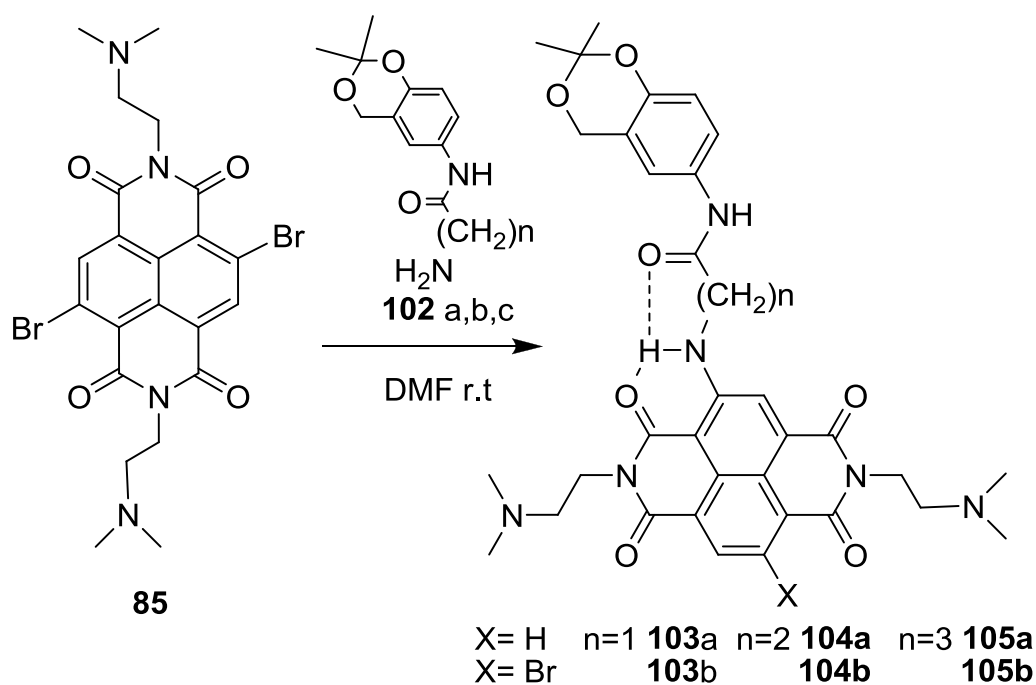
The synthetic approach exploited to achieve the synthesis of molecules illustrated in **Scheme 27** is similar to that used in for the tri substituted NDIs already described in the previous chapter. Particularly interesting, instead, is the general synthetic approach for the generation of the alcoholic QMP, which has been optimized and developed in this PhD work as depicted in **Scheme 30**. Such a 7 steps synthetic route is original and widely applicable for the preparation of a large number of derivatives, thus allowing a possible high throughput screening approach for the synthesis of different NDIs derivatives. The key step of this synthetic route is the acylation of

the amino intermediate **99**, by using a chloro-acylchloride, generating the amide **100** which can be functionalized as azide *via* SN and successively reduced to give the amine **102**.



Scheme 30. Synthetic protocol for the synthesis of new QMP. (i) H₂O/CaCO₃ MW (ii) CH₃COCH₃, PTSA (iii) H₂ Pt/C (iv) Chloroacetylchloride TEA/THF (v) NaN₃ DMF (vi) PPh₃ THF

The amines derivatives (**102**) so synthesized have been tethered to the NDI **85** according to a protocol similar to that described in the previous chapter (**Scheme 31**).



Scheme 31. Synthetic protocol for the coupling of amines **102** and the brominated NDI core.

FRET Melting Assays

Because the accomplishment of the synthesis of these new NDIs derivatives has been achieved in the very last part of this work, the biophysical studies are just preliminary. First of all we investigated the behavior of this third generation NDIs as G-4 ligands through FRET thermocycling, in order to estimate the effects brought by the modifications on molecular shape and dimension. The experimental conditions and the oligonucleotides used are impossible to those described in the previous chapter. As partially expected molecule **87** revealed to be the best ligand. That was probably due both to the absence of the bromine atom and the correct spacer length. Brominated derivatives or longer spacers are translated into a lower G-4 binding efficacy as already observed for the other NDIs derivatives discussed in this work. **Table 11** reports the telomeric G-4 melting temperatures obtained in the presence of 1 μM concentration of ligands.

Table 11. ΔT_m of binding NDI compounds at 1 μM conc, measured by FRET of the labeled oligonucleotide F21T in K^+ solution.

Compound	ΔT_m °C (1 μM)
87	22.0 \pm 0.3
88	11.0 \pm 0.8
89	12.0 \pm 0.3
90	16.0 \pm 0.5
91	8.5 \pm 0.4
92	10.0 \pm 0.6

By considering only the FRET melting values, this new generation of NDI derivatives does not represent an evolution in binding potency. In fact, at similar concentration (0.8 compared to 1

μM) only molecule **87** gave values comparable to those obtained for the chemically simpler NDIs **71**, **72** and **73**. Probably, such a dramatic difference is partially due to the absence of the quaternary ammonium salt, which could strongly contribute to the binding strength through electrostatic interactions with the oligonucleotide.

Does third generation NDIs induce parallel-like G-4 topology as consequence of the alkylation process? CD consideration.

Although FRET data suggested that the above molecules, except **87**, were not excellent G-4 binders, we also investigated their alkylating properties and selectivity towards different G-4 topologies. Despite the FRET melting values, we surprisingly found that the brominated molecule **88** was able to induce a selective topology switch from a mixed type to a parallel topology at 40 °C. Conversely, for molecule **87** such a feature was observed with significant lower intensity. The CD spectra reported in **Figure 35** clearly underline the last statement.

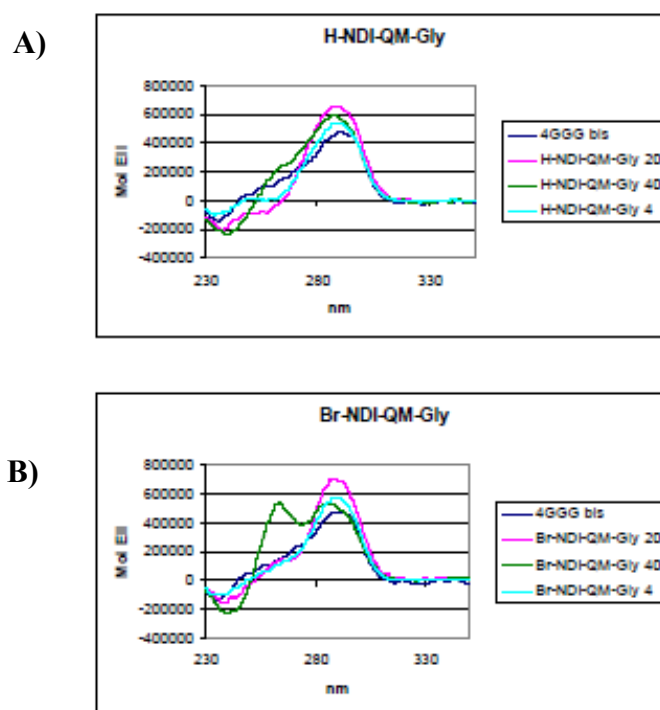


Figure 35. CD analysis of NDIs **87** (A) and **88** (B) at 4 (light blue), 20 (pink) and 40 °C (green) digested with *h-telo* oligonucleotide in the presence of K^+ 50 mM. The blue line is referred to the oligonucleotide without drug treatment.

Moreover, gel electrophoresis under denaturing condition (urea 7M) revealed a higher tendency for molecule **88** to undergo alkylation of the G-4 folded oligonucleotide. **Figure 36** reveals how the brominated derivative starts to alkylate the telomeric G-4 under concentrations around 60 nM. For higher concentration, in the μM range, the formation of a second adduct begins to be appraisable. Conversely, for molecule **87** higher concentrations are required in order to obtain comparable results.

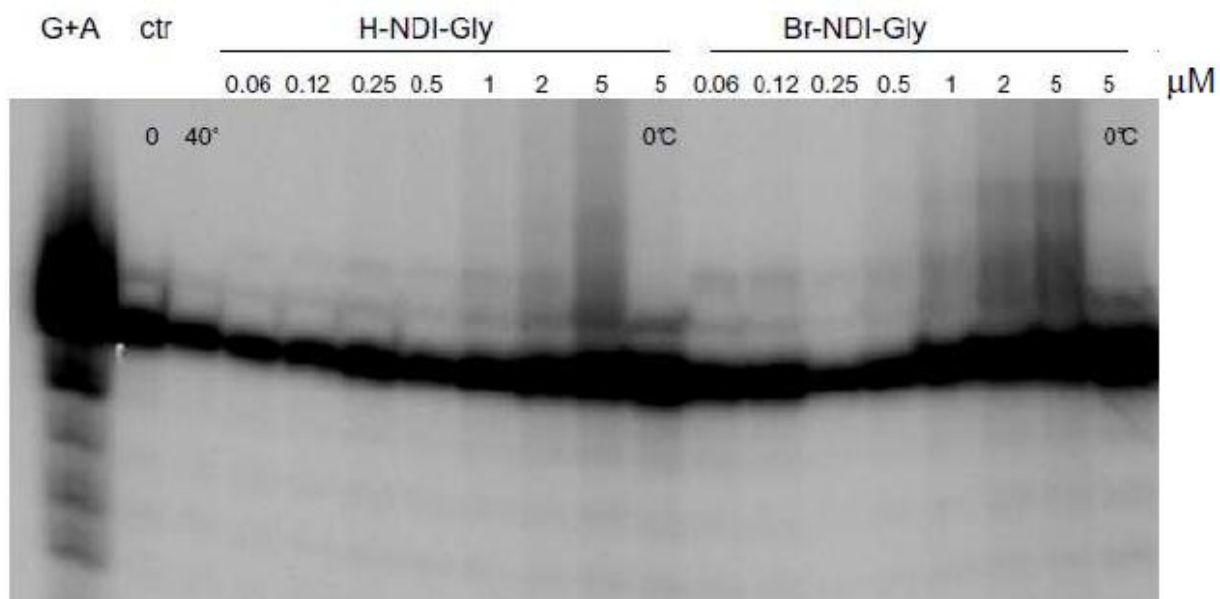


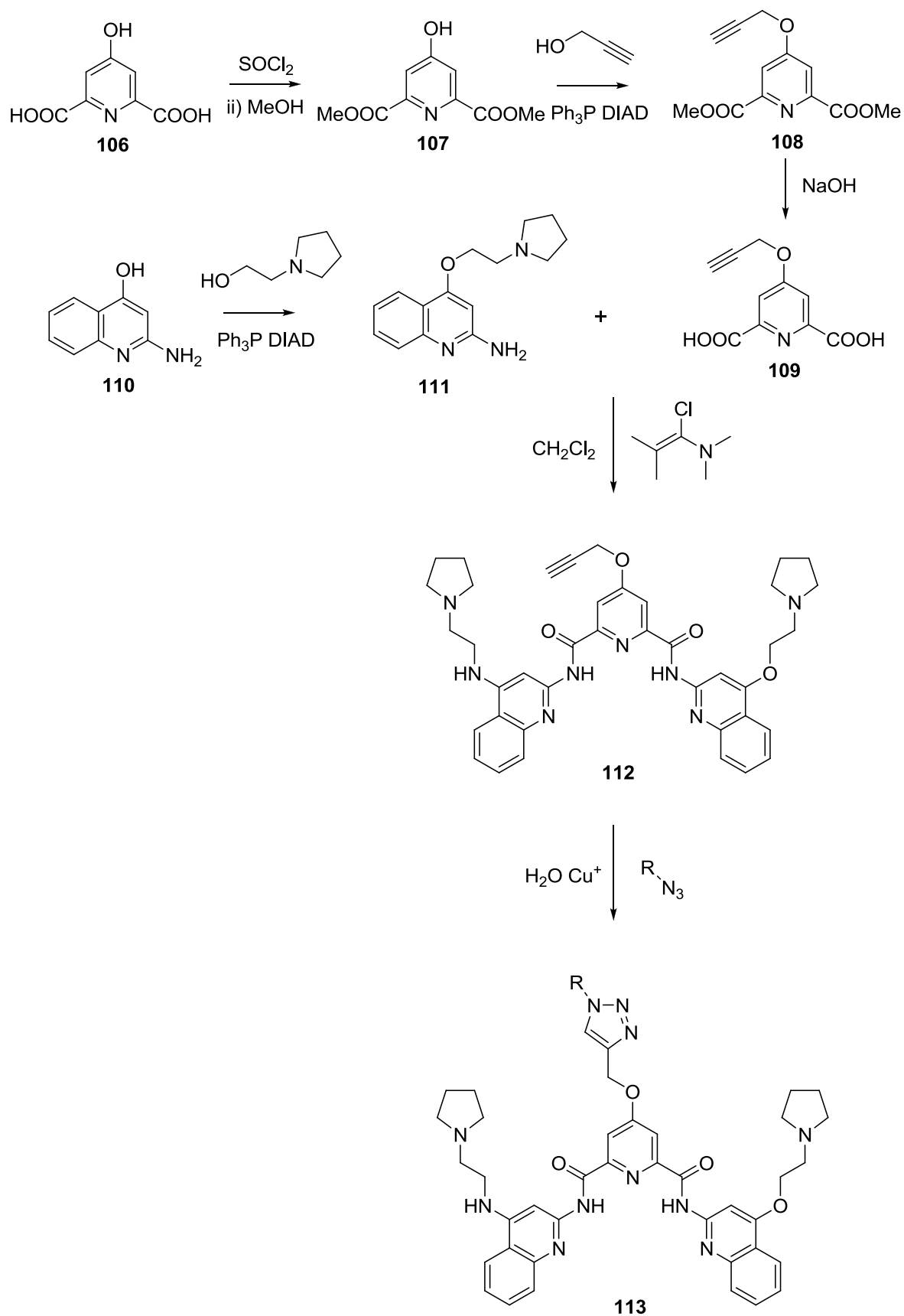
Figure 36. Alkylation effects of NDIs **87** and **88**. Alkylation of NDIs **87** and **88** at the 4GGG DNA level. The P^{32} 5'-end labeled 4GGG oligo was incubated with increasing amounts of NDIs (60nm - 5 μM) at 40°C to activate alkylation. The alkylated DNA (alk) was separated from the unreacted DNA (free) by 20% polyacrylamide 7 M urea denaturing gel.

Although a striking comparison between the alkylating results and the CD outcome is neither subsistent nor could be done, it is worthy to underline that the most powerful alkylating agent is the only one of this family inducing a topology switch at 40 °C (temperature at which the alkylation is triggered) even though it is not the best ligand according to FRET melting. Since we already reported that tri and tetra substituted NDIs are intrinsically capable of inducing a parallel

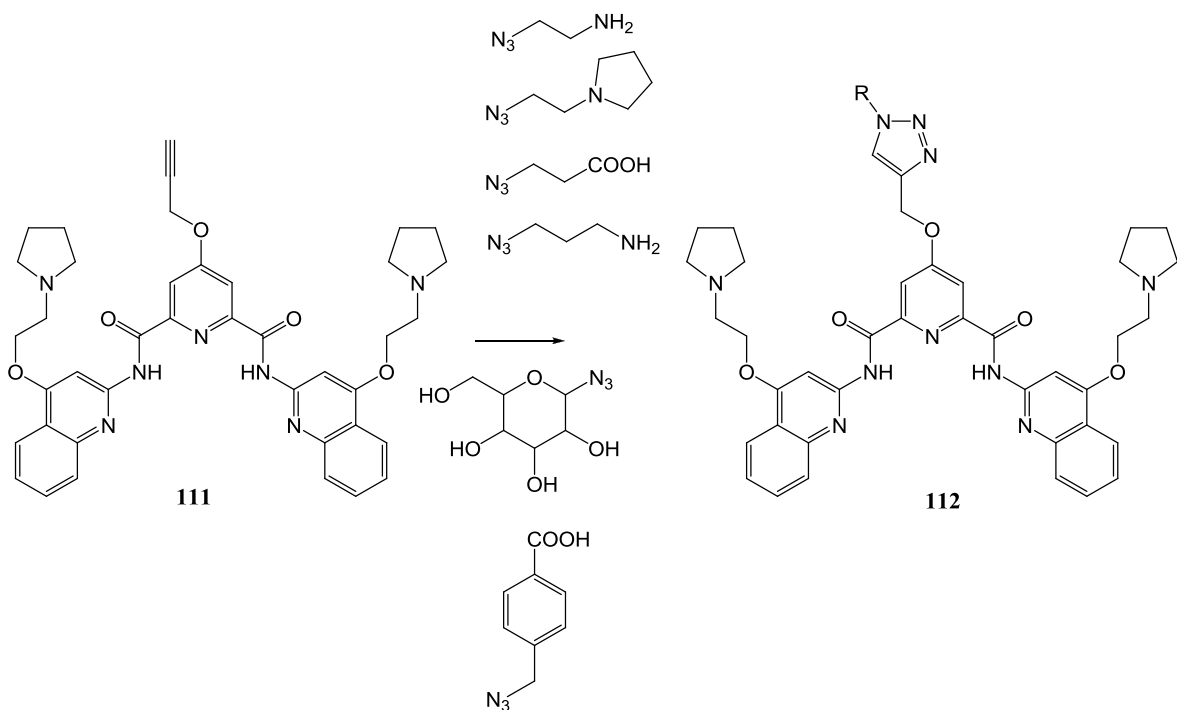
like topology as reversible binders (molecule **72**), we should not consider these experimental evidences as consequence of the alkylation. On the other hand, the simple alkylating NDI **50**, which should not stabilize any preferential topology according to literature, gave very similar results, thus suggesting that the alkylation process can strongly influence the conformational flexibility of the oligo strand, and a parallel-like topology rearrangement may eventually occurs as alkylation response. Further experiments are required in order to unravel this peculiar behavior.

New Raphaine Derivatives: Towards “in-situ” Synthesis of G-4 New Ligands.

As already mentioned this PhD project includes a reasearch contribution made at Cambridge University during a 6 month period spent in Balasubramanian’s group. Prof. Shankar Balasubramanian is one of the greatest experts in the G-4 field, as already cited in the introduction section of this work. Under the supervision of his co-worker Dr. Raphael Rodriguez we were able to start a new project which does not involve the alkylation process but is still aimed at unraveling G-4 relevance *in vivo*. Because of the very high efficacy of Raphaine A structure as G-4 binder, Dr. Rodriguez suggested to investigate how the introduction of more complex side chains in Raphaine molecule could be translated in terms of binding efficacy. Furthermore, exploiting the very efficient “click chemistry” protocol, we were able both to link a large number of chemically different appendages and to perform the reaction in the presence of G-4 organized oligonucleotides. In more details, we investigated if performing the reaction in the presence of the G-4 folded oligonucleotide gave a product distribution different from those obtained in solution. In other words we were looking for a template effect of the oligonucleotide in the click chemistry coupling. Such idea is summarized in **Scheme 33** together with the synthetic approach used to achieve the above derivatives preparation (**Scheme 32**).



Scheme 32. Synthetic protocol for the preparation of the new Raphaine derivatives explored during the Cambridge experience spent during the PhD.



Scheme 33. Reaction performed in the presence of different azides. The product distribution has been followed by HPLC either with or without a catalytic amount of *h-telo* G-4, with the aim to underline the possible template effect induced by the oligonucleotide.

Unfortunately we have not been able to follow by chromatography the experiments conducted in the presence of the oligonucleotides. Such an issue has been attributed to the high binding affinity with the oligonucleotides of the molecules generated by the “click reaction”. Therefore, even in strong denaturing conditions such as urea 8 M or NaOH or heating 50 °C, we have not been able to release the molecules generated from the *h-telo* oligonucleotide. Further experiments are presently underway in Cambridge with biotin functionalized oligonucleotides in order to concentrate them onto avidin beads and release the molecules by heating the latter. The product distribution under oligo free condition has been characterized in details so the experiments with biotinylated molecules should provide the first proof of concept of the project.

CONCLUSIONS

In this thesis we have described the design, the synthesis and the biophysical behavior of new molecular devices capable of selective cross linking towards G-4 folded oligonucleotides. New biocompatible activation protocols and original synthetic strategies have been developed in order to achieve both selectivity towards the target and triggerable cross linking activity. The preparation of a small library of new NDI and NI derivatives has been accomplished, together with a detailed study of the reactivity towards simple nucleophiles as well as nucleobases and different oligonucleotides. Moreover, the chemical improvement and evolution of the synthesized molecules led us to the generation of tri-substituted NDIs derivatives which showed strong selectivity for parallel like G-4 topology. *In cellulo* experiments and telomerase inhibition showed how the synthesized molecules still retain their activity in cellular environment and, incidentally, cytotoxicity values overlap *in vitro* activity.

To the best of our knowledge these results represent the very first case of engineered molecules capable of alkylating G-4 structures through non metal covalent interactions. Unraveling G-4 formation and functions *in vivo* is a crucial biological task; in this work we have developed a new generation of G-4 selective binders exploitable both for diagnostic and therapeutic purposes. These data altogether represent a little, useful step towards the understanding and hopefully targeted modulation of G-4 functions *in vivo*.

EXPERIMENTAL SECTION

1,8 Naphthalimides Derivatives Synthesis and Characterization.

Microwave imidization of 1,8-Naphthalic anhydride (14-17): General Procedure

Although the synthesis of similar NI derivatives has already been published,²⁰⁸ we manage to develop a new microwave based methodology. In this way, we were able to carry out the reaction in 1 h instead of 16 h, with higher yield. In more details, 500 mg (2.5 mmol) of 1,8-Naphthalic anhydride and 3.1 mmol of the respective amine (4-aminophenol, Tyramine) were suspended in 6 ml of pyridine. The mixture was irradiated during 1 h in a CEM oven, programmed to maintain a constant temperature (130 °C) with a maximal power output of 200 W. After cooling, the pyridine was removed under reduced pressure. The crude solid was then suspended in an HCl aqueous solution, filtered and washed first with acidic water and then twice with anhydrous EtOH.

The crude imides (**14**) and (**17**) were obtained as grey-violet (97% yield) and white-yellow solid (95% yield) respectively. These compounds have been used without further purification. The spectroscopic data found for the imide **14** were in agreement with those reported in literature.²⁶⁸

N-(4-hydroxyphenyl)-1,8-naphthalimide (14): Mp 239-241 °C; ¹H-NMR (CDCl₃): δ 6.98 (d, 2H), 7.15 (d, 2H), 7.85 (t, 2H), 8.30 (d, 2H), 8.70 (d, 2H); ¹³C-NMR (CDCl₃): δ 115.41, 122.69, 126.69, 127.21, 127.77, 129.84, 130.69, 131.42, 134.29, 157.36, 163.86. Anal. Calcd for C₁₈H₁₁NO₃: C, 74.73, H, 3.83; N, 4.84; O, 16.59. Found: C, 74.70, H, 3.86; N, 4.88.

N-[(4-hydroxyphenyl)ethyl]-1,8-naphthalimide (17): Mp 225-227 °C ; ¹H -NMR (DMSO-d₆): δ 2.80 (t, 2H, J = 8.0 Hz), 4.17 (t, 2H, J = 8.0 Hz), 6.69 (d, 2H, J = 8.4 Hz), 7.06 (d, 2H, J = 8.4 Hz), 7.84 (t, 2H, J = 8.0 Hz), 8.44 (m, 4H), 9.24 (s, 1H); ¹³C-NMR (DMSO-d₆): δ 32.77, 41.32, 115.24, 121.93, 127.16, 128.74, 129.50, 130.65, 131.22, 134.27, 155.78, 163.18. Anal. Calcd for C₂₀H₁₅NO₃: C, 75.70, H, 4.76; N, 4.41; O 15.13. Found: C, 75.72, H, 4.73; N, 4.48.

Mannich Reaction (10-13). General Procedure

500 mg of the respective 1,8-naphthalimide (**14,17**) were dissolved in anhydrous toluene (60 ml). 1.2 equivalents of N,N-dimethyl-methyleniminium chloride and 1.6 equivalents of K₂CO₃ were added to the solution. This mixture was allowed to reflux with vigorous stirring under nitrogen atmosphere for 4 h. After TLC control (EtOAc/MeOH 8:2), the solid suspension was filtrated and washed with 30 ml of ethyl acetate. The filtrated organic solution was dried under vacuum and the crude residue was purified by flash chromatography (EtOAc/MeOH 8:2). Such a procedure afforded **15** (59% Yield) or **18** (40% Yield).

N-[3-(dimethylamino)methyl-4-hydroxyphenyl]-1,8-naphthalimide (15): Mp = 210-211°C, ¹H-NMR (CDCl₃): δ 2.30 (s, 6H), 3.70 (s, 2H), 6.90 (d, 1H, J = 2.3 Hz), 7.0 (d, 1H, J = 8.5 Hz), 7.15 (dd, 1H, J = 2.4, 8.5 Hz), 7.85 (t, 2H, J = 7,3 Hz), 8.30 (d, 2H, J = 8.3 Hz) 8.70 (d, 2H, J = 7.3 Hz). ¹³C-NMR (CDCl₃): δ 44.33, 62.39, 108.27, 116.92, 122.20, 122.81, 126.03, 126.91, 128.20, 128.66, 131.46, 131.62, 134.06, 158.19, 164.57. Anal. Calcd for C₂₁H₁₈N₂O₃: C, 72.82; H, 5.24; N, 8.09; O,13.86. Found: C, 72.79; H, 5.27; N, 8.03.

N-[(3-(dimethylamino)methyl-4-hydroxyphenyl)ethyl]-1,8-naphthalimide (18): Mp = 185-188 °C; ¹H-NMR (CDCl₃): δ 2.30 (s, 6H), 2.94 (t, 2H, J = 8.4 Hz), 3.61 (s, 2H), 4.37 (t, 2H, J = 8.4 Hz), 6.78 (d, 1H, J = 8.2 Hz), 6.97 (d, 1H, J = 2.0 Hz), 7.17 (dd, 1H, J = 2.1, 8.2 Hz), 7.77 (t, 2H, J = 7.4 Hz), 8.22 (d, 2H, J = 7.4 Hz), 8.61 (d, 2H, J = 7.0 Hz); ¹³C-NMR (CDCl₃): δ 33.29, 41.94, 44.33, 62.70, 115.83, 121.78, 122.61, 126.80, 128.04, 128.77, 128.91, 129.06, 131.02, 131.49, 133.75, 156.46, 163.96. Anal. Calcd for C₂₃H₂₂N₂O₃: C, 73.78; H, 5.92; N, 7.48; O, 12.82. Found: C, 73.79; H, 5.89; N, 7.45

Exhaustive Methylation of Mannich bases (15-18). General Procedure

500 mg of the respective Mannich base (**15, 18**) were dissolved in CH₃CN (30 ml) and CH₃I (5 equivalents) was added dropwise. The solution was stirred at r.t. under nitrogen atmosphere until crashing out of a white solid is observed. To enhance solid precipitation 10 ml of Et₂O could be

added. The white solid was collected by filtration and washed twice with cold CH₃CN to give **16** (73% Yield) or **19** (75% Yield).

N-[3-(trimethylamino)methyl-4-hydroxyphenyl]-1,8-naphthalimide iodide (16): Mp = 256-257°C, ¹H-NMR (DMSO-d₆): δ 3.34 (s, 9H), 4.62 (s, 2H), 7.15 (d, 1H, J = 8.6 Hz), 7.35 (d, 1H, J = 2.4 Hz), 7.48 (dd, 1H, J = 2.3 Hz), 7.85 (t, 2H, J = 7.6 Hz), 8.50 (d, 2H, J = 5.1 Hz), 8.58 (d, 2H, J = 6.3 Hz). ¹³C-NMR (DMSO-d₆): δ 52.00, 62.78, 114.71, 116.30, 122.52, 126.85, 127.29, 127.77, 130.83, 131.45, 132.68, 134.55, 134.92, 157.05, 163.83. Anal. Calcd for C₂₂H₂₁IN₂O₃: C, 54.11; H, 4.33; I, 25.99; N, 5.74; O, 9.83. Found: C, 54.10; H, 4.38; I, 25.90; N, 5.72.

N-[(3-(trimethylamino)methyl-4-hydroxyphenyl)ethyl]-1,8-naphthalimide iodide (19): Mp = 251-256 °C, ¹H-NMR (DMSO-d₆): δ 2.87 (t, 2H, J = 7.6 Hz), 2.97 (s, 9H), 4.22 (t, 2H, J = 7.5 Hz), 4.39 (s, 2H), 6.85 (d, 1H, J = 8.3 Hz), 7.18 (dd, 1H, J = 2.0, 6.4 Hz), 7.27 (d, 1H, J = 1.8 Hz), 7.85 (t, 2H, J = 7.7 Hz), 8.44 (m, 4H), 10.14 (s, 1H); ¹³C-NMR (DMSO-d₆): δ 32.48, 41.11, 51.85, 63.00, 114.51, 116.06, 121.89, 127.25, 129.39, 130.69, 131.26, 132.41, 134.41, 134.72, 155.72, 163.26. Anal. Calcd for C₂₄H₂₅IN₂O₃: C, 55.82.01; H, 4.88; I, 24.58; N, 5.43; O, 9.30. Found: C, 55.80; H, 4.90; I, 24.55; N, 5.45.

Photoactivation of Naphthalimides 16 and 19. General Procedure

Photoreactivity of molecule **16** and **19** as alkylating agents has been performed according the following procedure. A Pyrex tube was filled with 10 ml of a 5 × 10⁻⁴M solution of **16** or **19** in H₂O/CH₃CN 1:1. To this solution the freshly distilled nucleophile was added until its concentration reaches 5 × 10⁻³M and, purge with N₂ flush was performed for 5 minutes. After that time the tube was irradiated in a multi lamp reactor fitted with four lamps centered at 310 nm for the required time (5-60 min). Conversion has been followed by analytical HPCL (H₂O added with 0.1% TFA and CH₃CN as eluent system).

Activation by Base Catalysis of Naphthalimides 16 and 19. General Procedure

Alkylating properties of molecules **16** and **19** towards different nucleophiles (amines, thiols and water) has also been investigated under thermal base catalysis. To a 5×10^{-4} M solution of **16** or **19** in a 1:1 mixture H₂O/CH₃CN, the freshly distilled nucleophile was added until its concentration reaches 5×10^{-3} M. Basic catalysis has been achieved according two different strategies: (i) by the use strong basic nucleophiles, such as amines, or (ii) by the employment of an aqueous carbonate buffer media (pH 10, NaHCO₃/Na₂CO₃) with nucleophiles displaying poor basicity. Conversion has been followed by analytical HPCL (H₂O added with 0.1% TFA and CH₃CN as eluent system).

Adduct 20: Yellow oil; ¹H-NMR (DMSO-d₆): δ 4.54 (s, 2H), 5.07 (bs, 1H), 6.88 (d, 1H, J = 8.4 Hz), 7.02 (dd, 1H, J = 2.4, 8.4 Hz), 7.23 (d, 1H, J = 2.2 Hz), 7.9 (t, 2H, J = 7.7 Hz), 8.3 (m, 4H), 9.6 (bs, 1H). ¹³C-NMR (DMSO-d₆): δ 58.01, 114.60, 122.69, 126.81, 127.20, 127.40, 127.59, 127.78, 129.16, 130.68, 131.43, 134.29, 153.75, 163.89. Anal. Calcd for C₁₉H₁₃NO₄: C, 71.47; H, 4.10; N, 4.39. O, 20.04. Found: C, 71.49; H, 4.09; N, 4.41.

Adduct 21: Yellow needles; Mp = 214-215°C; ¹H-NMR (CDCl₃): δ 1.70 (m, 6H), 3.22 (m, 4H), 3.75 (s, 2H), 6.90 (d, 1H, J = 2.4 Hz), 7.0 (d, 1H, J = 8.5 Hz), 7.15 (dd, 1H, J = 2.5, 8.5 Hz), 7.80 (t, 2H, J = 8.0 Hz), 8.25 (d, 2H, J = 7.4 Hz), 8.65 (d, 2H, J = 6.3 Hz). ¹³C-NMR (CDCl₃): δ 21.98, 25.55, 44.55, 53.79, 116.86, 121.86, 122.72, 125.98, 126.93, 128.35, 128.48, 128.52, 131.50, 131.60, 134.14, 158.24, 164.61. Anal. Calcd for C₂₄H₂₀N₂O₃: C, 74.59; H, 5.74; N, 7.25; O, 12.42. Found: C, 74.40; H, 5.85; N, 7.32.

Adduct 22: Pale yellow needles; Mp = 128-129°C; ¹H-NMR (CDCl₃): δ 0.90 (t, 3H, J = 7.3 Hz), 1.20 (t, 3H, J = 7.2 Hz), 1.45 (m, 2H), 1.65 (m, 2H), 2.65 (m, 2H), 2.75 (m, 2H), 4.00 (s, 2H), 6.90 (d, 1H, J = 2.2 Hz), 7.0 (d, 1H, J = 8.5 Hz), 7.15 (dd, 1H, J = 2.3, 8.3 Hz), 7.85 (t, 2H, J = 7.6 Hz), 8.30 (d, 2H, J = 8.2 Hz), 8.70 (d, 2H, J = 7.3 Hz). ¹³C-NMR (CDCl₃): δ 10.51, 13.81, 20.34, 27.95, 46.99, 52.54, 56.43, 117.36, 121.57, 122.77, 126.13, 126.92, 128.78, 129.00,

131.48, 131.61, 134.10, 158.06, 164.54. Anal. Calcd for C₂₅H₂₆N₂O₃: C, 74.60; H, 6.51; N, 6.96; O, 11.93. Found: C, 74.55; H, 6.72; N, 7.05.

Adduct 23: Yellow needles; Mp = 222-224° C; ¹H-NMR (CDCl₃): δ 2.65 (bs, 4H), 3.78 (m, 6H), 6.90 (d, 1H, J = 2.3 Hz), 7.0 (d, 1H, J = 8.5 Hz), 7.15 (dd, 1H, J = 2.3, 8.5 Hz), 7.85 (t, 2H, J = 8.5 Hz), 8.30 (d, 2H, J = 8.3 Hz), 8.70 (d, 2H, J = 8.3 Hz). ¹³C-NMR (CDCl₃): δ 52.88, 61.53, 66.67, 116.86, 121.23, 122.73, 126.40, 126.92, 128.37, 128.66, 128.91, 131.62, 131.48, 134.13, 157.66, 164.56. Anal. Calcd for C₂₃H₂₀N₂O₄: C, 71.12; H, 5.19; N, 7.21; O, 16.48. Found: C, 71.35; H, 5.10; N, 7.05.

Adduct 24: Yellow needles; Mp = 153-155° C; ¹H-NMR (DMSO-d₆): δ 1.30 (s, 9H), 4.00 (s, 2H), 6.90 (d, 1H, J = 8.5 Hz), 7.15 (dd, 2H, J = 2.3, 8.5 Hz), 7.95 (t, 2H, J = 8.5 Hz), 8.51 (m, 4H). ¹³C-NMR (DMSO-d₆): δ 26.59, 40.87, 42.12, 115.59, 121.96, 122.52, 126.50, 127.25, 127.77, 129.58, 129.95, 130.71, 131.45, 134.40, 156.99, 163.86. Anal. Calcd for C₂₃H₂₂N₂O₃: C, 73.78; H, 5.92; N, 7.48; O, 12.82. Found: C, 73.53; H, 5.98; N, 7.52.

Adduct 25: White dust; Mp = 215-216° C; ¹H-NMR (DMSO-d₆): δ 2.83 (m, 2H), 3.55 (m, 2H), 3.73 (s, 2H), 4.74 (bs, 1H), 6.93 (d, 1H, J = 8.4 Hz), 7.04 (dd, 1H, J = 2.4, 8 Hz), 7.16 (d, 1H, J = 2 Hz), 7.88 (t, 2H, J = 8 Hz), 8.48 (m, 4H), 9.7 (s, 1H). ¹³C-NMR (DMSO-d₆): 33.43, 37.55, 60.54, 114.74, 122.10, 124.87, 126.12, 126.63, 127.22, 127.75, 129.85, 130.16, 130.87, 133.75, 154.31, 163.28. Anal. Calcd for C₂₁H₁₇NO₄S: C, 66.47; H, 4.52; N, 3.69; O, 16.87; S, 8.45. Found: C, 66.45; H, 4.55; N, 3.72; S, 8.43.

Adduct 26: Yellow oil; ¹H-NMR (DMSO-d₆): δ 2.81 (t, 2H, J = 8.3 Hz), 4.19 (t, 2H, J = 8.2 Hz), 4.47 (d, 2H, J = 5.3 Hz), 4.96 (t, 1H, J = 5.3 Hz), 6.71 (d, 1H, J = 8.0 Hz), 6.91 (dd, 1H, J = 2.4, 8.0 Hz), 7.25 (d, 1H, J = 2.4 Hz), 7.89 (t, 2H, J = 8.0 Hz), 8.49 (m, 4H), 9.18 (s, 1H). ¹³C-NMR (DMSO-d₆): 33.03, 41.52, 58.16, 114.56, 122.09, 125.05, 127.24, 127.38, 127.46, 128.56, 129.49, 130.72, 131.32, 134.34, 152.58, 163.29. Anal. Calcd for C₂₁H₁₇NO₄: C, 72.61; H, 4.93; N, 4.03; O, 18.42. Found: C, 72.60; H, 4.95; N, 4.02.

Adduct 27: White solid; Mp = 145-150° C; ¹H-NMR (CDCl₃): δ 1.60 (m, 6H), 2.46 (bs, 4H), 2.92 (m, 2H), 3.62 (s, 2H), 4.34 (m, 2H), 6.76 (d, 1H, J = 8.2), 6.96 (d, 1H, J = 1.8 Hz), 7.16 (dd, 1H, J = 2.0, 8.1 Hz), 7.75 (t, 2H, J = 7.7 Hz), 8.19 (d, 2H, J = 7.6 Hz), 8.50 (d, 2H, J = 6.6 Hz); ¹³C-NMR (CDCl₃): δ 23.89, 25.74, 33.28, 41.95, 53.73, 61.97, 115.79, 121.48, 122.54, 126.79, 127.97, 128.87, 128.95, 131.00, 131.44, 133.76, 156.47, 163.89. Anal. Calcd for C₂₆H₂₆N₂O₃: C, 75.34; H, 6.32; N, 6.76; O, 11.58. Found: C, 75.35; H, 6.30; N, 6.72.

Adduct 28: Yellow needles; Mp = 112-115° C; ¹H-NMR (CDCl₃): δ 0.92 (t, 3H, J = 7.2 Hz), 1.08 (t, 3H, J = 7.2 Hz), 1.33 (m, 2H), 1.53 (m, 2H), 2.54 (m, 4H), 2.93 (m, 2H), 3.74 (s, 2H), 4.35 (m, 2H), 6.76 (d, 1H, J = 8.1 Hz), 6.99 (s, 1H), 7.15 (dd, 1H, J = 1.5, 8.0 Hz), 7.76 (t, 2H, J = 8.1 Hz), 8.21 (d, 2H, J = 8.2 Hz), 8.60 (d, 2H, J = 7.2 Hz); ¹³C-NMR (CDCl₃): 10.79, 13.84, 20.44, 28.48, 33.32, 41.99, 46.55, 52.46, 57.31, 115.89, 121.98, 122.55, 126.81, 127.99, 128.88, 131.02, 131.46, 133.79, 156.60, 163.92. Anal. Calcd for C₂₇H₃₀N₂O₃: C, 75.32; H, 7.02; N, 6.51; O, 11.15. Found: C, 75.35; H, 7.00; N, 6.55.

Adduct 29: White powder; Mp = 182-185° C; ¹H-NMR (CDCl₃): δ 2.48 (bs, 4H), 2.90 (m, 2H), 3.64 (s, 2H), 3.71 (bs, 4H), 4.32 (m, 2H), 6.76 (d, 1H, J = 8.17 Hz), 6.96 (d, 1H, J = 1.8 Hz), 7.16 (dd, 1H, J = 2.0, 8.1 Hz), 7.72 (t, 2H, J = 7.6 Hz), 8.18 (d, 2H, J = 8.2 Hz), 8.56 (d, 2H, J = 7.2 Hz); ¹³C-NMR (CDCl₃): 33.19, 41.84, 52.74, 61.66, 66.67, 115.95, 120.49, 122.51, 126.81, 127.97, 129.33, 129.38, 131.01, 131.44, 133.80, 155.86, 163.68. Anal. Calcd for C₂₅H₂₄N₂O₄: C, 72.10; H, 5.81; N, 6.73; O, 15.37. Found: C, 72.15; H, 5.78; N, 6.70.

Adduct 30: Yellow solid; Mp 132-135°C; ¹H-NMR (DMSO-d₆): δ 1.07 (s, 9H), 2.77 (t, 2H, J = 7.3 Hz), 3.78 (s, 2H), 4.15 (t, 2H, J = 7.3 Hz), 6.59 (d, 1H, J = 8.2 Hz), 6.96 (m, 2H), 7.83 (t, 2H, J = 7.4 Hz), 8.42 (m, 4H); ¹³C-NMR (DMSO-d₆): δ 27.95, 32.74, 41.36, 44.51, 50.50, 115.63, 121.93, 124.44, 126.89, 127.12, 127.74, 128.14, 128.22, 130.62, 131.22, 134.24, 156.57, 163.17. Anal. Calcd for C₂₅H₂₆N₂O₃: C, 74.60; H, 6.51; N, 6.96; O, 11.93. Found: C, 74.62; H, 6.49; N, 6.94.

Adduct 31: White solid; Mp = 190-194° C; ¹H-NMR (CDCl₃): δ 2.58 (m, 2H), 2.97 (t, 2H, J = 7.3 Hz), 3.77 (m, 2H), 3.84 (s, 2H), 4.42 (t, 2H, J = 7.3 Hz), 6.5 (bs, 1H), 6.75 (d, 1H, J = 8.1 Hz), 7.07 (dd, 1H, J = 2.0, 6.0 Hz), 7.14 (d, 1H, J = 2.0 Hz), 7.78 (t, 2H, J = 7.4 Hz), 8.25 (d, 2H, J = 7.4 Hz), 8.59 (d, 2H, J = 7.3 Hz). ¹³C-NMR(CDCl₃): δ 30.82, 31.99, 32.50, 33.15, 41.72, 61.49, 116.81, 122.37, 126.89, 129.68, 130.76, 131.18, 131.28, 131.50, 133.98, 143.50, 153.58, 164.09. Anal. Calcd for C₂₃H₂₁NO₄S: C, 67.79; H, 5.19; N, 3.44; O, 15.71; S, 7.87. Found: C, 67.82; H, 5.15; N, 3.42; S, 7.89.

Adduct 32: White needles; Mp = 273-274° C; ¹H-NMR (CDCl₃): δ 1.28 (m, 3 H), 2.08 (m, 2H), 2.72 (m, 1H), 3.06 (m, 1H), 3.68 (m, 1H), 3.95 (m, 1H), 5.32 (bs, 1H), 7.0 (m, 3H), 7.85 (t, 2H, J = 8.5 Hz), 8.30 (d, 2H, J = 8.3 Hz), 8.67 (d, 2H, J = 7.3Hz). ¹³C-NMR (CDCl₃): δ 14.98, 20.51, 26.09, 63.67, 96.99, 117.79, 122.78, 123.50, 126.91, 127.10, 127.48, 128.39, 128.93, 131.51, 131.61, 134.09, 152.35, 164.56. Anal. Calcd for C₂₃H₁₉NO₄: C, 73.98; H, 5.13; N, 3.75; O, 17.14. Found: C, 73.85; H, 5.03; N, 3.70.

Adduct 33: White needles; Mp = 168-170° C; ¹H-NMR (CDCl₃): δ 1.22 (t, 3H, J = 7.0 Hz), 2.04 (m, 2H), 2.63 (m, 1H), 2.94 (m, 3H), 3.69 (m, 1H), 3.94 (m, 1H), 4.38 (m, 2H), 5.26 (bs, 1H), 6.82 (d, 1H, J = 7.8 Hz), 7.10 (s, 1H), 7.15 (d, 1H, J = 8.2 Hz), 7.78 (t, 2H, J = 8.1 Hz), 8.23 (d, 2H, J = 8.2 Hz), 8.63 (d, 2H, J = 7.2 Hz); ¹³C-NMR(CDCl₃): 15.01, 20.43, 26.48, 33.43, 42.02, 63.52, 96.83, 116.81, 122.43, 122.61, 126.82, 127.71, 128.04, 129.63, 130.67, 131.05, 131.48, 133.79, 150.71, 163.93. Anal. Calcd for C₂₅H₂₃NO₄: C, 74.79; H, 5.77; N, 3.49; O, 15.94. Found: C, 74.82; H, 5.73; N, 3.52.

Naphthalendiimides as New Reductive Bis-Alkylating Agents. Synthesis and Characterization.

N,N'-bis[3-(dimethylamino)methyl-4-hydroxy-phenyl]-1,8,5,4-naphthalenetetracarboxylic diimide (35a): 2.0 g of 4-amino-2-[(dimethylamino)methyl]phenol dihydrochloride, prepared according published procedure, (8.4 mmol) and 1.07 g (4 mmol) of 1,4,5,8 tetracarboxylic

dianhydride were suspended in 20 ml of a mixture dioxane:DMF=9:1. TEA (1 ml) was added to the suspension and the mixture was allowed to reflux with vigorously stirring for 20 hrs, under nitrogen. The reaction mixture was cooled and poured into 30 ml of water. The resulting suspension was filtered and washed first with water and then twice with anhydrous EtOH. The N,N' bis[3-(dimethylamino)methyl-4-hydroxy]-1,8,5,4-naphthalenetetracarboxylic diimide was obtained as a pale green solid. M.p. > 350°C. ¹H NMR (DMSO-d⁶) δ, 2.25 (s, 12H, Me₂), 3.60 (s, 4H, CH₂), 6.90 (d, 2H, J = 7.4 Hz), 7.20 (d, 2H, J = 7.4 Hz), 7.25 (s, 2H), 8.70 (s, 4H), 9.70 (s, 2H). ¹³C NMR (DMSO-d⁶) δ, 41.87; 54.43; 116.05; 116.68; 126.24;126.64; 126.90; 130.55; 131.66; 132.93; 156.74; 163.03. Anal. Calcd for C₃₂H₂₈N₄O₆: C, 68.07; H, 5.00; N, 9.92; O, 17.00. Found: C, 68.14; H, 4.99; N, 9.90.

N,N'-bis[3-(trimethylamino)methyl-4-hydroxyphenyl]-1,8,5,4-naphthalenetetracarboxylic diimide iodide (35): 2.0 g (3.54 mmol) of diimide **35a** was suspended in CH₃CN (50 ml) and CH₃I (1.2 g; 8.5 mmol) was added. This suspension, refluxing under nitrogen, turned dark red color in a few minutes. After 3 hours the reaction was chilled and Et₂O (50 ml) was added with formation of red crystals. The suspension was filtered and washed twice with CH₃CN to give **4**, 2.5g (3 mmol, 84% yield) as a red-brownish solid. M.p.>350°C. ¹H NMR (DMSO-d⁶) δ, 3.1 (s, 18 H), 4.5 (s, 4 H), 7.10 (d, 2 H, J = 8,6 Hz), 7.4 (d, 2 H, J = 8.6 Hz), 7.50 (s, 2 H), 8.80 (s, 4 H), 10.9 (s, 2 H). ¹³C NMR (DMSO-d⁶) δ, 52.04; 62.81; 114.84; 116.43; 126.34; 126.63; 126.97; 130.53; 132.60; 134.82; 157.35;163.07. Anal. Calcd for C₃₄H₃₄I₂N₄O₆: C, 48.13; H, 4.04; I, 29.91; N, 6.60; O, 11.31. Found: C, 48.18; H, 4.02; I, 29.80; N, 6.63.

Activation by base catalysis. General procedure.

Base catalysis general method: The bis-alkylating properties of the diimide **35** have been activated by base catalysis in the presence of several nucleophiles (amines and thiols), according the following procedures:

Procedure A (For nucleophile with $pK_a > 8$). To a solution of **35** (50 ml, $\text{CH}_3\text{CN} : \text{H}_2\text{O} = 1 : 1$, 5×10^{-3} M) oxygen-purged with a N_2 flux, was added the nucleophile in order to reach a 5×10^{-2} M concentration. This solution was allowed to stand at 25 or 40°C and after 0.5-few hrs a pale yellow solid begins to form. After a few hrs the solution was concentrated under reduced pressure and the resulting suspension was cooled at 4°C for 12h. The solid was filtered and washed with cold anhydrous EtOH to provide the bis-alkylated adduct (**37-39**, **41-43**) in good yield (60-85 %).

Procedure B (For nucleophile with $pK_a < 8$): To 50 ml of a solution 5×10^{-3} M of the diimide **35** in a $\text{CH}_3\text{CN}:\text{H}_2\text{O}=1:1$ buffered to pH 8.5 with a $\text{Na}_2\text{CO}_3/\text{NaHCO}_3$ buffer, outgassed with a N_2 flux, was added the nucleophile in order to reach a concentration of 5×10^{-2} M. This solution was heated at 40°C for 12 hrs. After this time the CH_3CN was evaporated under vacuum and the suspension was kept at 4°C for 12 hrs. The solid was filtered and washed twice with cold water and anhydrous EtOH, to provide the bis-alkylated adducts (**40**, **44-46**) in good yield (55-70 %).

Activation by $\text{S}_2\text{O}_4^{2-}$ reduction. General procedure. In order to trap the nucleophiles by reductive activation of **35** a similar procedure to base catalytic method has been used. However lower concentration of substrate are requested in order to avoid assembling between **35** and its radical ion.

To 20 ml of an oxygen purged solution of the diimide **35** (5×10^{-4} M), was added the nucleophile in order to reach a concentration of 5×10^{-3} M and 2 ml of a $\text{Na}_2\text{S}_2\text{O}_4$ solution 0.1 M. The resulting violet solution is allowed to stand at 40°C for 4 hours. After this time the solution was chilled, treated with an air flux for 10 min. in order to consume the unreacted $\text{S}_2\text{O}_4^{2-}$. The CH_3CN was evaporated under vacuum and the product precipitated as a pale yellow solid.

Adduct 36: Pale yellow needles. M.p. $> 350^\circ\text{C}$. ^1H NMR ($\text{DMSO}-d^6$) δ , 4.40 (s, 4 H), 7.20 (d, 2 H, $J = 8.6$ Hz), 7.4 (d, 2 H, $J = 8.6$ Hz), 7.5 (s, 2 H), 8.8 (s, 4 H), 10.8 (s, 2 H). ^{13}C NMR ($\text{DMSO}-d^6$) δ , 64.6; 115.9; 117.2; 126.2; 126.9; 127.7; 131.0; 131.4; 132.9; 156.7; 163.1. Anal. Calcd for $\text{C}_{28}\text{H}_{18}\text{N}_2\text{O}_8$: C, 65.88; H, 3.55; N, 5.49; O, 25.07. Found: C, 65.77; H, 3.58; N, 5.45.

Adduct 37: Yellow needles. M.p. > 350°C. ^1H NMR (DMSO- d^6) δ , 1.10 (t, 12 H), 2.75 (q, 8 H), 3.70 (s, 4 H), 6.90 (d, 2 H, $J = 9.2$ Hz), 7.25 (d, 2 H, $J = 9.2$ Hz), 7.25 (s, 2 H), 8.6 (s, 4 H). ^{13}C NMR (DMSO- d^6) δ , 11.2; 45.9; 54.8; 115.5; 123.2; 126.1; 126.6; 127.0; 128.4; 128.8; 130.39; 157.5; 163.1. Anal. Calcd for $\text{C}_{36}\text{H}_{36}\text{N}_4\text{O}_6$: C, 69.66; H, 5.85; N, 9.03; O, 15.47. Found: C, 69.69; H, 5.84; N, 9.10.

Adduct 38: Yellow needles. M.p. > 350°C. ^1H NMR (DMSO- d^6) δ , 0.91 (t, 12 H); 1.10 (t, 12 H); 1.30 (q, 8 H); 1.5 (m, 8 H), 2.75 (m, 8 H), 3.75 (s, 4 H), 6.75 (d, 2 H, $J = 8.8$ Hz), 7.1 (d, 2 H, $J = 8.8$ Hz), 7.15 (s, 2 H), 8.7 (s, 4 H). ^{13}C NMR (DMSO- d^6) δ , 10.9; 13.8; 20.0; 28.2; 46.4; 52.0; 55.4; 115.5; 123.2; 126.06; 126.5; 127.0; 128.4; 128.9; 130.4; 157.5; 163.1. Anal. Calcd for $\text{C}_{40}\text{H}_{44}\text{N}_4\text{O}_6$: C, 70.99; H, 6.55; N, 8.28; O, 14.18. Found: C, 71.02; H, 6.58; N, 8.25.

Adduct 39: Pale yellow needles. M.p. > 350°C. ^1H NMR (CDCl_3) δ , 2.1 (d, 12 H), 2.5 (m, 2 H), 3.75 (s, 4 H), 6.9 (s, 2 H), 7.0 (d, 2 H, $J = 8.6$ Hz), 7.2 (d, 2 H, $J = 8.6$ Hz), 8.8 (s, 4 H). ^{13}C NMR (CDCl_3) δ , 30.8; 44.5; 62.5; 115.5; 117.0; 122.6; 125.1; 127.0; 127.9; 128.4; 131.3; 158.8; 163.2. Anal. Calcd for $\text{C}_{40}\text{H}_{44}\text{N}_4\text{O}_6$: C, 70.99; H, 6.55; N, 8.28; O, 14.18. Found: C, 71.09; H, 6.53; N, 8.21.

Adduct 40: Yellow needles. M.p. > 350°C. ^1H NMR (DMSO- d^6) δ , 3.70 (s, 20 H), 6.90 (d, 2 H, $J = 8.6$ Hz), 7.20 (d, 2 H, $J = 8.6$ Hz), 7.25 (s, 2 H), 8.75 (s, 4 H). ^{13}C NMR (DMSO- d^6) δ , 52.8; 58.0; 66.1; 115.4; 122.8; 126.3; 126.6; 127.0; 128.5; 129.7; 130.4; 156.3; 163.1. Anal. Calcd for $\text{C}_{36}\text{H}_{32}\text{N}_4\text{O}_8$: C, 66.66; H, 4.97; N, 8.64; O, 19.73. Found: C, 66.73; H, 5.00; N, 8.59.

Adduct 41: Characterized as hydrochloride (**41**·2HCl). Green needles. M.p. > 350°C. ^1H NMR (DMSO- d^6) δ , 2.75 (s, 18 H), 4.30 (s, 4 H), 7.20 (d, 2 H, $J = 8.6$ Hz), 7.4 (d, 2 H, $J = 8.6$ Hz), 7.5 (s, 2 H), 8.8 (s, 4 H), 10.0 (s, 4 H), 10.8 (s, 2 H). ^{13}C NMR (DMSO- d^6) δ , 25.1; 41.9; 54.6; 115.8; 116.0; 126.3; 126.6; 126.9; 130.9; 131.7; 132.9; 156.7; 163.0. Anal. Calcd for $\text{C}_{36}\text{H}_{38}\text{Cl}_2\text{N}_4\text{O}_6$: C, 62.34; H, 5.52; Cl, 10.22; N, 8.08; O, 13.84. Found: C, 62.29; H, 5.61; Cl, 10.19; N, 8.06.

Adduct 42: Yellow needles. M.p. > 350°C. ^1H NMR (DMSO- d^6) δ , 1.75 (s, 12 H), 3.5 (m, 8 H), 3.85 (s, 4 H), 6.80 (d, 2 H, $J = 8.8$ Hz), 7.25 (d, 2 H, $J = 8.8$ Hz), 7.25 (s, 2 H), 8.8 (s, 4 H). ^{13}C

NMR (DMSO-d⁶) δ , 25.5; 30.7; 53.3; 59.5; 115.5; 122.7; 126.3; 126.5; 126.90; 126.94; 127.0; 130.4; 156.3; 163.7. Anal. Calcd for C₃₈H₃₆N₄O₆: C, 70.79; H, 5.63; N, 8.69; O, 14.89. Found: C, 70.73; H, 5.65; N, 8.70.

Adduct 43: Yellow needles. M.p.>350°C. ¹H NMR (DMSO-d⁶) δ , 2.00 (m, 8 H), 3.10(m, 4 H), 3.5 (m, 4 H), 4.3(s, 4 H), 7.1(d, 2 H J = 8.6 Hz), 7.35(d, 2 H, J= 8,6 Hz), 7.50 (s, 2H), 8.7 (s, 4H)

¹³C NMR (DMSOd⁶) δ , 22.5; 51.5; 52.9; 116.0; 117.7; 126.3; 126.6; 126.9; 130.6; 131.4; 132.5; 156.4; 163.0. Anal. Calcd for C₃₆H₃₂N₄O₆: C, 70.12; H, 5.23; N, 9.09; O, 15.57. Found: C, 70.09; H, 5.25; N, 9.07.

Adduct 44: Yellow needles. M.p.>350°C. ¹H NMR (DMSO-d⁶) δ , 2.0 (m, 4 H), 2.1 (m, 2 H), 2.4 (m, 2 H), 3.2 (m, 2 H), 3.5 (m, 2 H), 3.7(m, 2 H), 3.9 (s, 6 H), 4.1(s, 4 H) , 7.1 (d, 2H, J = 8.65 Hz), 7.35 (d, 2 H, J= 8.65 Hz), 7.50 (s, 2H), 8.7 (s, 4H). ¹³C NMR (DMSO-d⁶) δ , 23.2; 29.4; 52.0; 52.6; 57.6; 65.0; 116.1; 117.2; 126.1; 126.4; 126.8; 130.7; 131.9; 132.6; 156.4; 163.0; 173.5. Anal. Calcd for C₄₀H₃₆N₄O₁₀: C, 65.57; H, 4.95; N, 7.65; O, 21.84. Found: C, 65.53; H, 4.99; N, 7.61.

Adduct 45: Yellow needles. M.p.>350°C. ¹H NMR (DMSO-d⁶) δ , 2.00 (s, 18 H), 4.30 (s, 4 H), 7.20 (d, 2 H, J = 8.8Hz), 7.4 (d, 2 H, J = 8.8 Hz), 7.5 (s, 2 H), 8.8 (s, 4 H), 10.8 (s, 2 H). ¹³C NMR (DMSO-d⁶) δ , 30.2; 45.3; 60.3; 115.8; 116.0; 126.3; 126.6; 126.9; 130.9; 131.7; 132.9; 156.7; 163.0. Anal. Calcd for C₃₆H₃₄N₂O₆S₂: C, 66.03; H, 5.23; N, 4.28; O, 14.66; S, 9.79. Found: C, 66.09; H, 5.25; N, 4.23; S, 9.73.

Adduct 46: Characterized as hydrochloride (**46·2HCl**). Pale green needles. M.p > 350°C. ¹H NMR (DMSO-d⁶) δ , 2.00 (s, 18 H), 4.30 (s, 4 H), 6.8 (m, 6 H), 7.10 (m, 4 H), 7.20 (d, 2 H, J= 8.7 Hz), 7.4 (d, 2 H, J = 8.7 Hz), 7.5(s, 2 H), 8.8 (s, 4 H), 10.0 (s, 2 H) 10.8 (s, 4 H). ¹³C NMR (DMSOd⁶) δ , 55.3; 115.0; 115.8; 116.0; 118.4; 126.3; 126.6; 126.9; 129.3; 130.6; 131.0; 132.8; 147.0; 157.0; 163.1. Anal. Calcd for C₄₀H₃₀Cl₂N₄O₆: C, 65.49; H, 4.12; Cl, 9.67; N, 7.64; O, 13.09. Found: C, 65.43; H, 4.16; Cl, 9.69; N, 7.62.

Adduct 47: Yellow solid. M.p.>350°C. $^1\text{H NMR}$ (DMSO- d_6) δ , 1.3 (t, 6 H), 2.00 (m, 4 H), 2.70 (m, 2 H), 3.0 (m, 2 H), 3.7 (m, 2 H), 4.0 (m, 2 H), 5.4 (dd, 2 H, $J = 2.7$ Hz), 7.1 (d, 2 H, $J = 8.6$ Hz), 7.35 (d, 2H, $J = 8.6$ Hz), 7.50 (s, 2 H), 8.70 (s, 4 H). $^{13}\text{C NMR}$ (DMSO- d_6), δ 15.1; 22.5; 51.5; 52.9; 116.0; 117.7; 126.3; 126.6; 126.9; 130.6; 131.4; 132.5; 156.4; 163.0. Anal. Calcd for $\text{C}_{36}\text{H}_{30}\text{N}_2\text{O}_8$: C, 69.89; H, 4.89; N, 4.53; O, 20.69. Found: C, 69.94; H, 4.90; N, 4.49.

Electrochemical Measurements.

Cyclic voltammetry (CV) were performed using an Amel 433/W polarographic analyser equipped with a standard three-electrode cell with a Platinum disk electrode as working electrode (2.0 mm diameter), a platinum wire as auxiliary electrode and a Ag/AgCl/KCl (4 M KCl saturated with AgCl) reference electrode. All potentials in the text are reported vs. Ag/AgCl/KCl (4 M KCl saturated with AgCl)

In degassed DMF using Bu_4NBF_4 0.1M, sweep rate 100 mV s^{-1} , although the processes for both the compounds were not perfectly reversible, **35a** showed a more reversible behaviour with peak separation of $70 \pm 10 \text{ mV}$ and $120 \pm 15 \text{ mV}$ for the first and the second process respectively. A similar behaviour has been found also in 0.1M Bu_4NBF_4 $\text{CH}_3\text{CN}:\text{H}_2\text{O} = 1:1$, at 100 mV s^{-1} ; in this case a defined second reduction, especially for **35**, were obtained. As expected, less negative peak potentials have been found in $\text{CH}_3\text{CN}:\text{H}_2\text{O}$, with respect to DMF.

Coulometric reductions were performed on a BAS 100B/W Version 2.3 and a BAS C3 Cell Stand with a 200 mL glass cell, using a carbon sponge working electrode, a platinum wire as auxiliary electrode set in a separated quartz tube and a Ag/AgCl/KCl (4 M KCl saturated with AgCl) reference electrode in degassed $\text{CH}_3\text{CN}:\text{H}_2\text{O} = 1:1$ solutions. Reduction were performed for the amine **35a** and its ammonium quaternary salt **35**, at -600 mV and -500 mV respectively. The formation of the anion radicals and their decay have been monitored as function of the time, recording the UV-Vis spectra on a HP-8452A DAD Spectrophotometer with a 661-500-QX Quarz Tauchsonde with 10 mm path length, HELLMA.

Methods and Computation Details.

All calculations were carried out using the Revision D.02 of Gaussian 03 program package. The geometric structures of the reactants (**48**, **48⁻** and **48⁻**) and the transition states (**TS-48**, **TS-48⁻** and **TS-48⁻**) located were fully optimized in the gas phase using the hybrid density functional B3LYP¹⁷ with the 6-31+G(d,p) basis set. It is known that diffuse functions are mandatory for a reliable evaluation of anion energies and in our reactive system a zwitterionic character is present in both the reactants **48⁻** and **48⁻** and related TSs (**TS-48⁻** and **TS-48⁻**). Thermal contributions (δG), to activation free energy were computed from B3LYP/6-31G(d) structures and harmonic frequencies, by using the harmonic oscillator approximation and the standard expressions for an ideal gas in the canonical ensemble at 298.15 K and 1 atm. The optimization of the stationary points in the solvent bulk were calculated via the self-consistent reaction field (SCRF) method using PCM as implemented in the D.02 version of Gaussian 03. The geometry optimizations in water solution for **TS-48** and **TS-48⁻** have been quite difficult, therefore to solve the problem the “loose” convergence criteria on geometry optimization was adopted. We were unable to optimize **TS-48⁻** in aqueous bulk, therefore for this TS we compute the solvation by single point calculation on B3LYP/6-31+G(d,p) gas phase geometry. The cavity is composed by interlocking spheres centered on non-hydrogen atoms with UA0 radii. Such a model includes the non-electrostatic terms (cavitation, dispersion, and repulsion energy) in addition to the classical electrostatic contribution.

Naphthalendiimides as selective G-4 Bis-Alkylating Agents. Synthesis and Characterization. Biophysical Assays.

Synthesis of the Intermediates

4-(aminomethyl)phenol. 4-hydroxybenzotrile (2.10 g, 17.6 mmol) was dissolved into 200 ml of anhydrous THF. The solution was added dropwise to a stirred suspension of LiAlH₄ (0.758g,

20 mmol) in THF (100 ml) under nitrogen atmosphere. Then the suspension was slowly heated to reflux. After 3 hrs the resulting yellow suspension was cooled with an ice bath and then the excess of hydride was decomposed by adding first dropwise ethyl acetate and then water until the total volume reached was 500 ml. The solution was extracted with ethyl acetate (40 ml for 3 times). The organic layers were collected, dried on sodium sulfate and the solvent was removed under vacuum. 4-(aminomethyl)phenol was obtained as a yellow oil (1.31 g, 61 % yield) and used for the next step without further purification. The spectroscopic data were in agreement with those reported in literature.

N-(4-hydroxybenzyl)acetamide: 4-(aminomethyl)phenol (1.10 g, 8.9 mmol) was suspended in 10 ml of a NaHCO₃ saturated solution by a vigorous stirring. Acetic anhydride (1.0 g, 9.8 mmol) was added dropwise to the stirring solution. Then, the resulting suspension was allowed to stand at room temperature. After 10 minutes the suspension was washed once with 5 ml of CHCl₃ in order to remove the excess of anhydride and then with ethyl acetate (4 x 20 ml).

The organic extracts were collected, dried with sodium sulfate and then the solvent was evaporated under vacuum to give N-(4-hydroxybenzyl)acetamide (1.54 g, yield 95%). The NMR spectrum of the crude was in agreement to that reported in literature.^[S3] The compound does not need further purifications.

N-(3-((dimethylamino)methyl)-4-hydroxybenzyl)acetamide: N-(4-hydroxybenzyl)acetamide (1.30 g, 10.4 mmol) was dissolved in 15 ml of anhydrous EtOH. Then 0.33g (10.9 mmol) of paraformaldehyde and 3.0 g (11.8 mmol) of a solution of dimethylamine in EtOH (20%) were added. This mixture was heated under reflux and nitrogen atmosphere for 2 hrs. The mixture was concentrated under vacuum and a yellow oil was obtained.

The oil was purified by column chromatography (eluent: EtOAc : MeOH = 8:2 v/v) to give the pure product as a yellow oil (1.64g, yield 71%). R_f0.25 (EtOAc-MeOH 8:2 v/v).

¹H NMR (300 MHz, CDCl₃, 25 °C, TMS): = 7.10 (d, ³J(H,H)=7.6Hz 1H), 6.90 (s, 1H), 6.75 (d, ³J(H,H)=7.6Hz 1H), 5.80 (s, 1H), 4.35 (d, ²J(H,H)=6.0Hz 2H), 3.60 (s, 2H), 2.30 (s, 6H), 2.05 (s, 3H).

N-(3-((dimethylamino)methyl)-4-hydroxyphenyl-methyl)amine dihydrochloride: 1.5 g of N-(3-((dimethylamino)methyl)-4-hydroxybenzyl)acetamide were dissolved in 15ml of aqueous HCl 10% and heated under reflux for 3h. The reaction mixture was chilled and the water removed under vacuum. The pink oil obtained was treated with 10 ml of EtOH absolute which is then evaporated in vacuum to provide N-(3-((dimethylamino)methyl)-4-hydroxyphenylethyl)amine dihydrochloride as a white crystals in quantitative yield.

N-(4-hydroxyphenethyl)acetamide: 5.0 g (28.8 mmol) of Tyramine hydrochloride were dissolved in 10 ml of a NaHCO₃ saturated solution. 3.0 g (29.4 mmol) of acetic anhydride were added slowly dropwise stirring the solution. After 5 min. the resulting suspension was allowed to stand at room temperature for additional 10 min, then it was washed with 5 ml of CHCl₃ in order to remove the unreacted anhydride. The water was further extracted with 4 x 20 ml of ethyl acetate. The organic phases were collected, dried with sodium sulfate and the solvent was removed under vacuum to give 4.9 g of N-(4-hydroxyphenethyl)acetamide. Yield 95%. The NMR data of the compound were in agreement to those reported in literature. This compound did not need further purification.

N-(3-((dimethylamino)methyl)-4-hydroxyphenethyl)acetamide: 1.3 g (8.4 mmol) of N-(4-hydroxyphenethyl)acetamide were dissolved in 15 ml of EtOH anhydrous. Then, 0.33 g (10.9 mmol) of paraformaldehyde and 3.0 g (11.8 mmol) of dimethylamine (solution 20%, in EtOH) were added. This mixture was heated under reflux and nitrogen atmosphere for 2 hrs. The mixture was concentrated in vacuum and a yellow oil was obtained. This oil was purified by column chromatography on silica gel (EtOAc : MeOH 8:2 v/v) to give the pure product as a yellow oil (1.2g , Yield 65%). R_f0,30 (EtOAc : MeOH 8:2 v/v).

^1H NMR (300 MHz, CDCl_3 , 25 °C, TMS) = 9.50 (s, 1H), 6.80 (d, $^3\text{J}(\text{H,H})=7.7\text{Hz}$ 1H), 6.7(s, 1H), 6.6 (d, $^3\text{J}(\text{H,H})=7.7\text{Hz}$ 1H), 3.7 (s, 2 H), 3.4 (t, $^3\text{J}(\text{H,H})=6.2\text{Hz}$ 2H), 2.7 (t, $^3\text{J}(\text{H,H})=6.2\text{Hz}$ 2H), 2.3 (s, 6H) 2.00 (s, 3H).

N-(3-((dimethylamino)methyl)-4-hydroxyphenylethyl)aminedihydrochloride: 1.2 g of N-(3-((dimethylamino)methyl)-4-hydroxyphenethyl)acetamide were dissolved in 15 ml of aqueous HCl 10% and heated under reflux for 3hrs. The reaction mixture was cooled at r.t. and the water removed under vacuum. 10 ml of EtOH anhydrous was mixed to the resulting pink oil and then evaporated under vacuum to provide N-(3-((dimethylamino)methyl)-4-hydroxyphenethyl)amine dihydrochloride as a pale pink crystals in quantitative yield.

4-(3-aminopropyl)phenol: The product, 4-(3-aminopropyl)phenol, was obtained as a yellow oil following the same protocol as for the reduction of 4-hydroxybenzonitrile. Yield 55%. The spectroscopic data were in agreement with the literature.

N-(3-(4-hydroxyphenyl)propyl)acetamide: The product was obtained as a yellow oil following the same protocol exploited for the acetylation of the Tyramine hydrochloride and 4-(aminomethyl)phenol. Yield 49%. The spectroscopic data were in agreement with the literature.

N-(3-(3-((dimethylamino)methyl)-4-hydroxyphenyl)propyl)acetamide: The product was obtained as a yellow oil following the same Mannich reaction procedure used for the synthesis of N-(3-(4-hydroxyphenyl)propyl)acetamide. The product was obtained as a yellow oil Yield 65%. ^1H NMR (300 MHz, CDCl_3 , 25 °C, TMS) = 6.90 (d, $^3\text{J}(\text{H,H})=7.9\text{Hz}$ 1H), 6.80 (s, 1H), 6.75 (s, $^3\text{J}(\text{H,H})=7.9$ 1H), 3.60 (s, 2H), 3.20 (m, 2H), 2.50 (m, 2H), 2.30 (s, 6H), 2.05 (s, 3H), 1.70 (m, 2H).

N-(3-((dimethylamino)methyl)-4-hydroxyphenylpropyl)aminedihydrochloride: 1.2 g of N-(3-((dimethylamino)methyl)-4-hydroxyphenyl)propyl)acetamide were dissolved in 15 ml of aqueous HCl 10% and heated under reflux for 3h. The reaction mixture was cooled at r.t. and the water removed under vacuum. The pink oil obtained was mixed with 10 ml of anhydrous EtOH,

which was then evaporated under vacuum to provide N-(3-((dimethylamino)methyl)-4-hydroxyphenyl)propyl)amine dihydrochloride as a pale pink solid in quantitative yield.

N,N'-bis[2-(3-(dimethylamino)methyl-4-hydroxyphenyl)methyl]-1,8-5,4-naphthalenetetracarboxylic bisimide (49a): 3.2g of N-(3-((dimethylamino)methyl)-4-hydroxyphenyl)methyl)amine dihydrochloride (12.6 mmol) and 1.61 g (6.0 mmol) of 1,4-5,8 tetracarboxylic dianhydride were suspended in 20 ml of a mixture dioxane/DMF 9:1. Under nitrogen atmosphere, 1 ml of TEA were added to the suspension and the mixture was allowed to reflux with vigorously stirring for 5 hrs. The reaction mixture was cooled at r.t. and poured into 30 ml of water. The resulting suspension was filtered and washed with water and cold EtOH anhydrous. The N,N'-bis[2-(3-(dimethylamino)methyl-4-hydroxyphenyl)methyl]-1,8-5,4-naphthalenetetracarboxylic bisimide was obtained as a pale yellow solid. Yield 91%. M.p.>350°C. ¹H NMR (300 MHz, CDCl₃, 25 °C, TMS): δ 8.80 (s, 4H), 7.40 (d, 2H, *J* = 6.9Hz), 7.20 (s, 2H), 6.85 (d, 2H, *J* = 6.9Hz), 5.20 (s, 4H), 3.60 (s, 4H), 2.30 (s, 12H). ¹³C NMR (300 MHz, CDCl₃, 25 °C, TMS): δ= 162.74; 157.76; 131.03; 130.95; 131.00; 129.55; 126.87; 126.61; 121.68; 115.91; 62.60; 44.37; 43.41. Anal. Calcd. for C₃₄H₃₂N₄O₆: C, 68.91; H, 5.44; N, 9.45; O, 16.20. Found C, 68.95; H, 5.40; N, 9.47.

N,N'-bis[2-(3-(trimethylamino)methyl-4-hydroxyphenyl)methyl]-1,8-5,4naphthalenetetracarboxylic bisimide iodide (49): 1.7 g (2.9 mmol) of the bisimide **4a** were suspended in 50 ml of CH₃CN and 1.2 g (8.5 mmol) of CH₃I was added. This suspension was refluxed under nitrogen atmosphere and in a few minutes the reaction mixture turned dark red. After heating 3 hrs at 80°C, the reaction was cooled at r.t.. Red solid formation was observed after addition of Et₂O (50 ml) to the reaction mixture. The suspension was filtered and washed with CH₃CN to give 2.7g (3.0 mmol) of **4** as a red-brownish solid. M.p.>350°C. Yield 92%. ¹H NMR (300 MHz, [D₆]DMSO, 25 °C, TMS): δ 10.30 (s, 2H), 8.70 (s, 4H), 7.50 (s, 2H), 7.40 (d, 2H, *J* =8.4 Hz), 6.90 (d, 2H, *J* =8.4Hz), 5.15 (s, 4H), 4.45 (s, 4H), 3.05 (s, 18H). ¹³C NMR ([D₆]DMSO, 25 °C, TMS): 162.72; 156.59; 134.88; 132.07; 130.71; 127.63; 126.38; 126.28; 116.09; 114.39; 62.91;

51.90; 42.7. Anal. Calcd. for C₃₆H₃₈I₂N₄O₆: C, 49.33; H, 4.37; I, 28.96; N, 6.39; O, 10.95. Found C, 49.35; H, 4.41; I, 28.93; N, 6.42.

N,N'-bis[2-(3-(dimethylamino)methyl-4-hydroxyphenyl)ethyl]-1,8-5,4naphthalenetetra carboxylic bisimide (50a): The same protocol used for the synthesis of **49a** was followed. 2.1 g of N-(3-((dimethylamino)methyl)-4-hydroxyphenylethyl)amine dihydrochloride (8.3 mmol) and 1.07 g (4.0 mmol) of 1,4-5,8 tetracarboxylic dianhydride were used. The N,N' bis[2-(3-(dimethylamino)methyl-4-hydroxyphenyl)ethyl]-1,8-5,4-naphthalenetetracarboxylic bisimide **50a** was obtained as a pale yellow solid, 2.20 g (yield 89%). M.p.>350°C ¹H NMR (300 MHz, CDCl₃, 25 °C, TMS): δ 8.70 (s, 4H), 7.20 (d, 2H, *J*=7.4 Hz), 7.00 (s, 2H), 6.80 (d, 2H, *J*=7.4 Hz), 4.40 (t, 4H, *J* = 8.1Hz), 3.75 (s, 4H), 2.90 (t, 4H, *J* = 8.1 Hz), 2.35 (s, 12H). ¹³C NMR ([D₆]DMSO, 25 °C, TMS): δ 162.46; 155.08; 132.92; 131.29; 130.48; 129.00; 126.27; 126.12; 116.34; 115.71; 54.54; 45.15; 32.43; 30.78. Anal. Calcd. for C₃₆H₃₆N₄O₆: C, 69.66; H, 5.85; N, 9.03; O, 15.47. Found C, 69.62; H, 5.88; N, 9.00.

N,N'-bis[2-(3-(trimethylamino)methyl-4-hydroxyphenyl)ethyl]-1,8-5,4-naphthalenetetra carboxylic bisimide iodide (50): The same protocol used for the synthesis of **49** was followed. 2.0 g (3.2 mmol) of the bisimide **5a** was used. 2.7g (3.0 mmol) of **5** as a red-brownish solid was obtained. M.p.>350°C. Yield 84%. ¹H NMR (300 MHz, [D₆]DMSO, 25 °C, TMS): δ 10.20 (s, 2H), 8.80 (s, 4H), 7.30 (s, 2H), 7.20 (d, 2H, *J* = 7.6Hz), 6.90 (d, 2H, *J* = 7.6Hz), 4.40 (s, 4H), 4.20 (t, 4H, *J* = 8.1Hz), 3.00 (s, 18H), 2.85 (t, 4H, *J* = 8.1Hz). ¹³C NMR ([D₆]DMSO, 25 °C, TMS): δ 162.50; 155.80; 134.72; 132.38; 130.47; 129.28; 126.30; 126.14; 116.15; 114.63; 63.06; 51.95; 41.60; 32.41. Anal. Calcd. for C₃₈H₄₂I₂N₄O₆: C, 50.46; H, 4.68; I, 28.06; N, 6.19; O, 10.61. Found C, 50.41; H, 4.71; I, 28.01; N, 6.16.

N,N'bis[2-(3-(dimethylamino)methyl-4-hydroxyphenyl)propyl]-1,8-5,4-naphthalenetetra carboxylic bisimide (51a): The same protocol used for the synthesis of **49a** was followed. 1.17g of N-(3-((dimethylamino)methyl)-4-hydroxyphenylpropyl)amine dihydrochloride (6.01 mmol) and 0.8 g (3.0 mmol) of 1,4-5,8 tetracarboxylic dianhydride were used. The N,N' bis[2-(3-

(dimethylamino)methyl-4-hydroxyphenyl)propyl]-1,8-5,4-naphthalenetetracarboxylic bisimide was obtained as a pale yellow solid. 2.2 g (yield 98%). M.p. > 350°C. ¹H NMR (300 MHz, CDCl₃, 25 °C, TMS): δ 8.75 (s, 4H), 7.35 (d, 2H, *J*=7.6Hz), 6.85 (s, 2H), 6.70 (d, 2H, *J*=7.6Hz), 4.25 (t, 4H, *J*=6.0Hz), 3.60 (s, 4H), 2.69 (t, 4H, *J*=6.0Hz), 2.30 (s, 12H), 2.10 (t, 4H, *J*=8.0Hz). ¹³C NMR (300 MHz, CDCl₃, 25 °C, TMS): δ 162.70; 155.99; 130.77; 128.22; 127.93; 126.48; 121.61; 126.12; 115.71; 62.74; 44.38; 40.70; 32.37; 29.44. Anal. Calcd. for C₃₈H₄₀N₄O₆: C, 70.35; H, 6.21; N, 8.64; O, 14.80 Found C, 70.37; H, 6.22; N, 8.86.

N,N'-bis[2-(3-(trimethylamino)methyl-4-hydroxyphenyl)propyl]-1,8-5,4-naphthalene tetracarboxylic bisimide iodide (51): The same protocol used for the synthesis of **49** was followed. 0.90 g (1.4 mmol) of the bisimide **51a** was used. 1.06g of **51** as a red-brownish solid was obtained M.p. > 350 °C. Yield 81%. ¹H NMR (300 MHz, [D₆]DMSO, 25 °C, TMS): δ= 10.15 (s, 2H), 8.60 (s, 4H), 7.25 (m, 4H), 6.85 (d, 2H, *J*=8.6Hz), 4.40 (t, 4H), 4.05 (s, 4H), 3.05 (s, 18H), 2.65 (t, 4H); 1.95 (t, 4H). ¹³C NMR ([D₆]DMSO, 25 °C, TMS): 163.07; 157.35; 134.82; 132.60; 130.53; 126.97; 126.63; 126.34; 116.43; 114.84; 62.81; 52.04. Anal. Calcd. for C₄₀H₄₆I₂N₄O₆: C, 51.51; H, 4.97; I, 27.21; N, 6.01; O, 10.29 Found C, 51.46; H, 4.93; I, 27.19; N, 6.06

NDIs Activation of the bis-alkylating properties by mild thermal digestion. General procedures.

In order to trap the nucleophiles by mild thermal digestion the following procedures were used:

Procedure A (for basic nucleophiles: pK_a > 8): To 50 ml of a solution 5x10⁻³M of the bisimides (**49-51**) in 1:1 CH₃CN/H₂O, outgassed with a N₂ flux, was added the nucleophile (5x10⁻²M). This solution is allowed to stand at 40°C and after 0.5 hrs a pale yellow precipitate starts to form. The reaction mixture was kept at 40°C for 4hrs. After this time the CH₃CN was evaporated under vacuum and the suspension was cooled at 4 °C for 12 hrs. The bis-alkylated adduct formed

was filtered and washed with cold anhydrous EtOH to provide the product in good yield (60-85 %).

Procedure B (for non-basic nucleophiles: $pK_b < 8$): To 50 ml of a solution $5 \times 10^{-3} M$ of the bisimides (**49-51**) in 1:1 CH_3CN/H_2O buffered to pH 8.5 with a $H_2PO_4^-/HPO_4^{2-}$ buffer, outgassed with a N_2 flux, was added the nucleophile ($5 \times 10^{-2} M$). This solution was heated at $40^\circ C$ for 12 hrs. After this time the CH_3CN was evaporated under vacuum and the suspension was kept at $4^\circ C$ for 12 hrs. The bis-alkylated adduct precipitated was filtered and washed with cold water and anhydrous EtOH to provide the product in fairly good yield (55-70 %).

Adduct 52: Pale yellow needle like solid. $M.p > 350^\circ C$. 1H NMR (300 MHz, $[D_6]DMSO$, $25^\circ C$, TMS): δ 10.20 (s, 2H), 8.70 (s, 4H), 7.30 (s, 2H), 7.20 (d, 2H, $J=7.9$ Hz), 6.90 (d, 2H, $J=7.9$ Hz), 4.30 (s, 4H), 4.20 (t, 4H); 2.9 (t, 4H). ^{13}C NMR ($[D_6]DMSO$, $25^\circ C$, TMS): δ 162.48; 155.80; 134.71; 132.37; 130.47; 129.30; 126.28; 126.13; 116.16; 114.63; 63.11; 51.99; 41.60; 32.41. Anal. Calcd. for $C_{32}H_{26}N_2O_8$: C, 67.84; H, 4.63; N, 4.94; O, 22.59 Found C, 67.81; H, 4.66; N, 4.95.

Adduct 53: Yellow needle like solid. $M.p > 350^\circ C$. 1H NMR (300 MHz, $CDCl_3$, $25^\circ C$, TMS): δ 8.80 (s, 4H), 7.10 (d, 2H, $J=8.1$ Hz), 7.00 (s, 2H), 6.75 (d, 2H, $J=8.1$ Hz), 4.40 (t, 4H, $J=7.8$ Hz), 3.75 (s, 4H); 2.95 (t, 4H, $J=7.8$ Hz); 2.60 (q, 8H, $J=7.1$ Hz); 1.10 (t, 12H, $J=7.1$ Hz). ^{13}C NMR (300 MHz, $CDCl_3$, $25^\circ C$, TMS): δ 162.58; 156.88; 132.90; 130.82; 128.78; 128.21; 126.52; 126.42; 122.11; 115.93; 56.80; 46.18; 42.38; 33.24; 11.12. Anal. Calcd. for $C_{40}H_{44}N_4O_6$: C, 70.99; H, 6.55; N, 8.28; O, 14.18. Found C, 71.03; H, 6.51; N, 8.33.

Adduct 54: Pale yellow needles. $M.p > 350^\circ C$. 1H NMR (300 MHz, $CDCl_3$, $25^\circ C$, TMS): δ 8.90 (s, 4H), 7.15 (d, 2H, $J=7.9$ Hz), 7.00 (s, 2H), 6.90 (d, 2H, $J=7.9$ Hz), 4.40 (t, 4H, $J=7.4$ Hz), 3.75 (s, 4H); 2.95 (t, 4H, $J=7.4$ Hz); 2.60 (m, 8H); 1.50 (q, 4H, $J=6.5$ Hz); 1.25 (q, 4H, $J=6.1$ Hz); 1.1 (t, 6H, $J=6.1$ Hz); 0.90 (t, 6H, $J=6.5$ Hz). ^{13}C NMR (300 MHz, $CDCl_3$, $25^\circ C$, TMS): δ 162.58; 156.79; 130.83; 128.78; 128.20; 126.52; 122.17; 115.88; 57.39; 52.49; 46.57; 44.38;

42.40; 33.26; 28.54; 20.46; 13.86; 10.84. Anal. Calcd. for $C_{44}H_{52}N_4O_6$: C, 72.11; H, 7.15; N, 7.64; O, 13.10 Found C, 72.13; H, 7.11; N, 7.68.

Adduct 55: Yellow needles. M.p. > 350°C. 1H NMR (300 MHz, $CDCl_3$, 25 °C, TMS): δ 8.80 (s, 4H), 7.10 (d, 2H, $J = 7.5$ Hz), 7.00 (s, 2H), 6.75 (d, 2H, $J = 7.5$ Hz), 4.45 (t, 4H, $J = 7.4$ Hz), 3.60 (t, 8H, $J = 7.1$ Hz); 3.00 (t, 8H, $J = 7.1$ Hz), 2.90 (t, 4H, $J = 7.4$ Hz). ^{13}C NMR (300 MHz, $CDCl_3$, 25 °C, TMS): δ 163.12; 156.34; 130.36; 129.72; 128.47; 126.98; 126.20; 122.79; 122.17; 115.88; 66.13; 58.01; 52.49; 46.57; 33.26. Anal. Calcd. for $C_{40}H_{40}N_4O_8$: C, 68.17; H, 5.72; N, 7.95; O, 18.16 Found C, 68.13; H, 5.70; N, 7.91.

Adduct 56: Yellow needles. M.p. > 350°C. 1H NMR (300 MHz, $CDCl_3$, 25 °C, TMS): δ 8.6 (s, 4H); 7.20 (d, 2H, $J = 7.7$ Hz); 7.00 (s, 2H); 6.75 (d, 2H, $J = 7.7$ Hz); 4.45 (t, 4H, $J = 7.8$ Hz); 3.60 (s, 4H); 3.0 (t, 4H, $J = 7.8$ Hz); 2.4 (m, 8H); 1.8 (m, 8H). ^{13}C NMR (300 MHz, $CDCl_3$, 25 °C, TMS): δ 163.56; 156.60; 130.82; 128.84; 128.28; 128.17; 126.57; 126.50; 122.45; 15.80; 58.66; 53.35; 42.34; 33.22; 23.53. Anal. Calcd. for $C_{40}H_{40}N_4O_6$: C, 71.41; H, 5.99; N, 8.33; O, 14.27 Found C, 71.38; H, 6.04; N, 8.30.

Adduct 57: Green crystals. M.p. > 350°C: 1H NMR (300 MHz, $CDCl_3$, 25 °C, TMS): δ 8.80 (s, 4H); 7.10 (d, 2H, $J = 7.8$ Hz), 7.00 (s, 2H), 6.85 (d, 2H, $J = 7.8$ Hz); 4.40 (t, 4H, $J = 7.7$ Hz); 4.00 (s, 4H); 2.90 (t, 4H, $J = 7.7$ Hz); 1.20 (s, 18H). ^{13}C NMR (300 MHz, $CDCl_3$, 25 °C, TMS): δ 162.58; 157.03; 130.85; 128.81; 128.39; 128.34; 126.53; 123.54; 116.43; 50.98; 45.95; 42.45; 33.29; 28.47. Anal. Calcd. for $C_{40}H_{44}N_4O_6$: C, 70.99; H, 6.55; N, 8.28; O, 14.18. Found: C, 70.92; H, 6.58; N, 8.22.

Adduct 58: Yellow needles. M.p. > 350°C. 1H NMR (300 MHz, $[D_6]DMSO$, 25 °C, TMS): δ 10.20 (s, 2H), 8.80 (s, 4H); 7.20 (d, 2H, $J = 7.9$ Hz), 7.0 (s, 2H), 6.85 (d, 2H, $J = 7.9$ Hz); 4.45 (s, 4H), 4.30 (t, 4H, $J = 7.6$ Hz); 3.15 (s, 18H), 3.00 (t, 4H, $J = 7.6$ Hz). ^{13}C NMR ($[D_6]DMSO$, 25 °C, TMS): δ 162.79; 157.12; 130.82; 128.81; 128.39; 128.34; 126.93; 126.51; 123.54; 116.43; 60.21; 45.95; 42.41; 38.29; 33.47 Anal. Calcd. for $C_{40}H_{42}N_2O_6S_2$: C, 67.58; H, 5.95; N, 3.94; O, 13.50; S, 9.02. Found C, 67.51; H, 5.98; N, 3.92; S, 9.00

Adduct 59: Yellow needles. m.p>350°C. ¹H NMR (300 MHz, [D₆]DMSO, 25 °C, TMS) δ=10.00 (s, 2H), 8.70 (s, 4H), 7.30(s, 2H), 7.20 (d, 2H, *J*=7.8 Hz), 6.90 (d, 2H, *J*=7.8 Hz), 5.1 (s, 4H), 4.30 (s, 4H). ¹³C NMR ([D₆]DMSO, 25 °C, TMS): δ 162.48; 155.80; 134.71; 132.37; 130.47; 129.30; 126.28; 126.13; 121.16; 115.93; 63.11; 62.58. Anal. Calcd. for C₃₀H₂₂N₂O₈: C, 66.91; H, 4.12; N, 5.20; O, 23.77 Found C, 67.01; H, 4.17; N, 5.26.

Adduct 60: Yellow needles. M.p > 350°C. ¹H NMR (300 MHz, CDCl₃, 25 °C, TMS): δ 8.70 (s, 4H), 7.30 (s, 2H), 7.00 (d, 2H, *J*=7.6 Hz), 6.90 (d, 2H, *J*=7.6 Hz), 5.1 (s, 4H), 4.20 (s, 4H) 2.60 (q, 8H, *J*=7.1 Hz); 1.1 (t, 12H, *J*=7.1 Hz). ¹³C NMR (300 MHz, CDCl₃, 25 °C, TMS): δ 163.70; 155.99; 131.29; 130.77; 128.22; 127.93; 126.48; 121.61; 115.71; 62.74; 44.38; 40.70; 32.37; 29.44. Anal. Calcd. for: C₃₈H₄₀N₄O₆ C, 70.35; H, 6.21; N, 8.64; O, 14.80. Found C, 70.33; H, 6.27; N, 8.62.

Adduct 61: Yellow needles. M.p > 350°C. ¹H NMR (300 MHz, [D₆]DMSO, 25 °C, TMS): δ=10.80 (s, 2H), 8.80 (s, 4H), 7.50(s, 2H), 7.40 (d, 2H, *J*=8.8 Hz), 7.20 (d, 2H, *J*=8.8 Hz), 5.1 (s, 4H), 4.30 (s, 4H), 3.00(s, 18H). ¹³C NMR ([D₆]DMSO, 25 °C, TMS): δ 163.44; 155.98; 132.55; 131.59; 130.99; 126.96; 126.72; 126.21; 116.02; 115.76; 62.18; 60.26; 45.78; 38.30. Anal. Calcd. for C₃₈H₃₈N₂O₆S₂: C, 66.84; H, 5.61; N, 4.10; O, 14.06; S, 9.39. Found C, 66.81; H, 5.55; N, 4.06; S, 9.34.

Adduct 62: Yellow needles. M.p > 350°C. ¹H NMR (300 MHz, [D₆]DMSO, 25 °C, TMS): δ 10.15 (s, 2H), 8.60 (s, 4H), 7.25 (d, 2H, *J*=8.0 Hz), 7.0 (s, 2H); 6.85 (d, 2H, *J*=8.0 Hz), 4.40 (t, 2H, *J*=7.5 Hz); 4.30 (s, 4H); 2.65 (t, 2H, *J*=7.5 Hz); 2.00 (m, 4H). ¹³C NMR ([D₆]DMSO, 25 °C, TMS): δ 163.23; 158.35; 134.82; 132.60; 130.53; 126.97; 126.63; 126.34; 116.43; 114.84; 62.81; 52.04; 33.25; 29.07. Anal. Calcd. for: C₃₄H₃₀N₂O₈ C, 68.68; H, 5.09; N, 4.71; O, 21.53. Found C, 68.71; H, 5.11; N, 4.74.

Adduct 63: Yellow needles. M.p > 350°C. ¹H NMR (300 MHz, CDCl₃, 25 °C, TMS): δ 8.70 (s, 4H), 7.10 (d, 2H, *J*=7.9 Hz), 7.00 (s, 2H), 6.90 (d, 2H, *J*=7.9 Hz), 4.40 (t, 4H, *J*=7.6 Hz), 3.70 (s, 4H); 2.95 (t, 4H, *J*=7.6 Hz); 2.60 (q, 8H, *J*=7.1 Hz); 2.10 (t, 4H, *J*=7.6 Hz) 1.1 (t, 12H, *J*=7.1

Hz). ^{13}C NMR (300 MHz, CDCl_3 , 25 °C, TMS): δ 162.17; 155.17; 132.91; 130.45; 128.79; 128.31; 126.55; 126.42; 122.09; 116.13; 57.39; 46.57; 44.38; 33.26; 28.54; 20.46. Anal. Calcd. for: $\text{C}_{42}\text{H}_{48}\text{N}_4\text{O}_6$ C, 71.57; H, 6.86; N, 7.95; O, 13.62. Found: C, 71.52; H, 6.88; N, 7.89.

Adduct 64: Yellow needles. M.p > 350°C. ^1H NMR (300 MHz, $[\text{D}_6]\text{DMSO}$, 25 °C, TMS): δ 10.10 (s, 2H), 8.70 (s, 4H), 7.00 (d, 2H, $J=7.7$ Hz), 6.90 (s, 2H), 6.90 (d, 2H, $J=7.7$ Hz), 4.25 (t, 4H, $J=6.0$ Hz), 3.60 (s, 4H), 2.69 (t, 4H, $J=6.0$ Hz), 2.00 (s, 18H), 2.10 (t, 4H, $J=8.0$ Hz). ^{13}C NMR ($[\text{D}_6]\text{DMSO}$, 25 °C, TMS): δ 163.04; 156.42; 132.46; 131.43; 130.56; 126.92; 126.62; 126.31; 117.75; 115.99; 62.90; 61.46; 32.37; 29.44; 22.47; 18.34. Anal. Calcd. for: $\text{C}_{42}\text{H}_{46}\text{N}_2\text{O}_6\text{S}_2$: C, 68.27; H, 6.27; N, 3.79; O, 12.99; S, 8.68. Found: C, 68.22; H, 6.21; N, 3.82; S, 8.69.

Adduct 65: Yellow needles. M.p > 350°C. ^1H NMR (300 MHz, CDCl_3 , 25 °C, TMS): δ 8.70 (s, 4H), 7.20 (d, 2H, $J=8.2$ Hz), 7.10 (s, 2H), 6.75 (d, 2H, $J=8.2$ Hz), 5.25 (dd, 2H, $J=2.7$ Hz), 4.40 (t, 4H, $J=8.0$ Hz), 3.90 (m, 2H), 3.60 (m, 2H), 3.00 (t, 4H, $J=8.0$ Hz), 2.60 (m, 2H), 2.00 (m, 2H), 1.30 (t, 6H, $J=7.0$ Hz). ^{13}C NMR (300 MHz, CDCl_3 , 25 °C, TMS): δ 162.59; 150.8; 130.85; 130.10; 129.60; 127.66; 126.56; 122.50; 116.91; 96.81; 63.55; 42.40; 33.35; 30.80; 26.43; 20.4; 15.02. Anal. Calcd. for $\text{C}_{40}\text{H}_{38}\text{N}_2\text{O}_8$: C, 71.20; H, 5.68; N, 4.15; O, 18.97. Found: C, 71.25; H, 5.77; N, 4.11.

G-quadruplex DNA Alkylation and Folding Induction.

For reaction with DNA, compounds were dissolved and diluted in DMSO, in order to obtain a final 2.5% DMSO. DNA sequences (Biosense) were: 4GGG: 5'-AGGGTTA GGGTTAGGGTTAGGG-3'; ss-scrambled-4GGG: 5'-GGATGTGAGTGTGAGTGTGAG-3' and its complementary strand 5'-CTCACACTCACACTCACATCC-3' to form ds-scrambled-4GGG; 2GGG: 5'-TACAGATAGTTAGGGTTAGGGTTA-3'. For DNA labeling reactions: 100 pmol of DNA were incubated with 1 μl (10 $\mu\text{Ci}/\mu\text{l}$) of $[\gamma\text{-}^{32}\text{P}]\text{ATP}$ and 10 units of T4 polynucleotide kinase (Fermentas) in 50 mM TRIS-HCl (pH 7.6), 10 mM MgCl_2 , 5 mM DTT, 0.1 mM

spermidine and 0.1 mM EDTA at 37°C for 30 min. After incubation, DNA was purified through MicroSpin G-25 columns (GE Healthcare). For alkylation experiment, 5-10 pmol of ³²P-labeled DNA were incubated with increasing drug amounts in phosphate buffer pH 7.4, 10 mM LiOH and 50 mM KCl. Samples were incubated at the indicated temperature and time and reactions were stopped by precipitation. For competition experiments, annealed-labeled 4GGG (3.9 pmol) and drug (2 μM **50**) were mixed with cold competitor-DNA (4GGG, ss- and ds-scrambled 4GGG) at increasing concentrations, so that the molar ratios competitor/labeled 4GGG were 0.5, 1, 2, 5 and 10. After 24 hrs incubation at 40°C, samples were precipitated. Alkylation products were then resolved in 20% polyacrylamide 7M urea sequencing gels. The NDI's ability to induce the G-quadruplex structure was tested by gel shift experiments. For G-4 folding induction, ³²P-labelled 2GGG and 5 μM cold 2GGG were annealed in phosphate buffer pH 7.4, containing 10 mM LiOH with or without 50 mM KCl. The annealed 2GGG was mixed with 25 μM of drug for increasing times at the indicated temperatures. Samples were loaded onto 16% polyacrylamide gel, containing 20 mM KCl.

Exonuclease I Digestion Assay.

For exonuclease I reaction, the alkylation product was resolved in 20% polyacrylamide 7M urea gel and purified by cutting and crashing the band of interest, and eluting the alkylated oligo in TE buffer for 2 hrs. The purified alkylated oligo was then precipitated and resuspended in exonuclease I reaction buffer. Exonuclease I was added at 10, 20 and 40 units and the reaction incubated for 30 min at 37°C or 50°C. The reaction was stopped by DNA precipitation and samples loaded onto 20% polyacrylamide 7M urea gel.

Circular Dichroism Measurements.

Oligonucleotide 4GGG circular dichroism spectra from 230 to 350 nm were recorded using 10 mm path length cells on a Jasco J 810 spectropolarimeter equipped with a NESLAB temperature controller. Before data acquisition, a 4 μ M 4GGG solution in Li_3PO_4 10mM, KCl 50 mM, pH 7.4, was prepared, heated at 95°C for 5 min and left to cool at room temperature over night. This solution was divided into four fractions: two were incubated 24 h at 25 and 40°C, respectively; **50** was added to a final concentration of 26 μ M to the remaining fractions and incubated 24 h at 25 and 40°C, respectively. The reported spectrum of each sample represents the average of 3 scans recorded with 1-nm step resolution at 25°C.

Cytotoxicity Assay.

Human embryonic kidney 293T cells (293T) were purchased from ATCC (ATCC number CRL-11268). 293T cells were grown as monolayers in Dulbecco's Modified Eagle Medium (Invitrogen, Italy) with 10% fetal bovine serum (FBS) supplemented with penicillin (100U/ml) and streptomycin (100 μ g/ml) in a humidified atmosphere with 5% CO_2 at 37 °C.

Cytotoxic effects on cell growth were determined by MTT assay. NDI compounds were dissolved and diluted into working concentrations with DMSO. Cells (1.75×10^4 cells/well) were plated onto 96-microwell plates to a final volume of 100 μ l and allowed an overnight period for attachment. At day 1, 1 μ l of each dilution of tested compounds was added per well in order to get a 1% final concentration of drug solvent per well; at day 2, medium was removed, cells washed with PBS and fresh medium was added. Control cells (without any compound, but with 1% drug solvent) were treated in the exact same conditions. Cell survival was evaluated by MTT assay: 10 μ l of freshly dissolved solution of MTT (5mg/ml in PBS) were added to each well and, after 4 h incubation, 100 μ l of solubilization solution (10% SDS, 0,01M HCl) were added. After overnight incubation at 37 °C, absorbance was read at 540 nm. Data were expressed as mean values of three individual experiments conducted in triplicate. The percentage of cell survival was calculated as

follows: cell survival = $(A_{\text{well}} - A_{\text{blank}}) / (A_{\text{control}} - A_{\text{blank}}) * 100$, where blank denotes medium without cells.

Tri and Tetra Naphthalendiimides as selective G-4 Bis-Alkylating Agents. Synthesis and Characterization. Biophysical Assays.

N-(4-hydroxybenzyl)tert-butylcarbamate (77). 3.95 g (28.8 mmol) of Tyramine were dissolved in 25 ml of THF. 9.42 g (43.2 mmol) of Di-tetr-Butyl dicarbonate in THF solution (5ml) were added slowly dropwise at the stirring the solution. The resulting suspension was allowed to stand at room temperature for 2 hours, then the solvent was removed under vacuum. The resulting crude product was solved in CH₃Cl and washed with a water solution of NaHCO₃. The organic phases were collected, dried with sodium sulfate and the solvent was removed under vacuum to give 4.9 g of brown/yellow oil (**xx**, 97% yield). The compound does not needs further purifications. ¹H NMR(200 MHz, CDCl₃) δ(ppm): 7.02 (d, 2H, J=8.0 Hz); 6.80 (d, 2H, J=8.0 Hz); 3.35 (m, 2H); 2.71 (t, 2H, J=6.6 Hz); 1.46 (s, 9H).

N-(3-((dimethylamino)methyl)-4-hydroxybenzyl)tert-butylcarbamate (78): N-(4-hydroxy benzyl)tert-butylcarbamate (2.46 g, 10.4 mmol) was dissolved in 15 ml of anhydrous EtOH. Then 0.33g (10.9 mmol) of paraformaldehyde and 3.0 g (11.8 mmol) of a solution of dimethylamine in EtOH (20%) were added. This mixture was heated under reflux and nitrogen atmosphere for 2 hrs. The mixture was concentrated under vacuum and a yellow oil was obtained. The oil was purified by column chromatography (eluent: EtOAc : MeOH = 8:2 v/v) to give the pure product as a yellow oil (1.4g, yield 47%). Rf 0.25 (EtOAc-MeOH 8:2 v/v).

¹H NMR (300 MHz, CDCl₃) δ(ppm): 9.28 (bs, 1H); 6.95 (d, 1H, J=6.3 Hz); 6.77 (d; 1H, J=6.3 Hz); 6.74 (s, 1H); 4.63 (bs, 1H); 3.30 (m, 2H); 2.67 (t, 2H, J=7.6 Hz); 2.32 (s, 6H); 1.43 (s, 12H).

¹³C NMR (CDCl₃) δ(ppm): 156.38; 155.82; 129.06; 128.78; 128.56; 121.75; 115.89; 78.96; 62.60; 44.33; 41.91; 35.18; 28.29.

N-(3-((morpholino)methyl)-4-hydroxybenzyl)tert-butylcarbamate (82): N-(4-hydroxybenzyl)tert-butylcarbamate (2.46 g, 10.4 mmol) was dissolved in 15 ml of anhydrous EtOH. Then 0.33g (10.9 mmol) of paraformaldehyde and 1.02 g (11.8 mmol) of morpholine were added. This mixture was heated under reflux and nitrogen atmosphere for 2 hrs. The mixture was concentrated under vacuum and a yellow oil was obtained. The oil was purified by column chromatography (eluent: EtOAc : MeOH = 8:2 v/v) to give the pure product as a yellow oil (1.74g, yield 50%).

¹H NMR (300 MHz, CDCl₃) δ(ppm): 6.97 (d, 1H, J=6.6 Hz); 6.79 (d, 1H, J=8.8 Hz); 6.73 (s, 1H); 4.67 (bs, 1H); 3.74 (bs, 4H); 3.66 (s, 2H); 3.29 (bs, 2H); 2.69 (bs, 2H); 2.56 (bs, 4H); 1.43 (s, 9H).

N-(3-((trimethylamino)methyl)-4-hydroxybenzyl)tert-butylcarbamate(80): (77) (1.47 g, 5.0 mmol) was suspended in 50 ml of CH₃CN and 0.33g (10.0 mmol) of CH₃I was added. This suspension was refluxed under nitrogen atmosphere. After heating 3 h at 80°C, the reaction was cooled at room temperature and the solvent was removed under vacuum to obtain a pure yellow solid (2.07g, yield 95%).

¹H NMR (200 MHz, CDCl₃) δ(ppm): 7.28 (m, 2H); 7.11 (m, 1H); 4.66 (bs, 2H); 3.30 (m, 2H); 3.23 (s, 9H); 2.73 (m, 2H); 1.44 (s, 9H).

Deprotection of tert-butylcarbamate: General Procedure

N-(3-((dimethylamino)methyl)-4-hydroxyphenylethyl)aminedihydrotrifluoroacetate(79): 300 mg of N-(3-((dimethylamino)methyl)-4-hydroxybenzyl)tert-butylcarbamate was hydrolyzed by stirring in a solution of trifluoroacetic acid (1.94 ml, 13 mmol) and dichloromethane (10 ml) in the presence of triethylsilane (0.8 ml, 2.5 mmol), at room temperature. The yields were almost

quantitative (93 %) using triethylsilane as carbocation scavenger. After stirring 2h., the solvent was removed in vacuo, the residue triturated with diethyl ether and product isolated by filtration.

^1H NMR (200 MHz, CDCl_3) δ (ppm): 7.28 (s, 1H); 6.94 (d, 1H, $J=8.6$ Hz); 6.74 (d, 1H, $J=8.5$ Hz); 6.73 (s, 1H); 6.05 (bs, 1H); 3.57 (s, 2H); 2.86 (t, 2H, $J=6.24$ Hz); 2.62 (m, 2H); 2.28 (s, 6H).

N-(3-((morpholino)methyl)-4-hydroxyphenylethyl)aminedihydrotrifluoroacetate (83): ^1H NMR (200 MHz, CDCl_3) δ (ppm): 7.39 (bs, 1H); 7.31 (d, 1H, $J=7.3$ Hz); 6.97 (d, 1H, $J=8.04$ Hz); 4.62 (bs, 2H); 4.52 (bs, 1H); 3.70 (m, 2H); 3.15 (s, 9H); 2.95 (m, 2H).

N-(3-((trimethylamino)methyl)-4-hydroxyphenylethyl)aminedihydrotrifluoroacetate (81): ^1H NMR (200 MHz, CDCl_3) δ (ppm): 7.01 (d, 1H, $J=6.6$ Hz); 6.80 (d, 1H, $J=5.8$ Hz); 6.76 (s, 1H); 3.79 (m, 4H); 3.69 (s, 2H); 2.90 (m, 2H); 2.66 (m, 2H); 2.58 (m, 4H).

Preparation of Key Intermediate NDI 85

The dibromo naphthalene bisanhydride (**84**) has been synthesized according to standard published procedures.

To a stirred suspension of di-bromo-dianhydride (600 mg, 0.001 mol) in glacial acetic acid (15 ml) N,N-dimethylethylamine (1.6 ml) was added. After stirring for 30 min at 130°C , the reaction mixture was cooled to room temperature and put into ice to induce a precipitation. The crude orange solid was filtered on Hirsch and purified by column chromatography (CHCl_3 : MeOH 9:1), yielding 20 (45%), 21 (26%)

N,N'-Di-(N,N-dimethylethyl)-2,6-dibromonaphthalene-1,4,5,8-tetra-carboxylic-acid-bisimide (85). Yellow-orange solid. ^1H NMR (200 MHz, CDCl_3 , 25°C , TMS). $\delta=$ 9.0 (s, 2H); 4.35 (m, 4H); 2.72 (m, 4H); 2.37 (s, 12H). Anal. Calcd. for $\text{C}_{22}\text{H}_{22}\text{Br}_2\text{N}_4\text{O}_4$: C, 46.66; H, 3.92; Br, 28.22; N, 9.89; O, 11.30. Found: C, 46.69; H, 3.89; Br, 28.18; N, 9.92.

N,N'-Di-(N,N-dimethylethyl)-2-bromonaphthalene-1,4,5,8-tetra-carboxylic acid bisimide (85a). Yellow solid. ^1H NMR (200 MHz, CDCl_3 , 25°C , TMS): $\delta=$ 8.94 (s, 1H), 8.84-8.76 (m,

2H), 4.37 (m, 4H), 2.69 (bs, 4H); 2.36 (s, 12H). Anal. Calcd. for $C_{22}H_{23}BrN_4O_4$: C, 54.22; H, 4.76; Br, 16.40; N, 11.50; O, 13.13. Found: C, 54.26; H, 4.71; Br, 16.41; N, 11.55.

Synthetic procedures for the generation of alcoholic QMP in third generation NDIs development

2-(hydroxymethyl)-4-nitrophenol (97): 2-(bromomethyl)-4-nitrophenol (**96**) 1.44g (6.2 mmol) was suspended in 40 ml of a 1:1 solution Dioxane-Water and treated at 100 W for 30 min in an open vessel Micro Wave reactor. The deep yellow solution was acidified with 1ml of HCl 10% and extracted 3 times with 30 ml of Ethyl Acetate. Organic layer were collected dried on Na_2SO_4 and the solvents removed in vacuo. The yellow oil obtained were crystallized in Toluene to afford 1.0g (5.9 mmol) of 2-(hydroxymethyl)-4-nitrophenol as yellow needle. Yield 95% 1H NMR (300 MHz, DMSO d_6 , 25 °C, TMS): δ = 11.07 (broad s, 1H), 8.21 (d, 1H J = 2.9 Hz), 8.02 (dd, 1H J_1 = 2.9 Hz, J_2 = 8.9 Hz), 6.94 (d, 1H J = 8.9 Hz), 5.35 (broad s, 1H), 4.55 (s, 2H) ^{13}C NMR (300 MHz, DMSO d_6 , 25 °C, TMS): δ = 160.69, 139.85, 130.51, 124.20, 122.89, 114.86, 57.62. Anal. Calcd $C_7H_7NO_4$: C, 49.71; H, 4.17; N, 8.28; O, 37.84. Found: C, 50.01; H, 4.12; N, 8.28.

2-(hydroxymethyl)-4-nitrophenolisopropylidenacetal (98): 2-(hydroxymethyl)-4-nitrophenol 1.0g (5.9 mmol) were dissolved in 40ml of acetone 5 ml of Dimethoxypropane and 0,05g of PTSA was then added. This solution was stirred at rt for 1h, the quantitative formation of the cyclic acetal is checked by direct TLC analysis (Cycloesane-Acetate of Ethyl 1:1). After total disappear of the reactant TEA 1ml is added and solvent is removed by vacuo, the yellow oil residue is dissolved in $CHCl_3$ and washed 3 times with a saturated solution of $NaHCO_3$. Organic layers were dried on Na_2SO_4 and solvent removed to afford 1.2g (5.85 mmol) of 2-(hydroxymethyl)-4-nitrophenol isopropylidenacetal as yellow solid. Yield 99% 1H NMR (300 MHz, $CHCl_3$, 25 °C, TMS): δ = 8.09 (dd, 1H J_1 = 2.47 Hz, J_2 = 9.18 Hz), 7.96 (d, 1H J = 2.47 Hz), 6.91 (d, 1H J = 9.18 Hz), 4.92 (s, 2H), 1.59 (s, H) ^{13}C NMR (300 MHz, $CHCl_3$, 25 °C, TMS):

δ = 156.77, 140.83, 125.37, 124.17, 121.17, 117.14, 116.96, 60.35, 24.64. Anal. Calcd C₁₀H₁₁NO₄: C, 57.41; H, 5.30; N, 6.70; O, 30.59. Found: C, 57.33; H, 5.22; N, 6.28.

2-(hydroxymethyl)-4-amino isopropylidenacetal (99): 1.2g of 2-(hydroxymethyl)-4-nitrophenol isopropylidenacetal (5.85 mmol) is dissolved in 35ml of EtOH abs and 0.05g of Pd/C 10% is added. The suspension is strongly stirred under H₂ atmosphere for 3h after that time Pd/C is filtered and solvent removed by vacuo. 2-(hydroxymethyl)-4-amino isopropylidenacetal is obtained as a yellow oil and purified by flash chromatography (Cyclohexane- Ethyl Acetate 1:1) to afford 0.890g (5.0 mmol). Yield 85% ¹H NMR (300 MHz, CHCl₃, 25 °C, TMS): δ = 7.09 (dd, 1H J₁ = 2.45 Hz, J₂ = 8.58 Hz), 6.76 (d, 1H, J = 2.45 Hz), 6.64 (dd, 1H, J = 8.58 Hz), 4.86 (s, 2H), 3.47 (s, 2H), 1.63 (s, 6H) ¹³C NMR (300 MHz, CHCl₃, 25 °C, TMS): δ = 143.86, 139.50, 119.97, 117.64, 115.66, 110.80, 98.92, 60.93, 24.53. Anal. Calcd C₁₀H₁₃NO₂: C, 67.02; H, 7.31; N, 7.82; O, 17.85. Found: C, 67.01; H, 7.32; N, 7.82.

2-chloro-N-(2,2-dimethyl-4H-benzo[d][1,3]dioxin-6-yl)acetamide (100): The isopropylidene acetal (n) 500mg (2.78 mmol) is dissolved in 15ml of dry THF and one ml of TEA was added; to this solution at 0 °C under stirring chloroacetylchlorid 0.56ml (0.35 mmol) was added dropwise. This solution was allowed to stand at 0°C under stirring for 2 hours, then 10ml of AcOEt was added. The suspension was washed with Water saturated with NaHCO₃ twice. Organic layers were collected dried on Na₂SO₄, solvent evaporation affords a brown solid which is purified on silica flash (Cyclohexane- Ethyl Acetate 8:2). Yield over 93%.

¹H NMR (300 MHz, CDCl₃, 25 °C, TMS): δ = 8.2 (s, 1H), 7.25 (d, 1H J = 2.4 Hz), 7.05 (dd, 1H J₁ = 2.4 Hz, J₂ = 8.7 Hz), 6.8 (d, 1H J = 8.7 Hz), 4.8 (s, 2H), 4.10 (s, 2H), 1.55 (s, 6H) ¹³C NMR (300 MHz, CDCl₃, 25 °C, TMS): δ = 163.72; 148.55; 129.36; 120.61; 119.73; 117.33; 117.01; 99.55; 60.70; 40.65; 24.54. Anal. Calcd C₁₂H₁₄N₁O₃Cl: C, 67.02; H, 7.31; N, 7.82; O, 17.85. Found: C, 67.12; H, 7.72; N, 7.78.

2-azido-N-(2,2-dimethyl-4H-benzo[d][1,3]dioxin-6-yl)acetamide (101): Compound **100** 500mg (1.96 mmol) was dissolved in DMF, and NaN₃ 500mg (7.9 mmol) was added in one

portion. The temperature of the solution was raised to 80°C, and stirring was continued at 80 °C for 10 h. The reaction was cooled to room temperature, and solvent was then evaporated off. The residue was dissolved in CHCl₃, washed with water three times, and dried over MgSO₄. The crude product was purified by SiO₂ flash chromatography (CH₂Cl₂ - *n*-hexane 2:1) to obtain pure 2-azido-N-(2,2-dimethyl-4H-benzo[d][1,3]dioxin-6-yl)acetamide (0.52 g, 90% yield) as a white powder.

¹H NMR (300 MHz, CDCl₃, 25 °C, TMS): δ= 7.9 (s, 1H), 7.30 (d, 1H J = 2.4 Hz), 7.10 (dd, 1H J₁ = 2.4 Hz, J₂ = 8.7 Hz), 6.75 (d, 1H J = 8.7 Hz), 4.9 (s, 2H), 4.10 (s, 2H), 1.50 (s, 6H) ¹³C NMR (300 MHz, CDCl₃, 25 °C, TMS): δ= 164.22; 148.41; 129.35; 120.42; 119.74; 117.37; 116.87; 99.56; 60.77; 52.82; 24.57 C₁₂H₁₄N₄O₃. Anal. Calcd.: C, 54.96; H, 5.38; N, 7.82; O, 21.36. Found: C, 55.02; H, 5.32; N, 7.88.

2-amino-N-(2,2-dimethyl-4H-benzo[d][1,3]dioxin-6-yl)acetamide (101): To a solution of azido-acetal in tetrahydrofuran 0.2g (0.76mmol) 20 mL were added triphenylphosphine 0.26g (1 mmol) and water (2 mL). The reaction mixture was stirred at room temperature for 16 h, and solvent was then evaporated off. The yellow oil obtained is dissolved in 2ml of EtOH and 2 drops of HCl conc were then added; 2-amino-N-(2,2-dimethyl-4H-benzo[d][1,3]dioxin-6-yl)acetamide chloridrate is obtained as white needle after one night at 4 °C. Yield 76%

¹H NMR (300 MHz, CDCl₃, 25 °C, TMS): δ= 8.25 (s, 1H), 7.35 (d, 1H J = 2.50 Hz), 7.10 (d, 1H J = 8.7 Hz), 6.80 (dd, 1H J₁ = 2.4 Hz, J₂ = 8.7 Hz), 4.81 (s, 2H), 4.15 (s, 2H), 3.75 (broad s, 2H), 1.52 (s, 6H) ¹³C NMR (300 MHz, CDCl₃, 25 °C, TMS): δ= 164.22; 148.41; 129.35; 120.42; 119.74; 117.37; 116.87; 99.56; 60.77; 52.82; 24.57 C₁₂H₁₆N₂O₃. Anal. Calcd.: C, 61.00; H, 6.83; N, 11.86; O, 20.32. Found: C, 61.09; H, 6.88; N, 11.88.

Microwave assisted synthesis of 70, 70a, 71, 71a, 75.

The NDI **85** (250 mg, 0.4 mmol) was treated in DMF in a closed vessel with the corresponding amine (0.6 mmol) at 180°C, 200 psi and 200W. After 3-10 min the violet solution was cooled at r.t and water (50 ml) was added to induce precipitation. The filtered crude were purified by HPLC using a C-18 reverse phase column (CH₃CN:H₂O 0.1%TFA, as eluent). Addition of HCl 1M solution to each chromatographic portion and solvent evaporation under vacuum afforded the adducts **70**, **70a**, **71**, **71a** and **75** as hydrochlorides.

***N,N'*-Bis-((dimethylamino)ethylamino)-2-((4-hydroxyphenyl)ethylamino)-1,4,5,8-naphthalenetetracarboxylic bisimide dihydrochloride (70·2HCl)**: Red solid. M.p.>350°C. ¹H NMR(300 MHz, CD₃OD) δ(ppm): 8.40 (d, 1H, J=7.8 Hz); 8.13 (d, 1H, J=7.8 Hz); 7.97 (s, 1H); 7.23 (d, 1H, J=8.5 Hz); 6.77 (d, 1H, J=8.5 Hz); 4.48 (m, 4H); 3.78 (t, 2H; J=6.8 Hz); 3.54 (m, 4H); 3.03 (s, 12 H); 3.01 (bs, 2H). ¹³C NMR (CD₃OD) δ(ppm): 167.47; 165.21; 164.96; 164.74; 157.71; 153.82; 132.37; 131.55; 130.96; 130.62; 129.04; 127.48; 125.57; 124.48; 121.52; 120.78; 116.96; 100.39; 57.80; 57.37; 46.12; 44.49; 44.39; 37.15; 36.78; 35.90. Anal. Calcd. for C₃₀H₃₅Cl₂N₅O₅: C, 58.44; H, 5.72; Cl, 11.50; N, 11.36; O, 12.98. Found C, 58.36; H, 5.70; Cl, 11.42; N, 11.21.

***N,N'*-Bis-((dimethylamino)ethylamino)-2-bromo-6-((4-hydroxyphenyl)ethylamino)-1,4,5,8-naphthalenetetracarboxylic bisimide dihydrochloride (70a·2HCl)**: Red solid. M.p.>350°C. ¹H NMR (300 MHz, CD₃OD) δ(ppm): 8.54 (s, 1H); 8.06 (s, 1H); 7.25 (d, 1H, J=8.5 Hz); 6.80 (d, 1H, J=8.5 Hz); 4.49 (m, 4H); 3.80 (t, 2H; J=6.9 Hz); 3.55 (m, 4H); 3.05 (s, 12 H); 2.86 (bs, 2H). ¹³C NMR (CD₃OD) δ(ppm): 167.20; 163.82; 163.10; 157.73; 153.25; 138.85; 134.45; 131.58; 131.12; 130.57; 130.05; 128.51; 124.44, 122.22; 121.18; 117.00; 100.55; 79.21; 57.61; 57.25; 46.16; 44.46; 37.59; 36.89; 35.82. Anal. Calcd. for C₃₀H₃₄BrCl₂N₅O₅: C, 51.81; H, 4.93; Br, 11.49; Cl, 10.20; N, 10.07; O, 11.50. Found C, 51.84; H, 5.00; Br, 11.46; Cl, 10.28; N, 10.12.

***N,N'*-Bis-((dimethylamino)ethylamino)-2-(2-(3-(dimethylamino)methyl-4-hydroxyphenyl)ethylamino)-1,4-5,8-naphthalenetetracarboxylic bisimide trihydrochloride (71·3HCl)**: Red solid. M.p.>350°C. ¹H NMR(300 MHz, CD₃OD) δ(ppm): 8.36 (d, 1H, J=7.8 Hz); 8.08 (d, 1H, J=7.8 Hz); 7.94 (s, 1H); 7.40 (s, 1H); 7.37 (d, 1H, J=8.4 Hz); 6.96 (d, 1H, J=8.4 Hz); 4.53-4.52 (m, 4H); 4.34 (s, 2H); 3.82 (t, 2H; J=6.8 Hz); 3.60-3.54 (m, 4H); 3.05 (s, 14 H); 2.90 (s, 6H). ¹³C NMR (CD₃OD) δ(ppm): 167.38; 165.14; 164.91; 164.69; 157.02; 153.67; 134.29; 133.85; 132.32; 131.54; 130.86; 128.98; 127.38; 125.59; 124.41; 121.30; 120.73; 118.28; 117.17; 100.52; 65.18; 57.57; 57.27; 45.91; 44.43; 44.35; 43.58; 37.19; 36.77; 35.74. Anal. Calcd. for C₃₃H₄₃Cl₃N₆O₅: C, 55.82; H, 6.10; Cl, 14.98; N, 11.84; O, 11.27. Found C, 55.78; H, 6.19; Cl, 15.03; N, 11.82.

***N,N'*-Bis-((dimethylamino)ethylamino)-2-bromo-6-(2-(3-(dimethylamino)methyl-4-hydroxyphenyl)ethylamino)-1,4-5,8-naphthalenetetracarboxylic bisimide trihydrochloride (71a·3HCl)**: Blue solid. M.p.>350°C. ¹H NMR (300 MHz, CD₃Cl₃ 25 °C, TMS) δ(ppm): 8.44 (s, 1H); 8.15 (s, 1H); 7.15 (d, 1H, J=8.2 Hz); 6.91 (s, 1H); 6.80 (d, 1H, J=8.2 Hz); 4.40-4.33 (m, 4H); 3.73 (m, 2H); 3.65 (s, 2H); 2.99 (m, 2H); 2.71 (bs, 4 H); 2.45 (s, 6H); 2.42 (s, 6H); 2.33 (s, 6H). ¹³C NMR (CD₃Cl) δ(ppm): 165.98; 163.20; 161.74; 156.71; 150.99; 149.48; 128.91; 128.62.; 128.42; 126.72; 123.88; 123.36; 122.80; 121.94; 118.42; 116.13; 108.30; 101.07; 62.67; 56.99; 56.77; 45.51; 44.90; 44.39; 43.96; 38.19; 37.73; 34.95; 30.81. Anal. Calcd. for C₃₃H₄₂BrCl₃N₆O₅: C, 50.24; H, 5.37; Br, 10.13; Cl, 13.48; N, 10.65; O, 10.14. Found C, 50.30; H, 5.39; Br, 10.08; Cl, 13.53; N, 10.61.

***N,N'*-Bis-((dimethylamino)ethylamino)-2,6-bis(2-(3-(dimethylamino)methyl-4-hydroxyphenyl)ethylamino)-1,4-5,8-naphthalenetetracarboxylic bisimide tetrahydrochloride (75·4HCl)**: Dark violet solid. M.p.>350°C. ¹H NMR (300 MHz, CD₃OD) δ(ppm): 8.50 (s, 2H); 7.17 (s, 4H); 6.82 (d, 2H, J=10.3 Hz); 4.57 (m, 4H); 4.26 (s, 4H); 3.60 (t, 4H, J=7.7 Hz); 3.31 (m, 4H); 3.04 (s, 12H); 2.84 (s, 12H); 2.72 (s, 4H). ¹³C NMR (CD₃OD) δ(ppm): 173.52; 165.38; 156.55; 152.50; 133.84; 133.61; 132.45; 126.45; 125.49; 124.96; 117.83; 116.71; 108.43; 58.77;

57.80; 44.84; 44.43; 43.52; 42.35; 37.40; 35.86; 28.28; 22.83. Anal. Calcd. for C₄₄H₆₀C₁₄N₈O₆: C, 56.29; H, 6.44; Cl, 15.11; N, 11.94; O, 10.23. Found C, 56.32; H, 6.41; Cl, 15.18; N, 12.00.

Exhaustive methylation of the amines 71, 71a.

The amine hydrochlorides were dissolved in a NaHCO₃ solution and extracted 3 times with CH₂Cl₂. After solvent evaporation under reduced pressure, the amine (2.9 mmol) was suspended in 50 ml of CH₃CN and 1.2 g (8.5 mmol) of CH₃I was added. This suspension was heated under reflux under nitrogen atmosphere for 3 hrs, within a few minutes the reaction mixture turned into dark red. The reaction was allowed to cool at r.t. and crashing out of a red solid was observed after addition of Et₂O (50 ml) to the reaction mixture. The suspension was filtered and washed with CH₃CN to give the quaternary ammonium salts **74** and **74a**.

***N,N'*-Bis-((trimethylamino)ethylamino)-2-(2-(3-(trimethylamino)methyl-4-hydroxyphenyl)ethylamino)-1,4-5,8-naphthalenetetracarboxylic bisimide triiodide (**74**):** Red solid. Yield 97% M.p.>350°C. ¹H NMR(300 MHz, D₂O) δ(ppm): 8.24 (d, 1H, J=7.8 Hz); 7.98 (d, 1H, J=7.9 Hz); 7.54 (s, 1H); 7.33 (d, 1H, J=1.8 Hz); 7.28 (d, 1H, J=6 Hz); 6.83 (d, 1H, J=8.8 Hz); 4.46 (m, 4H); 4.24 (s, 2H); 3.77 (t, 2H; J=5.77 Hz); 3.57 (m, 4H), 3.24 (s, 18H); 2.94 (s, 9H), 2.63 (bs, 2H). ¹³C NMR (D₂O) δ(ppm): 164.59; 163.37; 163.22; 162.66; 155.10; 152.12; 135.03; 133.37; 130.89; 130.29; 128.70; 126.01; 124.95, 124.20; 121.99; 120.52; 118.36; 116.66; 114.56; 98.20; 63.58; 62.21; 61.85; 53.38; 52.40; 44.29; 38.59; 34.25; 33.85. Anal. Calcd. for C₃₆H₄₉I₃N₆O₅: C, 42.12; H, 4.81; I, 37.09; N, 8.19; O, 7.79. Found C, 42.14; H, 4.78; I, 37.12; N, 8.22.

***N,N'*-Bis-((trimethylamino)ethylamino)-2-bromo-6-(2-(3-(trimethylamino)methyl-4-hydroxyphenyl)ethylamino)-1,4-5,8-naphthalenetetracarboxylic bisimide triiodide (**74a**):** Blue solid. Yield 97% M.p.>350°C. ¹H NMR (300 MHz, D₂O) δ(ppm): 8.54 (s, 1H), 7.78 (s, 1H); 7.28 (m, 2H); 6.82 (d, 1H, J=8.5 Hz); 4.53 (m, 4H); 4.27 (s, 2H); 3.85 (m, 2H); 3.63 (m, 4H);

3.27 (s, 18 H); 2.95 (s, 9H); 2.65 (bs, 2H). ^{13}C NMR (D_2O) $\delta(\text{ppm})$: 165.02; 163.84; 162.97; 162.55; 155.04; 151.78; 135.05; 133.46; 131.09; 130.59; 125.86, 123.91; 123.17; 122.19; 120.29; 116.68; 114.63; 99.05; 63.73; 62.27; 61.90; 53.36; 52.40; 45.70; 38.65; 34.46; 34.01. Anal. Calcd. for $\text{C}_{36}\text{H}_{48}\text{BrI}_3\text{N}_6\text{O}_5$: C, 39.11; H, 4.38; Br, 7.23; I, 34.44; N, 7.60; O, 7.24 Found C, 39.18; H, 4.41; Br, 7.22; I, 34.39; N, 7.64.

Nucleophilic aromatic substitution reaction at r.t.

The NDI **85** (250 mg, 0.4 mmol) was solved into 20 ml of DMF in a round bottom flask containing the corresponding amine (0.6 mmol). The mixture was stirred at r.t. for 8-48h under argon. The resulting red solution was poured in water (100 ml) and crashing out was observed. The collected solid was washed with water and purified by preparative HPLC chromatography ($\text{CH}_3\text{CN}:\text{H}_2\text{O}$ 0.1%TFA). HCl 1M solution was added to each chromatographic portion. Solvent evaporation under vacuum afforded the adducts **70**, **70a**, **71**, **71a** and **73**.

***N,N'*-Bis-((dimethylamino)ethylamino)-2-(2-(3-(N-morpholino)methyl-4-hydroxyphenyl)ethylamino)-1,4-5,8-naphthalenetetracarboxylic bisimide trihydrochloride (**71**·3HCl)**: Red solid. Yield 12%. M.p.>350°C. ^1H NMR (300 MHz, CD_3OD) $\delta(\text{ppm})$: 8.63 (d, 1H, $J=7.7$ Hz); 8.37 (d, 1H, $J=7.7$ Hz); 8.23 (s, 1H); 7.39 (s, 1H); 7.32 (dd, 1H, $J=8.3, 2.0$ Hz); 6.88 (d, 1H, $J=8.3$ Hz); 4.59-4.53 (m, 4H); 4.36 (s, 2H); 4.03-3.98 (m, 2H); 3.94-3.90 (m, 2H); 3.80-3.72 (m, 2H); 3.57 (bs, 4H); 3.42-3.39 (m, 2H); 3.32-3.21 (m, 4H); 3.04 (s, 12H). Anal. Calcd. for $\text{C}_{35}\text{H}_{45}\text{Cl}_3\text{N}_6\text{O}_6$: C, 55.89; H, 6.03; Cl, 14.14; N, 11.17; O, 12.76. Found C, 55.92; H, 6.08; Cl, 14.11; N, 11.15.

***N,N'*-Bis-((dimethylamino)ethylamino)-2-bromo-6-(2-(3-(N-morpholino)methyl-4-hydroxyphenyl)ethylamino)-1,4-5,8-naphthalenetetracarboxylic bisimide trihydrochloride (**71a**·3HCl)**: Violet solid. Yield 45%. M.p.>350°C. ^1H NMR(300 MHz, CD_3OD) $\delta(\text{ppm})$: 8.58 (s, 1H); 8.14 (s, 1H); 7.44 (s, 1H); 7.37 (d, 1H, $J=8.2, 2.0$ Hz); 6.93 (d, 1H, $J=8.2$ Hz); 4.55 (m, 4H); 4.4 (s, 2H); 4.06-4.03 (m, 2H); 3.90-3.87 (m, 2H); 3.85-3.80 (m, 2H); 3.61-3.57 (m, 4H); 3.47-

3.43 (m, 2H); 3.34-3.31 (m, 2H); 3.26-3.22 (m, 2H); 3.05 (s, 12H). ¹³C NMR (CD₃OD) δ(ppm): 167.35; 163.99; 163.22; 157.36; 153.32; 138.97; 134.88; 139.99; 131.45; 130.25; 128.75; 124.85; 124.66; 123.11; 122.15; 121.25; 117.30; 116.92; 100.91; 65.15; 57.53; 57.33; 57.25; 53.14; 45.94; 44.94; 44.42; 37.58; 36.93; 35.86. Anal. Calcd. for C₃₅H₄₄BrCl₃N₆O₆: C, 50.59; H, 5.34; Br, 9.62; Cl, 12.80; N, 10.11; O, 11.55. Found C, 51.03; H, 5.30; Br, 9.67; Cl, 12.86; N, 10.09.

***N,N'*-Bis-((dimethylamino)ethylamino)-2-(2-(3-(trimethylamino)methyl-4-hydroxyphenyl)ethylamino)-1,4-5,8-naphthalenetetracarboxylic bisimide trihydrochloride (73x3HCl)**: Red solid. Yield 6%. M.p.>350°C. ¹H NMR (300 MHz, CD₃Cl₃ 25 °C, TMS) δ(ppm): 8.67 (d, 1H, J=7.7 Hz); 8.38 (d, 1H, J=7.7 Hz); 8.27 (s, 1H); 7.36 (bs, 1H); 7.33 (d, 1H, J=8.6 Hz); 6.91 (d, 1H, J=8.6 Hz); 4.59 (bs, 4H); 4.31 (s, 2H); 3.93 (t, 2H, J=6.8 Hz); 3.60 (bs, 4H); 3.07 (bs, 2H); 3.06 (s, 15H); 2.87 (s, 6H). ¹³C NMR (CD₃OD) δ(ppm): 167.86; 165.56; 165.39; 165.15; 162.04; 161.56; 156.95; 154.14; 134.15; 133.83; 132.61; 131.59; 131.47; 129.72; 128.02; 125.78; 124.97; 121.60; 118.26; 117.02; 100.98; 58.72; 57.87; 57.50; 45.87; 44.48; 44.40; 43.56; 37.17; 36.80; 36.01. Anal. Calcd. for C₃₄H₄₅Cl₃N₆O₅: C, 56.39; H, 6.26; Cl, 14.69; N, 11.61; O, 11.05. Found C, 56.43; H, 6.23; Cl, 14.62; N, 11.66.

NDI derivative 87 ¹H NMR(300 MHz, CD₃OD) δ(ppm): 8.74 (s, 1H); 8.20 (s, 1H); 7.55 (bs, 1H); 7.36 (d, 1H, J=8.6 Hz); 6.77 (d, 1H, J=8.6 Hz); 4.66 (s, 2H); 4.58 (m, 4H); 4.52 (s, 2H); 3.59 (m, 4H); 3.06, (s, 12H).

¹³C NMR (CD₃OD) δ(ppm):163.99; 161.84; 139.17; 128.93; 122.56; 122.09; 121.65; 116.12; 60.92; 57.73; 57.26; 47.16; 44.49; 40.68; 37.59; 36.98.

NDI derivative 88 ¹H NMR (200 MHz, CD₃OD) δ(ppm): 8.53 (bs, 1H); 8.32 (bs, 1H); 7.99 (bs, 1H); 7.56 (bs, 1H); 7.32 (bs, 1H); 6.76 (d, 1H, J=8.6 Hz); 4.66 (bs, 2H); 4.56 (bs, 4H); 4.41 (bs, 2H); 3.58 (bs, 4H); 3.05 (s, 12H).

NDI derivative 89 ¹H NMR (200 MHz, CD₃OD) δ(ppm):8.55 (d, 1H, J=7.8 Hz); 8.30 (d, 1H, J= 6.7 Hz); 8.25 (s, 1H); 7.42 (bs, 1H); 7.23 (m, 2H); 4.58 (bs, 4H), 4.54 (bs, 2H); 4.02 (m, 2H); 3.51 (m, 4H); 3.03 (s, 6H); 3.02 (s, 6H); 2.85 (m, 2H).

NDI derivative 90 ^1H NMR(300 MHz, CD_3OD) δ (ppm): 8.59 (s, 1H); 8.26 (s, 1H); 7.30 (bs, 1H); 7.15 (dd, 1H, $J=8.5, 2.3$ Hz); 6.57 (d, 1H, $J=8.5$ Hz); 4.55 (bs, 4H); 4.47 (bs, 2H); 3.78 (t, 2H, $J=5.9$ Hz); 3.56 (bs, 2H); 3.49 (bs, 2H); 3.04 (s, 12H); 2.56 (t, 2H, $J=6.2$ Hz); 2.22 (t, 2H, $J=6$ Hz).

^{13}C NMR (CD_3OD) δ (ppm): 173.17; 167.23; 163.96; 163.79; 163.20; 153.46; 152.96; 138.87; 132.03; 130.17; 129.19; 128.74; 124.74; 124.52; 123.04; 122.18; 121.72; 121.58; 121.18; 115.79; 101.03; 60.94; 57.50; 57.28; 50.15; 49.87; 49.59; 49.30; 49.02; 48.74; 48.45; 44.47; 43.99; 37.62; 36.87; 35.25; 26.60.

NDI derivative 91 ^1H NMR(300 MHz, CD_3OD) δ (ppm): 8.41 (d, 1H, $J=7.7$ Hz); 8.15 (d, 1H, $J=7.8$ Hz); 8.11 (s, 1H); 7.37 (d, 1H, $J=2$ Hz); 7.17 (dd, 1H, $J=8.5, 2.2$ Hz); 6.61 (d, 1H, $J=8.6$ Hz); 4.55 (bs, 4H); 4.47 (bs, 2H); 3.74 (bs, 2H); 3.56 (bs, 2H); 3.49 (bs, 2H); 3.03 (s, 12H); 2.57 (t, 2H, $J=6.1$ Hz); 2.21 (t, 2H, $J=6.2$ Hz).

^{13}C NMR (CD_3OD) δ (ppm): 173.19; 167.35; 165.14; 164.81; 164.73; 153.87; 153.01; 132.31; 132.02; 130.87; 129.19; 129.09; 127.40; 125.58; 124.38; 122.02; 121.85; 121.41; 120.74; 115.91; 100.68; 61.01; 57.57; 57.31; 44.44; 44.39; 44.09; 43.94; 37.22; 36.75; 35.14; 26.60.

NDI derivative 87a ^1H NMR(200 MHz, CD_3OD) δ (ppm): 10.09 (s, 1H); 8.60 (s, 1H); 8.44 (d, 1H, $J=7.8$ Hz); 8.19 (d, 1H, $J=7.04$ Hz); 8.11 (s, 1H); 7.42 (d, 2H, $J=7.8$ Hz); 6.79 (d, 2H, $J=9.4$ Hz); 4.53 (bs, 4H); 4.36 (s, 2H); 3.57 (bs, 4H); 3.03 (s, 12H).

NDI derivative 88a ^1H NMR(200 MHz, CD_3OD) δ (ppm): 10.09 (s, 1H); 8.56 (s, 1H); 8.13 (s, 1H); 7.42 (d, 2H, $J=8.6$ Hz); 6.77 (d, 2H, $J=7.8$ Hz); 4.54 (bs, 4H); 4.43 (s, 2H); 3.55 (bs, 4H); 3.02 (s, 12H).

NDI derivative 89a ^1H NMR(300 MHz, CD_3OD) δ (ppm): 9.91 (s, 1H); 8.34 (d, 1H, $J=7.8$ Hz); 8.07 (d, 1H, $J=7.6$ Hz); 8.06 (s, 1H); 4.52 (t, 4H, $J=6.3$ Hz); 3.96 (t, 2H, $J=5.7$ Hz); 3.56 (t, 4H, $J=5.5$ Hz); 3.49 (t, 2H, $J=5.5$ Hz); 3.04 (s, 12H).

^{13}C NMR (CD_3OD) $\delta(\text{ppm})$: 169.77; 165.42; 163.17; 162.90; 162.77; 154.00; 151.65; 130.56; 130.05; 128.89; 127.18; 125.39; 123.80; 122.45; 121.95; 119.37; 118.72; 98.69; 55.70; 55.36; 42.60; 42.53; 38.98; 35.41; 35.33; 35.03.

NDI derivative 90a ^1H NMR(300 MHz, CD_3OD) $\delta(\text{ppm})$: 8.53 (s, 1H); 8.26 (s, 1H); 7.38 (d, 2H, $J=8.9$ Hz); 6.75 (d, 2H, $J=8.9$ Hz); 4.54 (t, 4H, $J=6.4$ Hz); 4.01 (t, 2H, $J=6.5$ Hz); 3.54 (m, 4H); 3.47 (m, 2H); 3.05 (s, 6H); 2.98 (s, 6H). ^{13}C NMR (CD_3OD) $\delta(\text{ppm})$: 171.56; 167.18; 163.85; 163.75; 163.04; 155.86; 153.10; 138.92; 131.85; 130.05; 128.72; 124.59; 124.42; 123.78; 122.88; 122.01; 121.30; 116.56; 100.85; 57.47; 57.18; 44.41; 40.79; 37.64; 37.13; 36.99.

NDI derivative 91a ^1H NMR(200 MHz, CD_3OD) $\delta(\text{ppm})$: 8.55 (d, 1H, $J=11.7$ Hz); 8.29 (d, 1H, $J=11.7$ Hz); 8.08 (s, 1H); 7.54 (s, 1H); 7.33 (s, 1H, $J=8.6$ Hz); 6.78 (d, 1H, $J=3.1$ Hz); 4.63 (bs, 2H); 4.50 (bs, 2H); 4.28 (bs, 2H); 4.25 (bs, 2H); 3.01 (s, 12H); 2.91 (bs, 2H).

NDI derivative 92a ^1H NMR (200 MHz, CD_3OD) $\delta(\text{ppm})$: 8.68 (s, 1H); 8.14 (s, 1H); 7.53 (s, 1H); 7.33 (bs, 1H); 6.76 (d, 1H, $J=9.4$ Hz); 4.64 (bs, 2H); 4.50 (bs, 2H); 4.30 (bs, 2H); 4.25 (bs, 2H); 2.91 (s, 12H); 2.79 (bs, 2H).

FRET-melting assay.

All oligonucleotides were purchased from Sigma-Aldrich. After an initial dilution at 1 mM concentration in purified water, further dilutions were carried out in the relevant buffer. FRET assay was performed with F21T ($5'$ -d(*FAM*- $\text{G}_3[\text{T}_2\text{AG}_3]_3$ -*Tamra*, with *FAM*: 6-carboxyfluorescein and *Tamra*: 6-carboxy-tetramethylrhodamine)-3'). Fluorescence melting curves were determined with a LightCycler II (Roche) real-time PCR machine, using a total reaction volume of 20 μL , with 0.25 μM of tagged oligonucleotide in a buffer containing 10 mM lithium cacodylate pH 7.4 and 50 mM KCl. After a first equilibration step at 30 $^\circ\text{C}$ during 2 minutes, a stepwise increase of 1 $^\circ\text{C}$ every minute for 65 cycles to reach 95 $^\circ\text{C}$ was performed and measurements were made after

each cycle with excitation at 470 nm and detection at 530 nm. The melting of the G-quadruplex was monitored alone or in the presence of various concentrations of compounds and/or of G4 competitor 27NHEG (5'-d(TGGGGAGGGTGGGGAGGGTGGGGGAAGG)-3'), double-stranded competitor ds26 (5'-d(CAATCGGATCGAATTCGATCCGATTG)-3') and single-stranded 4GGGscrambled (5'-d(GGATGTGAGTGTGAGTGTGAGG)-3'). Final analysis of the data was carried out using Excel and Sigma Plot software. Emission of FAM was normalized between 0 and 1, and T_m was defined as the temperature for which the normalized emission is 0.5 ΔT_m values are mean of 2-3 experiments \pm standard deviation.

For ionic strength experiments, the standard buffer containing 10 mM lithium cacodylate pH 7.4 and 50 mM KCl was added with LiCl 50, 100, 200, 400 or 940 mM.

CD analysis.

CD experiments were performed on a Jasco J 810 spectropolarimeter equipped with a NESLAB temperature controller and interfaced to a PC 100. A quartz cuvette with 5 mm path length was used for spectra recorded from 230 to 350 nm at 2 nm bandwidth, 0.1 nm step size, and 4 s time per point. The reported spectrum of each sample represents the average of 2 scans. Observed ellipticities were converted to mean residue ellipticity (θ) = deg x cm² x d mol⁻¹ (Mol. Ellip.). The oligomer 4GGG (5'-d(AGGG[TTAGGG]₃)-3') was diluted from stock to the correct concentration (4 μ M) in Li cacodylate buffer (10 mM, pH 7.4) with 50 mM KCl and then annealed by heating at 95 °C for 5 min, gradually cooled to room temperature, and incubated at 4 °C overnight. Compounds at 16 μ M final concentration were added either before or after 4GGG annealing. CD titrations were performed at a fixed 4GGG concentration (usually 3-4 μ M) with various concentrations (0–16 mol equiv) of ligands at 25 °C. All samples were allowed to equilibrate overnight. A buffer baseline was collected in the same cuvette and subtracted from the sample spectra. Final analysis of the data was carried out using Excel and Sigma Plot softwares.

For the thermal unfolding experiments, CD spectra were recorded from 20°C to 95°C, with temperature increase of 5°C, and processed as above. T_m and ΔH values were calculated according to the van't Hoff equation, applied for a two state transition from a folded to unfolded state, assuming that the heat capacity of the folded and unfolded states are equal²⁶⁹.

Alkylation Assays Experiments.

To measure the alkylation properties of **73** and **73a** towards 2'-deoxynucleotides, 200 nmol of drug and 1800 nmol of dG, dA, dC or dT were incubated in potassium phosphate buffer 50 mM, pH 7.4 for 24 h 40°C. The mixtures were loaded on a HPLC C18 reverse phase column (Eclipse XDB C18 column, Agilent Technologies), using solvent A: CH₃CN/TFA 0.01%, and solvent B: H₂O/TFA 0.01% as elution buffers, with a gradient 0-100% solvent A in 20 min and 100 μ l injection. Peaks were detected at 260 nm, and the adduct peaks were collected in Eppendorf tubes and dried at room temperature in Speed Vac UniVapo 100 H (UniEquip, Martinsried, Germany). Liquid chromatography mass spectrometry (LC-MS) was performed on a Time-of-Flight (TOF) mass analyser (Mariner ESI-TOF, Applied Biosystems, CA) Positive ion mass spectra were acquired on the ESI-TOF instrument by directly injecting 7 μ l of analyte solutions in CH₃CN:H₂O:HCOOH (50:49.5:0.5) at room temperature and with a 0.16 ml/min flow rate. The nozzle temperature was 140°C, while a constant flow of N₂ gas was kept at 0.35 l min \pm 1 to facilitate the spray. A three-points external calibration provided typical 100 p.p.m. accuracy.

For the oligonucleotide alkylation experiment by compound **74**, the gel-purified and desalted 4GGG oligonucleotide was 5'-end-labelled with [γ -³²P]ATP by T4 polynucleotide kinase and purified by MicroSpin G-25 columns (Amersham Biosciences, Europe). After purification, the oligonucleotide was resuspended in G4 buffer (LiOH 10 mM, pH 7.4, KCl 50 mM), heat-denatured and folded. Compound reactions with the labelled oligonucleotide (5 pmol/sample) were performed at 40°C in G4 buffer. These conditions were selected to maintain the stability of

the target oligonucleotide structures and to obtain thermal activation of the compound. After 24 h, samples were ethanol-precipitated, re-suspended in formamide gel-loading buffer, and heated at 95°C for 4 min. The reaction products were analyzed on 20% denaturing polyacrylamide gels and visualized by phosphorimaging analysis (Molecular Dynamics, Amersham Biosciences). Quantification was performed by ImageQuant software (Molecular Dynamics).

Cytotoxicity.

Telomerase-positive human cells were: lung carcinoma cells A549 (ATCC number CCL-185), human colorectal adenocarcinoma cells HT-29 (ATCC number HTB-38), and human melanoma (SK-Mel5). Cell lines were obtained from American Type Culture Collection (Rockville, MD). Cells were maintained as a monolayer in the logarithmic growth phase at 37°C in a 5% CO₂ humidified atmosphere, using Roswell Dulbecco's modified Eagle's medium supplemented with 10% fetal calf serum and penicillin (100 units/mL)/streptomycin (100 µg/mL) (A549 and HT-29) or 0.1% gentamycin (SK-Mel5). For A549 and HT-29 cytotoxic effects on tumor cell growth were determined by a MTT assay. QM compounds and TMP were dissolved and diluted into working concentrations with DMSO. Cells (1.75×10^4 cells/well) were plated onto 96-microwell plates to a final volume of 100 µL and allowed an overnight period for attachment. At day 1, 1 µL of each dilution of tested compounds was added per well to get a 1% final concentration of drug solvent per well; at day 2, medium was removed, cells washed with phosphate-buffered saline (PBS), and fresh medium was added. Control cells (without any compound but with 0.5% drug solvent) were treated in the exact same conditions. Cell survival was evaluated by a MTT assay: 10 µL of freshly dissolved solution of MTT (5 mg/mL in PBS) were added to each well, and after 4 h of incubation, 100 µL of solubilization solution [10% sodium dodecyl sulfate (SDS) and 0.01 M HCl] were added. After overnight incubation at 37 °C, absorbance was read at 540 nm. Data were expressed as mean values of three individual experiments conducted in triplicate. The percentage of cell survival was calculated as follows: cell survival = $(A_{\text{well}} - A_{\text{blank}})/(A_{\text{control}} -$

Ablank) $\times 100$, where blank denotes the medium without cells. For SK-Mel5, in the short-term cell growth assay, cells were seeded at 8.0×10^4 cells/well in a 6-well plate and exposed to increasing concentrations (0.005, 0.05, 0.5, 5.0 and 50 μM) of freshly dissolved **5**. Adherent cells were collected, counted in a particle counter (Coulter Counter, Coulter Electronics, Luton, UK) after 24 and 48 h of drug exposure and the IC_{50} values (drug concentration inhibiting cell growth by 50%) for each drug was calculated.

In the long-term cell growth assay, SK-Mel5 cells were seeded at 6.0×10^4 cells/ well in a 6-well plate and exposed to **73** at the final concentration of 0.25 μM . Every 48 h the culture medium was removed and fresh medium containing the drug was added to the cultures. Floating and adherent cells were collected and counted as described above every 48h of drug exposure.

Evaluation of telomerase activity. TRAP Assays.

Telomerase activity was measured on 1 μg of protein by the telomeric-repeat amplification protocol (TRAP) using the TRAPeze kit (Chemicon International, Canada), according to manufacturer's protocol. Each reaction product was amplified in the presence of a 36-bp internal TRAP assay standard (ITAS). A TSR8 quantitation standard (which serves as a standard to estimate the amount of product extended by telomerase in a given protein extract) was included for each set of TRAP assays. PCR amplification products were then resolved by polyacrylamide gel electrophoresis and visualized by autoradiography.

Immunoblotting analyses.

40 μg of protein extracts were fractioned by SDS-PAGE and transferred onto Hybond nitrocellulose membranes (GE Healthcare, Amersham, UK). Filters were blocked in PBS-Tween-20 in 5% skim milk and probed with an antibody raised against p21 (Abcam, Cambridge, UK) which was visualized by a SuperSignal[®] West PICO chemiluminescent

detection system (Thermo Scientific, Rockford, IL) after being probed with secondary anti-mouse horseradish peroxidase-linked whole antibody (Amersham Pharmacia Biotech, Uppsala, Sweden). β -actin was used as equal protein loading control.

New Raphaine Derivatives Synthesis

Chelidamic acid dimethyl ester (107)

Chelidamic acid **106** (10.0 g, 54.6 mmol) was dissolved in 100 ml SOCl_2 and refluxed overnight. The solvent was removed in vacuo and a yellow solid was obtained, which was quenched with 100 ml of freshly distilled MeOH at 0 °C. The excess solvent was then removed in vacuo. The crude product was dissolved in 200 ml of a sat. aq. NaHCO_3 solution and washed with 100 ml EtOAc. The aqueous layer was then recovered, acidified with conc. HCl to pH 4 and extracted with EtOAc. The organic layer was dried over MgSO_4 , filtered, and the solvent removed in vacuo to obtain the product as a white powder (3.4 g, 16.1 mmol, 29%).

^1H NMR (400 MHz, CDCl_3) δ H 7.39 (2H, br s), 3.92 (6H, s). The spectroscopic data were in agreement with the literature.

4-(prop-2-ynoxy)pyridine-2,6-dicarboxylic acid (109)

Chelidamic acid dimethyl ester (1.5 g, 7.1 mmol), propargylic alcohol (1.7 g, 10.5 mmol) and triphenylphosphine (3.7 g, 14.1 mmol) were dissolved in 50 ml freshly distilled THF and cooled to 0 °C. DIAD (1.9 ml, 9.9 mmol) was added dropwise under argon. The mixture was allowed to warm to rt and stirred for 3 d. The solvent was removed in vacuo and the product purified by column chromatography (50% EtOAc, 50% petroleum ether) to obtain the title compound as a white powder (1.7 g, 4.8 mmol, 68%).

^1H NMR (400 MHz, CDCl_3) δ H 7.79 (2H, s), 4.93 (1H, br s), 4.19 (2H, s, J 5.0 Hz), 3.58(1H, s).

^{13}C NMR (100 MHz, CDCl_3) δC 166.7, 165.0, 155.7, 150.0, 114.5, 80.0, 68.2, 53.2, 39.7, 28.3
108 was deprotected by adding a 2 M aq. soln. of NaOH dropwise to a soln. of **2a** in MeOH (typically 0.2 M) at rt. **109** was obtained as a white powder following a standard workup and was used without further purification

4-(2-Pyrrolidinyl-ethoxy)-quinolin-2-ylamine (111)

2-amino-quinolinone (1.0 g, 6.2 mmol), 2-(pyrrolidin-1-yl)ethanamine (1.5 g, 9.3 mmol) and triphenylphosphine (3.3 g, 12.6 mmol) were dissolved in 10 ml freshly distilled THF and cooled to 0 °C. DIAD (1.8 ml, 9.4 mmol) was added dropwise under argon. The mixture was allowed to warm to rt and stirred for 3 d. The solvent was removed in vacuo and the product purified by column chromatography (90% EtOAc, 10% MeOH) to obtain the title compound as a white powder (1.2 g, 4.0 mmol, 65%).

(400 MHz, CD_3OD) δH 8.00 (dd, $J = 8.0, 1.0$ Hz, 1H), 7.53 (dd, $J = 8.0, 1.5$ Hz, 1H), 7.48 (ddd, $J = 8.0, 6.5, 1.0$ Hz, 1H), 7.20 (ddd, $J = 8.0, 6.5, 1.5$ Hz, 1H), 6.28 (s, 1H), 4.33 (t, $J = 5.5$ Hz, 2H), 3.10 (t, $J = 5.5$ Hz, 2H), 2.81-2.73 (m, 4H), 1.94-1.82 (m, 4H)

Raphaine Derivative 112

Compound **109** (230 mg, 0.7 mmol) and 1-chloro-*N,N*,2-trimethyl-1-propenyl-amine (200 μl , 1.50 mmol) were dissolved in 10 ml DCM at 0 °C and stirred for 2 h. Triethylamine (250 μl , 1.8 mmol) was added dropwise and the solution stirred for 1 h at 0 °C. A solution of **111** (360 mg, 1.4 mmol) in 5 ml DCM was added slowly and the resulting mixture stirred at rt overnight. The solvent was removed in vacuo to yield a yellow waxy solid. Crystallization from MeCN yielded a white powder.

^1H NMR (400 MHz, CD_3OD) δH 8.48 (br d, $J = 8.0$ Hz, 2H), 8.21 (s, 2H), 8.17-8.12 (m, 2H), 8.12 (s, 2H), 8.01 (ddd, $J = 8.0, 6.5, 1.0$ Hz, 2H), 7.75 (ddd, $J = 8.0, 6.5, 1.0$ Hz, 2H), 4.98-4.93 (m, 4H), 4.69-4.63 (m, 2H), 4.07-3.99 (m, 4H), 3.97-3.85 (m, 4H), 3.61-3.53 (m, 2H), 3.48-3.34 (m, 4H), 2.36-2.08 (m, 8H);

^{13}C NMR (100 MHz, CD_3OD) δC 168.2, 167.2, 163.7, 151.0, 149.7, 139.5, 134.4, 127.6, 123.5, 121.3, 118.8, 113.9, 94.7, 66.4, 65.7, 55.2, 53.6, 39.1, 23.1

REFERENCES.

- (1) Gellman, S. H. *Chem Rev* **1997**, *97*, 1231.
- (2) Moellering, R. C., Jr. *Clin Infect Dis* **2006**, *42 Suppl 1*, S3.
- (3) Cerchia, L.; de Franciscis, V. *Trends Biotechnol* **2010**, *28*, 517.
- (4) Axarli, I.; Labrou, N. E.; Petrou, C.; Rassias, N.; Cordopatis, P.; Clonis, Y. D. *Eur J Med Chem* **2009**, *44*, 2009.
- (5) Gredicak, M.; Jeric, I. *Acta Pharm* **2007**, *57*, 133.
- (6) Frame, D. *Am J Health Syst Pharm* **2006**, *63*, S10.
- (7) Kelland, L. R.; Sharp, S. Y.; O'Neill, C. F.; Raynaud, F. I.; Beale, P. J.; Judson, I. R. *J Inorg Biochem* **1999**, *77*, 111.
- (8) Laginha, K. M.; Verwoert, S.; Charrois, G. J.; Allen, T. M. *Clin Cancer Res* **2005**, *11*, 6944.
- (9) Gellert, M.; Lipsett, M. N.; Davies, D. R. *Proc Natl Acad Sci U S A* **1962**, *48*, 2013.
- (10) Kruisselbrink, E.; Guryev, V.; Brouwer, K.; Pontier, D. B.; Cuppen, E.; Tijsterman, M. *Curr Biol* **2008**, *18*, 900.
- (11) Ou, T. M.; Lu, Y. J.; Tan, J. H.; Huang, Z. S.; Wong, K. Y.; Gu, L. Q. *ChemMedChem* **2008**, *3*, 690.
- (12) Guschlbauer, W.; Chantot, J. F.; Thiele, D. *J Biomol Struct Dyn* **1990**, *8*, 491.
- (13) Bang, I. *Biochem. Z.* **1910**, *26*, 293.
- (14) Rinaldi, R.; Branca, E.; Cingolani, R.; Di Felice, R.; Calzolari, A.; Molinari, E.; Masiero, S.; Spada, G.; Gottarelli, G.; Garbesi, A. *Ann N Y Acad Sci* **2002**, *960*, 184.
- (15) Oxford, G. S.; Gillespie, R. G. *Annu Rev Entomol* **1998**, *43*, 619.
- (16) Douglas, R. H.; Partridge, J. C.; Marshall, N. J. *Prog Retin Eye Res* **1998**, *17*, 597.
- (17) Tougard, P.; Chantot, J. F.; Guschlbauer, W. *Biochim Biophys Acta* **1973**, *308*, 9.
- (18) Zimmerman, S. B.; Cohen, G. H.; Davies, D. R. *J Mol Biol* **1975**, *92*, 181.
- (19) Zimmerman, S. B. *J Mol Biol* **1976**, *106*, 663.
- (20) Wheelhouse, R. T.; Jennings, S. A.; Phillips, V. A.; Pletsas, D.; Murphy, P. M.; Garbett, N. C.; Chaires, J. B.; Jenkins, T. C. *Journal of Medicinal Chemistry* **2006**, *49*, 5187.
- (21) De Cian, A.; Delemos, E.; Mergny, J. L.; Teulade-Fichou, M. P.; Monchaud, D. *J Am Chem Soc* **2007**, *129*, 1856.
- (22) Pinnavaia, T. J.; Marshall, C. L.; Mettler, C. M.; Fisk, C. L.; Miles, H. T.; Becker, E. D. *Journal of the American Chemical Society* **1978**, *100*, 3625.
- (23) Horvath, M. P.; Schultz, S. C. *J Mol Biol* **2001**, *310*, 367.
- (24) Haider, S.; Parkinson, G. N.; Neidle, S. *J Mol Biol* **2002**, *320*, 189.
- (25) Davis, J. T. *Angew Chem Int Ed Engl* **2004**, *43*, 668.
- (26) Feringa, B. L.; van Delden, R. A. *Angew Chem Int Ed Engl* **1999**, *38*, 3418.
- (27) Prins, L. J.; De Jong, F.; Timmerman, P.; Reinhoudt, D. N. *Nature* **2000**, *408*, 181.
- (28) Bouhoutsos-Brown, E.; Marshall, C. L.; Pinnavaia, T. J. *Journal of the American Chemical Society* **1982**, *104*, 6576.
- (29) Pinnavaia, T. J.; Miles, H. T.; Becker, E. D. *Journal of the American Chemical Society* **1975**, *97*, 7198.
- (30) Kawasaki, T.; Tokuhira, M.; Kimizuka, N.; Kunitake, T. *J Am Chem Soc* **2001**, *123*, 6792.
- (31) Brunsveld, L.; Vekemans, J. A.; Hirschberg, J. H.; Sijbesma, R. P.; Meijer, E. W. *Proc Natl Acad Sci U S A* **2002**, *99*, 4977.
- (32) Davis, A. V.; Yeh, R. M.; Raymond, K. N. *Proc Natl Acad Sci U S A* **2002**, *99*, 4793.

- (33) Fenniri, H.; Deng, B. L.; Ribbe, A. E.; Hallenga, K.; Jacob, J.; Thiagarajan, P. *Proc Natl Acad Sci U S A* **2002**, *99 Suppl 2*, 6487.
- (34) Henderson, E.; Hardin, C. C.; Walk, S. K.; Tinoco, I., Jr.; Blackburn, E. H. *Cell* **1987**, *51*, 899.
- (35) Sundquist, W. I.; Klug, A. *Nature* **1989**, *342*, 825.
- (36) Williamson, J. R.; Raghuraman, M. K.; Cech, T. R. *Cell* **1989**, *59*, 871.
- (37) Moine, H.; Mandel, J. L. *Science* **2001**, *294*, 2487.
- (38) Shafer, R. H.; Smirnov, I. *Biopolymers* **2000**, *56*, 209.
- (39) Arthanari, H.; Bolton, P. H. *Chem Biol* **2001**, *8*, 221.
- (40) Burge, S.; Parkinson, G. N.; Hazel, P.; Todd, A. K.; Neidle, S. *Nucleic Acids Res* **2006**, *34*, 5402.
- (41) Neidle, S. *Curr Opin Struct Biol* **2009**, *19*, 239.
- (42) Webba da Silva, M. *Chemistry* **2007**, *13*, 9738.
- (43) Luedtke, N. W. *CHIMIA International Journal for Chemistry* **2009**, *63*, 134.
- (44) Huppert, J. L. *Chem Soc Rev* **2008**, *37*, 1375.
- (45) Todd, A. K.; Johnston, M.; Neidle, S. *Nucleic Acids Res* **2005**, *33*, 2901.
- (46) Huppert, J. L.; Balasubramanian, S. *Nucleic Acids Res* **2005**, *33*, 2908.
- (47) Qin, Y.; Hurley, L. H. *Biochimie* **2008**, *90*, 1149.
- (48) De Cian, A.; Cristofari, G.; Reichenbach, P.; De Lemos, E.; Monchaud, D.; Teulade-Fichou, M. P.; Shin-Ya, K.; Lacroix, L.; Lingner, J.; Mergny, J. L. *Proc Natl Acad Sci U S A* **2007**, *104*, 17347.
- (49) Zagotto, G.; Sissi, C.; Moro, S.; Dal Ben, D.; Parkinson, G. N.; Fox, K. R.; Neidle, S.; Palumbo, M. *Bioorg Med Chem* **2008**, *16*, 354.
- (50) Shammass, M. A.; Shmookler Reis, R. J.; Akiyama, M.; Koley, H.; Chauhan, D.; Hideshima, T.; Goyal, R. K.; Hurley, L. H.; Anderson, K. C.; Munshi, N. C. *Mol Cancer Ther* **2003**, *2*, 825.
- (51) Shi, D. F.; Wheelhouse, R. T.; Sun, D.; Hurley, L. H. *J Med Chem* **2001**, *44*, 4509.
- (52) Sun, D.; Thompson, B.; Cathers, B. E.; Salazar, M.; Kerwin, S. M.; Trent, J. O.; Jenkins, T. C.; Neidle, S.; Hurley, L. H. *J Med Chem* **1997**, *40*, 2113.
- (53) Balasubramanian, S.; Neidle, S. *Curr Opin Chem Biol* **2009**, *13*, 345.
- (54) Watson, J. D.; Crick, F. H. *Nature* **1953**, *171*, 964.
- (55) Olovnikov, A. M. *J Theor Biol* **1973**, *41*, 181.
- (56) Shampay, J.; Szostak, J. W.; Blackburn, E. H. *Nature* **1984**, *310*, 154.
- (57) Greider, C. W.; Blackburn, E. H. *Cell* **1985**, *43*, 405.
- (58) Greider, C. W.; Blackburn, E. H. *Nature* **1989**, *337*, 331.
- (59) Blackburn, E. H.; Greider, C. W.; Henderson, E.; Lee, M. S.; Shampay, J.; Shippen-Lentz, D. *Genome* **1989**, *31*, 553.
- (60) Shippen-Lentz, D.; Blackburn, E. H. *Science* **1990**, *247*, 546.
- (61) Wellinger, R. J.; Ethier, K.; Labrecque, P.; Zakian, V. A. *Cell* **1996**, *85*, 423.
- (62) Vonderheide, R. H. *Oncogene* **2002**, *21*, 674.
- (63) Nakamura, T. M.; Morin, G. B.; Chapman, K. B.; Weinrich, S. L.; Andrews, W. H.; Lingner, J.; Harley, C. B.; Cech, T. R. *Science* **1997**, *277*, 955.
- (64) Nakamura, T. M.; Cooper, J. P.; Cech, T. R. *Science* **1998**, *282*, 493.
- (65) Blackburn, E. *Mt Sinai J Med* **1999**, *66*, 292.
- (66) Blasco, M. A. *Nat Rev Cancer* **2002**, *2*, 627.
- (67) Hogan, N. C.; Slot, F.; Traverse, K. L.; Garbe, J. C.; Bendena, W. G.; Pardue, M. L. *Genetics* **1995**, *139*, 1611.
- (68) Cenci, G.; Siriaco, G.; Gatti, M. *Genetica* **2003**, *117*, 311.
- (69) Nakamura, T. M.; Cech, T. R. *Cell* **1998**, *92*, 587.
- (70) Ly, H.; Xu, L.; Rivera, M. A.; Parslow, T. G.; Blackburn, E. H. *Genes Dev* **2003**, *17*, 1078.

- (71) Benson, J. D.; Chen, Y. N.; Cornell-Kennon, S. A.; Dorsch, M.; Kim, S.; Leszczyniecka, M.; Sellers, W. R.; Lengauer, C. *Nature* **2006**, *441*, 451.
- (72) Blackburn, E. H.; Greider, C. W.; Szostak, J. W. *Nat Med* **2006**, *12*, 1133.
- (73) Bodnar, A. G.; Ouellette, M.; Frolkis, M.; Holt, S. E.; Chiu, C. P.; Morin, G. B.; Harley, C. B.; Shay, J. W.; Lichtsteiner, S.; Wright, W. E. *Science* **1998**, *279*, 349.
- (74) Hahn, W. C.; Counter, C. M.; Lundberg, A. S.; Beijersbergen, R. L.; Brooks, M. W.; Weinberg, R. A. *Nature* **1999**, *400*, 464.
- (75) Masutomi, K.; Yu, E. Y.; Khurts, S.; Ben-Porath, I.; Currier, J. L.; Metz, G. B.; Brooks, M. W.; Kaneko, S.; Murakami, S.; DeCaprio, J. A.; Weinberg, R. A.; Stewart, S. A.; Hahn, W. C. *Cell* **2003**, *114*, 241.
- (76) Masutomi, K.; Possemato, R.; Wong, J. M.; Currier, J. L.; Tothova, Z.; Manola, J. B.; Ganesan, S.; Lansdorp, P. M.; Collins, K.; Hahn, W. C. *Proc Natl Acad Sci U S A* **2005**, *102*, 8222.
- (77) Dunham, M. A.; Neumann, A. A.; Fasching, C. L.; Reddel, R. R. *Nat Genet* **2000**, *26*, 447.
- (78) Chen, Y.; Dokmanovic, M.; Stein, W. D.; Ardecky, R. J.; Roninson, I. B. *Cancer Res* **2006**, *66*, 8749.
- (79) Compton, S. A.; Choi, J. H.; Cesare, A. J.; Ozgur, S.; Griffith, J. D. *Cancer Res* **2007**, *67*, 1513.
- (80) de Lange, T. *Genes Dev* **2005**, *19*, 2100.
- (81) Wang, F.; Podell, E. R.; Zaug, A. J.; Yang, Y.; Baciou, P.; Cech, T. R.; Lei, M. *Nature* **2007**, *445*, 506.
- (82) Shay, J. W. *Cancer Res* **2005**, *65*, 3513.
- (83) Shay, J. W.; Wright, W. E. *Nat Rev Drug Discov* **2006**, *5*, 577.
- (84) Hahn, W. C.; Stewart, S. A.; Brooks, M. W.; York, S. G.; Eaton, E.; Kurachi, A.; Beijersbergen, R. L.; Knoll, J. H.; Meyerson, M.; Weinberg, R. A. *Nat Med* **1999**, *5*, 1164.
- (85) Folini, M.; Brambilla, C.; Villa, R.; Gandellini, P.; Vignati, S.; Paduano, F.; Daidone, M. G.; Zaffaroni, N. *Eur J Cancer* **2005**, *41*, 624.
- (86) Kim, M. M.; Rivera, M. A.; Botchkina, I. L.; Shalaby, R.; Thor, A. D.; Blackburn, E. H. *Proc Natl Acad Sci U S A* **2001**, *98*, 7982.
- (87) Goldkorn, A.; Blackburn, E. H. *Cancer Res* **2006**, *66*, 5763.
- (88) Nosrati, M.; Li, S.; Bagheri, S.; Ginzinger, D.; Blackburn, E. H.; Debs, R. J.; Kashani-Sabet, M. *Clin Cancer Res* **2004**, *10*, 4983.
- (89) van Steensel, B.; Smogorzewska, A.; de Lange, T. *Cell* **1998**, *92*, 401.
- (90) Zaug, A. J.; Podell, E. R.; Cech, T. R. *Proc Natl Acad Sci U S A* **2005**, *102*, 10864.
- (91) Churikov, D.; Wei, C.; Price, C. M. *Mol Cell Biol* **2006**, *26*, 6971.
- (92) Li, G. Z.; Eller, M. S.; Firoozabadi, R.; Gilchrest, B. A. *Proc Natl Acad Sci U S A* **2003**, *100*, 527.
- (93) d'Adda di Fagagna, F.; Reaper, P. M.; Clay-Farrace, L.; Fiegler, H.; Carr, P.; Von Zglinicki, T.; Saretzki, G.; Carter, N. P.; Jackson, S. P. *Nature* **2003**, *426*, 194.
- (94) Zahler, A. M.; Williamson, J. R.; Cech, T. R.; Prescott, D. M. *Nature* **1991**, *350*, 718.
- (95) Schaffitzel, C.; Berger, I.; Postberg, J.; Hanes, J.; Lipps, H. J.; Pluckthun, A. *Proc Natl Acad Sci U S A* **2001**, *98*, 8572.
- (96) Wang, Y.; Patel, D. J. *Structure* **1993**, *1*, 263.
- (97) Parkinson, G. N.; Lee, M. P.; Neidle, S. *Nature* **2002**, *417*, 876.
- (98) Rodriguez, R.; Muller, S.; Yeoman, J. A.; Trentesaux, C.; Riou, J. F.; Balasubramanian, S. *J Am Chem Soc* **2008**, *130*, 15758.
- (99) Miyoshi, T.; Kanoh, J.; Saito, M.; Ishikawa, F. *Science* **2008**, *320*, 1341.
- (100) Tauchi, T.; Shin-Ya, K.; Sashida, G.; Sumi, M.; Nakajima, A.; Shimamoto, T.; Ohyashiki, J. H.; Ohyashiki, K. *Oncogene* **2003**, *22*, 5338.

- (101) Salvati, E.; Leonetti, C.; Rizzo, A.; Scarsella, M.; Mottolose, M.; Galati, R.; Sperduti, I.; Stevens, M. F.; D'Incalci, M.; Blasco, M.; Chiorino, G.; Bauwens, S.; Horard, B.; Gilson, E.; Stoppacciaro, A.; Zupi, G.; Biroccio, A. *J Clin Invest* **2007**, *117*, 3236.
- (102) Arnoult, N.; Shin-Ya, K.; Londono-Vallejo, J. A. *Cytogenet Genome Res* **2008**, *122*, 229.
- (103) Denchi, E. L.; de Lange, T. *Nature* **2007**, *448*, 1068.
- (104) Hemann, M. T.; Strong, M. A.; Hao, L. Y.; Greider, C. W. *Cell* **2001**, *107*, 67.
- (105) Londono-Vallejo, J. A. *Biochimie* **2008**, *90*, 73.
- (106) Howell, R. M.; Woodford, K. J.; Weitzmann, M. N.; Usdin, K. *J Biol Chem* **1996**, *271*, 5208.
- (107) Huppert, J. L.; Balasubramanian, S. *Nucleic Acids Res* **2007**, *35*, 406.
- (108) Verma, A.; Halder, K.; Halder, R.; Yadav, V. K.; Rawal, P.; Thakur, R. K.; Mohd, F.; Sharma, A.; Chowdhury, S. *J Med Chem* **2008**, *51*, 5641.
- (109) Xie, X.; Lu, J.; Kulbokas, E. J.; Golub, T. R.; Mootha, V.; Lindblad-Toh, K.; Lander, E. S.; Kellis, M. *Nature* **2005**, *434*, 338.
- (110) Todd, A. K.; Neidle, S. *Nucleic Acids Res* **2008**, *36*, 2700.
- (111) Eddy, J.; Maizels, N. *Nucleic Acids Res* **2008**, *36*, 1321.
- (112) Simonsson, T.; Pecinka, P.; Kubista, M. *Nucleic Acids Res* **1998**, *26*, 1167.
- (113) Phan, A. T.; Modi, Y. S.; Patel, D. J. *J Am Chem Soc* **2004**, *126*, 8710.
- (114) Ambrus, A.; Chen, D.; Dai, J.; Jones, R. A.; Yang, D. *Biochemistry* **2005**, *44*, 2048.
- (115) Siddiqui-Jain, A.; Grand, C. L.; Bearss, D. J.; Hurley, L. H. *Proc Natl Acad Sci U S A* **2002**, *99*, 11593.
- (116) Rankin, S.; Reszka, A. P.; Huppert, J.; Zloh, M.; Parkinson, G. N.; Todd, A. K.; Ladame, S.; Balasubramanian, S.; Neidle, S. *J Am Chem Soc* **2005**, *127*, 10584.
- (117) Fernando, H.; Reszka, A. P.; Huppert, J.; Ladame, S.; Rankin, S.; Venkitaraman, A. R.; Neidle, S.; Balasubramanian, S. *Biochemistry* **2006**, *45*, 7854.
- (118) Phan, A. T.; Kuryavyi, V.; Burge, S.; Neidle, S.; Patel, D. J. *J Am Chem Soc* **2007**, *129*, 4386.
- (119) Shirude, P. S.; Okumus, B.; Ying, L.; Ha, T.; Balasubramanian, S. *J Am Chem Soc* **2007**, *129*, 7484.
- (120) Bejugam, M.; Sewitz, S.; Shirude, P. S.; Rodriguez, R.; Shahid, R.; Balasubramanian, S. *J Am Chem Soc* **2007**, *129*, 12926.
- (121) Cogoi, S.; Xodo, L. E. *Nucleic Acids Res* **2006**, *34*, 2536.
- (122) Cogoi, S.; Paramasivam, M.; Spolaore, B.; Xodo, L. E. *Nucleic Acids Res* **2008**, *36*, 3765.
- (123) Soldatenkov, V. A.; Vetcher, A. A.; Duka, T.; Ladame, S. *ACS Chem Biol* **2008**, *3*, 214.
- (124) Kumari, S.; Bugaut, A.; Huppert, J. L.; Balasubramanian, S. *Nat Chem Biol* **2007**, *3*, 218.
- (125) Sacca, B.; Lacroix, L.; Mergny, J. L. *Nucleic Acids Res* **2005**, *33*, 1182.
- (126) Huppert, J. L.; Bugaut, A.; Kumari, S.; Balasubramanian, S. *Nucleic Acids Res* **2008**, *36*, 6260.
- (127) Kostadinov, R.; Malhotra, N.; Viotti, M.; Shine, R.; D'Antonio, L.; Bagga, P. *Nucleic Acids Res* **2006**, *34*, D119.
- (128) Darnell, J. C.; Jensen, K. B.; Jin, P.; Brown, V.; Warren, S. T.; Darnell, R. B. *Cell* **2001**, *107*, 489.
- (129) Gomez, D.; Lemarteleur, T.; Lacroix, L.; Mailliet, P.; Mergny, J. L.; Riou, J. F. *Nucleic Acids Res* **2004**, *32*, 371.
- (130) Arora, A.; Dutkiewicz, M.; Scaria, V.; Hariharan, M.; Maiti, S.; Kurreck, J. *RNA* **2008**, *14*, 1290.

- (131) Morris, M. J.; Basu, S. *Biochemistry* **2009**, *48*, 5313.
- (132) Halder, K.; Wieland, M.; Hartig, J. S. *Nucleic Acids Res* **2009**, *37*, 6811.
- (133) Bugaut, A.; Rodriguez, R.; Kumari, S.; Hsu, S. T.; Balasubramanian, S. *Org Biomol Chem* **2010**, *8*, 2771.
- (134) Kim, M. Y.; Vankayalapati, H.; Shin-Ya, K.; Wierzba, K.; Hurley, L. H. *J Am Chem Soc* **2002**, *124*, 2098.
- (135) Shin-ya, K.; Wierzba, K.; Matsuo, K.; Ohtani, T.; Yamada, Y.; Furihata, K.; Hayakawa, Y.; Seto, H. *J Am Chem Soc* **2001**, *123*, 1262.
- (136) Perry, P. J.; Reszka, A. P.; Wood, A. A.; Read, M. A.; Gowan, S. M.; Dosanjh, H. S.; Trent, J. O.; Jenkins, T. C.; Kelland, L. R.; Neidle, S. *J Med Chem* **1998**, *41*, 4873.
- (137) Perry, P. J.; Gowan, S. M.; Reszka, A. P.; Polucci, P.; Jenkins, T. C.; Kelland, L. R.; Neidle, S. *J Med Chem* **1998**, *41*, 3253.
- (138) Perry, P. J.; Read, M. A.; Davies, R. T.; Gowan, S. M.; Reszka, A. P.; Wood, A. A.; Kelland, L. R.; Neidle, S. *J Med Chem* **1999**, *42*, 2679.
- (139) Harrison, R. J.; Reszka, A. P.; Haider, S. M.; Romagnoli, B.; Morrell, J.; Read, M. A.; Gowan, S. M.; Incles, C. M.; Kelland, L. R.; Neidle, S. *Bioorg Med Chem Lett* **2004**, *14*, 5845.
- (140) Read, M. A.; Wood, A. A.; Harrison, J. R.; Gowan, S. M.; Kelland, L. R.; Dosanjh, H. S.; Neidle, S. *J Med Chem* **1999**, *42*, 4538.
- (141) Haider, S. M.; Parkinson, G. N.; Neidle, S. *J Mol Biol* **2003**, *326*, 117.
- (142) Mergny, J. L.; Maurizot, J. C. *Chembiochem* **2001**, *2*, 124.
- (143) White, E. W.; Tanious, F.; Ismail, M. A.; Reszka, A. P.; Neidle, S.; Boykin, D. W.; Wilson, W. D. *Biophys Chem* **2007**, *126*, 140.
- (144) Burger, A. M.; Dai, F.; Schultes, C. M.; Reszka, A. P.; Moore, M. J.; Double, J. A.; Neidle, S. *Cancer Res* **2005**, *65*, 1489.
- (145) Taetz, S.; Baldes, C.; Murdter, T. E.; Kleideiter, E.; Piotrowska, K.; Bock, U.; Haltner-Ukomadu, E.; Mueller, J.; Huwer, H.; Schaefer, U. F.; Klotz, U.; Lehr, C. M. *Pharm Res* **2006**, *23*, 1031.
- (146) Martins, C.; Gunaratnam, M.; Stuart, J.; Makwana, V.; Greciano, O.; Reszka, A. P.; Kelland, L. R.; Neidle, S. *Bioorg Med Chem Lett* **2007**, *17*, 2293.
- (147) Fedoroff, O. Y.; Salazar, M.; Han, H.; Chemeris, V. V.; Kerwin, S. M.; Hurley, L. H. *Biochemistry* **1998**, *37*, 12367.
- (148) Kern, J. T.; Kerwin, S. M. *Bioorg Med Chem Lett* **2002**, *12*, 3395.
- (149) Kerwin, S. M.; Chen, G.; Kern, J. T.; Thomas, P. W. *Bioorg Med Chem Lett* **2002**, *12*, 447.
- (150) Franceschin, M.; Pascucci, E.; Alvino, A.; D'Ambrosio, D.; Bianco, A.; Ortaggi, G.; Savino, M. *Bioorg Med Chem Lett* **2007**, *17*, 2515.
- (151) Sissi, C.; Lucatello, L.; Paul Krapcho, A.; Maloney, D. J.; Boxer, M. B.; Camarasa, M. V.; Pezzoni, G.; Menta, E.; Palumbo, M. *Bioorg Med Chem* **2007**, *15*, 555.
- (152) Mehta, A. K.; Shayo, Y.; Vankayalapati, H.; Hurley, L. H.; Schaefer, J. *Biochemistry* **2004**, *43*, 11953.
- (153) Clark, G. R.; Pytel, P. D.; Squire, C. J.; Neidle, S. *J Am Chem Soc* **2003**, *125*, 4066.
- (154) Cocco, M. J.; Hanakahi, L. A.; Huber, M. D.; Maizels, N. *Nucleic Acids Res* **2003**, *31*, 2944.
- (155) Mergny, J. L.; Lacroix, L.; Teulade-Fichou, M. P.; Hounsou, C.; Guittat, L.; Hoarau, M.; Arimondo, P. B.; Vigneron, J. P.; Lehn, J. M.; Riou, J. F.; Garestier, T.; Helene, C. *Proc Natl Acad Sci U S A* **2001**, *98*, 3062.
- (156) Hounsou, C.; Guittat, L.; Monchaud, D.; Jourdan, M.; Saettel, N.; Mergny, J. L.; Teulade-Fichou, M. P. *ChemMedChem* **2007**, *2*, 655.

- (157) Allain, C.; Monchaud, D.; Teulade-Fichou, M. P. *J Am Chem Soc* **2006**, *128*, 11890.
- (158) Alberti, P.; Ren, J.; Teulade-Fichou, M. P.; Guittat, L.; Riou, J. F.; Chaires, J.; Helene, C.; Vigneron, J. P.; Lehn, J. M.; Mergny, J. L. *J Biomol Struct Dyn* **2001**, *19*, 505.
- (159) Kaiser, M.; De Cian, A.; Sainlos, M.; Renner, C.; Mergny, J. L.; Teulade-Fichou, M. P. *Org Biomol Chem* **2006**, *4*, 1049.
- (160) Jantos, K.; Rodriguez, R.; Ladame, S.; Shirude, P. S.; Balasubramanian, S. *J Am Chem Soc* **2006**, *128*, 13662.
- (161) Shirude, P. S.; Gillies, E. R.; Ladame, S.; Godde, F.; Shin-Ya, K.; Huc, I.; Balasubramanian, S. *J Am Chem Soc* **2007**, *129*, 11890.
- (162) Rodriguez, R.; Pantos, G. D.; Goncalves, D. P.; Sanders, J. K.; Balasubramanian, S. *Angew Chem Int Ed Engl* **2007**, *46*, 5405.
- (163) Sun, D.; Guo, K.; Rusche, J. J.; Hurley, L. H. *Nucleic Acids Res* **2005**, *33*, 6070.
- (164) Dexheimer, T. S.; Sun, D.; Hurley, L. H. *J Am Chem Soc* **2006**, *128*, 5404.
- (165) Guo, K.; Pourpak, A.; Beetz-Rogers, K.; Gokhale, V.; Sun, D.; Hurley, L. H. *J Am Chem Soc* **2007**, *129*, 10220.
- (166) Izbicka, E.; Wheelhouse, R. T.; Raymond, E.; Davidson, K. K.; Lawrence, R. A.; Sun, D.; Windle, B. E.; Hurley, L. H.; Von Hoff, D. D. *Cancer Res* **1999**, *59*, 639.
- (167) Ren, J.; Chaires, J. B. *Biochemistry* **1999**, *38*, 16067.
- (168) Phan, A. T.; Kuryavyi, V.; Gaw, H. Y.; Patel, D. J. *Nat Chem Biol* **2005**, *1*, 167.
- (169) Parkinson, G. N.; Ghosh, R.; Neidle, S. *Biochemistry* **2007**, *46*, 2390.
- (170) Goncalves, D. P.; Rodriguez, R.; Balasubramanian, S.; Sanders, J. K. *Chem Commun (Camb)* **2006**, 4685.
- (171) Seenisamy, J.; Bashyam, S.; Gokhale, V.; Vankayalapati, H.; Sun, D.; Siddiqui-Jain, A.; Streiner, N.; Shin-Ya, K.; White, E.; Wilson, W. D.; Hurley, L. H. *J Am Chem Soc* **2005**, *127*, 2944.
- (172) Stanslas, J.; Hagan, D. J.; Ellis, M. J.; Turner, C.; Carmichael, J.; Ward, W.; Hammonds, T. R.; Stevens, M. F. *J Med Chem* **2000**, *43*, 1563.
- (173) Koepfel, F.; Riou, J. F.; Laoui, A.; Mailliet, P.; Arimondo, P. B.; Labit, D.; Petitgenet, O.; Helene, C.; Mergny, J. L. *Nucleic Acids Res* **2001**, *29*, 1087.
- (174) Riou, J. F.; Guittat, L.; Mailliet, P.; Laoui, A.; Renou, E.; Petitgenet, O.; Megnin-Chanet, F.; Helene, C.; Mergny, J. L. *Proc Natl Acad Sci U S A* **2002**, *99*, 2672.
- (175) Pennarun, G.; Granotier, C.; Gauthier, L. R.; Gomez, D.; Hoffschir, F.; Mandine, E.; Riou, J. F.; Mergny, J. L.; Mailliet, P.; Boussin, F. D. *Oncogene* **2005**, *24*, 2917.
- (176) Granotier, C.; Pennarun, G.; Riou, L.; Hoffschir, F.; Gauthier, L. R.; De Cian, A.; Gomez, D.; Mandine, E.; Riou, J. F.; Mergny, J. L.; Mailliet, P.; Dutrillaux, B.; Boussin, F. D. *Nucleic Acids Res* **2005**, *33*, 4182.
- (177) Schouten, J. A.; Ladame, S.; Mason, S. J.; Cooper, M. A.; Balasubramanian, S. *J Am Chem Soc* **2003**, *125*, 5594.
- (178) Keating, L. R.; Szalai, V. A. *Biochemistry* **2004**, *43*, 15891.
- (179) Maraval, A.; Franco, S.; Vialas, C.; Pratviel, G.; Blasco, M. A.; Meunier, B. *Org Biomol Chem* **2003**, *1*, 921.
- (180) Dixon, I. M.; Lopez, F.; Esteve, J. P.; Tejera, A. M.; Blasco, M. A.; Pratviel, G.; Meunier, B. *ChemBiochem* **2005**, *6*, 123.
- (181) Rajput, C.; Rutkaite, R.; Swanson, L.; Haq, I.; Thomas, J. A. *Chemistry* **2006**, *12*, 4611.
- (182) Ren, L.; Zhang, A.; Huang, J.; Wang, P.; Weng, X.; Zhang, L.; Liang, F.; Tan, Z.; Zhou, X. *ChemBiochem* **2007**, *8*, 775.
- (183) Reed, J. E.; Neidle, S.; Vilar, R. *Chem Commun (Camb)* **2007**, 4366.
- (184) Reed, J. E.; Arnal, A. A.; Neidle, S.; Vilar, R. *J Am Chem Soc* **2006**, *128*, 5992.

- (185) Dixon, I. M.; Lopez, F.; Tejera, A. M.; Esteve, J. P.; Blasco, M. A.; Pratviel, G.; Meunier, B. *J Am Chem Soc* **2007**, *129*, 1502.
- (186) Bertrand, H.; Monchaud, D.; De Cian, A.; Guillot, R.; Mergny, J. L.; Teulade-Fichou, M. P. *Org Biomol Chem* **2007**, *5*, 2555.
- (187) Tuntiwechapikul, W.; Lee, J. T.; Salazar, M. *J Am Chem Soc* **2001**, *123*, 5606.
- (188) Sato, S.; Kondo, H.; Nojima, T.; Takenaka, S. *Anal Chem* **2005**, *77*, 7304.
- (189) Redon, S.; Bombard, S.; Elizondo-Riojas, M. A.; Chottard, J. C. *Nucleic Acids Res* **2003**, *31*, 1605.
- (190) Bertrand, H.; Bombard, S.; Monchaud, D.; Teulade-Fichou, M. P. *J Biol Inorg Chem* **2007**, *12*, 1003.
- (191) Di Antonio, M.; Doria, F.; Richter, S. N.; Bertipaglia, C.; Mella, M.; Sissi, C.; Palumbo, M.; Freccero, M. *J Am Chem Soc* **2009**, *131*, 13132.
- (192) Chiang, Y.; Kresge, A. J.; Zhu, Y. *J Am Chem Soc* **2001**, *123*, 8089.
- (193) Veldhuyzen, W. F.; Shallop, A. J.; Jones, R. A.; Rokita, S. E. *J Am Chem Soc* **2001**, *123*, 11126.
- (194) Chiang, Y.; Kresge, A. J.; Zhu, Y. *J Am Chem Soc* **2002**, *124*, 6349.
- (195) Chiang, Y.; Kresge, A. J.; Zhu, Y. *J Am Chem Soc* **2002**, *124*, 717.
- (196) Veldhuyzen, W. F.; Pande, P.; Rokita, S. E. *J Am Chem Soc* **2003**, *125*, 14005.
- (197) Richter, S. N.; Maggi, S.; Mels, S. C.; Palumbo, M.; Freccero, M. *J Am Chem Soc* **2004**, *126*, 13973.
- (198) Verga, D.; Richter, S. N.; Palumbo, M.; Gandolfi, R.; Freccero, M. *Org Biomol Chem* **2007**, *5*, 233.
- (199) Doria, F.; Richter, S. N.; Nadai, M.; Colloredo-Mels, S.; Mella, M.; Palumbo, M.; Freccero, M. *J Med Chem* **2007**, *50*, 6570.
- (200) Weinert, E. E.; Dondi, R.; Colloredo-Melz, S.; Frankenfield, K. N.; Mitchell, C. H.; Freccero, M.; Rokita, S. E. *J Am Chem Soc* **2006**, *128*, 11940.
- (201) Verga, D.; Nadai, M.; Doria, F.; Percivalle, C.; Di Antonio, M.; Palumbo, M.; Richter, S. N.; Freccero, M. *J Am Chem Soc* **2010**, *132*, 14625.
- (202) Di Antonio, M.; Doria, F.; Mella, M.; Merli, D.; Profumo, A.; Freccero, M. *J Org Chem* **2007**, *72*, 8354.
- (203) Wintgens, V.; Valat, P.; Kossanyi, J.; Biczok, L.; Demeter, A.; Berces, T. *J Chem Soc Faraday T* **1994**, *90*, 411.
- (204) Cho, D. W.; Fujitsuka, M.; Choi, K. H.; Park, M. J.; Yoon, U. C.; Majima, T. *J Phys Chem B* **2006**, *110*, 4576.
- (205) Cho, D. W.; Fujitsuka, M.; Sugimoto, A.; Yoon, U. C.; Mariano, P. S.; Majima, T. *J Phys Chem B* **2006**, *110*, 11062.
- (206) Cho, D. W.; Fujitsuka, M.; Sugimoto, A.; Majima, T. *J Phys Chem A* **2008**, *112*, 7208.
- (207) Takahashi, S.; Nozaki, K.; Kozaki, M.; Suzuki, S.; Keyaki, K.; Ichimura, A.; Matsushita, T.; Okada, K. *J Phys Chem A* **2008**, *112*, 2533.
- (208) Cao, H.; Chang, V.; Hernandez, R.; Heagy, M. D. *J Org Chem* **2005**, *70*, 4929.
- (209) Kolosov, D.; Adamovich, V.; Djurovich, P.; Thompson, M. E.; Adachi, C. *J Am Chem Soc* **2002**, *124*, 9945.
- (210) Licchelli, M.; Biroli, A. O.; Poggi, A.; Sacchi, D.; Sangermani, C.; Zema, M. *Dalton T* **2003**, 4537.
- (211) Bojinov, V. B.; Georgiev, N. I.; Bosch, P. *J Fluoresc* **2009**, *19*, 127.
- (212) Tian, Y.; Su, F.; Weber, W.; Nandakumar, V.; Shumway, B. R.; Jin, Y.; Zhou, X.; Holl, M. R.; Johnson, R. H.; Meldrum, D. R. *Biomaterials* **2010**, *31*, 7411.
- (213) Georgiev, N.; Bojinov, V. *Journal of Fluorescence* **2010**, *1*.
- (214) Duke, R. M.; Gunnlaugsson, T. *Tetrahedron Lett* **2007**, *48*, 8043.
- (215) Veale, E. B.; Gunnlaugsson, T. *Journal of Organic Chemistry* **2008**, *73*, 8073.

- (216) Veale, E. B.; Tocci, G. M.; Pfeffer, F. M.; Kruger, P. E.; Gunnlaugsson, T. *Org Biomol Chem* **2009**, *7*, 3447.
- (217) Sami, S. M.; Dorr, R. T.; Alberts, D. S.; Remers, W. A. *J Med Chem* **1993**, *36*, 765.
- (218) Wamberg, M. C.; Walczak, K.; Andersen, L.; Hassan, A. A.; Pedersen, E. B. *Helv Chim Acta* **2006**, *89*, 1826.
- (219) Chen, Z.; Liang, X.; Zhang, H.; Xie, H.; Liu, J.; Xu, Y.; Zhu, W.; Wang, Y.; Wang, X.; Tan, S.; Kuang, D.; Qian, X. *J Med Chem* **2010**, *53*, 2589.
- (220) Nitiss, J. L.; Zhou, J.; Rose, A.; Hsiung, Y.; Gale, K. C.; Osheroff, N. *Biochemistry* **1998**, *37*, 3078.
- (221) Brana, M. F.; Castellano, J. M.; Moran, M.; Perez de Vega, M. J.; Romerdahl, C. R.; Qian, X. D.; Bousquet, P.; Emling, F.; Schlick, E.; Keilhauer, G. *Anticancer Drug Des* **1993**, *8*, 257.
- (222) Deady, L. W.; Desneves, J.; Kaye, A. J.; Finlay, G. J.; Baguley, B. C.; Denny, W. A. *Bioorg Med Chem* **2000**, *8*, 977.
- (223) Li, F.; Cui, J.; Guo, L.; Qian, X.; Ren, W.; Wang, K.; Liu, F. *Bioorg Med Chem* **2007**, *15*, 5114.
- (224) Yang, Q.; Yang, P.; Qian, X.; Tong, L. *Bioorg Med Chem Lett* **2008**, *18*, 6210.
- (225) Zhu, H.; Miao, Z. H.; Huang, M.; Feng, J. M.; Zhang, Z. X.; Lu, J. J.; Cai, Y. J.; Tong, L. J.; Xu, Y. F.; Qian, X. H.; Ding, J. *Neoplasia* **2009**, *11*, 1226.
- (226) Yang, Q.; Qian, X. H.; Xu, J. Q.; Sun, Y. S.; Li, Y. G. *Bioorgan Med Chem* **2005**, *13*, 1615.
- (227) Saito, I.; Takayama, M.; Sakurai, T. *Journal of the American Chemical Society* **1994**, *116*, 2653.
- (228) Kawai, K.; Osakada, Y.; Takada, T.; Fujitsuka, M.; Majima, T. *J Am Chem Soc* **2004**, *126*, 12843.
- (229) Kawai, K.; Osakada, Y.; Fujitsuka, M.; Majima, T. *Chem Commun (Camb)* **2006**, 3918.
- (230) Colloredo-Mels, S.; Doria, F.; Verga, D.; Freccero, M. *J Org Chem* **2006**, *71*, 3889.
- (231) Rogers, J. E.; Abraham, B.; Rostkowski, A.; Kelly, L. A. *Photochem Photobiol* **2001**, *74*, 521.
- (232) Rogers, J. E.; Le, T. P.; Kelly, L. A. *Photochem Photobiol* **2001**, *73*, 223.
- (233) Gosztola, D.; Niemczyk, M. P.; Svec, W.; Lukas, A. S.; Wasielewski, M. R. *The Journal of Physical Chemistry A* **2000**, *104*, 6545.
- (234) Land, E. J.; Porter, G.; Strachan, E. *Transactions of the Faraday Society* **1961**, *57*, 1885.
- (235) Maki, T.; Araki, Y.; Ishida, Y.; Onomura, O.; Matsumura, Y. *J Am Chem Soc* **2001**, *123*, 3371.
- (236) Surdhar, P. S.; Armstrong, D. A. *The Journal of Physical Chemistry* **1987**, *91*, 6532.
- (237) Rogers, J. E.; Kelly, L. A. *Journal of the American Chemical Society* **1999**, *121*, 3854.
- (238) Thalacker, C.; Roger, C.; Wurthner, F. *J Org Chem* **2006**, *71*, 8098.
- (239) Pschirer, N. G.; Kohl, C.; Nolde, F.; Qu, J.; Mullen, K. *Angew Chem Int Ed Engl* **2006**, *45*, 1401.
- (240) Guelev, V.; Sorey, S.; Hoffman, D. W.; Iverson, B. L. *J Am Chem Soc* **2002**, *124*, 2864.
- (241) Chu, Y.; Sorey, S.; Hoffman, D. W.; Iverson, B. L. *J Am Chem Soc* **2007**, *129*, 1304.

- (242) Okamoto, A.; Nakamura, T.; Yoshida, K.; Nakatani, K.; Saito, I. *Org Lett* **2000**, *2*, 3249.
- (243) Zhong, C. J.; Kwan, W. S. V.; Miller, L. L. *Chemistry of Materials* **1992**, *4*, 1423.
- (244) Abraham, B.; McMasters, S.; Mullan, M. A.; Kelly, L. A. *J Am Chem Soc* **2004**, *126*, 4293.
- (245) Modica, E.; Zanaletti, R.; Freccero, M.; Mella, M. *J Org Chem* **2001**, *66*, 41.
- (246) Xu, Y.; Ishizuka, T.; Kurabayashi, K.; Komiyama, M. *Angew Chem Int Ed Engl* **2009**, *48*, 7833.
- (247) Xu, Y.; Suzuki, Y.; Komiyama, M. *Angew Chem Int Ed Engl* **2009**, *48*, 3281.
- (248) Paramasivan, S.; Rujan, I.; Bolton, P. H. *Methods* **2007**, *43*, 324.
- (249) Yao, Y.; Wang, Q.; Hao, Y. H.; Tan, Z. *Nucleic Acids Res* **2007**, *35*, e68.
- (250) Hampel, S. M.; Sidibe, A.; Gunaratnam, M.; Riou, J. F.; Neidle, S. *Bioorg Med Chem Lett* **2010**, *20*, 6459.
- (251) Luu, K. N.; Phan, A. T.; Kuryavyi, V.; Lacroix, L.; Patel, D. J. *J Am Chem Soc* **2006**, *128*, 9963.
- (252) Ambrus, A.; Chen, D.; Dai, J.; Bialis, T.; Jones, R. A.; Yang, D. *Nucleic Acids Res* **2006**, *34*, 2723.
- (253) Vorlickova, M.; Chladkova, J.; Kejnovska, I.; Fialova, M.; Kypr, J. *Nucleic Acids Res* **2005**, *33*, 5851.
- (254) Viglasky, V.; Bauer, L.; Tluczkova, K. *Biochemistry* **2010**, *49*, 2110.
- (255) Jain, A. K.; Reddy, V. V.; Paul, A.; K, M.; Bhattacharya, S. *Biochemistry* **2009**, *48*, 10693.
- (256) Barbieri, C. M.; Srinivasan, A. R.; Rzuczek, S. G.; Rice, J. E.; LaVoie, E. J.; Pilch, D. S. *Nucleic Acids Res* **2007**, *35*, 3272.
- (257) Rezler, E. M.; Seenisamy, J.; Bashyam, S.; Kim, M. Y.; White, E.; Wilson, W. D.; Hurley, L. H. *J Am Chem Soc* **2005**, *127*, 9439.
- (258) Pilch, D. S.; Barbieri, C. M.; Rzuczek, S. G.; Lavoie, E. J.; Rice, J. E. *Biochimie* **2008**, *90*, 1233.
- (259) Fu, Y. T.; Keppler, B. R.; Soares, J.; Jarstfer, M. B. *Bioorg Med Chem* **2009**, *17*, 2030.
- (260) Parkinson, G. N.; Cuenca, F.; Neidle, S. *J Mol Biol* **2008**, *381*, 1145.
- (261) Tan, E.; Young, D.; McLaren, B.; Wright, A. *Australas J Dermatol* **2010**, *51*, 139.
- (262) Freccero, M.; Gandolfi, R.; Sarzi-Amade, M. *J Org Chem* **2003**, *68*, 6411.
- (263) Veldhuyzen, W. F.; Lam, Y. F.; Rokita, S. E. *Chem Res Toxicol* **2001**, *14*, 1345.
- (264) Rokita, S. E.; Yang, J.; Pande, P.; Greenberg, W. A. *J Org Chem* **1997**, *62*, 3010.
- (265) Freccero, M.; Di Valentin, C.; Sarzi-Amade, M. *J Am Chem Soc* **2003**, *125*, 3544.
- (266) Maxam, A. M.; Gilbert, W. *Methods Enzymol* **1980**, *65*, 499.
- (267) Kim, N. W.; Piatyszek, M. A.; Prowse, K. R.; Harley, C. B.; West, M. D.; Ho, P. L.; Coviello, G. M.; Wright, W. E.; Weinrich, S. L.; Shay, J. W. *Science* **1994**, *266*, 2011.
- (268) Paudel, S.; Nandhikonda, P.; Heagy, M. D. *J Fluoresc* **2009**, *19*, 681.
- (269) Greenfield, N. J. *Nat Protoc* **2006**, *1*, 2527.